# Seismic Design of Rigid Wall-Flexible Diaphragm Buildings

## An Alternative Procedure
## Second Edition

*FEMA P-1026 / October 2021*

FEMA

nehrp

# Seismic Design of Rigid Wall-Flexible Diaphragm Buildings: An Alternative Procedure

## Second Edition

Prepared by

APPLIED TECHNOLOGY COUNCIL
201 Redwood Shores Parkway, Suite 240
Redwood City, California 94065
www.ATCouncil.org

Prepared for

FEDERAL EMERGENCY MANAGEMENT AGENCY
Mai (Mike) Tong, Project Officer
William T. Holmes, Technical Advisor
Washington, D.C.

SECOND EDITION PROJECT TEAM

APPLIED TECHNOLOGY COUNCIL
Jon A. Heintz (Project Executive)
Justin Moresco (Project Manager)

PROJECT TECHNICAL COMMITTEE
Dominic J. Kelly (Project Technical Director)
Kelly Cobeen
John Lawson
Ben Schafer
Robert Tremblay

PROJECT REVIEW PANEL
Ryan Kersting (ATC Board Contact)
Phil Line
Bonnie Manley
David McCormick
Trent Nagele
Joe Steinbicker

PROJECT WORKING GROUP
Maria Koliou
Shahab Torabian

FIRST EDITION PROJECT TEAM

PRINCIPAL AUTHORS
John Lawson
Dominic J. Kelly

CONTRIBUTING AUTHORS
Andre Filiatrault
Maria Koliou

REVIEWERS
Kelly Cobeen
David McCormick

PROJECT MANAGEMENT COMMITTEE
William Holmes (Chair)
James R. Harris
John D. Hooper
Dominic J. Kelly
Barry H. Welliver

PROJECT REVIEW PANEL
Ryan Kersting
James Kramer
Trent Nagele
Joe Steinbicker
Doug Thompson


FEMA

PROJECT REVIEW PANEL WORKSHOP PARTICIPANTS
Thomas Gangel
Nathan Hauer
Philip Line
Bonnie Manley
Lawrence Novak

PROJECT OVERSIGHT
Mai Tong
Robert D. Hanson
Philip Schneider

## Notice



Cover photograph – Aerial view of a rigid wall-flexible diaphragm building (photo credit: Harsch Investment Properties/VLMK Engineering + Design).

# Foreword

The Federal Emergency Management Agency (FEMA) has the responsibility under the National Earthquake Hazards Reduction Program (NEHRP) for translation of new knowledge and research results to help improve seismic design of buildings in the United States. This updated FEMA NEHRP technical guidance document is to provide the supporting technical study results, comparative design examples, and explanations for the alternative seismic design procedure for rigid wall-flexible diaphragm (RWFD) buildings. This type of building, also known as a "big box" building, is typically used for warehouses or retail stores and has experienced severe damage or even collapse in past earthquakes.

It is known that the seismic performance of RWFD buildings is mostly related to the large displacement of flexible diaphragms under earthquake ground motions. The current traditional seismic design of RWFD buildings lacks a comprehensive consideration of the flexible diaphragm behavior. The new alternative RWFD procedure is intended to correct this weakness, and it has been shown to offer superior seismic performance for such buildings.

FEMA and the project officer are thankful to the Applied Technology Council (ATC), the chair and members of the Project Technical Committee, the Project Review Panel, the project technical advisor, and the ATC project manager for the significant effort they have devoted to update, review, and enhance the alternative design procedure of rigid wall-flexible diaphragm buildings. We are very glad that the alternative procedure has been approved in Part 1 of the 2020 *NEHRP Recommended Seismic Provisions for New Buildings and Other Structures* (FEMA P-2082) and has been accepted in ASCE/SEI 7-22, *Minimum Design Loads and Associated Criteria for Buildings and Other Structures*.

Federal Emergency Management Agency

# Preface

Rigid wall-flexible diaphragm (RWFD) buildings are ubiquitous throughout the United States and are commonly used for retail, storage, and distribution facilities. This report describes an alternative procedure for designing RWFD buildings that better reflects their expected seismic behavior by explicitly accounting for the response of their diaphragms. The expectation is that the alternative procedure will lead to designs that provide improved earthquake performance.

In 2018, the Applied Technology Council (ATC), with funding from the Federal Emergency Management Agency (FEMA) under Task Order Contract HSFE60-17-D-0002, commenced a series of projects to update FEMA P-1026, *Seismic Design of Rigid Wall-Flexible Diaphragm Buildings: An Alternate Procedure* (FEMA, 2015), which was published in March 2015. That edition of FEMA P-1026 was funded by FEMA and prepared by the National Institute of Building Sciences' Building Seismic Safety Council (BSSC). The publication was a result of a study on simplified designs administered by BSSC.

The alternative RWFD design procedure described in the 2015 report was incorporated into FEMA P-2082, *NEHRP Recommended Seismic Provisions for New Buildings and Other Structures* (FEMA, 2020a), and into ASCE/SEI 7-22, *Minimum Design Loads and Associated Criteria for Buildings and Other Structures* (ASCE, 2022). The objectives of this 2021 update to FEMA P-1026 are to amend the design procedure for consistency with provisions in ASCE/SEI 7-22, to incorporate newly available research and numerical studies on bare-steel-deck and wood diaphragms, and to expand the design examples to include bare-steel-deck diaphragms. This update also incorporates recommendations for future studies that could lead to further improvements to the design of RWFD buildings.

ATC is indebted to the Building Seismic Safety Council and all members of the project team that developed the 2015 version of the FEMA P-1026 report. ATC would like to thank Dominic Kelly, Project Technical Director, for his leadership in the update to FEMA P-1026. The Project Technical Committee for the update, consisting of Kelly Cobeen, John Lawson, Ben Schafer, and Robert Tremblay, reviewed the original report and incorporated significant

changes throughout. Shahab Torabian helped incorporate new material on steel-deck diaphragms, and Maria Koliou conducted additional numerical analysis related to wood diaphragms that built upon the work done in the development of the original FEMA P-1026 report. In particular, the update could not have been possible without the research on steel-deck diaphragms conducted by Ben Schafer and funded through the Cold-Formed Steel Research Consortium. The Project Review Panel for the update, consisting of Ryan Kersting, Phil Line, Bonnie Manley, David McCormick, Trent Nagele, and Joe Steinbicker, provided technical review, advice, and consultation at key stages of the work.

ATC also gratefully acknowledges Mike Tong (FEMA Project Officer) and Bill Holmes (FEMA Technical Advisor) for their input and guidance in the preparation of this report. Ayse Hortacsu and Veronica Cedillos assisted in ATC project management, and Carrie J. Perna and Ginevra Rojahn provided ATC report production services. The names and affiliations of all who contributed to this report are provided in the list of Project Participants at the end of this report.

Justin Moresco
ATC Director of Projects

Jon A. Heintz
ATC Executive Director

# Table of Contents

# List of Figures

# List of Tables

# Chapter 1
# Introduction

This report presents an alternative design procedure for earthquake resistance of one-story buildings with stiff and strong vertical elements coupled with flexible roof diaphragms. The report focuses on use of this alternative procedure for new buildings, while noting its possible application to the retrofit of existing buildings. Vertical elements permitted to be used with this procedure include concrete and masonry walls, as well as braced frames and other elements of similar in-plane stiffness. Herein, these structures are referred to as rigid wall-flexible diaphragm (RWFD) buildings. At the time of preparing this report, the alternative RWFD design procedure was expected to be incorporated into Section 12.10.4 and Section 12.2.3.4 of the forthcoming ASCE/SEI 7-22, *Minimum Design Loads and Associated Criteria for Buildings and Other Structures* (ASCE, 2022).

This alternative RWFD design procedure resulted from one of three studies that were part of the Building Seismic Safety Council's Simplified Design Program, a larger project to explore means of simplifying the seismic design of buildings. The goal of the RWFD study was to determine whether a set of stand-alone design provisions could be created for a single building type, in this case a RWFD, or "big box," building. This topic had the added potential to directly address the behavior of single-story RWFD buildings wherein the building's seismic response is dominated by the diaphragm instead of the vertical elements of the seismic-force-resisting system (SFRS).

The objectives of the study were:

- To develop an alternative design methodology for the horizontal roof diaphragm and the vertical elements of the SFRS that is relatively simple yet appropriately captures the unique behavior of single-story RWFD buildings, in which a building's response is dominated by the diaphragm instead of the vertical elements of the SFRS, and
- To base the alternative design procedure on design parameters, such as period, that are representative of the diaphragm's response, a response modification coefficient, and an overstrength factor that together account for diaphragm flexibility and performance.

The alternative RWFD design procedure was developed and evaluated using the procedure of FEMA P695, *Quantification of Building Seismic Performance Factors* (FEMA, 2009), to confirm that it would meet the performance intent of current building-code provisions. The results of these evaluations are presented in Appendix A through Appendix D.

In addition to this report, the reader is referred to FEMA P-2082, *NEHRP Recommended Seismic Provisions for New Buildings and Other Structures* (FEMA, 2020a), ASCE/SEI 7-22, and their associated commentaries.

## 1.1 The Need for a New Seismic Design Procedure for RWFD Buildings

Single-story buildings with concrete or masonry walls supporting lightweight wood or bare (untopped) steel deck roof diaphragms are common across North America and other parts of the world. The walls are strong and stiff in their planes in comparison to the strength and stiffness of the diaphragm in its plane. The current building-code provisions most frequently used for these buildings are those of the equivalent-lateral-force procedure in ASCE/SEI 7-22. This procedure, applicable to all buildings, incorporates the assumption that the primary flexibility and ductility of the SFRS occur in the vertical elements. The flexibility drives the dynamic amplification of the ground motion, and the ductility drives the dissipation of the energy of the dynamic response. However, the actual seismic behavior of these RWFD buildings is quite different. Evidence indicates that the dynamic behavior is largely dominated by the diaphragm's response instead of the walls' response. This is a significant departure from the underlying assumptions of the widely used equivalent-lateral-force procedure.

The past performance of RWFD buildings when subjected to moderate-to-strong earthquake shaking has demonstrated weaknesses, in particular in the out-of-plane wall connections between the tops of walls and diaphragms. Building code design provisions have addressed specific known weaknesses of RWFD buildings. Provisions specific to these buildings have evolved mostly as reactions to observed damage with little stated recognition of how these buildings respond differently to earthquakes than multi-story frame buildings or one-story buildings with rigid diaphragms.

There was therefore a need identified to address the diaphragm-dominated response of RWFD buildings in applicable design requirements. Several design approaches were considered, including a displacement-based design approach. The design method that was ultimately selected and that is addressed in this report serves the purpose of recognizing the effects of diaphragm yielding while being easily incorporated into the provisions of

ASCE/SEI 7-22. The use of this alternative RWFD procedure is recommended because it is anticipated to result in improved earthquake performance relative to the traditional design method.

## 1.2 Purpose of Report

The purpose of this report is to present the alternative seismic design procedure for RWFD buildings as incorporated into ASCE/SEI 7-22. The target audience is practicing engineers that design this type of building. The intention of this report is to convey design principles that practicing engineers can use in their designs to improve the seismic performance of RWFD buildings.

## 1.3 2021 Update to FEMA P-1026

The 2021 update to FEMA P-1026 incorporates:

- Amendments to the design methodology for consistency with provisions in ASCE/SEI 7-22,
- New numerical study information addressing bare steel deck diaphragms based on new steel deck diaphragm research, as described in Appendix D,
- Expanded design examples that include bare steel deck diaphragms,
- Updates to the wood diaphragm numerical studies to fully reflect design of the archetype buildings using the design methodology as incorporated into ASCE/SEI 7-22, as well as expanding the numerical studies to include archetypes reflecting variation in wall weight and reflecting a range of building heights, and
- Updated discussions of interest to the user, including a series of recommendations for future studies.

## 1.4 Introduction to the Alternative RWFD Procedure and Comparison to Traditional Practice

The alternative RWFD procedure is force based and similar to traditional design requirements for this type of building; however, unlike traditional provisions, the magnitude of the diaphragm design forces in the alternative procedure depends more on diaphragm properties than those of the vertical in-plane elements.

In the alternative RWFD procedure, the diaphragm is designed using an equivalent-lateral-force procedure but with a period applicable to the diaphragm alone, $T_{diaph}$, and a response modification coefficient applicable to

the diaphragm, $R_{diaph}$. This is a departure from traditional design practice in which the diaphragm forces are computed using a period and response modification coefficient applicable to the vertical system.

Also, the alternative procedure requires designing the end regions of a diaphragm for an amplified shear to better spread diaphragm yielding. Diaphragm chords are designed using forces computed with $R_{diaph}$ but without the amplification in the end regions. Collectors for buildings assigned to Seismic Design Category (SDC) C to SDC F are designed for a diaphragm force amplified by the diaphragm overstrength factor, $\Omega_{0\text{-}diaph}$. The alternative RWFD procedure is applicable to buildings constructed with wood structural panel diaphragms nailed to wood framing members or wood nailers, and steel deck diaphragms.

The vertical elements are permitted to be designed using the ASCE/SEI 7-22 Section 12.2.3.4 two-stage analysis method. This can be thought of as similar to the Section 12.2.3.2 two-stage analysis procedure for a multi-story building with a flexible upper portion and a stiff lower portion. For the one-story RWFD building, the diaphragm is the flexible portion, and the in-plane walls or other vertical elements are the stiff portion.

The seismic design forces to the vertical elements in each horizontal direction consider separately: (1) the effective seismic weight tributary to the diaphragm responding as a function of the diaphragm period, and (2) the effective seismic weight tributary to the vertical element responding as a function of the vertical element period.

Included in ASCE/SEI 7-22 are conditions in which the in-plane deflections of the horizontal diaphragm and the vertical SFRS elements must be checked. The diaphragm deflections are commonly computed using SDPWS, *ANSI/AWS Special Design Provisions for Wind and Seismic* (AWC, 2021), for wood structural panel diaphragms and DDM04, *Diaphragm Design Manual* (SDI, 2015) for steel deck diaphragms. When using the alternative RWFD procedure, a deflection amplification coefficient, $C_{d\text{-}diaph}$, specifically derived for the diaphragm is provided to compute the design earthquake displacement. The vertical-SFRS-element design earthquake displacements are computed using their elastic displacements amplified by the $C_d$ factor appropriate for the wall or stiff vertical SFRS. These displacements are used to check the deformation requirements of ASCE/SEI 7-22 Section 12.12 and the *P*-delta effect provisions of Section 12.8.7.

The alternative RWFD design procedure is outlined in Figure 1-1, along with an outline for traditional design practice. The list of design steps

demonstrates both similarities and differences between the alternative design procedure and traditional design practice. Many of the differences have been discussed above. The similarities are substantial in that both procedures are force-based and the steps for each procedure can be aligned with one another. Many of the alternative RWFD provisions, such as those for out-of-plane wall forces, wall anchorage, and diaphragm crossties, are identical to those used in traditional practice.

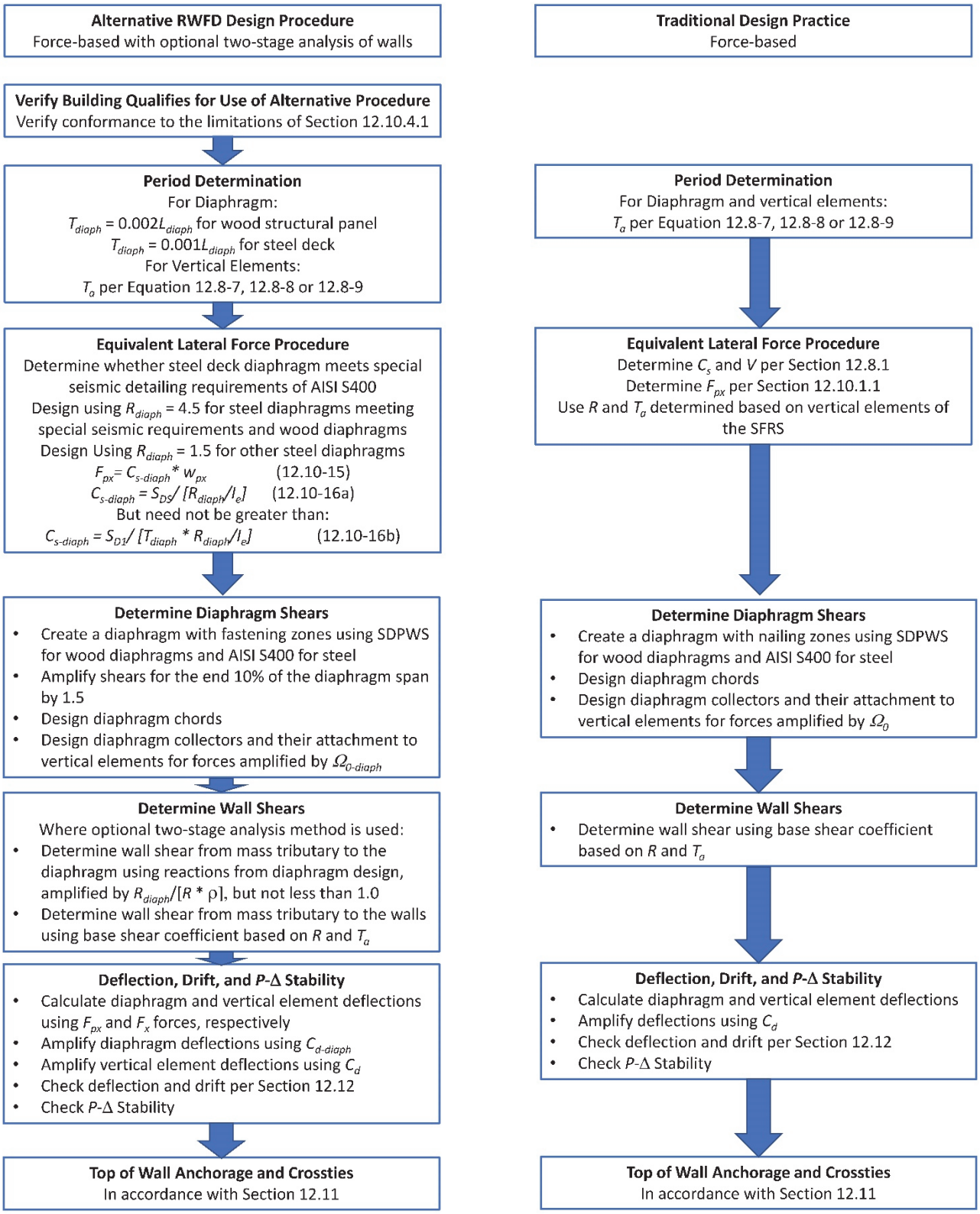


Figure 1-1 Comparison of design steps for the alternative RWFD procedure and traditional practice. All equation numbers are based on ASCE/SEI 7-22.

## 1.5 Implementation of the Alternative RWFD Design Procedure

The alternative RWFD design procedure has been incorporated into Section 12.10.4 and Section 12.2.3.4 of ASCE/SEI 7-22. Section 12.10.4 addresses seismic design of diaphragms in RWFD structures. With this new section added, the user of ASCE/SEI 7-22 has a choice of diaphragm design in accordance with: (1) Section 12.10.1 and Section 12.10.2; (2) Section 12.10.3; or (3) the new provisions of Section 12.10.4. The diaphragm seismic design provisions in ASCE/SEI 7-22 Section 12.10.1 and Section 12.10.2 are the traditional design method, long included in ASCE/SEI 7. ASCE/SEI 7-22 Section 12.10.3 is an alternative method, first included in the 2016 edition of ASCE/SEI 7. ASCE/SEI 7-22 Section 12.10.4 provides another alternative design method that is only permitted for one-story RWFD structures and is the subject of this report. For a given diaphragm, one of these three methods will need to be selected and implemented. Where a group of diaphragms is similar enough in elevation that they would be anticipated to interact, the use of one diaphragm design method for the group of diaphragms is recommended. Unless otherwise noted, references in this report to "alternative procedure" are to the procedures of ASCE/SEI 7-22 Section 12.10.4. Further, all references to ASCE/SEI 7 are to the 2022 version unless otherwise noted.

ASCE/SEI 7-22 Section 12.2.3.4 incorporates another provision based on the RWFD studies. This section provides a two-stage analysis procedure, where seismic forces to the vertical elements are treated differently based on whether they are generated by mass tributary to the longer-period diaphragm, or tributary to the short-period vertical elements.

Also new in ASCE/SEI 7-22 are procedures for seismic design using multi-period response spectra that will be required when performing response spectra design, and in other limited conditions. This is noted here in order to clarify that it is not intended that the multi-period spectra be used when implementing the RWFD provisions of Section 12.10.4 and Section 12.2.3.4; these sections are intended to be used in combination with equivalent-lateral-force provisions, with seismic design based on the design earthquake spectral response acceleration parameters $S_{DS}$ and $S_{D1}$, determined in accordance with ASCE/SEI 7-22 Section 11.4.4.

ASCE/SEI 7-22 is expected to be adopted into the 2024 *International Building Code* (IBC), making the RWFD provisions broadly available for use by designers once the 2024 IBC has been adopted by state and local jurisdictions. Until the 2024 IBC is adopted, use of the alternative RWFD

procedure for new construction could be permitted by the building official on a case-by-case basis, as permitted by Section 104.11 of the 2018 IBC (ICC, 2018).

## 1.6 Scope and Limitations of the Alternative Procedure

The alternative RWFD design procedure presented in this report is applicable to the design of one-story RWFD buildings. ASCE/SEI 7-22 Section 12.10.4.1 identifies a series of seven scoping limitations, all of which must be met to use the procedure. These are discussed in Section 5.3 of this report. In general, the alternative procedure is intended to be used with one-story structures with wood structural panel or steel deck diaphragms and with vertical elements of concrete or masonry walls or other vertical systems judged to be of similar rigidity. Use is limited to diaphragms or diaphragm segments spanning to vertical elements or collectors to vertical elements on all diaphragm edges. Section 12.10.4.1 limitations include details of the geometry and the construction of these one-story buildings.

As noted in the introduction to this chapter, this report and the affiliated ASCE/SEI 7-22 provisions address application of the alternative RWFD procedure to new buildings. It is possible to use the concepts introduced in this alternative procedure in the retrofit of existing buildings; however, the details of such application have not been developed. A designer wishing to use the concepts in an existing building retrofit will need to develop a proposed design methodology and obtain the concurrence of the building official.

## 1.7 Overview of Report Contents

The following is an overview of the contents of this report.

Chapter 2 provides a description of RWFD buildings and the performance of these buildings in past earthquakes.

Chapter 3 describes traditional design practice using design examples addressing both wood structural panel and steel deck diaphragms and finishes with a discussion of the shortcomings of traditional design practice. The traditional code-design procedure is presented before the alternative procedure, so that shortcomings of traditional practice can be brought to light, followed in Chapter 4 by discussion of how these shortcomings are addressed.

Chapter 4 describes the development of the alternative procedure for the design of RWFD buildings. It presents estimated period formulae applicable to flexible diaphragms and discusses computation of the overall building

fundamental period. It recommends the use of a diaphragm response modification coefficient and provides values for a diaphragm deflection amplification factor and a diaphragm overstrength factor. It also demonstrates that increasing the diaphragm strength in the end regions of the diaphragm results in better distribution of diaphragm yielding. The final section of this chapter summarizes the steps required to implement the alternative RWFD design procedure.

Chapter 5 illustrates implementation of the alternative RWFD design procedure by presenting design examples for both wood structural panel and steel deck diaphragm buildings. The examples include design of both the diaphragms and the vertical elements.

Chapter 6 demonstrates calculation of diaphragm deflection for both wood structural panel and steel deck diaphragms. It then describes use of the diaphragm deflection to check against the deformation requirements of ASCE/SEI 7-22 Section 12.12 and the *P*-delta effects of Section 12.8.7.

Chapter 7 provides comparisons of key design results from traditional practice relative to the alternative RWFD design procedure. This includes a comparison of the required diaphragm nailing for each procedure for a wood diaphragm and required diaphragm fasteners for a steel deck diaphragm.

Chapter 8 provides a list of future studies recommended on this topic. Included are recommendations related to the alternative RWFD procedure and also recommendations addressing the broader group of RWFD buildings, independent of design procedure. Recommendations for both future provisions development and future research are provided.

Chapter 9 provides conclusions.

Appendix A, Appendix B, and Appendix C document the FEMA P695 evaluations of performance of RWFD buildings that were conducted as part of the initial RWFD study that led to the 2015 edition of FEMA P-1026. Performance evaluation of buildings with wood diaphragms designed using both the traditional practice and the alternative RWFD provisions are included. Also incorporated are several updates to the original studies, including studies of the effects of wall weight and height.

Appendix D documents additional studies that were completed to extend the alternative RWFD provisions to include steel deck diaphragms. Included are both new testing and new numerical studies.

# Chapter 2
# Description of RWFD Buildings and Their Performance in Earthquakes

RWFD buildings have been a common building type for many decades, particularly in the western United States, where seismic hazards are high. The performance of these buildings during major earthquakes has been well documented and has highlighted recurring vulnerabilities. Recent code changes have been implemented to address these vulnerabilities, but they have not yet been tested by a major earthquake.

## 2.1 Description of Typical RWFD Structures

Structures containing rigid walls with flexible diaphragms are ubiquitous in cities in the United States. Often labeled as "big-box" buildings, these structures are the mainstay for retail, storage, and distribution facilities for large companies. These buildings are favored by developers and owners for providing the most cost-effective approach to enclosing large floor spaces while providing durable and secure perimeters. Additionally, smaller RWFD buildings occur in other commercial environments, such as strip malls and office parks.

RWFD buildings incorporate concrete or masonry walls, which are considered rigid in-plane, with flexible horizontal in-plane wood or bare steel deck roof diaphragm systems (Figure 2-1 and Figure 2-2). These rigid walls act as shear walls to provide seismic shear resistance. Concrete wall systems are most often site-cast precast panels, usually referred to as tilt-up or tilt-wall panels (ACI, 2015). These highly cost-efficient and versatile enclosures are common in many markets across the United States, including in high-seismic zones. Plant-cast precast concrete walls and concrete block masonry are also very popular perimeter shear wall systems enclosing these structures; the relative popularity varies significantly from one regional market to another. These rigid wall systems inherently contain large perimeter seismic masses relative to the roof diaphragm seismic mass. Details of how these buildings are constructed can be found in *Engineering Tilt-Up* (Mays and Steinbicker, 2013).

Figure 2-1 RWFD building with a wood structural panel diaphragm (photo credit: Panelized Structures).

Figure 2-2 RWFD building with a bare steel deck diaphragm (photo credit: Vulcraft/Verco Group – A Division of Nucor).

Roof diaphragms in these buildings consist either of wood structural panel or bare steel deck diaphragms, depending upon the regional preferences or building uses and needs. Wood structural panel diaphragms are common in the western and southwestern United States, especially in high-seismic-hazard regions. Plywood, or more recently oriented strand board (OSB), is fastened with nails to wood framing to provide a structural diaphragm as well as a roofing substrate. More commonly encountered today, these wood structural panels are fastened to wood nailer plates that are factory installed on top of a steel open-web joist and joist-girder roof support structure. This "hybrid" system is popular because of the speed and cost-efficiency that it combines. The in-plane shear strength and stiffness of these diaphragms are a function of the wood structural panel thickness and grade, as well as nail size and spacing. The wood structural panel diaphragms are relatively flexible, weak, and lightweight compared with the surrounding stiff, strong, and heavy walls.

Bare steel deck diaphragms are more popular outside of the West, Southwest, and Pacific Northwest. The steel decking is fastened to supporting open-web steel joists and adjacent deck panels with welds or screws; with power-actuated fasteners (PAFs), which are also called power-driven fasteners; and sometimes with an assortment of other proprietary fasteners. The in-plane shear strength and stiffness of these diaphragms are a function of the steel deck gage, deck profile, joist spacing, and fastener type and spacing (SDI, 2015). Unlike composite steel decking topped with concrete—a popular floor and roof system in multistory buildings—bare steel deck diaphragms are relatively lightweight, weak, and flexible in-plane compared with the surrounding walls.

Regional differences in the fastening of bare steel deck diaphragms also exist. In the western United States, interlocking deck profiles with proprietary side-lap punching is common. In comparison, nested deck profiles with screwed side-laps are common in the eastern United States. Although arc spot welds are used throughout the country, PAF use for deck-to-structure connections is increasing in popularity.

Another regional difference for bare steel deck diaphragms is the use of C-shaped wall configurations in the eastern United States, where seismic demands are low or moderate. This configuration, which is commonly used for larger buildings with expansion joints, includes walls along the three exterior sides of a building but with no vertical element, such as braced frames, along the edge of a diaphragm at the expansion joint. This system is not used in the western United States. As discussed in Chapter 8, the alternative procedure is not applicable to C-shaped wall configurations.

## 2.2 Similar Buildings with Braced Frames

A seismic response like that of a RWFD building is expected to occur for buildings that incorporate rigid braced frames in combination with or instead of concrete or masonry walls as the vertical elements of the SFRS. In very large distribution warehouses, interior braced frames are commonly used to reduce the horizontal roof diaphragm spans. The design methodology presented herein is applicable to these situations. The principal difference is that, unlike concrete or masonry walls, the braced frames often are not much stronger than the diaphragm. The proportions of the walls are driven more by the need for functional enclosure of the space and for out-of-plane loading than for adequate in-plane strength. These considerations usually drive the design to a solution that has in-plane strength far more than code demands. The same is generally not true for steel braced frames. Thus, the braced frames are more likely to deform inelastically than walls would. This inelastic brace behavior would likely reduce the diaphragm deformations, and given that the diaphragm is relatively flexible, it would likely not result in amplified torsional response.

The stiffness of the braced frames relative to the diaphragm is another potential difference. The first edition of this document included a requirement for the stiffness of the vertical elements to be three times that of the diaphragm. ASCE/SEI 7-22 provisions do not include this requirement; however, the intention is not for soft braces, such as tension-only rod bracing or buckling-restrained braced frames, to be appropriate to mix with walls. This is discussed in Chapter 8 with a recommendation for further study.

Some metal building structures could also be included in a broader definition of RWFD buildings. The important factor to consider is the relative horizontal stiffness or period of vibration of the roof diaphragm compared to the vertical elements of the SFRS. Metal buildings with tension/compression bracing for the vertical system and a large steel deck diaphragm could also have seismic behavior dominated by the diaphragm; however, metal buildings with repetitive steel frames, tension-only bracing for the vertical system, or X-braced roof diaphragms likely will not be dominated by diaphragm behavior to the extent assumed in this alternative design procedure.

## 2.3 Seismic Performance History

The seismic performance of RWFD buildings has often been poor. The first documented failures of RWFD buildings due to seismic ground motions were warehouses at Elmendorf Air Force Base near Anchorage, Alaska in 1964. Designed in 1951 for a lateral force of only 8 percent of gravity under an

allowable stress design approach (NRC, 1973), a partial steel rod X-braced diaphragm below a wood roof structure failed at the diaphragm boundaries due to inadequate shear transfer, causing two buildings to completely collapse (Figure 2-3). A few years later, the 1971 San Fernando earthquake tested this building type again with strong seismic ground motions. Because of the high density of RWFD buildings in the region, coupled with poor out-of-plane wall anchorage practices, significant failures caught the attention of the engineering community and quickly resulted in new code provisions.

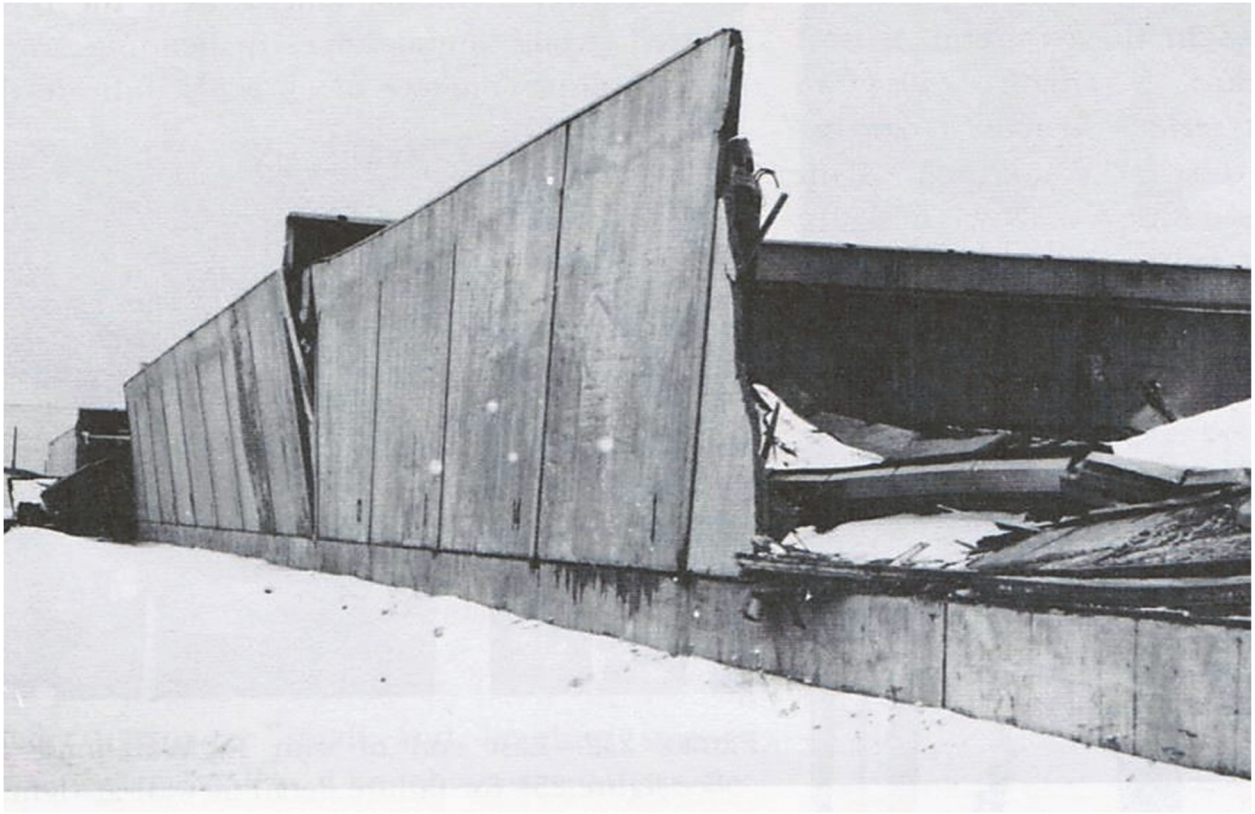

Figure 2-3 Collapse of a RWFD building at Elmendorf Air Force Base (photo credit: U.S. Air Force).

Thus far, the performance history of RWFD buildings has largely been dominated by the poor performance of the out-of-plane anchorage attaching the heavy walls to the lightweight roof diaphragms (SEAONC, 2001). Wall-to-roof separations and partial collapses have been documented in the 1971 San Fernando earthquake (USGS, 1971), 1984 Morgan Hill earthquake (EERI, 1985), 1987 Whittier Narrows earthquake (Hamburger et al., 1988), 1989 Loma Prieta earthquake (Phipps and Jirsa, 1990), 1992 Landers/Big Bear earthquakes (Shipp, 2010), and the 1994 Northridge earthquake (SSC, 1995). Because the earthquakes in which wall anchorage failures have been observed have occurred in California (Figure 2-4 and Figure 2-5), and because the RWFD building roof systems in California are predominately wood structural panel, observed wall anchorage failures have historically

been in wood diaphragms. However, an example of a bare steel deck diaphragm failure (Shipp, 2010; Brandow, 2010), which has been attributed to design load path deficiencies, was observed during the 1992 Landers Earthquake.

Figure 2-4 Partial collapse of a RWFD building with a steel deck diaphragm in Yucca Valley during the 1992 Landers Earthquake (photo credit: Gregg Brandow).

Figure 2-5 Partial collapse of a RWFD Building in the 1994 Northridge earthquake (photo credit: EERI).

In reaction to the repeated failures of the wall anchorage system in these buildings in the western United States, the *Uniform Building Code* (UBC) provisions have, multiple times, become more stringent and required higher design forces for out-of-plane wall anchorage (Figure 2-6). Based on observations following the 1994 Northridge earthquake, the current wall anchorage provisions are contained in ASCE/SEI 7-22 Section 12.11.2 and prescribe maximum expected design forces without relying upon connection ductility (SEAOC, 1999). These design force levels and detailing requirements for out-of-plane wall anchorage have remained largely unchanged since they were introduced into the 1997 *Uniform Building Code* (ICBO, 1997) and are anticipated to be carried forward through the 2024 IBC without change. Since that time, the current practice and force levels of anchoring heavy walls to the flexible diaphragms have not been tested by a strong earthquake event. A comprehensive summary of the building code's wall anchorage provisions evolution for RWFD buildings based on historical seismic events is provided in SEAONC (2001), Koliou et al. (2017), and Lawson et al. (2018).

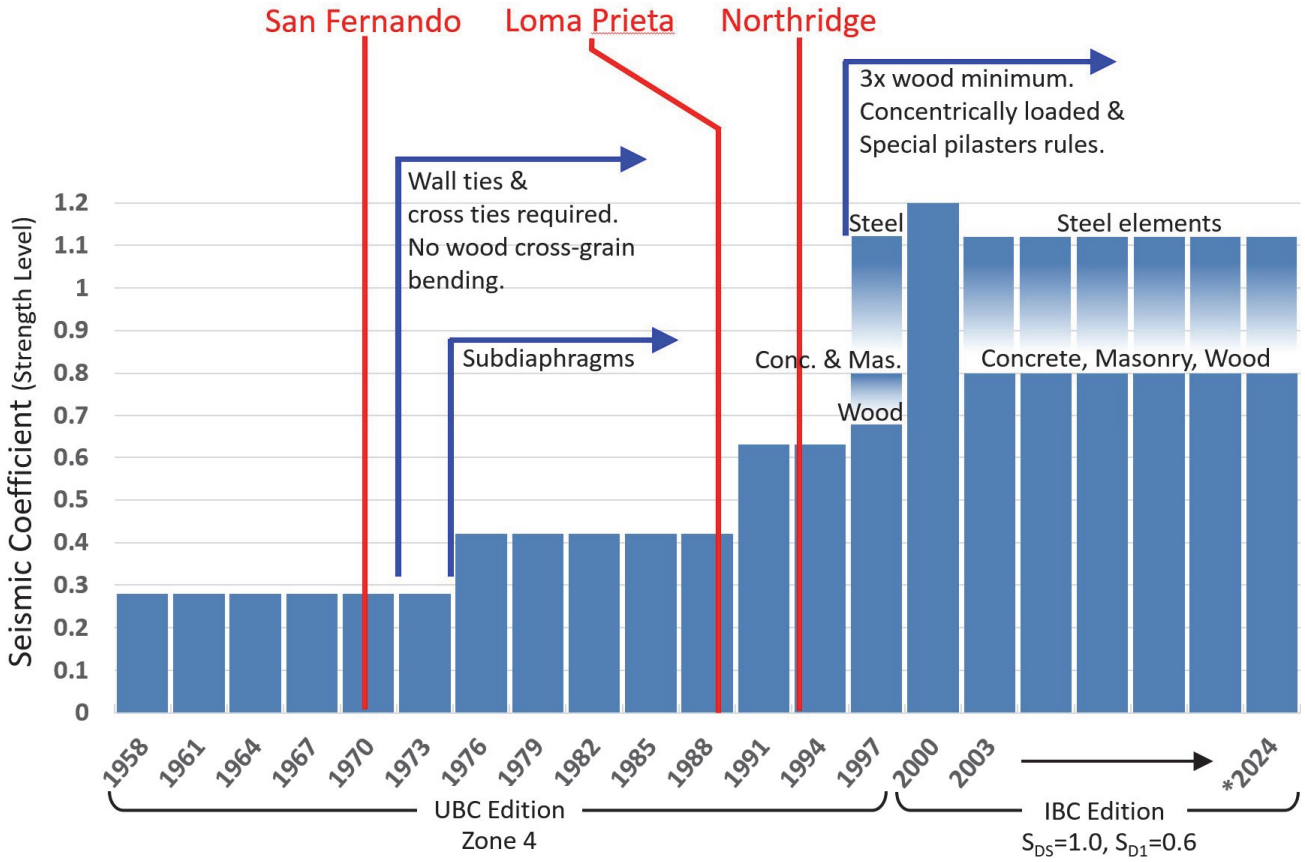


Figure 2-6 Evolution of wall anchorage code provisions (figure credit: Lawson et al., 2018 with update by Lawson, 2021).

Observation of earthquake damage to the in-plane rigid shear walls or the main flexible roof diaphragm has been rare, except for collateral damage from the out-of-plane wall anchorage issues. The perimeter shear walls often consist of largely solid wall portions with relatively few penetrations, resulting in in-plane lateral strength significantly greater than that required for seismic forces. This inherent overstrength of the shear walls transfers the inelastic building behavior into the diaphragm. It is important to consider that the out-of-plane detachment of the heavy walls from the diaphragm in the past may have protected the diaphragm from experiencing in-plane seismic forces which could have led to global failure. The overstrength of the walls, combined with higher wall-anchorage and collector force levels required by current code, could potentially make diaphragm yielding more critical for RWFD buildings in future earthquakes.

# Chapter 3

# Traditional Design Practice Example

Although the out-of-plane wall anchorage provisions for RWFD buildings have dramatically evolved after each damaging earthquake, code-based seismic design methodologies for the diaphragm and vertical elements of the SFRS have remained fairly consistent. The traditional practice is to engineer the SFRS using the equivalent-lateral-force (ELF) procedure of ASCE/SEI 7-22 Section 12.8. This procedure assumes the predominant structural response is closely associated with the vertical elements of the SFRS. Under the ELF procedure, seismic forces are based on the assumption of lumped masses at story levels, supported on flexible elements that represent the lateral stiffness of shear walls or frames traditionally defining the SFRS. The period of the SFRS is key to determining the code-based seismic forces. Additionally, the overstrength factor, $\Omega_o$, and deflection amplification factor, $C_d$, are determined based on the vertical elements of the SFRS. Diaphragm design loads have traditionally been determined from the building's base shear and story forces using ASCE/SEI 7-22 Section 12.10.1.

## 3.1 Example Building Description (Traditional Practice)

To illustrate the concepts presented in this report, designs of example buildings are presented. The example buildings represent common concrete tilt-up wall buildings with a low-sloped wood structural panel or bare steel deck roof diaphragm (Figure 3-1).

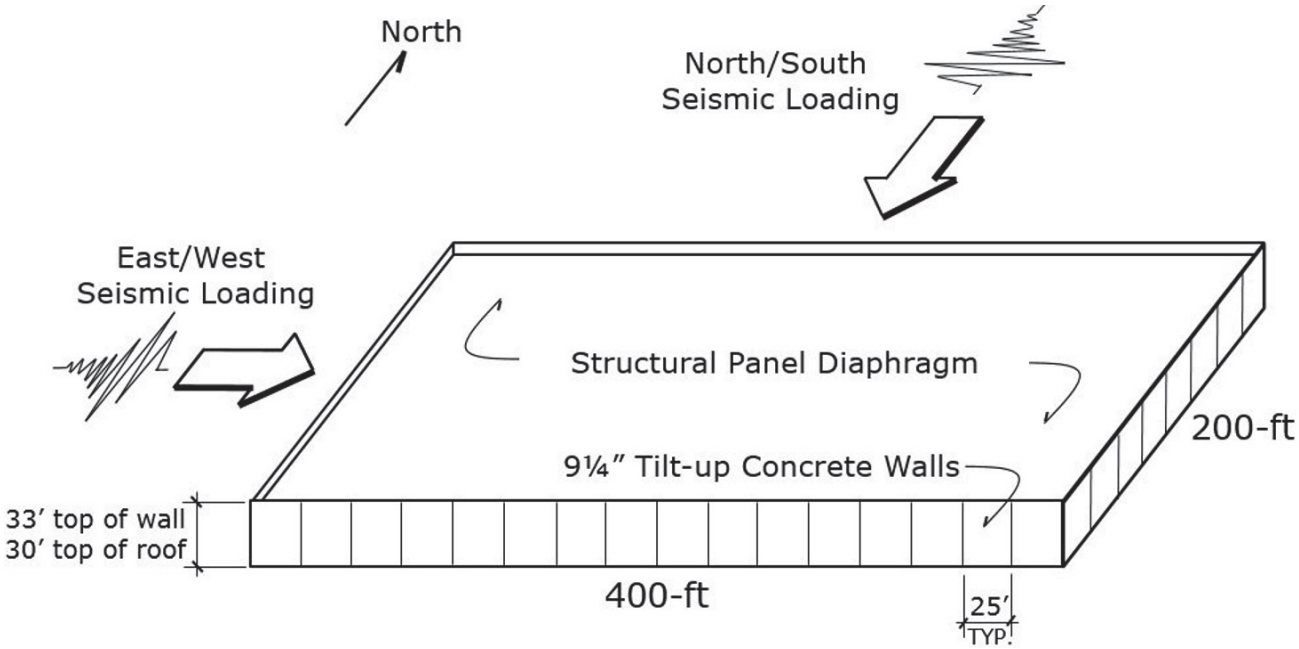


Figure 3-1 Example RWFD building.

**Codes and Standards**

- ASCE/SEI 7-22, *Minimum Design Loads and Associated Criteria for Buildings and Other Structures*
- AISI S310-20, *North American Standard for the Design of Profiled Steel Diaphragm Panels* (AISI, 2020a)
- DDM04, *Diaphragm Design Manual*, Fourth Edition and Errata
- SDPWS-2021, *ANIS/AWS Special Design Provisions for Wind and Seismic*

**Seismic-Force-Resisting System**

- Bearing-wall system consisting of intermediate precast concrete shear walls supporting a flexible diaphragm of wood structural panel or bare steel deck construction.

**Seismic and Site Data**

- Design earthquake spectral response acceleration parameters: $S_{DS}$ = 1.0 and $S_{D1}$ = 0.6 (and $S_1$ = 0.5 given)
- Risk Category = II (ASCE/SEI 7-22 Table 1.5-1)
- Seismic Design Category (SDC) = D
- Redundancy Factor, $\rho$ = 1.0 (computed for the walls and given for the diaphragm in accordance with ASCE/SEI 7-22 Section 12.3.4.1)

**Wind and Snow**

- Assumed not to govern the design

**Perimeter Walls**

- Wall Thickness = 9.25 inches of concrete (150 pcf, $f_c' = 4000$ psi)
- Height = 30 feet to roof with another 3 feet for the parapet

**Structural Wood Panel Roof Structure**

- Panelized hybrid roof structure (Lawson, 2013)
- Structural-I sheathing (15/32" OSB wood structural panel)
- Pre-engineered/pre-manufactured open-web steel joists and joist-girders with full-width wood nailers (popular hybrid system).
- Bay size is 50 feet in the north/south and east/west directions and joist spacing is 8 feet. The joists are oriented in the north/south direction.
- All wood is Douglas-fir/Larch (DF/L), S-Dry
- Roof Dead Load = 12 psf assumed as a design load

**Bare Steel Deck Roof Structure**

- Profiled steel deck sheathing (wide-ribbed B-Deck)
- Pre-engineered/pre-manufactured open-web steel joists and joist-girders
- Bay size is 50 feet in the north/south and east/west directions and joist spacing is 6.25 feet. The joists are oriented in the north/south direction.
- Roof Dead Load = 12 psf assumed as a design load

Following common practice, the ELF procedure and the provisions of ASCE/SEI 7-22 will be utilized for this design example unless otherwise noted.

Typically, the building inventory comprising RWFD buildings consists of concrete or masonry shear walls. In SDC C and higher, the permitted types of concrete and masonry shear wall systems are intermediate precast concrete shear walls, special reinforced concrete shear walls, and special reinforced masonry shear walls. While special reinforced concrete and special masonry shear walls benefit from higher response modification coefficients, additional detailing and analysis provisions are applicable, so they are less frequently used. As a result, in one-story tilt-up concrete buildings, intermediate precast shear wall systems are most common. In SDC D and above, this SFRS has a height limitation of 40 feet, except in single-story storage warehouses where

the limitation extends to 45 feet, per ASCE/SEI 7-22 Table 12.2-1. The use of the intermediate precast shear wall system will be illustrated for these building examples.

## 3.2 Determine Fundamental Building Period (Traditional Practice)

For a concrete shear wall building, the approximate fundamental period, $T_a$, under current practice is obtained using ASCE/SEI 7-22 Equation 12.8-7 with the coefficients $C_T = 0.020$ and $x = 0.75$. For this building, the average roof height, $h_n$, is 30 feet.

$$T_a = C_T h_n^x = (0.02)30^{0.75} = 0.26 \text{ seconds} \qquad \text{ASCE/SEI 7-22 Eq. 12.8-7}$$

Alternatively, Equation 12.8-9 could have been used. Because this example involves a regular structure five stories or fewer in height having a period, $T_a$, less than 0.5 seconds, the seismic response coefficient, $C_s$, can be based on $S_{DS} = 1.0$ (Section 12.8.1.3). However, in our example, $S_{DS}$ already equals 1.0, thus the design spectral response accelerations and SDC remain as originally given.

## 3.3 Base Shear Using the ELF Procedure (Traditional Practice)

Using ASCE/SEI 7-22 Section 12.6 in conjunction with Table 12.6-1, the ELF procedure of Section 12.8 is most commonly used to determine the seismic base shear coefficient for RWFD buildings.

ASCE/SEI 7-22 Section 12.8.1 defines the seismic base shear, $V$, as the seismic response coefficient, $C_s$, multiplied by the effective seismic weight, $W$:

$$V = C_s W \qquad \text{ASCE/SEI 7-22 Eq. 12.8-1}$$

$$C_s = \frac{S_{DS}}{R / I_e} \qquad \text{ASCE/SEI 7-22 Eq. 12.8-3}$$

where $R$ is the response modification coefficient, and $I_e$ is the importance factor. Because these tilt-up concrete walls will be considered load-bearing, intermediate precast shear walls, the following seismic performance factors are applicable to the building:

$R = 4$ Response modification coefficient

$\Omega_o = 2½$ Overstrength factor

$C_d = 4$ Deflection amplification factor

In addition, the importance factor described in ASCE/SEI 7-22 Section 11.5 is obtained from Table 1.5-2 based on the building's given Risk Category:

$I_e$ = 1.0 Importance factor

Therefore,

$$C_s = \frac{S_{DS}}{R / I_e} = \frac{1.0}{4 / 1.0} = 0.25$$

Checking the maximum limit for $C_s$ with Equation 12.8-4, where $T \leq T_L$:

$$C_{s\,max} = \frac{S_{D1}}{T\left(R / I_e\right)} = \frac{0.6}{0.26\left(4 / 1.0\right)} = 0.58 > 0.25 \text{ OK}$$

Checking the minimum allowed value for $C_s$, ASCE/SEI 7-22 Equation 12.8-6 and Equation 12.8-7 are applicable. In this example, $S_1$ given as 0.5 is noted as being less than 0.6*g*, therefore, Equation 12.8-7 need not be checked.

$C_{s\,min} = 0.044 S_{DS} I_e = 0.044(1.0)(1.0) = 0.044 < 0.25$ OK

$C_{s\,min} = 0.01 < 0.25$ OK ASCE/SEI 7-22 Eq. 12.8-6

The calculated value for $C_s = 0.25$ is between the maximum and minimum allowed values.

$C_{s\ governs} = 0.25$

Substituting into Equation 12.8-1, we obtain the base shear equation for the building for each orthogonal axis direction of the structure, which is used to determine the design forces in the shear walls.

$V = C_s W = 0.25W$

## 3.4 Diaphragm Design Forces Using the ELF Procedure (Traditional Practice)

Because the traditional code practice is based on a classical vibration model using lumped masses (at the diaphragm level) elevated on a flexible column (frames or shear walls), the diaphragm's forces are assumed to be closely associated with the response of the vertical elements of the SFRS.

The following formula is used in current practice to determine the total seismic force $F_{px}$ on the diaphragm at a given level of a building in each direction.

$$F_{px} = \frac{\sum_{i=x}^{n} F_i}{\sum_{i=x}^{n} w_i} w_{px}$$ ASCE/SEI 7-22 Eq. 12.10-1

As determined, the base shear for this building is $V = 0.25W$. Because it is a one-story building, Equation 12.10-1 simply becomes the following:

$F_{px} = 0.25w_{px}$

$F_{px}$ shall not be less than:

$0.2S_{DS}I_e w_{px} = 0.2(1.0)(1.0)w_{px} = 0.2w_{px}$ ASCE/SEI 7-22 Eq. 12.10-2

but need not exceed:

$0.4S_{DS}I_e w_{px} = 0.4(1.0)(1.0)w_{px} = 0.4w_{px}$ ASCE/SEI 7-22 Eq. 12.10-3

Based on the criteria given in Section 12.10.1.1, $F_{px} = 0.25w_{px}$. Therefore, traditional practice dictates for diaphragm design in each direction to use $F_p = 0.25w_p$.

Using a flat-beam analogy, where the diaphragm is idealized as a simply supported beam spanning between supporting walls, north/south seismic forces are resisted by shear walls on grid lines A and J, and east/west seismic forces are resisted by shear walls on grid lines 1 and 5. For this building, it is not required to combine both orthogonal directions based on ASCE/SEI 7-22 Section 12.5.1.1 and Section 12.5.4. Each orthogonal uniform load across this flat-beam model is illustrated in Figure 3-2.

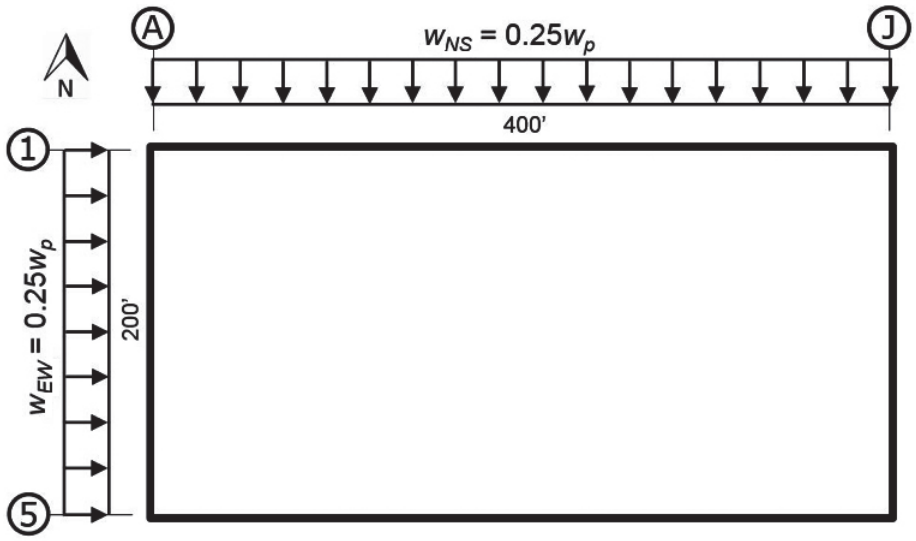


Figure 3-2 Diaphragm loading model (both orthogonal directions shown).

The uniformly distributed loads $w_{NS}$ and $w_{EW}$ applied laterally to the diaphragm are computed using the diaphragm lengths and unit weights and the tributary wall heights and unit weights:

$$w_{NS} = 0.25(12 \text{ psf})(200') + 2\left[0.25(116 \text{ psf})33'\left(\frac{33'}{2}\right)\left(\frac{1}{30'}\right)\right] = 1653 \text{ plf}$$

$$w_{EW} = 0.25(12 \text{ psf})(400') + 2\left[0.25(116 \text{ psf})33'\left(\frac{33'}{2}\right)\left(\frac{1}{30'}\right)\right] = 2253 \text{ plf}$$

where:

Roof dead load = 12 psf

Wall dead load = 116 psf (9¼" thick at 150 pcf)

Roof height = 30'-0" (above floor)

Top of wall = 33'-0" (above floor)

The maximum design shears are now computed using simple statics on the uniformly loaded flat beam model. Because of the building's regular shape and uniformly distributed mass, the loading diagram will be uniform, and the reactions $V_{NS}$ at grid lines A and J will be equal (see Figure 3-3).

North/south diaphragm shear:

$$V_{NS} = w_{NS}\frac{400 \text{ ft}}{2} = 1653\frac{400 \text{ ft}}{2} = 330{,}600 \text{ lbs, maximum}$$

North/south unit shear:

$$v_{NS} = \frac{V_{NS}}{200 \text{ ft}} = \frac{330{,}600}{200 \text{ ft}} = 1653 \text{ plf, maximum}$$

East/west diaphragm shear:

$$V_{EW} = w_{EW}\frac{200 \text{ ft}}{2} = 2253\frac{200 \text{ ft}}{2} = 225{,}300 \text{ lbs, maximum}$$

East/west unit shear:

$$v_{EW} = \frac{V_{EW}}{400 \text{ ft}} = \frac{225{,}300}{400 \text{ ft}} = 563 \text{ plf, maximum}$$

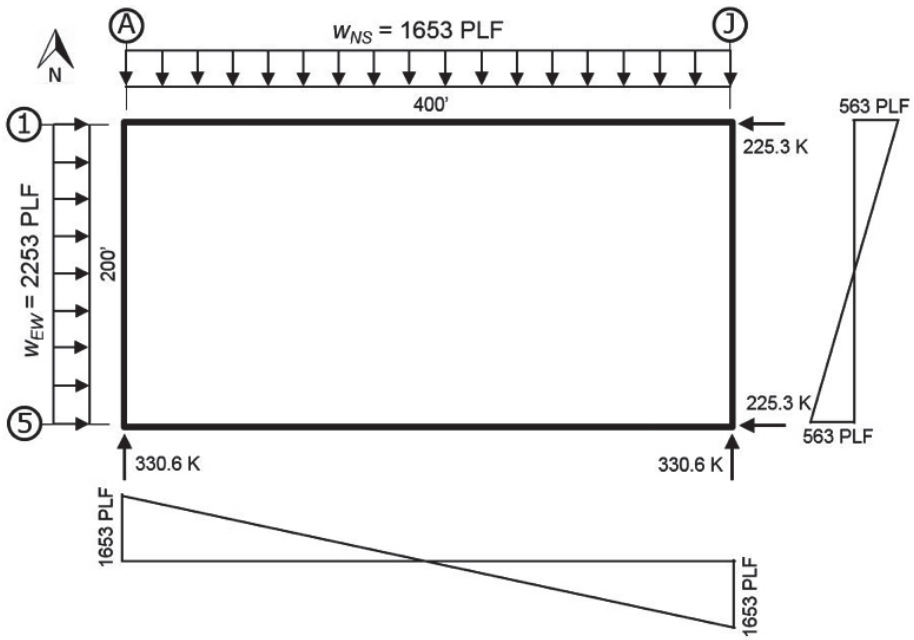


Figure 3-3 Diaphragm shear distribution in both orthogonal directions.

## 3.5 North/South Diaphragm Shear Design (Traditional Practice)

### *3.5.1 Wood Structural Panel Diaphragm Design*

In Section 3.4, the maximum diaphragm shears were determined for each orthogonal direction. ASCE/SEI 7-22 Section 12.5.4 does not require simultaneous load from two directions in this building. The highest unit shear demand is in the north/south direction with $v_{NS}$ = 1653 plf (unfactored). The nominal diaphragm shear capacities are provided in SDPWS-2021 Table 4.2A and Table 4.2B for a wide range of blocked diaphragm conditions. Panelized roof systems are commonly blocked based on their modular arrangement. Many engineers still use the Allowable Stress Design (ASD) format for timber design, even though the published nominal resistance values for diaphragms can be easily converted to strength format. This example will follow ASD convention for the timber diaphragm design.

The basic loading combinations involving earthquake loading are given in ASCE/SEI 7-22 Section 2.4.5, where load combination (8) will govern the design.

$$1.0D + 0.7E_v + 0.7E_h \quad (3\text{-}1)$$

where $D$ is the dead load, $E_v$ is the vertical seismic load, and $E_h$ is the horizontal seismic load. ASCE/SEI 7-22 Section 12.4.2.1 and Section 12.4.2.2 define $E_h = \rho Q_E$ and $E_v = 0.2S_{DS}D$ respectively, resulting in

$$(1.0 + 0.14S_{DS})D + 0.7\rho Q_E \quad (3\text{-}2)$$

where $\rho$ is the redundancy factor and $Q_E$ is the effect of horizontal seismic forces. When considering horizontal seismic loads on a structural diaphragm, vertical loading is not considered when evaluating the lateral diaphragm unit shear stress. Thus, the applicable load combination is simplified using $D = 0$. Additionally, the redundancy factor ($\rho$) is set to 1.0 for typical diaphragms per ASCE/SEI 7-22 Section 12.3.4.1. Therefore, the applicable basic load combination reduces to $0.7Q_E$.

$v_{NS(ASD)} = 0.7v_{NS} = 0.7(1653) = 1157$ plf

$v_{EW(ASD)} = 0.7v_{EW} = 0.7(563) = 394$ plf

Using these unit shear values, the designer may enter either SDPWS-2021 Table 4.2A or Table 4.2B to select a diaphragm assembly with an appropriate shear capacity. 15/32-inch Structural I sheathing is traditionally used as a minimum thickness in panelized construction (Lawson, 2013). The panelized sheathing system is inherently fully blocked and typically follows layout Case 2 (east/west loading) and Case 4 (north/south loading) illustrated in SDPWS-2021 Table 4.2A and Table 4.2B. SDPWS-2021 Table 4.2A and Table 4.2B are at a nominal strength level, and ASD seismic design values are obtained by dividing by a factor of 2.8 in accordance with SDPWS-2021 Section 4.1.4.

In the north/south direction, the ASD unit shear demand is greater than the maximum ASD capacities obtained from SDPWS-2021 Table 4.2A, thus reference to the high-load diaphragm shears in Table 4.2B will be necessary. The on-center (o.c.) nail spacing shown here requires thicker framing to prevent splitting. The capacity is reduced from the table nominal strength value to allowable stress design value by dividing by a factor of 2.8 per SDPWS-2021 Section 4.1.4.

**Design Solution**

- 15/32" Structural I sheathing
- 10d nails in two lines at 2½" o.c. boundaries and continuous north/south edges, 3" o.c. other edges
- 10d nails in one line at 12" o.c. intermediate (field)
- 4× framing at adjoining edges
- CAPACITY = 3610/2.8 = 1289 plf (ASD)
- $v_{NS(ASD)} = 0.7v_{NS} = 0.7(1653) = 1157$ plf < 1289 plf OK

The construction of this diaphragm system is illustrated in Figure 3-4.

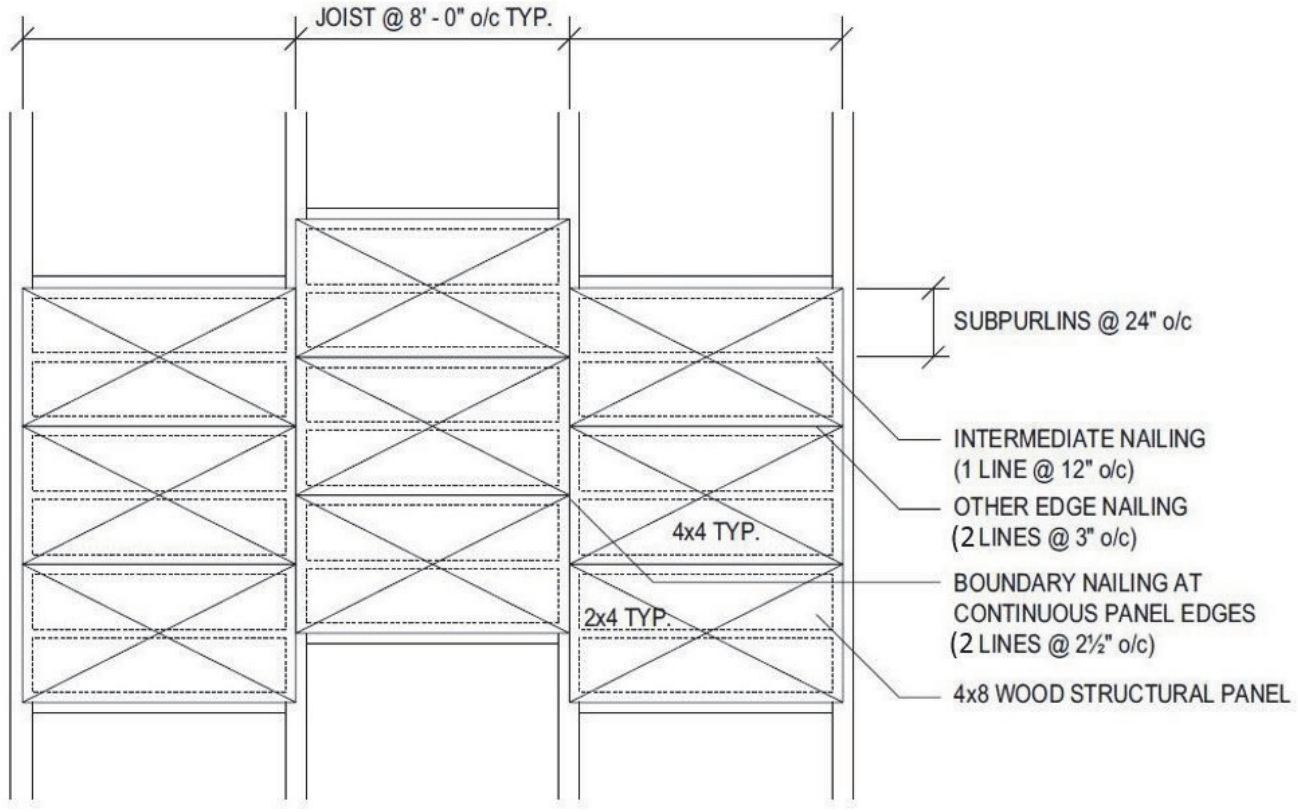


Figure 3-4 Sheathing layout and nailing for a panelized roof system (Lawson, 2013).

For a building this size, it is not efficient to install the heavy diaphragm nailing required at the boundary over the entire roof structure. Because the shear demands diminish towards the center of the diaphragm span, it is permitted to reduce the nailing and subpurlin widths as the corresponding unit shears also reduce. For this example, Table 3-1 identifies various diaphragm nailing configurations from the SDPWS-2021 that will be utilized at different portions of this building. The ASD shear values are simply the nominal strengths listed in SDPWS-2021 Table 4.2A and Table 4.2B divided by a factor of 2.8 per Section 4.1.4. For a panelized roof structure, layout cases 2 and 4 are applicable.

**Table 3-1 Diaphragm Nailing Schedule (Cases 2 and 4)**

| 15/32″ Structural I OSB Sheathing with 10d Nails (0.148″ dia x 2 long minimum) | | | | | |
|---|---|---|---|---|---|
| Nailing Zone | Framing Width at Adjoining Edges | Lines of Nails | Nailing per Line at Boundary and Continuous Edges | Nailing per Line at Other Edges | ASD Allowable Shear (plf) |
| 1 | 2x | 1 | 6″ o.c. | 6″ o.c. | 320 |
| 2 | 2x | 1 | 4″ o.c. | 6″ o.c. | 425 |
| 3 | 2x | 1 | 2½″ o.c. | 4″ o.c. | 640 |
| 4 | 3x | 1 | 2″ o.c. | 3″ o.c. | 820 |
| 5 | 4x | 2 | 2½″ o.c. | 4″ o.c. | 1005 |
| 6 | 4x | 2 | 2½″ o.c. | 3″ o.c. | 1289 |

At the diaphragm boundaries (grid lines A and J), Nailing Zone 6 was determined to be acceptable. At some location inward as the diaphragm shears diminish, Nailing Zone 5 will become acceptable. The transition from Nailing Zone 6 to Nailing Zone 5 may be solved using statics as follows:

Shear Demand (ASD) = Shear Capacity (ASD)

$0.7[330{,}600 \text{ lbs} - (1653 \text{ plf})x] = 1005 \text{ plf} (200 \text{ ft})$

where:

$x$ = the demarcation distance from the diaphragm boundary

Solving for $x$ obtains:

$x = 26.3$ feet

Because a panelized roof system typically consists of 8-foot-wide wood structural panels, the joist spacing module is also 8 feet, and the transition should be increased to the next 8-foot increment. In this case, it is increased to $x = 32$ feet.

The transition locations between Nailing Zones 5 and 4, Nailing Zones 4 and 3, Nailing Zones 3 and 2, and Nailing Zones 2 and 1 for the north-south loading direction are found using the same process resulting in Table 3-2.

**Table 3-2 Diaphragm Nailing Zone Shear Checks**

| Nailing Zone | Distance from Boundary | Strength Level Unit Shear | ASD Unit Shear | ASD Allowable Shear Capacity |
|---|---|---|---|---|
| 6 | 0 feet | $v_{max}$ = 1653 plf | $v_{ASD}$ = 1157 plf | 1289 plf |
| 5 | 32 feet | $v_{max}$ = 1389 plf | $v_{ASD}$ = 972 plf | 1005 plf |
| 4 | 64 feet | $v_{max}$ = 1124 plf | $v_{ASD}$ = 787 plf | 820 plf |
| 3 | 96 feet | $v_{max}$ = 860 plf | $v_{ASD}$ = 602 plf | 640 plf |
| 2 | 128 feet | $v_{max}$ = 595 plf | $v_{ASD}$ = 417 plf | 425 plf |
| 1 | 152 feet | $v_{max}$ = 397 plf | $v_{ASD}$ = 278 plf | 320 plf |

The resulting nailing zone layout for the north/south loading is shown in Figure 3-5.

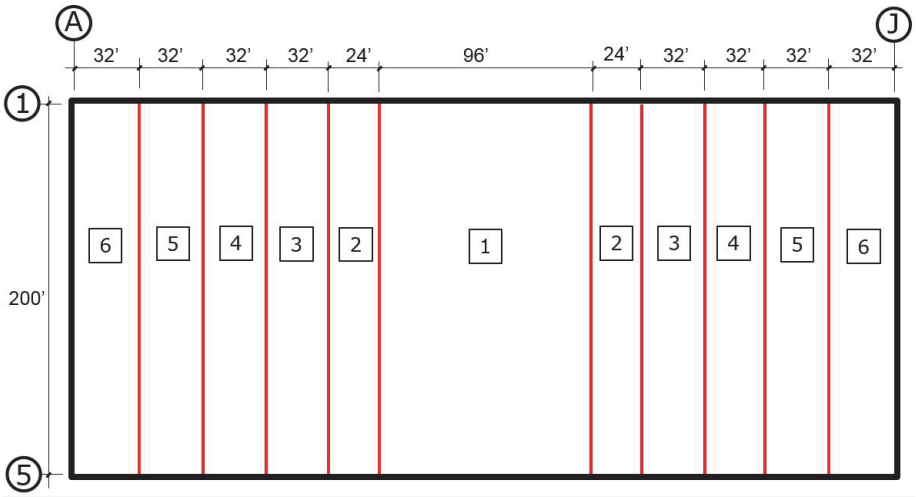


Figure 3-5 North/south nailing zone layout.

An additional check when designing wood diaphragms is to check their plan aspect ratios against the limitations in the SDPWS-2021 Table 4.2.2. For blocked diaphragms such as those that occur in panelized construction, the maximum aspect ratio is $L/W$ = 4:1. In this example, the north/south loading direction is the critical $L/W$ ratio:

$L/W = 400/200 = 2.0 < 4$ OK

### 3.5.2 *Bare Steel Deck Diaphragm Design Example (Mechanical Fasteners)*

This example will follow LRFD for design of a bare steel deck diaphragm. The basic loading combinations involving earthquake loading are given in ASCE/SEI 7-22 Section 2.3.6, where load combination (6) will govern the design.

$$1.2D + E_v + E_h + L + 0.2S \quad (3\text{-}3)$$

where $L$ is the live load, $S$ is the snow load, and $E_v$ and $E_h$ are as previously defined. ASCE/SEI 7-22 Section 12.4.2.1 and Section 12.4.2.2 define $E_h = \rho Q_E$ and $E_v = 0.2 S_{DS} D$ respectively, resulting in:

$$(1.2 + 0.2S_{DS})D + \rho Q_E + L + 0.2S \quad (3\text{-}4)$$

When considering horizontal seismic loads on a structural diaphragm, the vertical loading is not considered when evaluating the lateral diaphragm unit shear stress. Thus, the applicable load combination is simplified using $D = 0$, $L = 0$, and $S = 0$. Additionally, the redundancy factor $\rho$ is set to 1.0 for typical diaphragms per ASCE/SEI 7-22 Section 12.3.4.1. Therefore, the applicable basic load combination reduces to $Q_E$.

The highest unit shear demands in the north/south and east/west directions were determined previously and are:

$v_{NS(LRFD)} = v_{NS} = 1653$ plf

$v_{EW(LRFD)} = v_{EW} = 563$ plf

The design process is inherently an iterative process, and the diaphragm shear strength needs to be calculated for different diaphragm assemblies to find appropriate shear strengths for shear demands. The nominal diaphragm shear capacities are calculated per AISI S310-20. Alternatively, the design values can be taken from the design tables of DDM04 or manufacturers' design tables or software.

1.5-inch wide-rib (WR) steel deck, a common type of deck for bare steel deck diaphragms, is selected for the roof (see Figure 3-6). Using the unit shear demands, the designer can calculate the diaphragm capacity for different combinations of steel deck thickness, fastener type, and spacing, and select an appropriate diaphragm assembly with mechanical fasteners. Per AISI S310-20 Table B1.1-1, the LRFD seismic design values are obtained by multiplying by a resistance factor ($\phi$) of 0.7 when the strength of mechanical fasteners limits shear strength. When the diaphragm shear strength is limited by shear buckling, the design values are obtained by multiplying by a resistance factor ($\phi$) of 0.8.

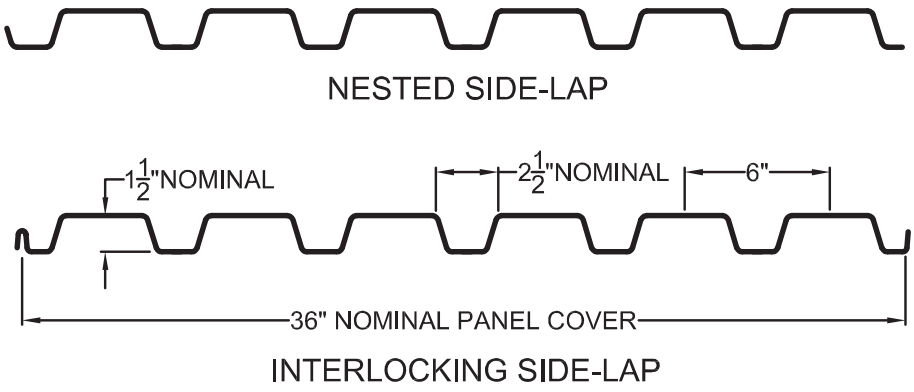


Figure 3-6 WR deck dimensions (see DDM04 for further details).

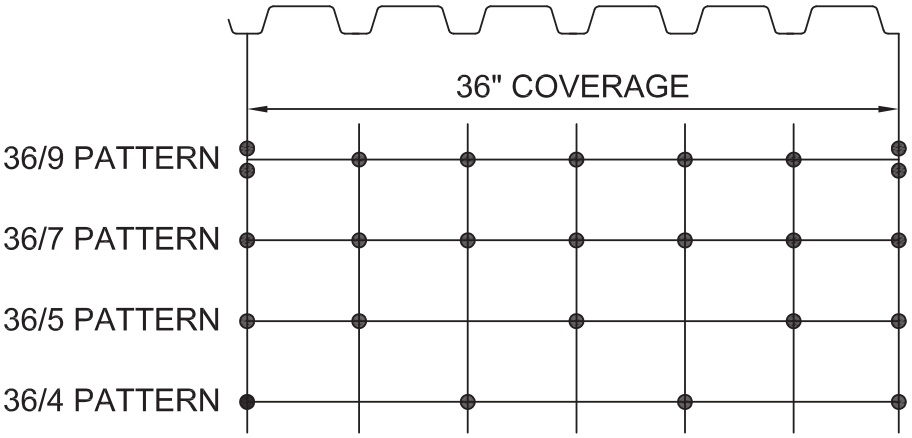


Figure 3-7 Typical fastener attachment patterns (see DDM04 for further details).

**Design Solution**

- 1.5-inch WR, 18 gage nestable steel deck ($F_y$ = 50 ksi, $F_u$ = 62 ksi)
  - Design thickness = 0.0474 inches
  - Support fastening: PAF with shaft diameter, $d_s$ = 0.16 inches
  - Side-lap fastening: 16 #12 screws within joist span
  - Fastener layout: 36/7 (see Figure 3-7)
  - Span: 6.25 feet
- Shear strength limited by fasteners: $\phi_{df} S_{nf}$ = (0.7)2914 = 2040 plf (LRFD)
- Shear strength limited by buckling: $\phi_{db} S_{nb}$ = (0.8)7324 = 5859 plf (LRFD)
- CAPACITY = min ($\phi_{df} S_{nf}$, $\phi_{db} S_{nb}$) = 2040 plf (LRFD)
- $v_{NS(LRFD)}$ = 1653 plf < 2040 plf OK

It is not efficient for a building this size to install the heavy steel deck and fastening at the boundary over the entire roof structure. Since the shear demands diminish towards the center of the diaphragm span, it is permitted to reduce the thickness of the steel deck and the number or size of fasteners as the corresponding unit shears also reduce. For this example, Table 3-3 identifies various diaphragm designs that will be utilized at different portions of this building. The LRFD shear capacity values are calculated per AISI S310-20 and require a few iterations to find the desirable capacities.

**Table 3-3 Diaphragm Design Zones**

| 1.5-inch WR Nestable ($F_y$ = 50 ksi, $F_u$ = 62 ksi)<br>Span (Joist spacing) = 6.25 ft<br>Support Fastening: PAF (shaft diameter, $d_s$ = 0.16 in.) | | | | | | |
|---|---|---|---|---|---|---|
| **Zone** | **Steel Deck** | **Steel Deck Design Thickness** | **Support Fastener Layout** | **Side-lap Fastener** | **Number of Side-lap Fasteners per Span** | **LRFD Shear Capacity** |
| 3 | 18 gage | 0.0474 in. | 36/7 | #12 Self-drilling Screw | 16 | 2040 plf |
| 2 | 20 gage | 0.0358 in. | 36/7 | #12 Self-drilling Screw | 9 | 1135 plf |
| 1 | 22 gage | 0.0295 in. | 36/7 | #10 Self-drilling Screw | 6 | 701 plf |

At the diaphragm boundaries (grid lines A and J), Zone 3 was determined to be acceptable. At some location inward as the diaphragm shears diminish, Zone 2 will become acceptable. The transition from Zone 3 to Zone 2 can be solved using statics as follows:

Shear Demand (LRFD) = Shear Capacity (LRFD)

330,600 lbs − (1653 plf)$x$ = 1135 plf (200 ft)

where:

$x$ = the demarcation distance from the diaphragm boundary

Solving for $x$ obtains:

$x$ = 62.7 feet

Since the joist spacing is 6.25 feet, the transition should be increased to the next 6.25-foot increment, and one span is added to overlap between the zones. In this case, it is increased to $x$ = 75 feet.

The transition locations between Zones 2 and 1 for the north-south loading direction are found using the same process resulting in Table 3-4.

**Table 3-4 Diaphragm Zone Shear Checks**

| Zone | Distance from Boundary | Strength Level Unit Shear | LRFD Unit Shear | LRFD Shear Capacity |
|---|---|---|---|---|
| 3 | 0 | $v_{max}$ = 1653 plf | $v_{LRFD}$ = 1653 plf | 2040 plf |
| 2 | 75 feet | $v_{max}$ = 1033 plf | $v_{LRFD}$ = 1033 plf | 1135 plf |
| 1 | 125 feet | $v_{max}$ = 620 plf | $v_{LRFD}$ = 620 plf | 701 plf |

The resulting zone layout for the north/south loading is shown in Figure 3-8.

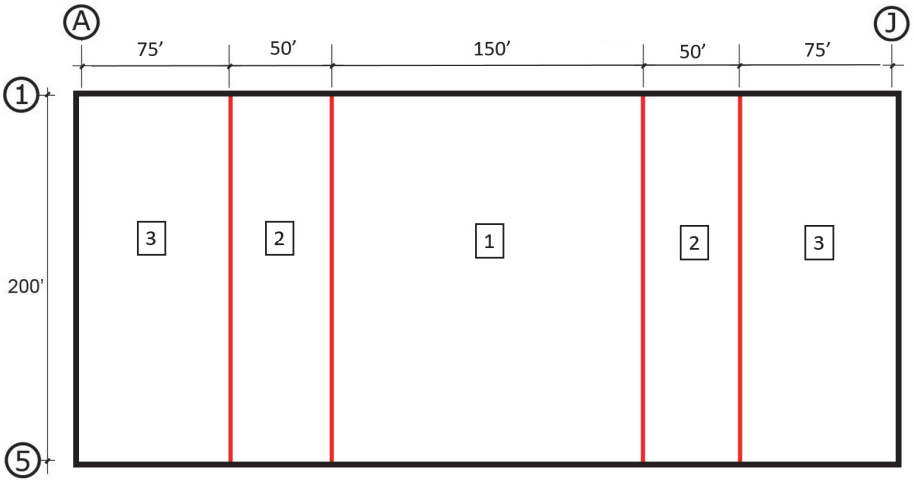


Figure 3-8 North/south zone layout.

### *3.5.3 Bare Steel Deck Diaphragm Design Example (Welded Fasteners)*

Similar to Section 3.5.2 for mechanical fasteners, AISI S310-20 is used to design steel deck diaphragms with welded fasteners. Using the unit shear demands, the designer can calculate the diaphragm capacity for different combinations of steel deck thickness, welded fastener type, and spacing, and select an appropriate diaphragm assembly with welded fasteners. Per AISI S310-20 Table B1.1-1, the LRFD seismic design values are obtained by multiplying by a resistance factor ($\phi$) of 0.55 when the strength of welded fasteners limits shear strength. When the diaphragm shear strength is limited by shear buckling, the design values are obtained by multiplying by a resistance factor ($\phi$) of 0.8.

**Design Solution**

- 1.5-inch WR, 20 gage interlocking steel deck ($F_y$ = 50 ksi, $F_u$ = 62 ksi)
  - Design thickness = 0.0358 inches
  - Support fastening: 3/4-inch arc spot weld
  - Side-lap fastening: top arc seam weld, L=1.5 inches E60-XX

- Fastener layout: 36/7
- Span: 6.25 feet

- Strength limited by fasteners: $\phi_{df}S_{nf}$ = 0.55(3136) = 1725 plf (LRFD)
- Shear strength limited by buckling: $\phi_{db}S_{nb}$ = 0.8(4800) = 3840 plf (LRFD)
- CAPACITY = min($\phi_{df}S_{nf}$, $\phi_{db}S_{nb}$) =1725 plf (LRFD)
- $v_{NS(LRFD)}$ = 1653 plf < 1725 plf OK

Table 3-5 identifies various diaphragm designs that will be utilized at different portions of this building.

**Table 3-5 Diaphragm Design Zones**

| 1.5-inch WR Interlocking ($F_y$ = 50 ksi, $F_u$ = 62 ksi)<br>Span (Joist Spacing) = 6.25 ft<br>Support Fastening: 3/4" Arc Spot Weld<br>Side-lap Fastening: Arc Seam Weld, L=1.5" E60-XX or Button Punch | | | | | | |
|---|---|---|---|---|---|---|
| **Zone** | **Steel Deck** | **Steel Deck Design Thickness** | **Support Fastener Layout** | **Side-lap Fastener** | **Number of Side-lap Fasteners per Span** | **LRFD Shear Capacity** |
| 3 | 20 gage | 0.0358 in. | 36/7 | Top Arc Seam Weld | 5 | 1725 plf |
| 2 | 20 gage | 0.0358 in. | 36/7 | Button Punch | 9 | 739 plf |
| 1 | 20 gage | 0.0358 in. | 36/7 | Button Punch | 3 | 577 plf |

Since the joist spacing is 6.25 feet, the transition between the zones should fall at 6.25-foot increments. The transition locations between Zones 3 and 2, and Zones 2 and 1 for the north-south loading direction are provided in Table 3-6.

**Table 3-6 Diaphragm Zone Shear Checks**

| Zone | Distance from Boundary | Strength Level Unit Shear | LRFD Unit Shear | LRFD Shear Capacity |
|---|---|---|---|---|
| 3 | 0 | $v_{max}$ = 1653 plf | $v_{LRFD}$ = 1653 plf | 1725 plf |
| 2 | 118.75 feet | $v_{max}$ = 620 plf | $v_{LRFD}$ = 620 plf | 739 plf |
| 1 | 137.5 feet | $v_{max}$ = 517 plf | $v_{LRFD}$ = 517 plf | 577 plf |

The resulting zone layout for the north/south loading is shown in Figure 3-9.

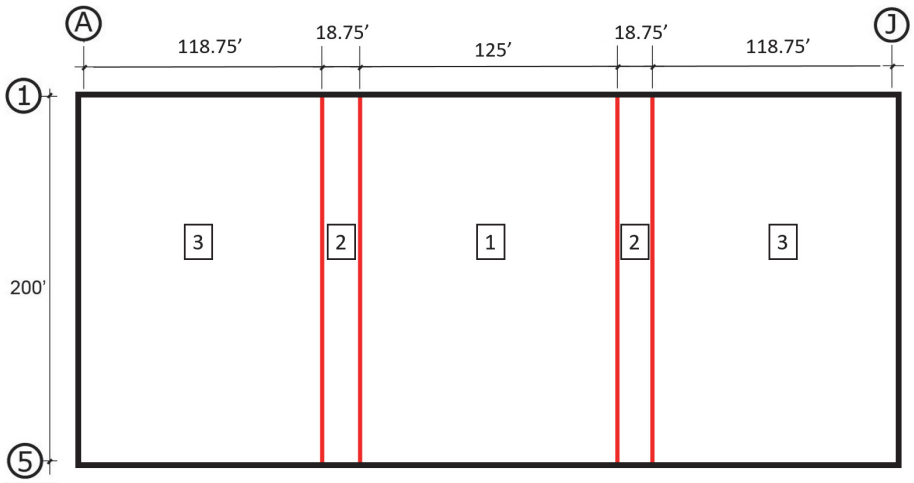


Figure 3-9 North/south zone layout.

## 3.6 North/South Diaphragm Chord Design (Traditional Practice)

The chord design is similar for both structural wood panel and bare steel deck diaphragms.

Recall that a flexible diaphragm may be considered a flat horizontal beam where the shear resistance is obtained by the wood structural panel sheathing or bare steel deck across the roof surface. However, tensile forces from horizontal bending are not considered to be resisted by the sheathing but by perimeter chords acting in tension and compression.

To resist bending efficiently, the diaphragm chords are traditionally placed at the extreme sides of the diaphragm. In buildings with masonry or concrete perimeter walls, these chords are often steel ledger angles or channels at the roofline. Chord forces are determined using simple statics, as illustrated in Figure 3-10. Maximum chord forces will occur at the center of the diaphragm's span, where the maximum moment occurs.

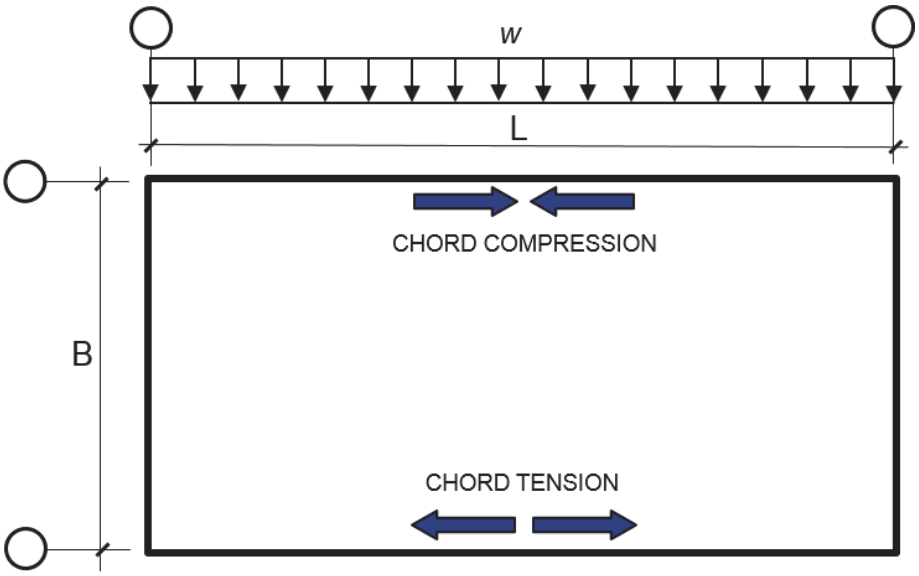


w = distributed diaphragm load
L = diaphragm span length
B = diaphragm breadth (width)

$$Chord\ T = C = \frac{wL^2}{8B}$$

Figure 3-10 Diaphragm chord forces.

Using the equations in Figure 3-10, the maximum chord force (in tension, *T*, or compression, *C*) for our building example is determined:

$$T = \frac{M}{B} = \frac{w_{EW} L^2}{8B} = \frac{1653\text{plf}(400)^2}{8(200)} = 165{,}300 \text{ lbs} \qquad (3\text{-}5)$$

Assuming the chord is connected to the wall, and thus fully braced, then the chord capacity in tension and compression is equal to the squash capacity of the member. The chord is designed here using LRFD with ASTM A36 Steel ($F_y$ = 36 ksi). Consulting ASCE/SEI 7-22 Section 2.3.6, the applicable load factor for seismic forces is 1.0. The area of steel ($A_s$) required is:

$$A_s = \frac{T}{\phi F_y} = \frac{165.3}{0.9(36)} = 5.10 \text{ in.}^2$$

Using an L5×5×5/8 rolled steel angle satisfies this chord demand.

L5×5×5/8 steel area, $A_s$ = 5.90 in.$^2$ > 5.10 in.$^2$

## 3.7 East/West Diaphragm Shear Design (Traditional Practice)

### *3.7.1 Wood Structural Panel Diaphragm Design*

Similar to the north/south loaded direction, the orthogonal east/west direction will also require consideration using the same sequential process. In Section 3.5, the maximum diaphragm shear in the east/west direction was determined

to be $v_{EW}$ = 563 plf (unfactored). Converting to allowable stress design (ASD), the maximum diaphragm shear is as follows:

$$v_{EW(ASD)} = 0.7v_{EW} = 0.7(563) = 394 \text{ plf}$$

As before, SDPWS-2021 Table 4.2A is used to select diaphragm nailing with an appropriate shear capacity. In the north/south loaded direction, Case 4 is the loading configuration, but for the east/west direction this becomes a Case 2 configuration. The applicable case determines the nail spacing along the continuous adjoining panel edges in the direction parallel to load. Comparing the diaphragm's shear demand with Table 3-1 of Section 3.5, Nailing Zone 2 is selected:

$$v_{EW(ASD)} = 394 \text{ plf} < 425 \text{ plf (Nailing Zone 2)}$$

At some distance away from the diaphragm boundary (walls at grid lines 1 and 5), Nailing Zone 1 in Table 1 will be acceptable due to the diminishing unit diaphragm shears. Using the same approach as done in the north/south direction, the location of the nailing zone transition from Zone 2 to 1 is found and Table 3-7 is developed.

**Table 3-7 Diaphragm Nailing Zone Shear Checks**

| Nailing Zone | Distance from Boundary | Strength Level Unit Shear | ASD Unit Shear | Allowable Shear Capacity |
|---|---|---|---|---|
| 2 | 0 feet | $v_{max}$ = 563 plf | $v_{ASD}$ = 394 plf | 425 plf |
| 1 | 20 feet | $v_{max}$ = 451 plf | $v_{ASD}$ = 315 plf | 320 plf |

Combining the nailing requirements for the north/south loading with the east/west loading results in Figure 3-11.

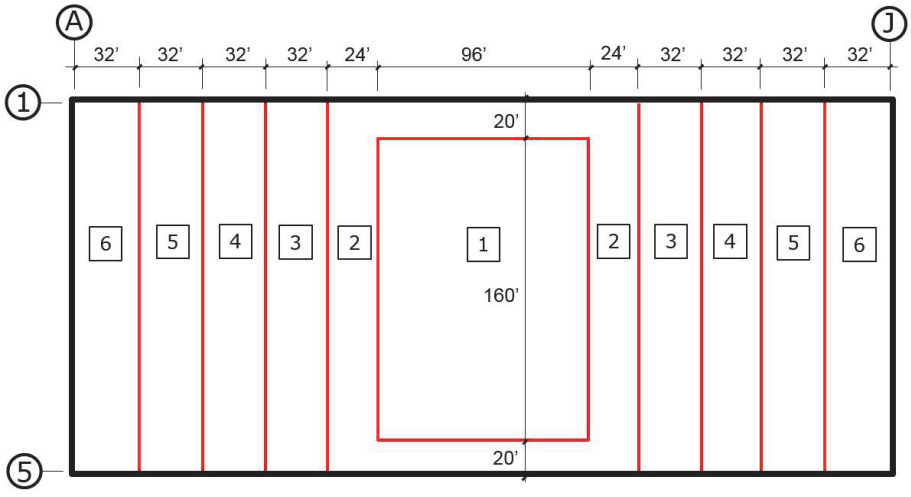


Figure 3-11 North/south and east/west nailing zones combined.

### 3.7.2 Bare Steel Deck Diaphragm Design Example (Mechanical Fasteners)

In Section 3.5, the maximum factored diaphragm shear in the east/west direction was determined to be $v_{EW(LRFD)}$ = 563 plf (factored). As before, AISI S310-20 is used to determine the diaphragm shear capacity. Comparing the diaphragm's shear demand with Table 3-3 of Section 3.5.2, Zone 1 is the weakest section but is still adequate:

$v_{EW(LRFD)}$ = 563 plf < 701 plf (Zone 1)

Therefore, the diaphragm design per Table 3-2 and Figure 3-3 is adequate for the east/west direction as well. This is generally the desired outcome as it would be uncommon to have zones for the roof in both directions for bare steel deck roof diaphragms.

### 3.7.3 Bare Steel Deck Diaphragm Design Example (Welded Fasteners)

In Section 3.5, the maximum factored diaphragm shear in the east/west direction was determined to be $v_{EW(LRFD)}$ = 563 plf (factored). Comparing the diaphragm's shear demand with Table 3-5 of Section 3.5.3, Zone 1 is sufficient as follows:

$v_{EW(LRFD)}$ = 563 plf < 577 plf (Zone 1)

Similar to the mechanically fastened solution, the diaphragm design per Table 3-6 and Figure 3-9 is adequate for the east/west direction.

## 3.8 East/West Diaphragm Chord Design (Traditional Practice)

The diaphragm chord design is similar for both structural wood panel and bare steel deck diaphragms.

With the diaphragm chords placed at the extreme sides of the diaphragm, the maximum chord forces in the east/west loaded direction are computed as follows:

$$T = \frac{M}{B} = \frac{w_{EW} L^2}{8B} = \frac{2253\text{plf}(200)^2}{8(400)} = 28{,}100 \text{ lbs}$$

Following the same assumptions as in the north/south direction, the required area of the steel chord using LRFD is:

$$A_s = \frac{T}{\phi F_y} = \frac{28.1}{0.9(36)} = 0.87 \text{ in.}^2$$

Using an L4×4×1/4 rolled steel angle as a practical minimum size satisfies this chord demand.

L4×4×1/4 steel area, $A_s = 1.93$ in.$^2 > 0.87$ in.$^2$

## 3.9 Shear Wall Force Using the ELF Procedure (Traditional Practice)

The design of shear walls is similar for both structural wood panel and bare steel deck diaphragms.

For a single-story building, the diaphragm's support reactions are the basis of the applied loads to the shear wall lines. The flexible diaphragm with its tributary mass will generate a lateral force near the top of the wall, $F_{v1}$. Additionally, the rigid concrete in-plane walls have significant self-weight that will also generate lateral forces near their centers of mass, $F_{v2}$. See Figure 3-12 and Figure 3-13.

As determined previously in Section 3.4, the diaphragm reactions to the shear walls based on $\rho = 1.0$ are as follows:

$F_p = V_{NS} = 330{,}600$ lbs (north/south)

$F_p = V_{EW} = 225{,}300$ lbs (east/west)

Because these forces were not controlled by the upper and lower bounds of ASCE/SEI 7-22 Equation 12.10-2 and Equation 12.10-3, they can be used for design of the shear walls. However, these diaphragm reaction forces need to be amplified to an appropriate shear wall design force if the redundancy factor for the SFRS is greater than 1.0. This is because, per ASCE/SEI 7-22 Section 12.3.4.1, $\rho$ is permitted to be set equal to 1.0 for diaphragm design but not for shear wall design.

$$F_{v1} = F_p \times \rho$$

where for this example $\rho = 1.0$ (computed). Therefore, the amplification equals 1.0, and the shear wall design forces from the diaphragm in each orthogonal direction are as follows:

$F_{v1} = 330{,}600$ lbs (north/south)

$F_{v1} = 225{,}300$ lbs (east/west)

Next, the lateral seismic force generated from the walls' self-weight must be included for design. Because this is a single-story building, the self-weight seismic force, $F_{v2}$, is simply the wall line's self-weight multiplied by the base shear coefficient, $C_s$, and any applicable redundancy factor, $\rho$, for the building. The base shear coefficient, $C_s$, for both axes of the building was determined in Section 3.3.

$$F_{v2} = C_s W = 0.25 W_{p\text{-}wall}$$

For the north/south direction, the wall's self-weight, $W_{p\text{-}wall}$, is computed as:

$W_{p\text{-}wall}$ = 116 psf × 200 ft × 33 ft = 765,600 lbs

Therefore:

$F_{v2} = 0.25W_{p\text{-}wall} = 0.25(765{,}600) = 191{,}400$ lbs

Therefore, the total shear wall design force, $F_v$, for the north/south direction is:

$F_v = F_{v1} + F_{v2} = 330{,}600 + 191{,}400$

$F_v$ = 522,000 lbs or 522 kips

For the east/west direction, the wall's self-weight, $W_{p\text{-}wall}$, is computed as:

$W_{p\text{-}wall}$ = 116 psf × 400 ft × 33 ft = 1,531,200 lbs

Therefore:

$F_{v2} = 0.25W_{p\text{-}wall} = 0.25(1{,}531{,}200) = 382{,}800$ lbs

Therefore, the total shear wall design force, $F_v$, for the east/west direction is:

$F_v = F_{v1} + F_{v2} = 225{,}300 + 382{,}800$

$F_v$ = 608,100 lbs or 608 kips

Figure 3-12 and Figure 3-13 illustrate the forces acting on the shear walls providing lateral resistance in the north/south and east/west directions respectfully. The design forces at the base of the shear walls are 522 kips north/south and 608 kips east/west. These forces include the entire weight of the walls and are appropriate for the design of shear forces that transfer to the slab on ground or foundation. In-plane shear design considerations for tilt-up concrete shear walls may be found in other sources (Mays and Steinbicker, 2013).

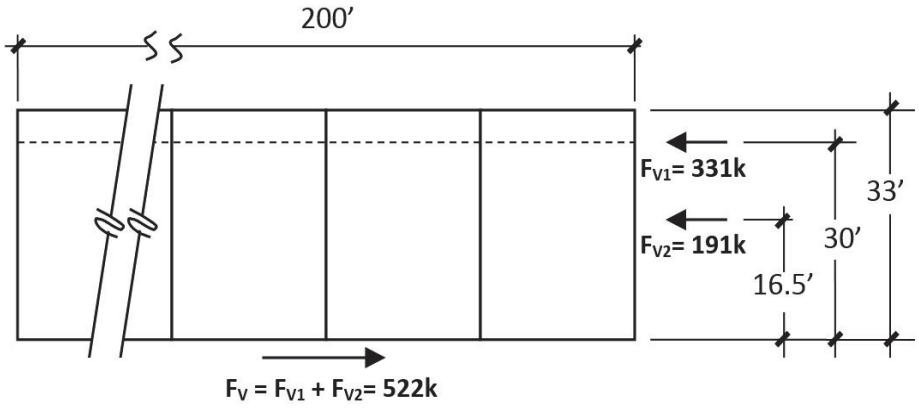


Figure 3-12 North/south lateral design forces acting on the shear walls (Lines A & J).

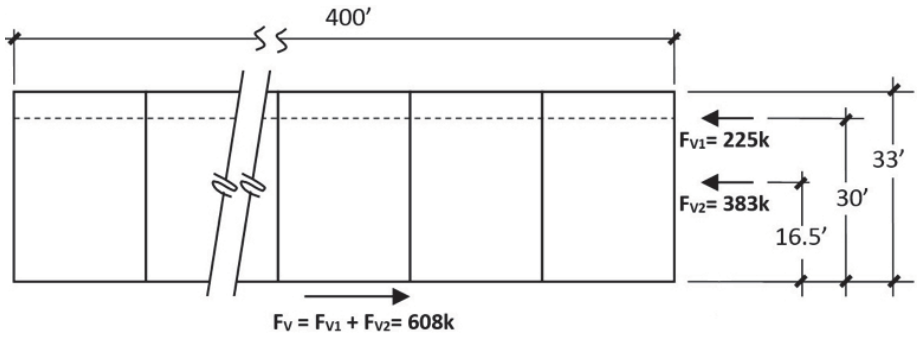


Figure 3-13 East/west lateral design forces acting on the shear walls (Lines 1 & 5).

## 3.10 Shortcomings of Traditional Practice

Section 3.1 through Section 3.9 have detailed the seismic design of a RWFD building using traditional ELF and diaphragm design methods (i.e., ASCE/SEI 7-22 Sections 12.8, 12.10.1, and 12.10.2). This section describes some of the shortcomings of traditional design methods, which motivated development of the alternative RWFD design methodology.

The simplistic model assumed by the ELF procedure fails to capture the actual behavior of RWFD buildings. The ELF procedure assumes that the seismic response consists primarily of deforming vertical elements of the SFRS and that the horizontal diaphragm is rigid (i.e., deformation of the diaphragm is not considered). However, for most RWFD structures, the primary seismic response is dominated by the deformation of the horizontal flexible diaphragm. Therefore, a more accurate structural representation is needed to capture the flexible diaphragm dominating the response.

The ELF procedure also is inappropriately based on the assumption that the primary inelastic behavior is in the vertical wall or frame system, instead of the roof diaphragm. The seismic response modification coefficient, $R$, the overstrength factor, $\Omega_o$, and the deflection amplification factor, $C_d$, in ASCE/SEI 7-22 Table 12.2-1 are used to estimate the strength demands, capacities, and deflections on systems that are designed using linear methods while responding in the nonlinear range. Under traditional design methods, the selection of $R$, $\Omega_o$, and $C_d$ for design is solely based on the performance characteristics of the SFRS's vertical elements. In reality, the inelastic behavior is likely to be in the horizontal diaphragm, and the traditional ELF procedure fails to characterize this diaphragm response adequately. Also, under traditional methods, flexible diaphragms and rigid concrete diaphragms are all designed as if they have the same seismic response and performance.

Under traditional methods, the seismic diaphragm shears used for design are directly related to the type of vertical elements used in the SFRS. In fact, some engineers routinely select special reinforced concrete shear walls ($R = 5$) in their design (instead of intermediate precast, $R = 4$) to reduce the diaphragm design shears and allow the diaphragm to span farther. The same motive drives some engineers to place girder support columns adjacent to the intermediate precast shear walls, converting the bearing wall system ($R = 4$) to a building frame system ($R = 5$) in one direction. The selection of the SFRS based on a desired diaphragm load outcome fails to recognize the likely building behavior. Traditional seismic design provisions in ASCE/SEI 7-22 may unintentionally encourage this practice.

Because RWFD buildings typically have excessive strength in the shear walls as compared with the diaphragms, it is unrealistic to expect the yielding to be in the walls even though the response modification coefficient, $R$, is based on that assumption. Past failures have typically been out-of-plane wall detachments, and building codes have responded to these failures by increasing the out-of-plane wall anchorage design force. Should failure of out-of-plane wall anchorage be prevented, diaphragm yielding and potential failure may become the critical behavior. The ELF procedure of ASCE/SEI 7-22 as currently applied to RWFD buildings does not account for this diaphragm behavior.

Finally, numerical studies conducted in the development of the alternative RWFD design method indicate that the current out-of-plane wall anchorage forces of ASCE/SEI 7-22 Section 12.11.2.1 may not adequately capture wall anchorage forces for diaphragms with shorter spans. Although the current provisions indicate reduced wall anchorage forces for diaphragms with spans less than 100 feet, the numerical studies identified a pattern of increased anchorage forces in the range of 100-foot diaphragm spans relative to longer diaphragm spans. Further discussion of this topic can be found in Koliou et al. (2017).

# Chapter 4

# Development of the Alternative RWFD Design Procedure

The shortcomings of traditional diaphragm design methods are detailed in Section 3.10. Chapter 4 discusses how these shortcomings were considered and addressed in the numerical studies that led to the development of the alternative RWFD design procedure. Chapter 4 also provides background on key parameters considered in the development of the alternative design methodology. Most, but not all, of the information addressed by this chapter was incorporated into ASCE/SEI 7-22.

With seismic response dominated by the horizontal diaphragm in RWFD structures, it is more appropriate that design forces be developed around the diaphragm's behavior. Furthermore, because the inelastic behavior in a RWFD building is typically located in the diaphragm, it is more appropriate that the seismic system capacity be developed around the overstrength and ductility of the diaphragm, rather than those of the vertical elements of the SFRS. An alternative procedure based on the diaphragm's response has the potential to better provide the seismic performance targeted by building-code seismic design provisions.

A more appropriate method of establishing seismic design loads for buildings dominated by diaphragm response is to consider the diaphragm's period relative to the design spectral acceleration. As an example, ASCE/SEI 41-17, *Seismic Evaluation and Retrofit of Existing Buildings* (ASCE/SEI, 2017), uses this approach in the *Linear Static Procedure* for existing one-story RWFD buildings by estimating the diaphragm-dominated building period and then establishing a pseudo-lateral force on the system. A number of other sources have proposed methods for estimating flexible diaphragm periods and their corresponding pseudo-lateral forces (Freeman et al., 2002; PEER, 2004; SEAONC, 2001). With a more accurate period based on the dominant building response, the force-based procedures of ASCE/SEI 7-22 can be used more appropriately. Furthermore, the use of an ELF approach with a response modification coefficient, $R$, an overstrength factor, $\Omega_o$, and a

deflection amplification factor, $C_d$, related to the diaphragm's design, construction, and detailing, is expected to produce more rational results.

Both the inelastically acting horizontal diaphragm and the SFRS vertical elements need a unified design methodology. The fact that RWFD buildings have a flexible upper portion (the diaphragm) supported in series with a rigid lower portion (the walls or other vertical elements) make them ideally suited to be designed similar to the two-staged ELF procedure of ASCE/SEI 7-22 Section 12.2.3.2. This approach is often used for residential podium-type structures where three- or four-story wood shear wall buildings are supported on masonry or concrete shear wall parking structures. This approach permits the two portions to be analyzed for seismic loading independently, and then combined as appropriate. As the seismic forces are handed off from one portion to another, they are adjusted to reflect the next portion's expected seismic performance influenced by its period and stipulated response modification coefficient ($R$).

The developers of the alternative RWFD diaphragm design provisions set out to incorporate these improvements into the resulting methodology. This chapter details considerations in the development of the alternative RWFD procedure.

## 4.1 Determination of Building and Diaphragm Period

A primary objective of the alternative RWFD design methodology is a design considering seismic response and seismic performance factors associated with a building with seismic response dominated by the flexible diaphragm instead of the vertical elements of the SFRS. The diaphragm period ($T_{diaph}$) is an important parameter in determining a more realistic seismic response. The following describes approaches considered in the development of the alternative RWFD provisions.

A number of approaches have been proposed in the past to more accurately estimate the periods of various flexible-diaphragm-dominated buildings (Koliou, 2014). One such approach is the fundamental period equation within ASCE/SEI 41-17 for one-story buildings with flexible diaphragms.

$$T_a = \sqrt{0.1\Delta_w + 0.078\Delta_d} \qquad \text{ASCE 41-17 Eq. 7-19}$$

where:

$T_a$ = fundamental period in sec. in the direction of consideration

$\Delta_w$ = maximum in-plane wall displacement in inches at 1.0g

$\Delta_d$ = maximum diaphragm displacement in inches at 1.0g

While this equation has credibility from the fact that it is formally adopted in an ASCE standard, it has been criticized as being derived from an improper flexural beam idealization for the diaphragm instead of a more realistic shear beam idealization. Wilson et al. (2013) derived an equation based on shear beam behavior and recommends that the diaphragm component, $0.078\Delta_d$, be revised to $0.066\Delta_d$ within the ASCE/SEI 41-17 procedure. With this modification, the following equation for the fundamental period of one-story buildings with flexible diaphragms becomes:

$$T_a = \sqrt{0.1\Delta_w + 0.066\Delta_d} \quad (4\text{-}1)$$

Equation 4-1 is mathematically derived and provides a valuable approach provided that accurate wall and diaphragm displacements can be computed. However, this equation is better suited for analyzing existing structures than it is for design because it requires one to compute the wall and diaphragm deflections. For design, an estimate of the period is needed to establish wall and diaphragm design forces. One cannot compute the deflections of the walls and diaphragm until after these elements have been designed, which is typical of most design problems

To meet the objective of developing a design methodology that is simple to implement and accounts for diaphragm flexibility, a simple period approximation, $T_a$, was desired. The research conducted by Koliou (2014) proposed simple separate period formulas, $T_a$, for RWFD buildings with wood or bare steel deck diaphragms based on results of semi-empirical analyses using numerical models of 23 archetypes designed per ASCE/SEI 7-10 (the edition that was available at the time of the RWFD study). The design seismic demand for the 23 archetypes was based on the upper bound of design spectral response accelerations for SDC D, designated as SDC $D_{max}$. For the purposes of creating an initial group of archetypes for evaluation under FEMA P695, this period $T_a$ was selected to be the algebraic sum of $T_{diaph}$ and $T_{walls}$. The period formula $T_a = T_{diaph} + T_{walls}$ tracks closely with Equation 4-1 developed by Wilson et al. for wood diaphragms less than 250-feet long. For lengths over 250 feet, the proposed formulas provide a smaller period than Wilson's equation (Koliou, 2014). The approximate period equations represent the elastic building period prior to a shift in the period due to inelastic behavior. More information on the development of these formulas is provided in Appendix B and Appendix C.

Equation 4-2 and Equation 4-3 were developed empirically from the results obtained from 23 archetype building configurations involving 33-feet-high, 9¼-inch-thick concrete tilt-up walls in a high-seismic-hazard region. In general, archetypes with more or less mass will have a corresponding

diaphragm design with more or less stiffness, thus offsetting the mass variation. Therefore, the proposed period formulas are thought to be reasonably independent of mass. An additional study was conducted of two archetypes, one with lightweight walls and another with heavyweight walls both designed under the alternative procedure. Using the naming convention given in Appendix B with results in Appendix C, archetype HWL_21_N_OSB_P1026_01 is designed with heavy concrete walls (116 psf), and archetype HWL_21_N_OSB_P1026_04 of identical size is designed with lightweight walls (10 psf) on the longitudinal sides. The elastic period for the heavyweight wall archetype is computed as 0.94 seconds, and the lightweight archetype is computed as 0.93 seconds. This similarity of building periods supports the belief that Equation 4-2 and Equation 4-3 are reasonably independent of the building's wall mass.

Another characteristic found to have little influence on building period is the diaphragm's aspect ratio, primarily because the diaphragm deformations were found to be overwhelmingly shear dominated. $T_{diaph}$ is simply based on the diaphragm's span, $L_f$, and $T_{walls}$ is based on ASCE/SEI 7-22 provisions for concrete or masonry shear wall buildings. The reader is cautioned that the equation for $T_{walls}$ was developed for shear wall buildings of various heights with heavy floor and roof masses, and thus it will probably overestimate the period for this type of building. Still, it serves a useful purpose for this discussion.

For wood structural panel diaphragms the following were developed (Koliou, 2014):

$$T_{diaph} = 0.002L_f \qquad (4\text{-}2)$$

$$T_{walls} = \frac{0.0019}{\sqrt{C_w}} h_n \qquad \text{ASCE/SEI 7-22 Eq. 12.8-10}$$

For steel deck diaphragms the following were developed (Koliou, 2014) and later confirmed by additional steel-deck diaphragm numerical studies:

$$T_{diaph} = 0.001L_f \qquad (4\text{-}3)$$

$$T_{walls} = \frac{0.0019}{\sqrt{C_w}} h_n \qquad \text{ASCE/SEI 7-22 Eq. 12.8-10}$$

where:

$L_f$ = The span, in feet, of the horizontal flexible diaphragm being considered; the span is measured between vertical elements that provide lateral support to the diaphragm in the direction considered.

$h_n$ = The structural height defined in ASCE/SEI 7-22 Section 11.2.

$C_w$ = Shear wall coefficient for concrete and masonry walls per ASCE/SEI 7-22 Equation 12.8-11.

$$= \frac{100}{A_B}\sum_{i=1}^{x}\left(\frac{h_n}{h_x}\right)^2 \frac{A_i}{1+0.83\left(\frac{h_i}{D_i}\right)^2}$$

$A_B$ = area of base of structure in ft$^2$

$A_i$ = web area of shear wall $i$ in ft$^2$

$D_i$ = length of shear wall $i$ in ft

$h_i$ = height of shear wall $i$ in ft

$x$ = number of shear walls in the building effective in resisting lateral forces in the direction under consideration

For our example wood-diaphragm building, the following illustrates use of Equation 4-2 to estimate the diaphragm's approximate period, $T_{diaph}$, and ASCE/SEI 7-22 Eq. 12.8-10 to estimate the walls' approximate period, $T_{walls}$; however, the two periods will not be combined to estimate a building period, $T_a$, out of concern that this would overestimate the building period and underestimate the seismic load effect. The same calculations can be repeated for steel deck diaphragms.

$T_{diaph} = 0.002L_f$

$$T_{walls} = \frac{0.0019}{\sqrt{C_w}}h_n$$

Compute building area $A_B$:

$A_B = 200 \text{ ft} \times 400 \text{ ft} = 80{,}000 \text{ ft}^2$

This building is comprised of a series of equal, 25-foot-long concrete tilt-up wall panels acting as shear walls around the building perimeter. Thus, all parameters for each wall $i$ are the same.

$$A_i = 25 \text{ ft} \times \frac{9.25 \text{ in.}}{12} = 19.3 \text{ ft}^2\text{/wall}$$

$D_i = 25$ feet

$h_i = 30$ feet

In the transverse direction (north/south), there are eight wall panels along each line of resistance, or a total of sixteen panels in the considered direction ($x = 16$). Similarly, in the longitudinal direction (east/west), there are thirty-

two panels total in the considered direction ($x = 32$). Thus, the shear wall coefficient, $C_w$, is different in each orthogonal direction.

North/south:

$$C_w = \frac{100}{80{,}000}(16)\left(\frac{30}{30}\right)^2 \frac{19.3}{1+0.83\left(\frac{30}{25}\right)^2} = 0.176$$

$$T_{diaph} = 0.002(400 \text{ ft}) = 0.800 \text{ sec}$$

$$T_{walls} = \frac{0.0019}{\sqrt{0.176}} 30 \text{ ft} = 0.136 \text{ sec}$$

Using this alternative approach, the north-south diaphragm period alone is estimated at 0.800 seconds. This compares with the code's current approximate period of 0.26 seconds for the building using ASCE/SEI 7-22 Equation 12.8-8 or 0.136 seconds using Equation 12.8-10.

East/west:

$$C_w = \frac{100}{80{,}000}(32)\left(\frac{30}{30}\right)^2 \frac{19.3}{1+0.83\left(\frac{30}{25}\right)^2} = 0.352$$

$$T_{diaph} = 0.002(200 \text{ ft}) = 0.400 \text{ sec}$$

$$T_{walls} = \frac{0.0019}{\sqrt{0.352}} 30 \text{ ft} = 0.096 \text{ sec}$$

Using this alternative approach, the east-west diaphragm period is estimated at 0.400 seconds. This compares with the code's current approximation for the building of 0.26 seconds using ASCE/SEI 7-22 Equation 12.8-8 or 0.096 seconds using Equation 12.8-10. Determination of periods used when implementing the alternative RWFD procedure is further discussed in Section 4.5 and Chapter 5 of this report. It is of note that in the ASCE/SEI 7-22 incorporation of the alternative RWFD design procedure, the diaphragm period, $T_{diaph}$, is used for diaphragm seismic design, while the designer is able to choose from multiple methods for calculation of the approximate period, $T_a$, associated with the walls.

## 4.2 Response Modification Coefficient, *R*, Selection

A primary objective of the RWFD numerical studies was to identify seismic response and seismic performance factors considering response dominated by the flexible roof diaphragm instead of the vertical elements of the SFRS. The structural response modification coefficient, *R,* is an important parameter

to estimate strength demands on systems that are designed using linear methods, such as the ELF procedure, but may respond in the nonlinear range when subject to strong ground motions. *R* coefficients in ASCE/SEI 7-22 are largely based on judgment. Historically, validation of seismic performance coefficients was simply based on observations following major earthquakes.

While learning from earthquakes is invaluable when validating current design factors, a more systematic form of validation is needed when proposing new *R* coefficients and new design procedures. The methodology contained in FEMA P695 (FEMA, 2009) was developed specifically to provide a means to evaluate an SFRS proposed for adoption into building codes, but the methodology also can be used to evaluate proposed design procedures. The primary objectives of a FEMA P695 study are to obtain an acceptably low probability of collapse of the SFRS under risk-targeted maximum considered earthquake ($MCE_R$) ground motions and to provide a uniform protection against collapse across various structural systems. An appropriate FEMA P695 evaluation must develop representative nonlinear models that include both detailed design information of the system as well as comprehensive test data on the post-yield performance of system components and subassemblies. The procedure evaluates the probability of collapse during strong earthquake shaking while accounting for a variety of possible ground motions, uncertainties, and a range of building configurations representing the design space.

An appropriate response modification coefficient unique to the diaphragm, $R_{diaph}$, was determined by a trial-and-error process using FEMA P695. The first trial evaluated traditional ASCE/SEI 7-22 designs using intermediate precast (tilt-up) concrete shear walls ($R = 4$) with both wood and steel deck diaphragms. The results showed that inelastic behavior occurred in the diaphragms instead of the in-plane walls, confirming the need for a diaphragm-based approach. Even though the diaphragm design capacity was intentionally stepped down (zoned) to efficiently follow the shear demand reduction towards the diaphragm interior, as is often done in practice, the analysis results indicated that inelastic response of the diaphragm was concentrated adjacent to the supporting shear walls.

Because the inelastic behavior was not well distributed across the diaphragm, the localized inelastic response near the shear wall supports was quickly overwhelmed by the limited ability of the connectors to dissipate large amounts of energy, which led to global building failure of some of the archetypes. This phenomenon was observed in both the steel and wood deck diaphragm analyses. The FEMA P695 analysis results for archetypes using *R* equal to 4 for the intermediate precast wall system did not meet the margin

against collapse required by the FEMA P695 methodology, thus indicating revised *R*-coefficients and/or a new design approach might be appropriate to improve performance to meet intended targets. A detailed description of the implementation of FEMA P695 evaluations for use on this project and the numerical computer model are contained in Appendix A.

A direct approach to improving the margin against collapse identified for RWFD buildings designed using existing practice is to design the flexible diaphragms using a response modification coefficient, $R_{diaph}$, that represents the ductility and overstrength of the diaphragm instead of the walls. During the RWFD numerical studies it was identified that two approaches could be taken to assigning a value or values to $R_{diaph}$: (1) assign a single reduced $R_{diaph}$ value and design the diaphragm assuming a linear distribution of design shear along the diaphragm's span length; or (2) assign a value to $R_{diaph}$ but amplify the design shear in targeted zones within the diaphragm, to encourage the spread of yielding across more of the diaphragm's length. Based on the FEMA P695 results for the traditional design procedure, approach (1) requires an $R_{diaph}$ value significantly less than 4 to obtain acceptable performance during an $MCE_R$ event if design shear is assumed to be distributed linearly along the diaphragm span length. Approach (2), in which the inelastic diaphragm behavior is spread away from the diaphragm boundaries by designing for amplified shear in targeted zones, has the potential of requiring a less punitive $R_{diaph}$ over much of a diaphragm's span length. Such an approach is discussed in the following subsection.

### *4.2.1 Encouraging Distributed Inelastic Behavior*

The RWFD numerical studies demonstrated that the performance of a diaphragm during strong earthquake shaking can be improved if yielding is spread over a large portion of a diaphragm's span instead of focused at the boundaries. Further, the spread of diaphragm yielding is improved if the location of initial yielding is shifted away from the diaphragm boundaries. This can be achieved either by intentionally weakening a portion of the diaphragm's interior or by increasing the strength-to-demand ratio of the diaphragm near its boundaries.

Distributing the inelastic behavior deeper into the diaphragm also requires that the diaphragm connectors that yield first exhibit sufficient positive post-yield stiffness behavior. In other words, once the critical connectors begin to yield, they need to resist increasing load to enable connectors elsewhere in the diaphragm to reach their yield loads. The connectors that yield must also have sufficient post-yield deformability, so the diaphragm as a whole has adequate post-yield deformability to provide the required collapse resistance.

The overall diaphragm deformability increases if connector yielding spreads over a large portion of the diaphragm. Also, the spread of yielding reduces the deformation demand on individual connectors. The hysteretic responses of the nail connectors in wood structural panel diaphragms have sufficient positive post-yield stiffness to effectively spread yielding from a location of first yield that is not at the diaphragm boundaries. This combination of favorable connector post-yield response and location of first yield at an interior location of the diaphragm results in spread of the yielding over a large portion of the diaphragm's span. In the case of bare steel deck diaphragms, certain mechanical fasteners in combination with the deck profile were found to have adequate post-yield strength gain and deformation capacity to allow for spreading of diaphragm yielding, as detailed in Appendix D. Special-seismic-detailing requirements were implemented in AISI S400-20, *North American Standard for Seismic Design of Cold-Formed Steel Structural Systems* (AISI, 2020b), and utilized in ASCE/SEI 7-22 for bare steel deck diaphragms that provide sufficient inelasticity. For diaphragm detailing, such as welded connections that do not meet the special detailing provisions, $R_{diaph}$ is instead adjusted to provide near elastic level demands.

Using the numerical model developed for the FEMA P695 evaluation, several archetypes were designed with varying degrees of weakening below current code-level design forces at the diaphragm interior. A series of incremental dynamic analyses (for the purposes of FEMA P695 collapse assessment methodology) were conducted. It was observed that relative weakening of the diaphragm interior assists in protecting the perimeter boundary areas from excessive inelastic demand and increases the overall margin against building collapse. Additional information on these studies is contained in Koliou (2014) and Koliou et al. (2016a, 2016b). Similar results were obtained using a combination of weakening interior portions of the diaphragm below current code-level forces and amplifying the design shear forces in the end regions of the diaphragm span, which is the approach used for the alternative RWFD design procedure as incorporated into ASCE/SEI 7-22.

In smaller buildings with shorter diaphragm spans and low shear demands, a minimum fastener size at maximum spacing is provided uniformly across the entire diaphragm, thus not permitting intentional weakening. To address this situation, the RWFD numerical studies evaluated the effect of designing for amplified shears across the entire diaphragm span. The studies found that acceptable performance would still be achieved, but the performance would be somewhat reduced, as discussed in Appendix C.

One potential concern with the spread of diaphragm yielding is its impact on the cost of repair. If diaphragm yielding occurs over a larger percentage of the roof area, a larger area of the diaphragm may require repair following an earthquake. A potential tradeoff between improved collapse resistance and cost of repairs may exist. Initial studies by Koliou et al. (2016d) have shown that the proposed alternative design is cost-efficient in terms of repair costs (economic losses) compared to traditional design per ASCE 7 Section 12.10.1 and Section 12.10.2.

### *4.2.2 Diaphragm Response Modification Coefficient and Shear Amplification*

An assumed linear distribution of design shear along the diaphragm span requires $R_{diaph}$ to be less than 4, but $R_{diaph}$ could potentially be increased if design shear is amplified in targeted areas near the diaphragm boundaries to spread yielding within the diaphragm. Based on this premise, the FEMA P695 collapse assessment methodology was applied to a set of archetype buildings with weakened interior portions of a diaphragm and a strengthened perimeter. Trial and error was used to evaluate different values of $R_{diaph}$ with different nonlinear shear distributions along the length of the diaphragm span. From this study, the alternative RWFD procedure was developed for one-story RWFD buildings.

The FEMA P695 evaluation included a set of buildings of various sizes, shapes, and seismic exposures, designed by incorporating a new approximate building period, reducing the strength of the interior diaphragm portions with a response modification coefficient $R_{diaph} = 4.5$ (instead of 4), and strengthening the diaphragm boundary regions (a minimum width of 10 percent of the diaphragm span at each end) with 50 percent more capacity. The initial studies by Koliou (2014) used a building period for diaphragm design of $T_a = T_{diaph} + T_{walls}$, and the FEMA P695 evaluation showed a significant improvement in the collapse capacity and met all collapse margin targets required to show equivalency to the seismic performance intent of the building code. The alternative RWFD design procedure ultimately incorporated a period for diaphragm design of simply $T_{diaph}$. The FEMA P695 evaluation of these archetypes was updated to incorporate design based on $T_{diaph}$. These results are incorporated as part of the 2021 update to this report. The updated results again showed significant improvement in the collapse capacity and met all collapse margin targets required. A summary of the FEMA P695 assessment studies and results for the alternative design procedure is contained in Appendix C and Appendix D.

## 4.3 Deflection Amplification Factor, $C_{d\text{-}diaph}$, Selection

Deflections are used in design to check for deformation compatibility, *P*-delta effects, property line setbacks, and separation at seismic joints. Diaphragms in RWFD buildings are expected to go into the inelastic range during a design earthquake; however, the design forces used to compute diaphragm deflections are based on elastic behavior. Thus, the computed elastic deformations must be amplified to get realistic values. Essentially, this amplification is partially reversing the process that the response modification coefficient, *R*, provided to the design-level forces.

FEMA P695 defines $C_d$ as the response modification coefficient, *R*, divided by a numerical coefficient that is a function of damping. Using this formulation, the value of $C_{d\text{-}diaph}$ computed in accordance FEMA P695 assuming 2 percent damping is equal to 1.25 times the value of the response modification coefficient, *R* (See Appendix Section C.3). However, for the case where bare steel deck diaphragms with special-seismic detailing and wood diaphragms are designed according to the alternative RWFD provisions, a deflection amplification factor, $C_{d\text{-}diaph}$, of 3.0 (less than $R_{diaph}$ of 4.5) was deemed appropriate for several reasons: (1) the boundary zones are designed for 1.5 times the design shear value equating to $R_{diaph}$ of 3.0 at the boundaries; (2) inelastic deformations in diaphragms concentrate at the diaphragm perimeter and at transitions in strength and stiffness (e.g., transitions in fastening patterns) leaving large portions of the diaphragm elastic; and (3) numerical studies underlying FEMA P-1026 found that the ratio of median design-basis earthquake drift to yield drift (approximation of predicted drift) was between 1.4 and 2.9, with an average value of 2.1, suggesting that $C_{d\text{-}diaph}$ of 3.0 is conservative. For this reason, $C_{d\text{-}diaph}$ is assigned as 3.0 in the ASCE/SEI 7-22 provisions for these diaphragm systems. $C_{d\text{-}diaph}$ is assigned as 1.5 for bare steel deck diaphragms not meeting the special-seismic-detailing provisions. Discussion of numerical study information relating to $C_{d\text{-}diaph}$ for the diaphragm is presented in Appendix C.

The diaphragm deflection for design earthquake shaking can be obtained by first computing the elastic deflection for design earthquake forces using the equations of the SDPWS-2021for wood structural panel diaphragms and AISI S310-20 for bare steel deck diaphragms, and then multiplying this value by the diaphragm's $C_{d\text{-}diaph}$.

## 4.4 Overstrength Factor, $\Omega_{0\text{-}diaph}$, Selection

In some cases, the building code dictates using special load combinations with overstrength to prevent critical elements from being the weak links during seismic shaking. The overstrength factor, $\Omega_{0\text{-}diaph}$, is used to increase the design forces to appropriate design levels for this purpose. When conducting a study under FEMA P695, a suitable overstrength factor, $\Omega_{0\text{-}diaph}$, can be determined for the proposed structural system being considered.

Because inelastic behavior is expected in the diaphragm, the use of a unique overstrength factor, $\Omega_{0\text{-}diaph}$, tied to the diaphragm is more appropriate for the design of diaphragm collectors and their connections to vertical elements than the traditional procedure that uses the $\Omega_0$ associated with vertical elements. For this study a diaphragm overstrength value of 2 was computed in accordance with FEMA P695. This value is noted to have been representative of the FEMA P695 numerical study results for high-seismic demands; it was judged not necessary to use the higher $\Omega_{0\text{-}diaph}$ value identified in the moderate-seismic-demand studies. See Appendix C for additional information. As adopted into ASCE/SEI 7-22, the value of $\Omega_{0\text{-}diaph}$ need not exceed the response modification coefficient, $R$; this leads to the assignment of $\Omega_{0\text{-}diaph}$ equal to 1.5 for steel deck diaphragms not meeting the special-seismic-detailing requirements.

## 4.5 Overview of the Alternative RWFD Design Procedure

The alternative RWFD design procedure can be thought of as a two-stage approach to designing a RWFD building: first, the diaphragm is designed using its own response modification coefficient, period, and detailing rules, and second, the vertical elements of the SFRS are designed using either the traditional ASCE/SEI 7-22 ELF procedures of Section 12.8 or the RWFD two-stage analysis procedures of ASCE/SEI 7-22 Section 12.2.3.4.

The alternative design procedure is only permitted to be used when the building complies with all of the limitations of ASCE/SEI 7-22 Section 12.10.4.1, as discussed in Section 5.3. The two-stage analysis procedures of ASCE/SEI 7-22 Section 12.2.3.4 are only permitted to be used when the diaphragms are designed in accordance with ASCE/SEI 7-22 Section 12.10.4.

The following provides an overview of the steps required to implement the alternative design procedure using ASCE/SEI 7-22 Section 12.10.4 and Section 12.2.3.4. Notations used are consistent with the ASCE/SEI 7-22 provisions.

1. A response modification coefficient of the diaphragm, $R_{diaph}$, equal to 4.5 is assigned for bare steel deck diaphragms meeting the special-seismic-detailing requirements and wood diaphragms. $R_{diaph}$ is taken as 1.5 for steel deck diaphragm not meeting the special-seismic-design requirements.

2. The wood diaphragm period is determined using Equation 4-2 and the bare steel deck diaphragm is determined using Equation 4-3:

$$T_{diaph} = 0.002L_f \quad (4\text{-}2)$$

$$T_{diaph} = 0.001L_f \quad (4\text{-}3)$$

where:

$L_f$ = the span, in feet, of the horizontal flexible diaphragm being considered; the span is measured between vertical elements that provide lateral support to the diaphragm in the direction being considered.

3. $C_{s\text{-}diaph}$ is determined in accordance with ASCE/SEI 7-22 Equation 12.10-16a and Equation 12.10-16b:

$$C_{s\text{-}diaph} = \frac{S_{DS}}{R_{diaph}/I_e} \quad \text{ASCE/SEI 7-22 Eq. 12.10-16a}$$

$$C_{s\text{-}diaph} = \frac{S_{D1}}{T_{diaph}\left(R_{diaph}/I_e\right)} \quad \text{ASCE/SEI 7-22 Eq. 12.10-16b}$$

4. Diaphragm design shears are computed using the following force acting on the diaphragm:

$$F_{px} = C_{s\text{-}diaph}w_{px} \quad \text{ASCE/SEI 7-22 Eq. 12.10-15}$$

where:

$F_{px}$ = the force acting on the diaphragm

$w_{px}$ = the tributary seismic weight applicable to the diaphragm including the tributary weight of the walls acting out-of-plane.

5. For diaphragm spans greater than 100 feet, the diaphragm design shears are increased by a shear amplification factor of 1.5 for the end 10 percent of the diaphragm span at each end. For diaphragm spans of 100 feet or less, the shear amplification is applied throughout the diaphragm. This amplified shear is applicable to the design of the diaphragm and design

for shear transfer between the diaphragm and the walls or other vertical elements.

6. Diaphragm chords are designed for the diaphragm flexure resulting from diaphragm loads computed using $F_{px}$ in Step 4 without the amplification in Step 5.

7. In SDC D, E, and F, the collectors and their connections to vertical elements are designed for the forces computed from the design diaphragm shears collected, without the 1.5 shear amplification factor in Step 5, and amplified by a diaphragm overstrength factor, $\Omega_{0\text{-}diaph}$, equal to 2.0. For steel deck diaphragms not meeting the special-seismic-detailing provisions, $\Omega_0$ is permitted to be capped at the $R_{diaph}$ value of 1.5.

8. Where the optional two-stage analysis procedure is used, the vertical elements of the SFRS (e.g., shear walls) are designed for in-plane forces using the ELF procedure of ASCE/SEI 7-22 Section 12.8 but with the force from the diaphragm as computed in Step 4 amplified by $R_{diaph}/(R/\rho)$ but not less than 1.0. The response modification coefficient, $R$, is assigned the value for the type of vertical system being engineered. The approximate period, $T_a$, is computed using ASCE/SEI 7-22 Equation 12.8-8, Equation 12.8-9, or Equation 12.8-10 for the shear walls. This period, for the type of building envisioned, is anticipated to always be small enough to be in the constant acceleration portion of the design spectrum. Acceleration computed using $R$ and $T_a$ is applied to the seismic mass of the in-plane walls.

9. Deflections are computed for the diaphragm and the wall system. Elastic diaphragm deflection, $\delta_{e\text{-}diaph}$, is computed using the force level, $F_{px}$, in Step 4, along with SDPWS-2021 Section 4.2.2 or AISI S310-20 Section D.5. The elastic diaphragm deflection should be amplified by a deflection amplification factor for the diaphragm, $C_{d\text{-}diaph}$, equal to 3.0 for steel deck diaphragms meeting the special-seismic-detailing requirements and wood diaphragms, and equal to 1.5 for steel deck diaphragms not meeting the special-seismic-detailing requirements:

$$\delta_{DE\text{-}diaph} = \frac{C_{d-diaph}\delta_{e-diaph}}{I_e}$$

Deflection of the wall system should be computed for design-level forces and amplified by $C_d$ for the wall system.

$$\delta_{DE\text{-}wall} = \frac{C_{d-wall}\delta_{e-wall}}{I_e}$$

In SDC D, E, and F, the computed deflection is used to check for deformation compatibility in accordance with ASCE/SEI 7-22 Section 12.12.4. This includes checking that the gravity system is able to maintain required vertical-load-carrying strength for the calculated diaphragm deflection. If appropriate, the computed deflections are used to determine required seismic separations or property setbacks in accordance with ASCE/SEI 7-22 Section 12.12.2, and requirements for members spanning between structures per Section 12.12.3.

10. Second order *P*-delta effects for the building are checked in accordance with ASCE/SEI 7-22 Section 12.8.7, but both diaphragm and wall deflections should be included. The diaphragm deflection component can be reduced to approximately two-thirds of the maximum diaphragm deflection because the diaphragm tributary seismic weight on average moves approximately two-thirds of the diaphragm deflection plus the deflection of the in-plane walls.
11. Out-of-plane wall forces and out-of-plane top-of-wall anchorage forces and detailing requirements are designed in accordance with Section 12.11.1 and Section 12.11.2 of ASCE/SEI 7-22.

# Chapter 5

# Implementation of the Alternative RWFD Design Procedure

This chapter provides an explanation of how to implement the alternative RWFD design procedure and includesa redesign of the example buildings introduced in Chapter 3 as a way to demonstrate and explain the procedure. Section 5.1 illustrates a building design with a wood structural panel diaphragm, and Section 5.2 illustrates a building design with a bare steel deck roof diaphragm.

## 5.1 Wood Structural Panel Diaphragm Design Example

### *5.1.1 A Two-Stage ELF Procedure*

Conceptually, a RWFD building is simply a flexible diaphragm structure supported by a more rigid structure below. The flexible diaphragm is in series with the rigid walls or other stiff elements, and could be viewed as a vertical combination of SFRSs under ASCE/SEI 7-22 Section 12.2.3.1. This is similar to today's common podium buildings, with a flexible SFRS at the upper floors supported on a rigid SFRS at the lower floors.

The two-stage ELF procedure of ASCE/SEI 7-22 Section 12.2.3.2 for vertical combination of systems, first introduced into the 1988 *Uniform Building Code* (ICBO, 1988), is commonly used in practice today for podium structures. This philosophy has been adapted for use in the alternative design procedure for RWFD buildings in Section 12.2.3.4. When an upper flexible portion is supported by a lower rigid portion, a two-stage procedure encourages the consideration of two different structural periods ($T$) and two different response modification coefficients ($R$) in series within the same building to determine the applied seismic design forces to each portion. Furthermore, two separate overstrength factors ($\Omega_o$) and deflection amplification factors ($C_d$) may be utilized when appropriate, with one pair of $\Omega_o$ and $C_d$ values for the diaphragm and another for the rigid vertical elements.

The two-stage analysis procedure for vertical combination of systems within ASCE/SEI 7-22 Section 12.2.3.2 limits its applicability to situations where the period of the entire structure is not greater than 1.1 times the period of the upper portion considered as a separate structure. Additionally, applicability is also limited to situations where the lower portion is at least ten times stiffer than the upper portion. These limitations were established to account for the uncertainty of the structure's behavior when the differences in the stiffnesses or periods are small.

The limitations for a two-stage analysis procedure for vertical combinations of systems described in the preceding paragraph were deemed unnecessary to the alternative RWFD design procedure presented in ASCE/SEI 7-22 Section 12.2.3.4. This decision was made because the procedure was validated using the FEMA P695 collapse assessment methodology with a wide range of diaphragm and wall stiffnesses, as well as diaphragm and building periods, that often fall below the stiffness ratio thresholds. Thus, some influence or interaction between the walls and diaphragm due to stiffnesses or periods that begin to approach each other is already reflected in the FEMA P695 validation.

The original edition of this document suggested that the alternative RWFD procedure should only be considered valid as long as the approximate period of the wood structural panel diaphragm computed in accordance with Equation 4-2 was at least three times the approximate period of the shear walls computed using ASCE/SEI 7-22 Equation 12.8-10; however, ASCE/SEI 7-22 Section 12.10.4.1 takes a more direct way to address this criterion by providing a list of acceptably rigid SFRSs in lieu of a required period comparison. Further discussion on this topic and the recommendation for further study is provided in Section 8.1.1 of this report.

For the two-stage analysis, the first stage (diaphragm design forces) and the second stage (shear wall design forces) are provided in Section 5.1.2 through Section 5.1.10 and in Section 5.1.11, respectively.

### *5.1.2 First Stage—Diaphragm Design*

The first stage of the analysis involves design of the diaphragm as a separate structure using an ELF procedure in each direction. As previously discussed, special seismic response modification coefficients, overstrength factors, and deflection amplification factors have been established for the flexible diaphragm composed of nailed wood structural panels or bare steel deck. Additionally, the SFRS supporting the diaphragm is limited to specific rigid systems.

$$T_{diaph} = 0.002L_f \quad (4\text{-}2)$$

$$T_{walls} = \frac{C_q}{\sqrt{C_w}} h_n \quad \text{ASCE/SEI 7-22 Eq. 12.8-10}$$

where:

$C_q$, $C_w$, and $h_n$ are per ASCE/SEI 7-22 Section 12.8.2.1

**Seismic Performance Factors**

$R_{diaph}$ = 4.5 provided an amplified shear boundary zone is incorporated into the diaphragm (ASCE/SEI 7-22 Section 12.10.4.2.1)

$\Omega_{o\ diaph}$ = 2.0 for the design of collectors, etc. (ASCE/SEI 7-22 Section 12.10.4.2.4)

$C_{d\ diaph}$ = 3.0 for the calculation of diaphragm deflections (ASCE/SEI 7-22 Section 12.10.4.2.5)

$\rho$ = 1.0 (ASCE/SEI 7-22 Section 12.3.4.1)

The design spectral accelerations will be the same as in the traditional design practice example in Chapter 3. As previously given:

$S_{DS}$ = 1.0 (short period)

$S_{D1}$ = 0.6 (1-second period based on $S_1$ = 0.5)

SDC = D

### *5.1.3 Diaphragm Design Coefficient, $C_s$, Using the ELF Procedure*

ASCE/SEI 7-22 Section 12.8.1 defines the seismic base shear as:

$$V = C_s W \quad \text{ASCE/SEI 7-22 Eq. 12.8-1}$$

where:

$$C_s = \frac{S_{DS}}{R / I_e} \quad \text{ASCE/SEI 7-22 Eq. 12.8-3}$$

and need not exceed:

$$C_s = \frac{S_{D1}}{T\left(R / I_e\right)} \quad \text{ASCE/SEI 7-22 Eq. 12.8-4}$$

Because the flexible diaphragm is supported by the significantly stiffer rigid shear walls, the diaphragm will be viewed as a separate structure with its base at the roof-to-wall interface. This philosophy extends the ELF procedure to diaphragms where the diaphragm force $F_{px}$ is be represented as

$$F_{px} = C_{s\text{-}diaph}(w_{px}) \quad \text{ASCE/SEI 7-22 Eq 12.10-15}$$

Now with the ability to differentiate between the wall's and diaphragm's response modification coefficients, a unique $C_{S\text{-}diaph}$ is initially obtained for the diaphragm.

$$C_{s\text{-}diaph} = \frac{S_{DS}}{R_{diaph} / I_e} = \frac{1.0}{4.5 / 1.0} = 0.222 \qquad \text{ASCE/SEI 7-22 Eq 12.10-16a}$$

With the greater flexibility of the diaphragm compared to the walls, it is now possible that the upper bound for $C_{s\text{-}diaph}$ using Equation 12.10-16b may govern, indicating that the seismic response is off the plateau of the design spectrum.

Before the upper bound for $C_{s\text{-}diaph}$ can be computed, the approximate fundamental period of the diaphragm in each orthogonal axis direction must be considered. The north/south (transverse) loading direction will be considered first, followed by the east/west (longitudinal) loading direction.

**North/South Direction**

As previously determined in Section 4.1:

$T_{diaph}$ = 0.800 sec — ASCE/SEI 7-22 Section 12.10.4.2.1

$T_{wall}$ = 0.136 sec — ASCE/SEI 7-22 Equation 12.8-9

For engineers using ASCE/SEI 41-17 to evaluate existing RWFD buildings, standard practice has been to use the building's period $T_a$ from ASCE/SEI 41-17 Equation 7-19 to develop pseudo forces for the diaphragm. However, engineers using ASCE/SEI 7-22's two-stage procedure design the upper flexible portion considering its own isolated period. There is some inconsistency between how the period is selected between these two approaches.

In Koliou (2014), the RWFD numerical model analyzed 17 building archetypes whose wood diaphragms were designed using the building's full period $T_a = T_{diaph} + T_{walls}$, similar to the ASCE/SEI 41-17 approach, and the results were found to be acceptable under the FEMA P695 collapse assessment methodology. However, situations where the walls may behave more like frames could cause the diaphragm design forces to become unconservative due to the longer design period utilized. ASCE/SEI 7-22 Section 12.10.4.2.1 requires design of the diaphragm for its own approximate period without including the walls' contribution. This results in a shorter period causing the diaphragm design forces to be comparatively higher for very large buildings whose spectral design acceleration is off the constant acceleration plateau. Using this approach, the results of the FEMA P695

study involving 21 building archetypes with wood diaphragms were found to be acceptable. These results are summarized in Appendix C.

Returning back to the computation of $C_{s\text{-}diaph}$ for the purposes of determining the diaphragm's design force, a check of the upper limit for $C_{s\text{-}diaph}$ is necessary where $T \le T_L$. Using the building period $T_{diaph} = 0.800$ seconds, $C_{s\text{-}diaph}$ need not be greater than:

$$C_{s\text{-}diaph} = \frac{S_{D1}}{T_{diaph}\left(R_{diaph} / I_e\right)} = \frac{0.6}{0.800\left(4.5/1.0\right)} = 0.167 < 0.222$$

ASCE/SEI 7-22 Eq. 12.10-16b

The fundamental period is longer than the transition period, $T_s$, equal to 0.6 seconds, so the fundamental period is off the design spectrum's constant acceleration plateau and into the $1/T$ region (i.e., constant velocity region) of the spectrum.

Thus:

$C_{s\text{-}diaph} = 0.167$

Substituting into Equation 12.10-15, we obtain the diaphragm force equation for the north/south direction of the structure, which is used to determine the design forces acting on the diaphragm.

$F_{px\ N/S} = C_{s\text{-}diaph} w_{px}$

$F_{px\ N/S} = 0.167 w_{px}$

**East/West Direction**

As previously determined in Section 4.1:

$T_{diaph} = 0.400$ sec — ASCE/SEI 7-22 Section 12.10.4.2.1

$T_{wall} = 0.096$ sec — ASCE/SEI 7-22 Eq. 12.8-9

By definition, RWFD buildings require the vertical portions of the SFRS to be relatively stiffer than the horizontal diaphragm, and the use of a shear wall system in the east/west direction complies with this requirement under Section 12.10.4.1.

Checking the upper limit for $C_{s\text{-}diaph}$ where $T \le T_L$:

$$C_{s\text{-}diaph} = \frac{S_{D1}}{T_{diaph}\left(R_{diaph} / I_e\right)} = \frac{0.6}{0.400\left(4.5/1.0\right)} = 0.333$$

ASCE/SEI 7-22 Eq. 12.10-16b

The fundamental period is short enough to be on the design spectrum's plateau, and Eq. 12.10-16b does not control, thus:

$C_{s\text{-}diaph} = 0.222$

Substituting into Equation 12.10-15, we obtain the diaphragm force equation for the east/west direction of the structure, which is used to determine the design forces in the diaphragm.

$$F_{px\ E/W} = C_{s\text{-}diaph} w_{px}$$

$$F_{px\ E/W} = 0.222 w_{px}$$

Each of the uniformly distributed diaphragm design loads $0.167w_{px}$ and $0.222w_{px}$ in the north/south and east/west directions, respectfully, are different than the traditional practice value of $0.25w_p$. These differences are attributed to recognition of the longer period of the long-spanning diaphragm in the north/south direction and better distribution of yielding along the diaphragm spans reflected in the response modification coefficient ($R = 4.5$ instead of 4). However, this increase in $R$ also requires an amplification of design shear in the end regions of the diaphragm that will be explained in Section 5.1.5. This amplification of the diaphragm design shears is effectively a local reduction of $R_{diaph}$ relative to a value of 4.5 in the diaphragm end regions.

### *5.1.4 Diaphragm Forces Using the ELF Procedure*

Using our flat-beam analogy, north/south seismic forces are resisted by shear walls on grid lines A and J, and east/west seismic forces are resisted by shear walls on grid lines 1 and 5. A uniformly distributed load across this flat-beam is illustrated in Figure 5-1.

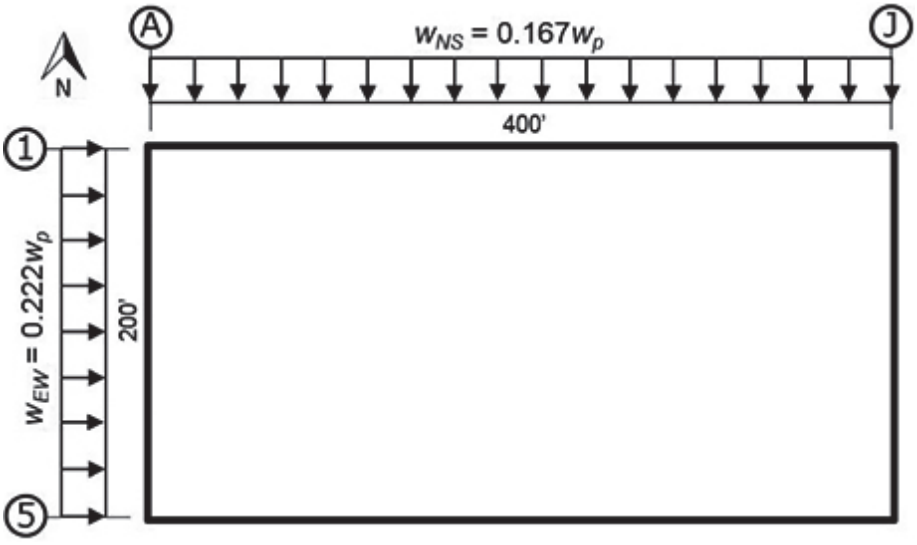


Figure 5-1 Diaphragm loading model (alternative RWFD procedure).

The uniform loads $w_{NS}$ and $w_{EW}$ applied laterally to the diaphragm are computed using the diaphragm lengths and its unit weights, and the tributary wall heights and its unit weights:

$$w_{NS} = 0.167(12 \text{ psf})(200') + 2\left[0.167(116 \text{ psf})33'\left(\frac{33'}{2}\right)\left(\frac{1}{30'}\right)\right]$$

$$= 1104 \text{ plf}$$

$$w_{EW} = 0.222(12 \text{ psf})(400') + 2\left[0.222(116 \text{ psf})33'\left(\frac{33'}{2}\right)\left(\frac{1}{30'}\right)\right]$$

$$= 2000 \text{ plf}$$

where:

Roof dead load = 12 psf

Wall dead load = 116 psf (9¼" thick at 150 pcf)

Roof height = 30'-0"

Top of wall = 33'-0" (above floor)

The maximum design shears are now computed using simple statics on the uniformly loaded flat beam model. Because of the building's symmetry, diaphragm shear $V_{NS}$ at grid lines A and J will be equal (see Figure 5-2).

North-south diaphragm shear:

$$V_{NS} = w_{NS}\frac{L}{2} = 1104\frac{400 \text{ ft}}{2} = 220{,}800 \text{ lbs}$$

North-south unit shear:

$$v_{NS} = \frac{V_{NS}}{200 \text{ ft}} = \frac{220{,}800}{200 \text{ ft}} = 1104 \text{ plf, maximum}$$

East-west diaphragm shear:

$$V_{EW} = w_{EW}\frac{L}{2} = 2000\frac{200 \text{ ft}}{2} = 200{,}000 \text{ lbs}$$

East-west unit shear:

$$v_{EW} = \frac{V_{EW}}{400 \text{ ft}} = \frac{200{,}000}{400 \text{ ft}} = 500 \text{ plf, maximum}$$

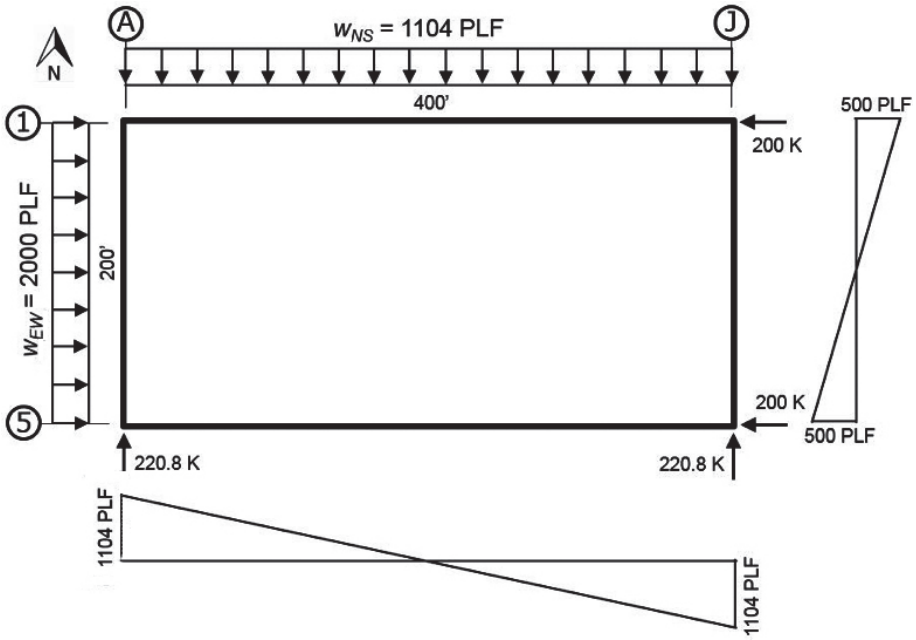


Figure 5-2 Diaphragm shear distribution.

### *5.1.5 North/South Diaphragm Shear Design*

The diaphragm design for the shears follows a similar approach as that outlined in Section 3.5, which illustrates traditional practice. In Section 5.1.4, the maximum diaphragm shears were determined for each orthogonal direction; however, performance was found to improve in the FEMA P695 assessment results when inelastic behavior was better distributed, and this was accomplished in part by providing overstrength in the amplified shear boundary zones of the diaphragm. More specifically, the 10 percent of the diaphragm's length 0.10*L* at each end is designed for 1.5 times more diaphragm shear than otherwise would have been computed. Figure 5-3 illustrates the design shear distribution across the diaphragm in each direction.

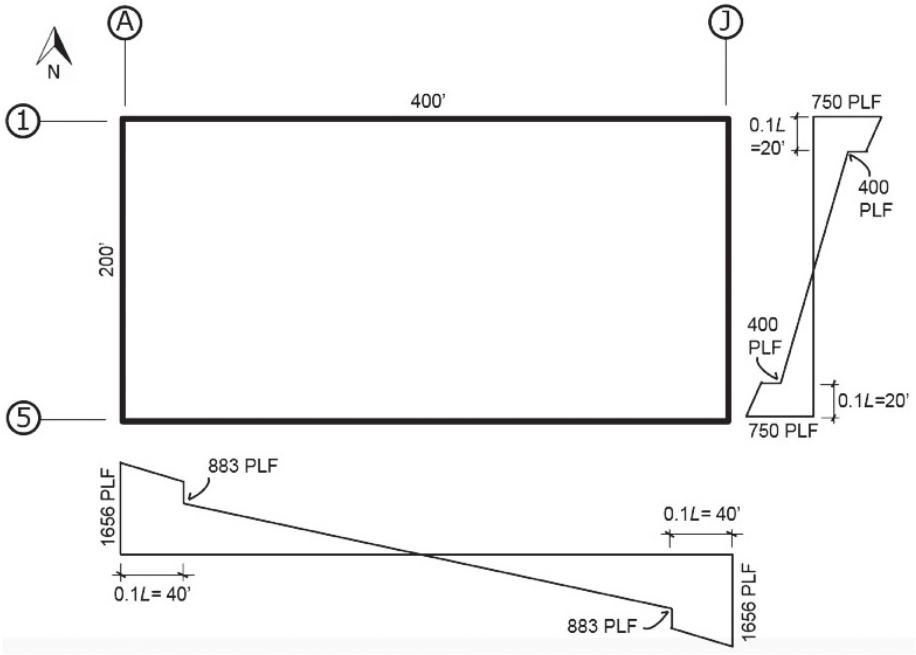


Figure 5-3 Shear diagrams for the diaphragm design with the 1.5× factor.

As observed in Figure 5-3, the worst unit shear demand is in the north/south direction with $v_{NS} = 1104 \times 1.5 = 1656$ plf (unfactored). The nominal diaphragm shear capacities are provided in SDPWS- 2021 Table 4.2A and Table 4.2B for a wide range of blocked diaphragm conditions. As done in Section 3.5.1 for traditional design, an ASD approach using the blocked panelized roof system will be followed.

$v_{NS\ (ASD)} = 0.7v_{NS} = 0.7(1656) = 1159$ plf

$v_{EW\ (ASD)} = 0.7v_{EW} = 0.7(750) = 525$ plf

Using these unit shear values, the designer enters either SDPWS-2021 Table 4.2A or Table 4.2B to select a diaphragm assembly with an appropriate shear capacity for 15/32-inch Structural I sheathing with 10d nails. For the ASD approach, table values are divided by a factor of 2.8 per SDPWS-2021 Section 4.1.4.

In the north/south direction, the ASD unit shear demand is greater than the maximum ASD capacities obtained from SDPWS-2021 Table 4.2A, thus reference to the high-load diaphragm shears in Table 4.2B will be necessary. The on-center (o.c.) nail spacing shown here requires thicker framing to prevent splitting. The capacity is reduced from the table nominal strength value to an allowable stress design value by dividing by 2.8.

**Design Solution**

- 15/32"-thick Structural I sheathing
- 10d nails in two lines at 2 ½" o.c. boundaries and continuous north/south edges, 3" o.c. other edges
- 10d nails in one line at 12" o.c. intermediate (field)
- 4× framing width at adjoining edges
- CAPACITY = 3610/2.8 = 1289 plf (ASD)
- $v_{NS\ (ASD)} = 0.7v_{NS} = 0.7(1656) = 1159$ plf < 1289 plf OK

The construction of this diaphragm system is illustrated in Figure 3-4.

The nailing and subpurlin widths may be reduced as the corresponding unit shears also reduce. For this example, Table 5-1 identifies various diaphragm nailing configurations from the SDPWS-2021 that will be utilized at different portions of this building. The ASD shear values are simply the nominal strengths listed in SDPWS-2021 Table 4.2A and Table 4.2B divided by a factor of 2.8 per Section 4.1.4. Note that the framing and nailing listed for Zones 1 to 6 in Table 5-1 are the same as those listed for Zones 1 to 6 in Table 3.1 for the traditional practice design example in Chapter 3.

**Table 5-1 Diaphragm Nailing Schedule (Cases 2 and 4)**

| 15/32″ Structural I OSB Sheathing (DOC PS 2 [NIST, 2004]) with 10d nails (0.148″ dia x 2″ long minimum) | | | | | |
|---|---|---|---|---|---|
| **Nailing Zone** | **Framing Width at Adjoining Edges** | **Lines of Nails** | **Nailing per line at Boundary & Continuous Edges** | **Nailing per line at Other Edges** | **ASD Allowable Shear (plf)** |
| 1 | 2x | 1 | 6″ o.c. | 6″ o.c. | 320 |
| 2 | 2x | 1 | 4″ o.c. | 6″ o.c. | 425 |
| 3 | 2x | 1 | 2½″ o.c. | 4″ o.c. | 640 |
| 4 | 3x | 1 | 2″ o.c. | 3″ o.c. | 820 |
| 5 | 4x | 2 | 2½″ o.c. | 4″ o.c. | 1005 |
| 6 | 4x | 2 | 2½″ o.c. | 3″ o.c. | 1289 |

At the diaphragm boundaries (grid lines A and J), Nailing Zone 6 was determined to be acceptable. At some location inward as the diaphragm shears diminish, Nailing Zone 5 will become acceptable. The transition from Nailing Zone 6 to Nailing Zone 5 may be located using statics as follows:

$$\begin{aligned} \text{Shear Demand (ASD)} &= \text{Shear Capacity (ASD)} \\ 0.7[V_{NS} - (w_{NS})x](1.5) &= (1005 \text{ plf})B \\ 0.7[220{,}800 \text{ lbs} - (1104 \text{ plf})x](1.5) &= 1005 \text{ plf}\,(200 \text{ ft}) \end{aligned} \qquad (5\text{-}1)$$

where:

$x$ = the demarcation distance from the diaphragm boundary.

Solving for $x$ obtains:

$x$ = 26.6 feet

Because a panelized roof system typically consists of 8-foot-wide wood structural panels, the joist spacing module is also 8 feet, and the transition should be increased to the next 8-foot increment. In this case, it is increased to $x$ =32 feet; however, this leaves only 8 feet more until the shear demand dramatically reduces at 0.1$L$ = 40 feet from the boundary, as seen in Figure 5-3. Therefore, it is elected to provide Nailing Zone 6 across the entire amplified shear boundary zone of the diaphragm.

It is important to observe that the potential transition location from Nailing Zone 6 to Nailing Zone 5 selected occurs within the 0.1$L$, or 40-foot, wide boundary strip, thus Equation 5-1 is still valid with the 1.5 factor included. If the first nailing zone transition occurs at or past 0.1$L$ from the boundary shear element, the 1.5 shear amplification factor in Equation 5-1 may be omitted.

Latitude in locating potential nailing zone transitions farther away from the diaphragm boundary is possible within the end regions where shear is amplified, at the transition between amplified and non-amplified shear, and within the interior portions of the diaphragm where shear is not amplified. The basis for this latitude is the results of analyses of archetypes in which the nailing pattern at the boundary is used for the entire diaphragm span (Appendix C.5). Although these archetypes did not perform as well as the archetypes with multiple nailing zones, they met the acceptable performance criteria.

After 0.1$L$, the shear demand drops dramatically and some potential nailing zone assemblies may be skipped entirely. The transition locations between Nailing Zones 5 and 4, Nailing Zones 4 and 3, Nailing Zones 3 and 2, and Nailing Zones 2 and 1 for the north-south loading direction are found using the same process resulting in Table 5-2; however, it is important to recognize that the 1.5 shear amplification factor is only on the outer 0.1$L$ portions.

Because the shear diagram (Figure 5-3) has a large stepped reduction in the design shear at 0.1$L$, Nailing Zones 5 and 4 are not utilized. This significant transition in nailing from Nailing Zone 3 to 6 may catch framers by surprise; or worse it could be confusing and lead to field errors. As such, engineers

should consider this construction aspect in their structural observation program.

**Table 5-2 Diaphragm Nailing Zone Shear Checks**

| Nailing Zone | Distance from Boundary | Maximum Unit Shear | ASD Unit Shear | Allowable Shear Capacity |
|---|---|---|---|---|
| 6 | 0 feet | $v_{max}$ = 1656 plf | $v_{ASD}$ = 1159 plf | 1289 plf |
| 5 | - | - | - | 1005 plf |
| 4 | - | - | - | 820 plf |
| 3 | 40 feet | $v_{max}$ = 883 plf | $v_{ASD}$ = 618 plf | 640 plf |
| 2 | 96 feet | $v_{max}$ = 574 plf | $v_{ASD}$ = 401 plf | 425 plf |
| 1 | 120 feet | $v_{max}$ = 442 plf | $v_{ASD}$ = 309 plf | 320 plf |

The resulting nailing zone layout for the north/south loading is shown in Figure 5-4.

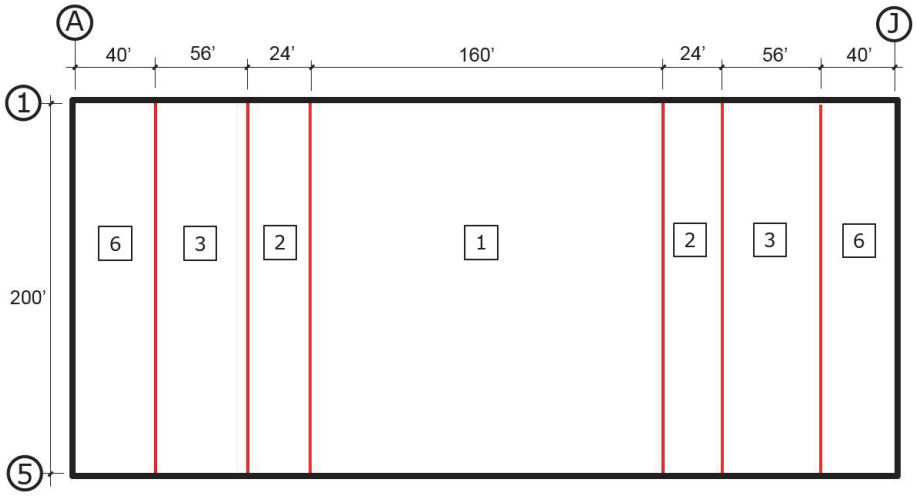


Figure 5-4 North/south nailing zone layout.

When designing wood diaphragms, the diaphragm aspect ratio must also be checked against the limitations in the SDPWS-2021 Table 4.2.2. For blocked diaphragms such as those that occur in panelized construction, the maximum aspect ratio is $L/W$ = 4:1. In this example, the north/south loading direction is the critical $L/W$ ratio.

$L/W = 400/200 = 2.0 < 4$ OK

### *5.1.6 North/South Diaphragm Shear Transfer to Walls (and Collectors)*

As the diaphragm shear reaches the diaphragm boundary, this seismic force must be transferred to the vertical SFRS, or as in this example, the concrete shear walls. Traditionally, this transfer has been through a wood ledger at

the inside face of wall. Occasionally, no parapets are utilized in the architectural design, and a wood nailer is provided at the top of wall in place of a ledger. With the alternative RWFD design procedure, the diaphragm boundary nailing to the wood ledger/nailer and the ledger/nailer's bolting to the shear walls are designed using the diaphragm shear force with the 1.5 shear amplification factor to encourage the spreading of yielding within the diaphragm.

This example utilizes steel ledgers as discussed in Section 3.6. Even in wood diaphragms, steel ledgers have become very popular in large RWFD buildings, utilizing steel angles or channels bolted to the inside face of the shear walls. When these steel ledgers are combined with wood nailers on the top leg or flange at the diaphragm interface, the provisions mentioned above for shear transfer still apply to the interface of the wood nailers to the steel ledgers and steel ledgers to the walls.

However, it has also become popular to omit the wood nailer and directly fasten the wood structural panel to the steel ledger with PAFs. These proprietary fasteners typically have an ICC-ES approval, however there is no cyclic test data available to evaluate the post-yield behavior for fastening wood structural panels to steel. Justification may be necessary through IBC Section 104.11's procedure for alternative materials, design and methods of construction. It is recommended that the design incorporate the overstrength factor, $\Omega_{o\text{-}diaph}$.

Ledger bolting capacities into the concrete or masonry shear walls shall comply with ACI 318-19, *Building Code Requirements for Structural Concrete and Commentary* (ACI, 2019), or TMS 402-16, *Building Code Requirements for Masonry Structures* (TMS, 2016), respectfully.

### *5.1.7 North/South Diaphragm Chord Design*

Recall that a flexible diaphragm may be thought of as a flat horizontal beam where the shear resistance is obtained by the wood structural panel sheathing across the roof surface and the flexural resistance is obtained from perimeter chords. As illustrated in the traditional-practice design of Section 3.6, these chords are steel ledger angles at the roof line. Chord forces are determined using simple statics as shown in Figure 3.6, and the design force is a uniformly distributed load without the 1.5 shear amplification design factor. Maximum chord forces will occur at the center of the diaphragm's span where the maximum moment occurs.

The maximum tensile chord force for our building example is determined as follows:

$$T = \frac{M}{B} = \frac{w_{NS}L^2}{8B} = \frac{1104 \text{ plf}(400)^2}{8(200)} = 110{,}400 \text{ lbs}$$

The chord is designed here using LRFD with ASTM A36 Steel ($F_y$ = 36 ksi). Consulting ASCE/SEI 7-22 Section 2.3.6, the applicable LRFD load factor for seismic forces is 1.0. The area of steel required is:

$$A_S = \frac{T}{\phi F_y} = \frac{110.4}{0.9(36)} = 3.41 \text{ in.}^2$$

Using an L5×5×3/8 rolled steel angle satisfies this chord demand.

L5×5×3/8 Steel Area, $A_S$ = 3.65 in.$^2$ > 3.41 in.$^2$

This chord size is smaller than that found using the traditional design practice, primarily because the diaphragm seismic design force is less due to the impact of the longer diaphragm period.

### *5.1.8 East/West Diaphragm Shear Design*

Similar to the north/south loaded direction, the orthogonal east/west direction will also require consideration using the same sequential process. In Section 5.1.5, the maximum diaphragm shear in the east/west direction was determined to be $v_{EW}$ = 750 plf (unfactored) including the 1.5 shear amplification factor; and converting to ASD, the maximum diaphragm shear is as follows:

$v_{EW(ASD)} = 0.7v_{EW} = 0.7(750) = 525$ plf

As before, SDPWS-2021 Table 4.2A is used to select diaphragm nailing with an appropriate shear capacity. In the north/south loaded direction, Case 4 is the loading configuration, but for the east/west direction this becomes a Case 2 configuration. The applicable case determines the nail spacing along the continuous adjoining panel edges in the direction parallel to load. Comparing the diaphragm's shear demand with the capacities of Table 5-1, Nailing Zone 3 is selected:

$v_{EW(ASD)}$ = 525 plf < 640 plf (Nailing Zone 3)

At some distance away from the diaphragm boundary (walls at grid lines 1 and 5), Nailing Zone 2 in Table 5-1 will be acceptable due to the diminishing unit diaphragm shears. With the dramatic drop in design shear at 0.1$L$ = 20 feet, Nailing Zone 2 can be skipped altogether. Using the same approach as done in the north/south direction, the locations of the transition from Nailing Zone 3 to 2 and Nailing Zone 2 to 1 are found and shown in Table 5-3.

**Table 5-3 Diaphragm Nailing Zone Shear Checks**

| Nailing Zone | Distance from Boundary | Maximum Unit Shear | ASD Unit Shear | Allowable Shear Capacity |
|---|---|---|---|---|
| 3 | 0 feet | $v_{max}$ = 750 plf | $v_{ASD}$ = 525 plf | 640 plf |
| 2 | - | - | - | 425 plf |
| 1 | 20 feet | $v_{max}$ = 400 plf | $v_{ASD}$ = 280 plf | 320 plf |

Combining the nailing requirements for the north/south loading with the east/west loading results in Figure 5-5.

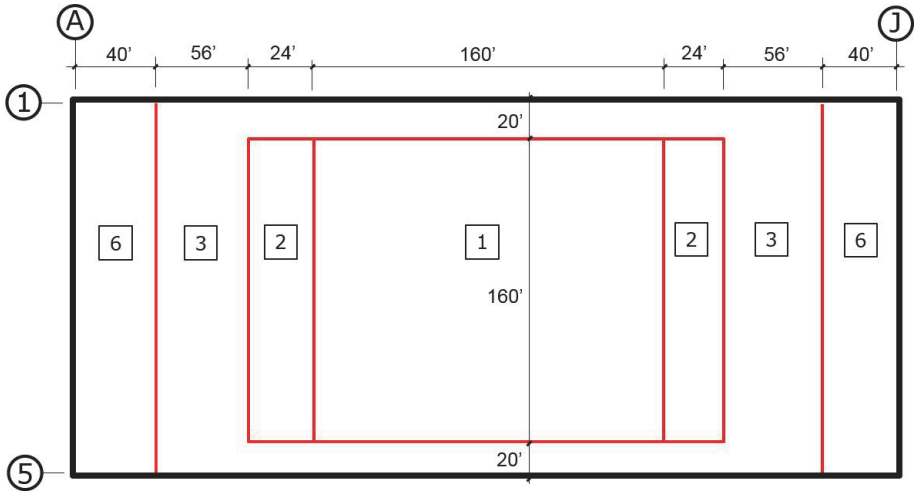


Figure 5-5 North/south and east/west nailing zones combined layout.

### *5.1.9 East/West Diaphragm Shear Transfer to Walls (and Collectors)*

Similar to the north/south diaphragm force design, the seismic diaphragm shears must be transferred to the vertical concrete shear walls. As discussed in Section 5.1.6, the shear transfer is designed with the 1.5 shear amplification factor.

Unlike the north/south force direction, the diaphragm boundaries resisting east/west seismic forces along grid lines 1 and 5 do not have uniform boundary nailing. While most of the length contains Nailing Zone 3 requirements, the first and last 40 feet of this wall line contain Nailing Zone 6 requirements, whose stiffness may attract more load. In this example, as well as that designed to traditional practice, there is a possibility that the shear transfer to the steel ledger is non-uniform; however, the steel ledger was designed as the diaphragm chord in Section 5.1.7 and contains sufficient strength to drag and redistribute the shear load appropriately to the shear wall elements. This is especially true when the diaphragm chord design is based on the maximum force at midspan, yet the chord design remains consistent along the entire wall line. This discussion is simply an observation of

predicted behavior; however, traditional design practice routinely assumes a uniform shear transfer into the wall line.

### 5.1.10 East/West Diaphragm Chord Design

With the diaphragm chords placed at the extreme sides of the diaphragm, the maximum chord forces in the east/west loaded direction are computed in a similar fashion as the north/south direction:

$$T = \frac{M}{B} = \frac{w_{NS}L^2}{8B} = \frac{2000 \text{ plf}(200)^2}{8(400)} = 25{,}000 \text{ lbs}$$

The required area of the steel chord is:

$$A_S = \frac{T}{\phi F_y} = \frac{25.0}{0.9(36)} = 0.77 \text{ in.}^2$$

Using an L4×4×1/4 rolled steel angle as a practical minimum size satisfies this chord demand.

L4×4×1/4 Steel Area $A_S = 1.93 \text{ in.}^2 > 0.77 \text{ in.}^2$

### 5.1.11 Second Stage—Shear Wall Force Using the ELF Procedure

The second stage of the two-stage analysis is the design of the heavy in-plane shear walls, whose period does not involve the diaphragm component, and is thus comparatively small. However, the shear forces include the diaphragm mass as well as a portion of the perpendicular out-of-plane walls and in-plane walls.

Additionally, the response modification coefficient ($R$) and redundancy factor ($\rho$) for the design of the in-plane walls will be as specified within ASCE/SEI 7-22 for that specific SFRS.

The design of the SFRS can follow the two-stage analysis procedure for one-story structures with flexible diaphragms and rigid vertical elements described in ASCE/SEI 7-22 Section 12.2.3.4. Determining the lateral design forces for the in-plane shear walls involves a conversion of the diaphragm design force contribution based on $R_{diaph}$ into the shear wall design forces based on $R$ and $\rho$ of the SFRS. Forces contributed by the effective seismic weight tributary to the diaphragm shall be the reactions from diaphragm forces determined in accordance with Section 12.10.4.2.1, amplified by the ratio of $R_{diaph}$ divided by $R/\rho$ of the vertical SFRS. This conversion is always an amplification, and thus this ratio shall not be taken as less than 1.0.

Note that the 1.5 shear amplification factor applied to the shear design of the diaphragm end regions per ASCE/SEI 7-22 Section 12.10.4.2.2 is not included in the conversion to wall forces.

This section illustrates this design procedure in each orthogonal direction on the example building.

Because the building is being evaluated as two different seismically behaving portions, the force to the in-plane shear walls will have two significant components. The flexible diaphragm with its tributary mass will generate a lateral force near the top of the wall, $F_{v1}$. Additionally, the rigid concrete in-plane walls have significant self-weight that will also generate lateral forces near their centers of mass, $F_{v2}$.

First, diaphragm forces imparted into the shear walls will be converted to be consistent with the expected seismic performance of an intermediate precast shear wall system. The diaphragm forces used for the design of the shear walls below will not include the 1.5 shear amplification factor used to design the diaphragm end regions.

As determined previously in Section 5.1.4, the diaphragm reactions to the shear walls based on $R_{diaph} = 4.5$ are as follows.

North/south diaphragm reactions:

$F_p = V_{NS} = 220{,}800$ lbs

East/west diaphragm reactions:

$F_p = V_{EW} = 200{,}000$ lbs

These diaphragm reaction forces need to be amplified to an appropriate shear wall design force.

North/south:

$$F_{v1} = F_p \times \left( \frac{R_{diaph}}{R / \rho} \right)$$

where:

$$\left( \frac{R_{diaph}}{R / \rho} \right) = \frac{4.5}{4 / 1.0} = 1.125 > 1.0 \text{ OK}$$

$F_{v1} = 220{,}800 \times 1.125$

$F_{v1} = 248{,}400$ lbs

East/west:

$$F_{v1} = F_p \times \left( \frac{R_{diaph}}{R / \rho} \right)$$

where:

$$\left( \frac{R_{diaph}}{R / \rho} \right) = \frac{4.5}{4 / 1.0} = 1.125 > 1.0 \text{ OK}$$

$F_{v1}$ = 200,000 × 1.125

$F_{v1}$ = 225,000 lbs

Second, the lateral seismic force generated from the wall self-weight must be included for design. The wall self-weight will have a seismic response unique to its own period of vibration, and the ELF procedure's base shear equation will be evaluated.

ASCE/SEI 7-22 Section 12.8.1 defines the seismic base shear as:

$$V = C_s W \qquad \text{ASCE/SEI 7-22 Eq. 12.8-1}$$

where:

$$C_s = \frac{S_{DS}}{R / I_e} \qquad \text{ASCE/SEI 7-22 Eq. 12.8-3}$$

Now working with the intermediate precast concrete shear walls ($R$ = 4) instead of the diaphragm ($R_{diaph}$ = 4.5), a unique $C_S$ is obtained for the shear wall design. Per Equation 12.8-3:

$$C_s = \frac{S_{DS}}{R / I_e} = \frac{1.0}{4 / 1.0} = 0.25$$

An upper bound for $C_s$ must now be computed using the approximate period of the rigid shear walls using Equation 12.8-4. As previously determined, the approximate $T_{walls}$ is different in each orthogonal direction when using Equation 12.8-10. The north/south (transverse) loading direction will be considered first, followed by the east/west (longitudinal) loading direction.

**North/South Direction**

$T_a = T_{walls}$ = 0.136 sec

Checking the upper limit for $C_s$ where $T \leq T_L$

$$C_{s\,max} = \frac{S_{D1}}{T(R / I_e)} = \frac{0.6}{0.136(4 / 1.0)} = 1.10 > 0.25$$

As expected for rigid shear walls, the fundamental period is short enough to be on the design spectrum's constant acceleration plateau, thus preliminarily $C_s$ equals 0.25. Checking the minimum allowed value for $C_s$, ASCE/SEI 7-22 Equation 12.8-6 is applicable. In this example, $S_1$ is given as 0.5*g*: therefore, Equation 12.8-7 is not applicable.

$$C_{s\,min} = 0.044 S_{DS} I_e = 0.44(1.0)(1.0) = 0.044 < 0.25 \quad \text{OK}$$

ASCE/SEI 7-22 Eq. 12.8-6

The calculated value of $C_s = 0.25$ is above the minimum allowed value.

$$C_{s\,governs} = 0.25$$

Substituting into Equation 12.8-1, we obtain the lateral force $F_{v2}$ equation for the shear wall self-weight, $W_{p\text{-}wall}$, for the north/south direction of the structure.

$$F_{v2} = C_s W = 0.25 W_{p\text{-}wall}$$

The wall self-weight, $W_{p\text{-}wall}$, is computed as:

$$W_{p\text{-}wall} = 116 \text{ psf} \times 200 \text{ ft} \times 33 \text{ ft} = 765{,}600 \text{ lbs}$$

Therefore:

$$F_{v2} = 0.25 W_{p\text{-}wall} = 0.25(765{,}600) = 191{,}400 \text{ lbs}$$

Therefore, the total shear wall design force, $F_v$, for the north/south direction is:

$$F_v = F_{v1} + F_{v2} = 248{,}400 + 191{,}400$$

$$F_v = 439{,}800 \text{ lbs or } 440 \text{ kips}$$

**East/West Direction**

Because the east/west load direction has the same $R_{wall}$ and $\rho_{wall}$, and because $T_a$ is smaller than in the north/south direction, the seismic response coefficient, $C_s$, is still on the constant acceleration plateau, $F_{v2} = 0.25 W_{p\text{-}wall}$.

$$F_v = F_{v1} + F_{v2} = 225{,}000 + 0.25 W_{p\text{-}wall}$$

The wall self-weight $W_{p\text{-}wall}$ is computed as:

$$W_{p\text{-}wall} = 116 \text{ psf} \times 400 \text{ ft} \times 33 \text{ ft} = 1{,}531{,}200 \text{ lbs}$$

Therefore:

$$F_{v2} = 0.25 W_{p\text{-}wall} = 0.25(1{,}531{,}200) = 382{,}800 \text{ lbs}$$

Therefore, the total shear wall design force, $F_v$, for the east/west direction is:

$$F_v = F_{v1} + F_{v2} = 225{,}000 + 382{,}800$$

$$F_v = 607{,}800 \text{ lbs or } 608 \text{ kips}$$

Figure 5-6 and Figure 5-7 illustrate the forces acting on the shear walls providing lateral resistance in the north/south and east/west directions, respectfully. The design forces at the base of the shear walls are 440 kips north/south and 608 kips east/west. These forces include the entire weight of the walls and are appropriate for the design of shear forces that transfer to the slab on ground or foundation.

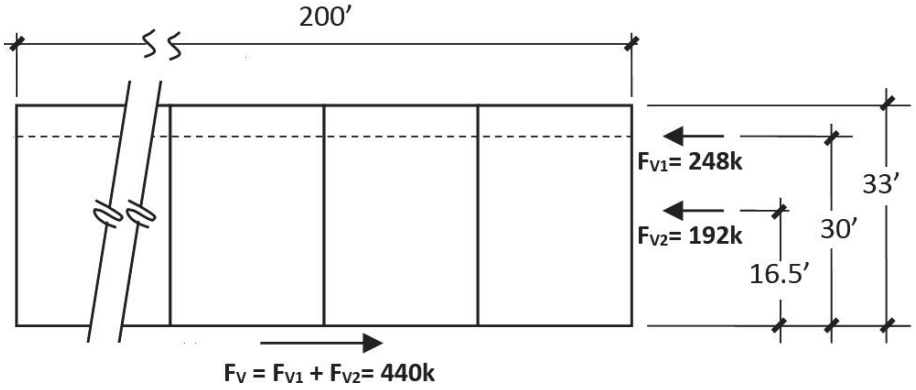


Figure 5-6 North/south lateral design forces acting on the shear walls (Lines A & J).

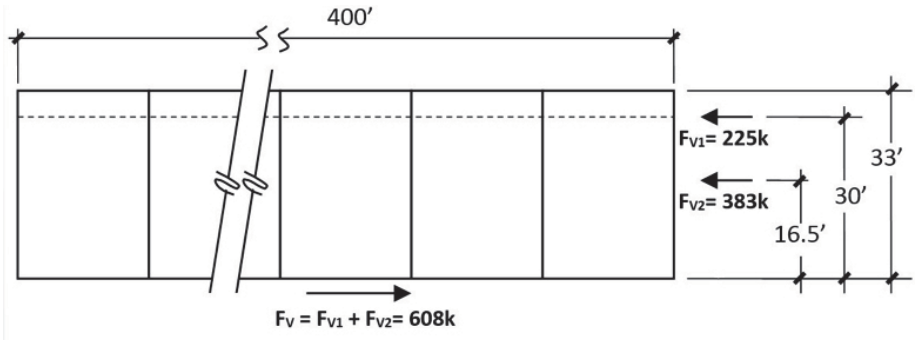


Figure 5-7 East/west lateral design forces acting on the shear walls (Lines 1 & 5).

## 5.2 Bare Steel Deck Diaphragm Design Example

Consider the design of a bare steel deck diaphragm with mechanical connectors that satisfy the special seismic detailing requirements in Section F3.5 of AISI S400-20, as detailed in Section 5.2.5 below.

### *5.2.1 A Two-Stage ELF Procedure*

Similar to the two-stage ELF procedure provided for structural wood diaphragm design in Section 5.1.1, bare steel deck diaphragms are designed using a two-stage ELF procedure. The first stage (diaphragm design forces) and the second stage (shear wall design forces) are provided in Section 5.2.2 through Section 5.2.10 and in Section 5.2.11, respectively.

### 5.2.2 First Stage—Diaphragm Design

The first stage of the analysis involves design of the bare steel deck diaphragm as a separate structure using an ELF procedure in each direction. The bare steel deck diaphragms will be designed using the same seismic performance factors used for the wood structural panel diaphragm provided in Section 5.1.2. The diaphragm period needs to be calculated using the following equation per ASCE/SEI 7-22 Section 12.10.4.2.1:

$T_{diaph} = 0.001L_f$

The design spectral accelerations, $S_{DS} = 1.0$ and $S_{D1} = 0.6$, will be same as the traditional design practice example in Chapter 3 and as followed in Section 5.1.2 for the wood diaphragm example.

### 5.2.3 Diaphragm Design Coefficient, $C_s$, Using the ELF Procedure

Because the flexible diaphragm is supported by the significantly stiffer rigid shear walls, the diaphragm will be viewed as a separate structure with its base at the roof-to-wall interface. Using the ELF procedure summarized in Section 5.1.3, the diaphragm design coefficient for the bare steel deck diaphragm is

$$C_{s\text{-}diaph} = \frac{S_{DS}}{R_{diaph} / I_e} = \frac{1.0}{4.5 / 1.0} = 0.222 \qquad \text{ASCE/SEI 7-22 Eq 12.10-16a}$$

Since it could be possible that the upper bound for $C_{s\text{-}diaph}$ using Equation 12.10-16b governs due to high flexibility of long-span diaphragms, the approximate fundamental period of the diaphragm in each orthogonal axis direction must be considered. The north/south (transverse) loading direction will be considered first, followed by the east/west (longitudinal) loading direction.

**North/South Direction**

$T_{wall}$ was previously determined in Section 4.1, and $T_{diaph}$ can be calculated as follows:

$T_{diaph} = 0.001(400 \text{ ft}) = 0.400 \text{ sec}$

$T_{wall} = 0.136 \text{ sec}$

As discussed in section 5.1.3, ASCE/SEI 7-22 requires design of the diaphragm for its own approximate period using equations in ASCE/SEI 7-22 Section 12.10.4.2.1 without including the walls' contribution.

For the purposes of determining the diaphragm's design force, a check of the upper limit for $C_{s\text{-}diaph}$ is necessary where $T \leq T_L$. Using the diaphragm period $T_{diaph} = 0.400$ seconds, $C_{s\text{-}diaph}$ need not be greater than:

$$C_{s\text{-}diaph} = \frac{S_{D1}}{T_{diaph}\left(R_{diaph} / I_e\right)} = \frac{0.6}{0.400\left(4.5/1.0\right)} = 0.333$$

ASCE/SEI 7-22 Eq. 12.10-16b

The fundamental period is shorter than the transition period, $T_s$, equal to 0.6 seconds, so the fundamental period is on the design spectrum's constant acceleration plateau and Eq. 12.10-16b does not control.

Thus:

$C_{s\text{-}diaph} = 0.222$

Substituting into Equation 12.10-15, we obtain the diaphragm force equation for the north/south direction of the structure, which is used to determine the design forces acting on the diaphragm.

$F_{px\ N/S} = C_{s\text{-}diaph} w_{px}$

$F_{px\ N/S} = 0.222 w_{px}$

**East/West Direction**

$T_{wall}$ was previously determined in Section 4.1, and $T_{diaph}$ can be calculated as follows:

$T_{diaph}$ = 0.001(200 ft) = 0.200 sec

$T_{wall}$ = 0.096 sec

By definition, RWFD buildings require the vertical portions of the SFRS to be stiffer than the horizontal diaphragm, and the use of a shear wall system in the east/west direction complies with this requirement under ASCE/SEI 7-22 Section 12.10.4.1.

Checking the upper limit for $C_{s\text{-}diaph}$ where $T \leq T_L$:

$$C_{s\text{-}diaph} = \frac{S_{D1}}{T_{diaph}\left(R_{diaph} / I_e\right)} = \frac{0.6}{0.200\left(4.5/1.0\right)} = 0.666$$

ASCE/SEI 7-22 Eq. 12.10-16b

The fundamental period is short enough to be on the design spectrum's plateau and Equation 12.10-16b does not control, thus:

$C_{s\text{-}diaph} = 0.222$

Substituting into Equation 12.10-15, we obtain the diaphragm force equation for the east/west direction of the structure, which is used to determine the design forces in the diaphragm.

$$F_{px\ E/W} = C_{s\text{-}diaph} w_{px}$$
$$F_{px\ E/W} = 0.222 w_{px}$$

The uniformly distributed diaphragm design load $0.222w_{px}$ in the north/south and east/west directions are different than the traditional practice value of $0.25w_p$. These differences are attributed to better distribution of yielding along the diaphragm spans reflected in the response modification coefficient ($R_{diaph}$ =4.5 instead of $R$ = 4, noting here that $R_{diaph}$ would not change even if the vertical SFRS system $R$ changed due to the selection of a different system). However, this increase in $R_{diaph}$ also requires an amplification of design shear in the end regions of the diaphragm, as detailed in Section 5.2.5. This amplification of the diaphragm design shears is effectively a local reduction of $R_{diaph}$ relative to a value of 4.5 in the diaphragm end regions.

### *5.2.4 Diaphragm Forces Using the ELF Procedure*

Using our flat-beam analogy, north/south seismic forces are resisted by shear walls on grid lines A and J, and east/west seismic forces are resisted by shear walls on grid lines 1 and 5. A uniformly distributed load across this flat-beam is illustrated in Figure 5-8.

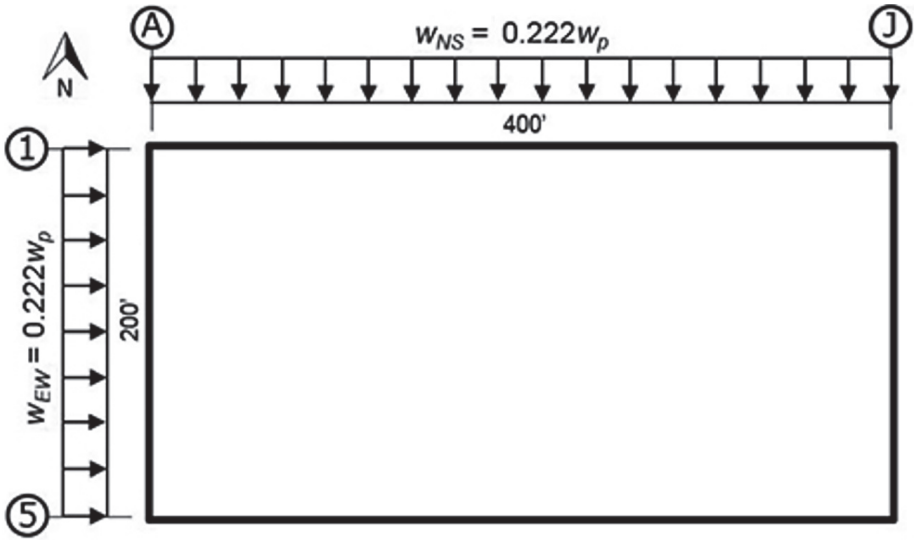


Figure 5-8 Diaphragm loading model (alternative RWFD procedure).

The uniform loads $w_{NS}$ and $w_{EW}$ applied laterally to the diaphragm are computed using the diaphragm lengths and unit weights, and the tributary wall heights and unit weights:

$$w_{NS} = 0.222(12\text{ psf})(200') + 2\left[0.222(116\text{ psf})33'\left(\frac{33'}{2}\right)\left(\frac{1}{30'}\right)\right]$$

$$= 1468\text{ plf}$$

$$w_{EW} = 0.222(12\text{ psf})(400') + 2\left[0.222(116\text{ psf})33'\left(\frac{33'}{2}\right)\left(\frac{1}{30'}\right)\right]$$

$$= 2000\text{ plf}$$

where:

Roof dead load = 12 psf

Wall dead load = 116 psf (9¼" thick at 150 pcf)

Roof height = 30'-0"

Top of wall = 33'-0" (above floor)

The maximum design shears are now computed using simple statics on the uniformly loaded flat beam model. Because of the building's symmetry, diaphragm shear $V_{NS}$ at grid lines A and J will be equal (see Figure 5-9).

North-south diaphragm shear:

$$V_{NS} = w_{NS}\frac{L}{2} - 1468\frac{400\text{ ft}}{2} = 293{,}600\text{ lbs}$$

North-south unit shear:

$$v_{NS} = \frac{v_{NS}}{200\text{ ft}} = \frac{293{,}600}{200\text{ ft}} = 1468\text{ plf, maximum}$$

East-west diaphragm shear:

$$V_{EW} = w_{EW}\frac{L}{2} = 2000\frac{200\text{ ft}}{2} = 200{,}000\text{ lbs}$$

East-west unit shear:

$$v_{EW} = \frac{V_{EW}}{400\text{ ft}} = \frac{200{,}000}{400\text{ ft}} = 500\text{ plf, maximum}$$

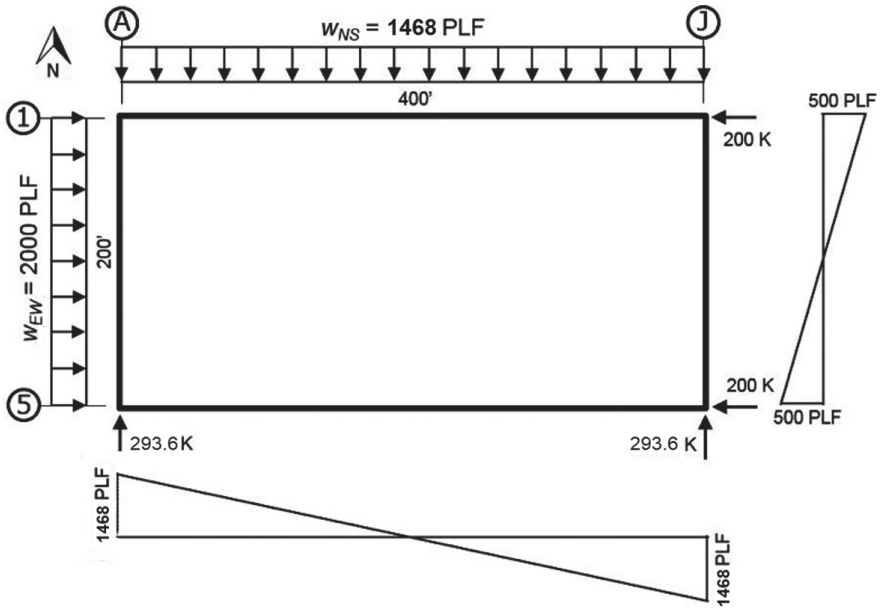


Figure 5-9 Diaphragm shear distribution.

### *5.2.5 North/South Diaphragm Shear Design*

The diaphragm design for the shears follows a similar approach as that outlined in Section 3.5, which illustrates traditional practice. In Section 5.2.4 above, the maximum diaphragm shears were determined for each orthogonal direction; but as mentioned earlier, performance was found to improve when inelastic behavior was better distributed, and this was accomplished in part by providing overstrength in the amplified shear boundary zones of the diaphragm. More specifically, 10 percent of the diaphragm's length ($0.10L$) at each end is designed for 1.5 times the original computed diaphragm shear. Figure 5-10 illustrates the design shear distribution across the diaphragm in each direction.

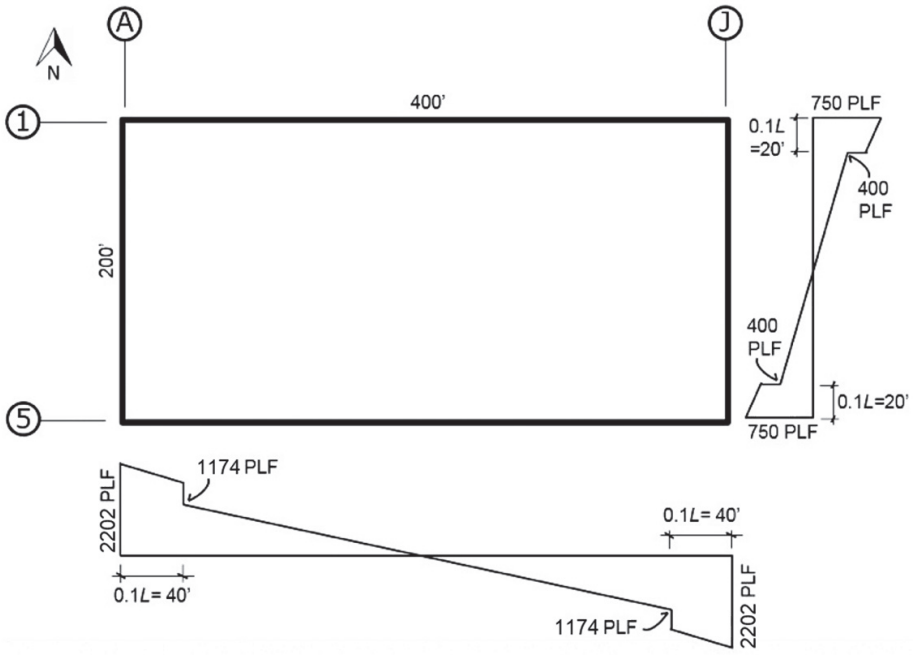


Figure 5-10 Shear diagrams for the diaphragm design with the 1.5× factor.

As observed in Figure 5-10, the worst unit shear demand is in the north/south direction with $v_{NS} = 1468 \times 1.5 = 2202$ plf. Consistent with Section 3.5 for current design, an LRFD approach will be followed:

$$v_{NS\ (LRFD)} = 1.0 v_{NS} = 2202 \text{ plf}$$

$$v_{EW\ (LRFD)} = 1.0 v_{EW} = 750 \text{ plf}$$

Similar to Section 3.5.2 for traditional bare steel deck diaphragm design, the nominal diaphragm shear capacities are calculated per AISI-S310-20 for different combinations of steel deck thickness, fastener type, and spacing. Alternatively, the design values can be taken from the design tables of DDM04 or manufacturers' design tables or software.

Per AISI S310-20 Table B1.1-1, the LRFD seismic design values are obtained by multiplying by a resistance factor ($\phi$) of 0.7 when the strength of mechanical fasteners limits shear strength. When the diaphragm shear strength is limited by shear buckling, the design values are obtained by multiplying by a resistance factor ($\phi$) of 0.8.

The steel deck panel type and thickness, steel deck material, connection type, pattern of the steel deck structural connection perpendicular and parallel to the steel deck ribs, sidelap screw size, and the slide lap connector spacing are selected to satisfy AISI S400-20 Section F3.5.1.

**Design Solution**

- 1.5-inch WR (see Figure 3-6), 16 gage nestable steel deck ($F_y$ = 50 ksi, $F_u$ = 62 ksi)
  - Design thickness = 0.0598 inches
  - Support fastening: PAF with shaft diameter, $d_s$ = 0.16 inches
  - Side-lap fastening: #14 screws @ 6" o.c. within joist span
  - Fastener layout: 36/7 (see Figure 3-7)
  - Span: 6.25 feet
- Shear strength limited by fasteners: $\phi_{df} S_{nf}$ = (0.7)3412 = 2388 plf (LRFD)
- Shear strength limited by buckling: $\phi_{db} S_{nb}$ = (0.8)10358 = 8286 plf (LRFD)
- CAPACITY = min $(\phi_{df} S_{nf}, \phi_{db} S_{nb})$ = 2388 plf (LRFD)
- $v_{NS(LRFD)}$ = 2202 plf < 2388 plf OK

The selected PAF for the structural connection and the selected fastener size for the sidelap connection conform to the special seismic detailing requirements of AISI S400-20 Section F3.5.1.1 and Section F3.5.1.2, as further discussed in Appendix D. Accordingly, the selected bare steel deck meets the special seismic detailing requirements per AISI S400-20 Section F3.5 and is eligible to use the $R_{diaph}$ = 4.5 utilized in this design. Ramifications of not meeting the detailing requirement are discussed in Section 5.2.12.

It is not efficient for a building this size to install the heavy steel deck and fastening at the boundary over the entire roof structure. For this example, Table 5-4 identifies a series of diaphragm zones that may be utilized at different portions of this building. The LRFD shear values are calculated per AISI S310-20, which generally requires some iteration to find the desired capacities.

**Table 5-4 Diaphragm Design Zones**

| 1.5-inch WR Nestable ($F_y$ = 50 ksi, $F_u$ = 62 ksi)<br>Span (Joist Spacing) = 6.25 ft<br>Support Fastening: PAF (shaft diameter, $d_s$ = 0.16 in.) | | | | | | |
|---|---|---|---|---|---|---|
| **Zone** | **Steel Deck** | **Steel Deck Design Thickness** | **Support Fastener Layout** | **Side-lap Fastener** | **Side-lap Fastener Spacing** | **LRFD Shear Resistance** |
| 4 | 16 gage | 0.0598 in. | 36/7 | #14 Self-drilling Screw | 6.0 in. | 2388 plf |
| 3 | 18 gage | 0.0474 in. | 36/7 | #14 Self-drilling Screw | 6.0 in. | 1905 plf |
| 2 | 20 gage | 0.0358 in. | 36/7 | #12 Self-drilling Screw | 8.3 in. | 1135 plf |
| 1 | 22 gage | 0.0295 in. | 36/7 | #10 Self-drilling Screw | 9.3 in. | 818 plf |

At the diaphragm boundaries (grid lines A and J), Zone 4 was determined to be acceptable. Assuming a base unit of joists spaced at 6.25 feet, all transitions would occur in 6.25-foot increments. The 16 gage deck employed in Zone 4 is heavy and transition to a lighter gage deck would likely be made as quickly as possible. Here, per Table 5-4 and Table 5-5, the zones are stepped down from 16 gage to 22 gage as efficiently as possible. Final selection of the length of the end zone, and all specified zones is an optimization between materials, fabrication, and erection costs—the provided solution is just one possible answer.

**Table 5-5 Diaphragm Zone Shear Checks**

| Zone | Distance from Boundary | Strength Level Unit Shear | LRFD Unit Shear | LRFD Shear Resistance |
|---|---|---|---|---|
| 4 | 0 | $v_{max}$ = 2202 plf | $v_{LRFD}$ = 2202 plf | 2388 plf |
| 3 | 37.5 feet | $v_{max}$ = 1789 plf | $v_{LRFD}$ = 1789 plf | 1905 plf |
| 2 | 62.5 feet | $v_{max}$ = 1009 plf | $v_{LRFD}$ = 1009 plf | 1135 plf |
| 1 | 100 feet | $v_{max}$ = 734 plf | $v_{LRFD}$ = 734 plf | 818 plf |

The resulting zone layout for the north/south loading is shown in Figure 5-11.

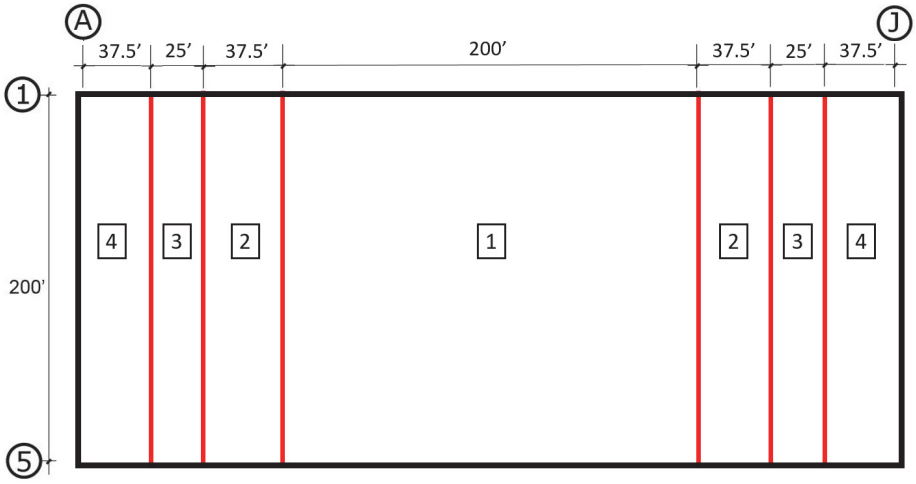


Figure 5-11 North/south zone layout.

### 5.2.6 North/South Diaphragm Shear Transfer to Walls and Collectors

As the diaphragm shear reaches the diaphragm boundary, this seismic force must be transferred to the vertical SFRS, or as in this example the concrete shear walls. Steel angles or channels bolted to the inside face of the shear walls are common in this application when parapets are desired. With the alternative RWFD design procedure, the diaphragm boundary connectors to the steel support/ledger and the support/ledger to the inside face of the shear walls are designed using the diaphragm shear force with the 1.5 shear amplification factor to encourage the spreading of yielding within the diaphragm.

Collector connection capacities into the concrete or masonry shear walls shall comply with ACI 318-19 or TMS 402-16 provisions, respectfully.

### 5.2.7 North/South Diaphragm Chord Design

As illustrated in the traditional practice design of Section 3.6, these chords are selected to be steel ledger angles at the roof line. Chord forces are determined using simple flat horizontal beam statics as shown in Figure 3-6, and the design force is a uniformly distributed load without the 1.5 shear amplification design factor. Maximum chord forces will occur at the center of the diaphragm's span where the maximum moment occurs.

The maximum tensile chord force for the building example is determined as follows:

$$T = \frac{M}{B} = \frac{w_{NS}L^2}{8B} = \frac{1468 \text{ plf}\left(400\right)^2}{8\left(200\right)} = 146{,}800 \text{ lbs}$$

The chord is designed here using LRFD with ASTM A36 Steel ($F_y$ = 36 ksi). Consulting ASCE/SEI 7-22 Section 2.3.6, the applicable LRFD load factor for seismic forces is 1.0. The area of steel required is:

$$A_S = \frac{T}{\phi F_y} = \frac{146.8}{0.9(36)} = 4.53 \text{ in.}^2$$

Using an L5×5×1/2 rolled steel angle satisfies this chord demand.

L5×5×1/2 Steel Area $A_S = 4.75 \text{ in.}^2 > 4.53 \text{ in.}^2$

This chord size is smaller than that found using the traditional design practice, primarily because the diaphragm seismic design force is less due to the impact of the higher response modification factor.

### 5.2.8 East/West Diaphragm Shear Design

In Section 5.2.5, the maximum factored diaphragm shear in the east/west direction was determined to be $v_{EW(LRFD)}$ = 750 plf (unfactored), including the 1.5 shear amplification factor. AISI S310-20 design method is used to determine the diaphragm shear capacity. Comparing the diaphragm's shear demand with the capacities in Table 5-5, Zone 1 is selected:

$v_{EW(LRFD)}$ = 750 plf < 818 plf (Zone 1)

Thus, the diaphragm layout per Figure 5-11 is adequate for the east/west direction.

### 5.2.9 East/West Diaphragm Shear Transfer to Walls and Collectors

Similar to the north/south diaphragm force design, the seismic diaphragm shears must be transferred to the vertical concrete shear walls. As discussed in Section 5.2.6, the shear transfer is designed with the 1.5 shear amplification factor.

Unlike the north/south force direction, the diaphragm boundaries resisting east/west seismic forces along grid lines 1 and 5 do not have uniform boundary fastening. While most of the length contains Zone 1 requirements, the first and last 62.5 feet of this wall line contain Zone 3 and 4 requirements, whose stiffness may attract more load. In this example, as well as that designed to traditional practice, there is a possibility that the shear transfer to the steel ledger angle is non-uniform; however, the steel angle is designed as the diaphragm chord in Section 5.2.7 and contains sufficient capacity to drag and redistribute the shear load appropriately to the shear wall elements. This is especially true when the diaphragm chord design is based on the maximum force at midspan, yet the chord design remains consistent along the entire wall line. This discussion is simply an observation of predicted behavior;

however, traditional design practice routinely assumes a uniform shear transfer into the wall line.

### 5.2.10 East/West Diaphragm Chord Design

The chord design in east/west direction is similar to the chord design in structural wood design example provided in Section 5.1.10. Thus, L4×4×1/4 hot-rolled steel angle satisfies the chord demand.

### 5.2.11 Second Stage—Shear Wall Force Using the ELF Procedure

The second stage of the two-stage analysis involves the design of the heavy in-plane shear walls. This section illustrates this design procedure in each orthogonal direction on the example building.

As discussed in Section 5.1.11, the building is evaluated as two different seismically behaving portions, and therefore the force to the in-plane shear walls will have two significant components. The flexible diaphragm with its tributary mass will generate a lateral force near the top of the wall, $F_{v1}$. Additionally, the rigid concrete in-plane walls have significant self-weight that will also generate lateral forces near their centers of mass, $F_{v2}$.

First, diaphragm forces imparted into the shear walls will be converted to be consistent with the expected seismic performance of an intermediate precast shear wall system. The diaphragm forces used for the design of the shear walls below will not include the 1.5 shear amplification factor used to design the diaphragm end regions.

As determined previously in Section 5.2.4, the diaphragm reactions to the shear walls based on $R_{diaph} = 4.5$ are as follows.

North/south diaphragm reactions:

$F_p = V_{NS} = 293{,}600$ lbs

East/west diaphragm reactions:

$F_p = V_{EW} = 200{,}000$ lbs

These diaphragm reaction forces need to be amplified to an appropriate shear wall design force.

North/south:

$$F_{v1} = F_p \times \left( \frac{R_{diaph}}{R / \rho} \right)$$

where:

$$\left(\frac{R_{diaph}}{R/\rho}\right) = \frac{4.5}{4/1.0} = 1.125 > 1.0 \text{ OK}$$

$F_{v1}$ = 293,600 × 1.125

$F_{v1}$ = 330,300 lbs

East/west:

$$F_{v1} = F_p \times \left(\frac{R_{diaph}}{R/\rho}\right)$$

where:

$$\left(\frac{R_{diaph}}{R/\rho}\right) = \frac{4.5}{4/1.0} = 1.125 > 1.0 \text{ OK}$$

$F_{v1}$ = 200,000 × 1.125

$F_{v1}$ = 225,000 lbs

Second, the lateral seismic force generated from the wall self-weight must be included for design. The wall self-weight will have a seismic response unique to its own period of vibration; therefore, the ELF procedure's base shear equation will be evaluated.

ASCE/SEI 7-22 Section 12.8.1 defines the seismic base shear as:

$V = C_s W$ ASCE/SEI 7-22 Eq. 12.8-1

where $C_s$ is calculated in Section 5.1.11:

$C_s$ = 0.25

Substituting into ASCE/SEI 7-22 Equation 12.8-1, we obtain the lateral force $F_{v2}$ equation for the shear wall self-weight, $W_{p\text{-}wall}$, for the north/south direction of the structure.

$F_{v2} = C_s W = 0.25 W_{p\text{-}wall}$

The wall self-weight, $W_{p\text{-}wall}$, is computed as:

$W_{p\text{-}wall}$ = 116 psf × 200 ft × 33 ft = 765,600 lbs

Therefore:

$F_{v2} = 0.25 W_{p\text{-}wall} = 0.25(765{,}600) = 191{,}400$ lbs

Therefore, the total shear wall design force, $F_v$, for the north/south direction is:

$F_v = F_{v1} + F_{v2} = 330{,}300 + 191{,}400$

$F_v$ = 521,700 lbs or 521.7 kips

The east/west load direction is similar to the structural wood example in Section 5.1.11, where:

$F_v$ = 607,800 lbs or 608 kips

Figure 5-12 and Figure 5-13 (similar to Figure 5-7) illustrate the forces acting on the shear walls providing lateral resistance in the north/south and east/west directions, respectfully. The design forces at the base of the shear walls are 522 kips north/south and 608 kips east/west. These forces include the entire weight of the walls and are appropriate for the design of shear forces that transfer to the slab on ground or foundation.

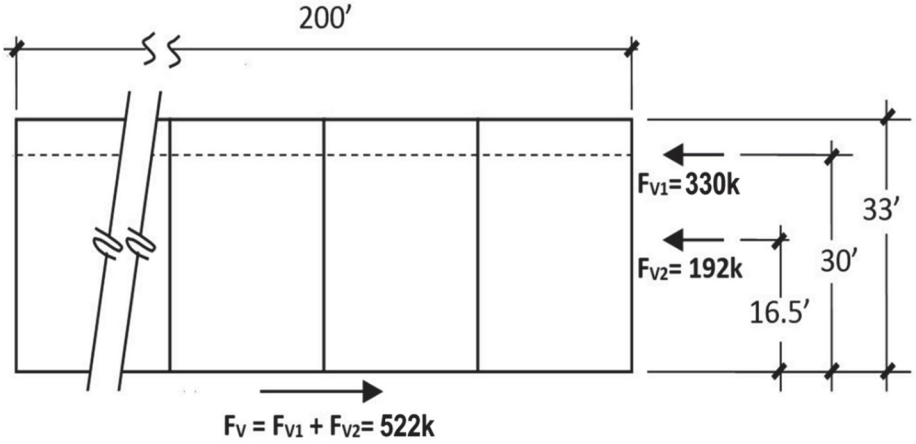


Figure 5-12 North/south lateral design forces acting on the shear walls (Lines A & J).

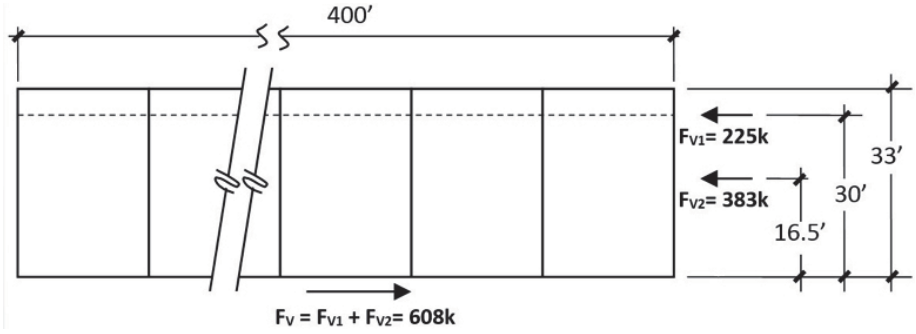


Figure 5-13 East/west lateral design forces acting on the shear walls (Lines 1 & 5) (repeated).

### *5.2.12 Bare Steel Deck Diaphragm Design with Welded Connectors (Non-Conforming to Special Seismic Detailing)*

For bare steel deck diaphragms that do not meet the special seismic detailing requirements in Section F3.5 of AISI S400-20, $R_{diaph}$ = 1.5 per ASCE/SEI 7-22, and a near-elastic design is enforced. As detailed in Torabian and Schafer (2021) and discussed in Appendix D, this generally applies for bare steel deck diaphragms with welded structural connectors. Appendix D

details that although welds have remarkable stiffness and strength, with traditional detailing they have limited ductility, limited post-peak residual force capacity, and strong degradation under cyclic loads. Although some system-level ductility is still possible in welded bare steel deck diaphragm systems, their redistribution potential is limited and near elastic design is recommended. See Appendix D for a complete discussion.

Here we provide the calculations summarizing the impact of using $R_{diaph}$ = 1.5; however, a complete design is not provided. For this case, the diaphragm's seismic design coefficient for bare steel deck is:

$$C_{s\text{-}diaph} = \frac{S_{DS}}{R_{diaph} / I_e} = \frac{1.0}{1.5 / 1.0} = 0.67 \qquad \text{ASCE/SEI 7-22 Eq 12.10-16a}$$

Again, the upper bound for $C_{s\text{-}diaph}$ should be checked.

**North/South Direction**

Using the diaphragm period $T_{diaph}$ = 0.4 seconds, $C_{s\text{-}diaph}$ need not be greater than:

$$C_{s\text{-}diaph} = \frac{S_{D1}}{T_{diaph}\left(R_{diaph} / I_e\right)} = \frac{0.6}{0.400\left(1.5 / 1.0\right)} = 1.0$$

ASCE/SEI 7-22 Eq. 12.10-16b

Equation Eq. 12.10-16b does not control, therefore:

$C_{s\text{-}diaph} = 0.67$

and the design forces acting on the diaphragm are:

$F_{px\ N/S} = C_{s\text{-}diaph} w_{px}$

$F_{px\ N/S} = 0.67 w_{px}$

**East/West Direction**

In the east/west direction $T_{diaph}$ = 0.2 seconds and checking the upper limit for $C_{s\text{-}diaph}$ where $T \le T_L$

$$C_{s\text{-}diaph} = \frac{S_{D1}}{T_{diaph}\left(R_{diaph} / I_e\right)} = \frac{0.6}{0.200\left(1.5 / 1.0\right)} = 2.0$$

ASCE/SEI 7-22 Eq. 12.10-16b

Equation Eq. 12.10-16b does not control, therefore:

$F_{px\ E/W} = 0.67 w_{px}$

The implications of these force levels are significant. The required unit shears to be carried are summarized in Figure 5-14 and may be compared with Figure 5-10 for a bare steel deck that meets the special seismic detailing.

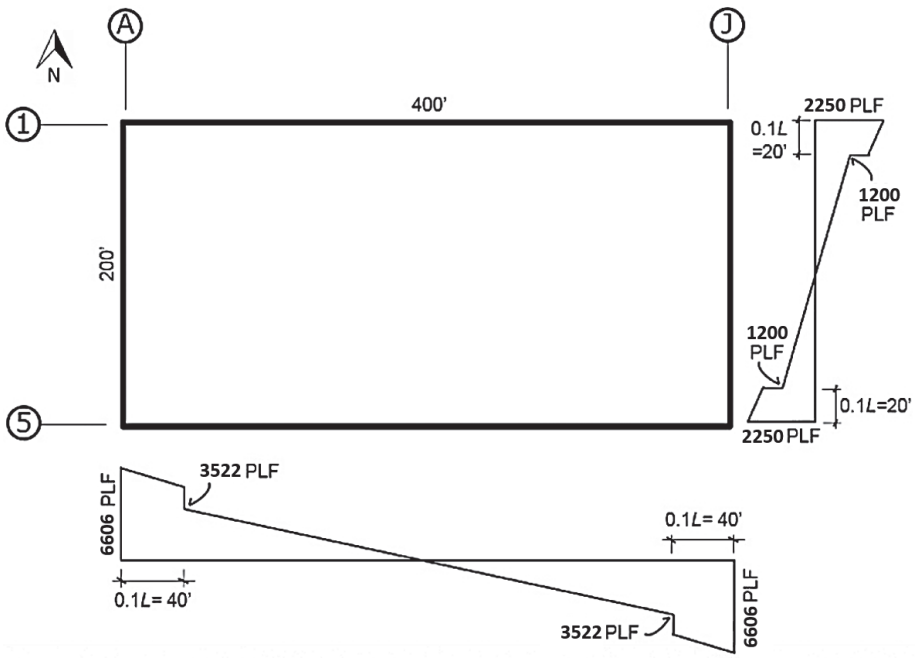


Figure 5-14 Shear diagrams for the diaphragm design with the 1.5x factor in the base of a steel deck roof that does not meet special seismic detailing.

**Design Solution**

- 1.5-inch WR, 16 gage nestable steel deck ($F_y$ = 50 ksi, $F_u$ = 62 ksi)
  - Design thickness = 0.0598 inches
  - Support fastening: 3/4-inch arc spot weld
  - Side-lap fastening: top arc seam weld, L = 1.5 inches E60-XX @ 6" o.c.
  - Fastener layout: 36/14/7
  - Span: 6.25 feet
- Shear strength limited by fasteners: $\phi_{df} S_{nf}$ = (0.55)13904 = 7647 plf (LRFD)
- Shear strength limited by buckling: $\phi_{db} S_{nb}$ = (0.8)10358 = 8286 plf (LRFD)
- CAPACITY = min ($\phi_{df} S_{nf}$, $\phi_{db} S_{nb}$) = 7647plf (LRFD)
- $v_{NS(LRFD)}$ = 6606 plf < 7647 plf OK

To meet the maximum demands would require 50 ksi, 16 gage deck with 36/14/7 arc spot weld (diameter = 0.75 inches) pattern and 1.5-inch top arc seam welded sidelap spaced no more than 6 inches, as shown above. This demonstrates that the expected elastic demands on the roof are significant

and represent a significant departure from the traditional design of Chapter 3. Traditional practice, where the vertical SFRS is assumed to provide ductility for the diaphragm, provides a significant reduction in diaphragm demands. Here, consistent with studied RWFD building behavior, the vertical and horizontal systems are separated and the diaphragm itself must provide ductility to receive a reduction in seismic force levels. Appendix D discusses this in more detail.

In comparison to traditional design, the near-elastic-level diaphragm forces are significantly greater. It is worth noting that if the diaphragm span is quite long (and thus the period is quite long) or the vertical SFRS is non-ductile (and thus the response modification factor, *R*, is quite low), the near-elastic-level demands on the diaphragm for a bare steel deck diaphragm that does not meet the special seismic detailing requirements can be much closer or even lower in comparison to traditional design.

## 5.3 Limitations and Adaptations of the Alternative RWFD Design Procedure

The alternative RWFD design procedure was presented in this chapter for a very basic single-story, rectangular building with solid walls and no interior vertical SFRS elements. Often the design of much larger buildings is necessary, and these situations often require interior vertical elements of the SFRSs to keep the diaphragm shears manageable. For these one-story buildings with multiple-span diaphragms, each diaphragm span can be evaluated separately, and appropriately combined and adjusted as the design load is brought to the vertical SFRS.

As part of the ASCE/SEI 7-22 alternative RWFD design procedure, Section 12.10.4.1 identifies a series of seven limitations, all of which must be met in order to use the procedure. These are:

- All portions of the diaphragm are to be designed using the alternative RWFD procedure in both orthogonal directions. Mixing of diaphragm design procedures is not permitted. Adjacent diaphragms occurring at close enough elevations that they will be interacting are recommended to be designed with the same procedure so that the same behavior can be anticipated; interaction of diaphragms designed using mixed procedures has not been studied.
- The diaphragm is to consist of either:
    - A wood structural panel diaphragm designed in accordance with SDPWS-2021 and fastened to wood framing members or wood

nailers with sheathing nailing in accordance with the SDPWS-2021 Section 4.2 nominal shear capacity tables, or

- A bare steel deck diaphragm meeting the requirements of AISI S400-20 and AISI S310-20.

- Toppings of concrete or similar materials that affect diaphragm strength or stiffness are not to be placed over the wood structural panel or bare steel deck diaphragm. Where toppings affect the stiffness of the diaphragm, the computation of the diaphragm period and resulting diaphragm design forces are outside of what is included in the design procedure. Prohibited materials are noted in the ASCE/SEI 7-22 commentary.
- The diaphragm does not contain horizontal structural irregularities, as specified in ASCE/SEI 7-22 Table 12.3-1, except that Horizontal Structural Irregularity Type 2 is permitted. Reentrant corners are thought to be prevalent in the building stock. Because flexible diaphragms are dominated by shear deformation behavior, reentrant corners are not thought to influence seismic performance in a manner that would make inclusion inappropriate.
- The diaphragm is rectangular in shape or is divisible into rectangular segments for purpose of seismic design, with vertical elements of the SFRS or collectors provided at each end of each rectangular segment span. This limitation prohibits use of the procedure for buildings with walls that are at an angle to the primary axes or are curved. It requires that there be a stiff vertical element of the SFRS supporting all four sides of each rectangular segement, whether the diaphragm is directly connected to the vertical element or connected through a collector. Cantilevered diaphragms or diaphragms that resist forces through rotation are not permitted; this exclusion includes buildings with "C-shaped" lateral resisting configurations with concrete or masonry walls on three sides and no vertical SFRS on the fourth side.
- The vertical elements of the SFRS are limited to one or more of the following:
  - concrete shear walls,
  - precast concrete shear walls,
  - masonry shear walls,
  - steel concentrically braced frames,
  - steel and concrete composite braced frames, or

- steel and concrete composite shear walls.

  The list of vertical systems allowed is intended as a simple and direct means to limit application to vertical systems that are sufficiently rigid compared with the diaphragms. The systems in this list were identified for inclusion in the design procedure based on being judged to be inherently rigid at design and maximum-considered-earthquake force levels for in-plane force relative to the diaphragm's anticipated flexibility. Should the vertical SFRS elements not be rigid compared to the diaphragm, use of this alternative RWFD design procedure might be of reduced benefit. Refer to Section 8.1.1 for further discussion on the use of less-stiff braced frames, such as tension-only braces.

- The vertical elements of the seismic-force-resisting system are designed in accordance with Section 12.8, except that they shall be permitted to be designed using the two-stage analysis procedure of Section 12.2.3.4, where applicable.

All of the ASCE/SEI 7-22 Section 12.10.4.1 limitations are discussed in the ASCE/SEI 7-22 commentary. Notably, these limitations are intended to bring the systems in-line with the assumptions inherent in the development of the alternative RWFD design procedure presented herein.

Situations involving two or more stories, non-rectangular diaphragm systems, vertical SFRSs outside the limitations of ASCE/SEI 7-22 Section 12.10.4.2.1, and other characteristics beyond these scoping provisions have not been properly evaluated to determine whether the alternative RWFD design procedure is appropriate. Caution is needed before this design procedure is applied to situations that fall outside of the archetype inventory that was investigated. Some areas for further study are listed in Chapter 8.

# Chapter 6
# Diaphragm Deflection Check

Seismic ground motion typically causes more lateral deformation in the diaphragm than in the walls of RWFD buildings. The magnitude of the diaphragm deflections can be large enough to impact the building's structural integrity, compromise the attached non-structural elements, or cause the building to pound against adjacent structures. Large diaphragm deflections may also result in excessive *P*-delta effects, causing instability that leads to collapse.

ASCE/SEI 7-22 Section 12.12.2 limits diaphragm deflections to the amount that will permit the attached elements to maintain their structural integrity and continue supporting their prescribed loads. The intent is to prevent substantial damage to structural elements and their connections, the failure of which can lead to local structural collapse. This requirement is also intended to prevent excessive *P*-delta effects that could lead to sidesway collapse. For non-structural elements, the intent is to prevent failure of connections that could result in a localized collapse hazard. To evaluate these aspects of structural design, the engineer needs to compute the approximate building deformation as a combination of the deflection of the diaphragm and the vertical elements of the SFRS.

## 6.1 Wood Diaphragm Building Deflection Checks

### *6.1.1 Deflection of North/South Diaphragm*

For the wood diaphragm building example, the diaphragm deflection in the north/south direction will be greater than that in the east/west direction, and thus only the north/south direction will be checked. Procedures for computing horizontal diaphragm deflections under lateral loading are found in SDPWS-2021. Equation 4.2-1 in Section 4.2.3 provides a simplified method of computing deflections of wood structural panel diaphragms by considering the contribution of flexural bending, shear deformation, nail slip and chord slip.

$$\delta_{dia} = \frac{5vL^3}{8EAW} + \frac{0.25vL}{1000G_a} + \frac{\sum x\Delta_c}{2W} \qquad \text{SDPWS-2021 Eq. 4.2-1}$$

where:

$\delta_{dia}$ = maximum mid-span diaphragm deflection determined by elastic analysis, in.

$v$ = Maximum diaphragm shear, ft (assuming a uniformly loaded rectangular diaphragm)

$L$ = horizontal span of diaphragm, ft

$W$ = diaphragm span depth, ft

$E$ = chord's modulus of elasticity, psi

$A$ = cross-sectional area of chord, in.$^2$

$G_a$ = apparent diaphragm shear stiffness, kips/in

$\Delta_c$ = chord slip at each connection, in.

$x$ = distance from chord splice to nearest support, ft

For our diaphragm example, the following parameters are determined below:

$v$ = 1104 plf (Section 5.1.4)

$L$ = 400 ft

$W$ = 200 ft

$E$ = 29,000,000 psi

$A$ = L5×5×5×3/8 = 3.65 in.$^2$ (Section 5.1.7)

$G_a$ = 24 kips/in. Zone 1 (Table 4.2A)

= 15 kips/in. Zone 2 (Table 4.2A)

= 20 kips/in. Zone 3 (Table 4.2A)

= 51 kips/in. Zone 6 (Table 4.2B)

$\Delta_c$ = 0 (welded chord connections assumed with no slip)

The contribution from flexural deformation ($5vL^3/8EAW$) is derived from a horizontal beam with a uniformly applied distributed load. The term $EA$ represents in this example the steel chord stiffness; however, the concrete walls themselves can also provide significant flexural stiffness to the diaphragm. Therefore, this equation generally overestimates the flexural contribution to diaphragm displacement.

$$\delta_{dia\ flexure} = \frac{5vL^3}{8EAW} = \frac{5(1104\text{ plf})(400\text{ ft})^3}{8(29{,}000{,}000\text{ psi})(3.65\text{ in}^2)(200\text{ ft})} = 2.09\text{ in.}$$

The panel shear deformation and nail slip contribution (0.25vL/1,000Ga) is derived from a horizontal beam with a uniformly applied distributed load, uniform shear stiffness, and uniform diaphragm nailing. In general, the shear deformation between two points at distance, $L_i$, apart, under constant shear, $v$,

is simply $vL_i/G_a$. In a simply supported beam with a uniformly distributed load, the shear is not constant but decreases linearly, and thus the average shear, $v_{ave}$, between the two points is applicable, $v_{ave}L_i/G_a$. Because the average shear is half the maximum shear, $v_{ave} = 0.5v$, and the distance to the maximum deformation at midspan, $L_i$, is half the total span, $L$:

$$L_i = 0.5L \tag{6-1}$$

With the apparent shear stiffness, $G_a$, in kips/inch, the shear deformation contribution becomes:

$$\delta_{dia\ shear} = \frac{v_{ave}L_i}{1000G_a} = \frac{0.5v(0.5L)}{1000G_a} = \frac{0.25vL}{1000G_a} \tag{6-2}$$

This matches the shear deformation term in SDPWS-2021 Equation 4.2-1.

For efficiency reasons, large diaphragms seldom have uniform diaphragm nailing across the building, and thus the shear deformation term needs to be modified. For a diaphragm with various strips of different nailing zones, there are several approaches to this modification. As previously discussed, the shear deformation between two points at distance, $L_i$, apart under an average shear of $v_{ave}$ is:

$$\delta_{dia\ shear} = \frac{v_{ave}L_i}{1000G_a}$$

With multiple nailing zone strips of width, $L_i$, and apparent shear stiffness, $G_{ai}$, in kips/inch, and average shears, $v_{i\ ave}$, the total shear deformation at midspan can be computed as the summation of each strip's contribution between the edge and the midspan of the diaphragm:

$$\delta_{dia\ shear} = \sum \frac{v_{i\ ave}L_i}{1000G_a} \tag{6-3}$$

where:

$v_{i\ ave}$ = the average diaphragm shear within each shear stiffness (nailing) zone

$L_i$ = the length of each shear stiffness zone measured perpendicular to loading

$G_{ai}$ = the apparent shear stiffness of each shear stiffness zone being considered

This approach assumes the nailing zones are continuous strips oriented from north to south, as illustrated in Figure 5-4; however, the east/west diaphragm design caused Nailing Zone 3 to wrap around Nailing Zone 1, as illustrated in Figure 5-5. To simplify the analysis, the additional nailing from Nailing

Zone 3 (north and south of Nailing Zone 1) will be ignored, which will result in an overestimate of diaphragm deformation (conservative). Table 6-1 provides an organized approach to the computation working from grid A to the midspan. This format allows each different nailing zone strip to be evaluated separately.

**Table 6-1 Shear Deformation and Nail Slip Computation Table**

| Nailing Zone | $v_{left}$ (plf) | $v_{right}$ (plf) | $v_{i\ ave}$ (plf) | $L_i$ (ft) | $G_a$ (kip/in.) | $\frac{v_{i\ ave}L_i}{1000G_a}$ |
|---|---|---|---|---|---|---|
| 6 | 1104 | 883 | 994 | 40 | 51 | 0.78 in. |
| 3 | 883 | 574 | 729 | 56 | 20 | 2.04 in. |
| 2 | 574 | 442 | 508 | 24 | 15 | 0.81 in. |
| 1 | 442 | 0 | 221 | 80 | 24 | 0.74 in. |
| | | | | | $\sum$ = | 4.37 in. |

$$\delta_{dia\ shear} = \sum \frac{v_{i\ ave}L_i}{1000G_a} = 4.37 \text{ in.}$$

The chord slip contribution to diaphragm deformation [$(\Sigma(x\Delta_c)/2w$] is assumed to be zero because of the use of welded chord splices ($\Delta_c = 0$).

$$\delta_{dia\ chord\ slip} = \frac{\sum x\Delta_c}{2W} = 0 \text{ in.}$$

Considering all the diaphragm deflection contributions we obtain:

$$\delta_{dia} = \delta_{dia\ flexure} + \delta_{dia\ shear} + \delta_{dia\ chord\ slip} = 2.09 + 4.37 + 0 = 6.46 \text{ in.}$$

Because the applicable load combination involves 1.0$E$, this unfactored diaphragm deflection is also the elastic deflection at strength-based design loads. But recall that the seismic coefficient, $C_s$, in Section 5.3 involves dividing the maximum expected building response by the diaphragm's response modification coefficient, $R_{diaph}$. To properly estimate the diaphragm's maximum expected inelastic deflection, the earlier effects of dividing by $R$ must be reversed in part, and this is accomplished with the use of the deflection amplification factor, $C_{d\text{-}diaph}$. ASCE/SEI 7-22 Equation 12.8-16 may be used to compute the maximum design earthquake displacement of the diaphragm:

$$\delta_{DE\text{-}diaph} = \frac{C_{d-diaph}\delta_{e-dia}}{I_e}$$

$C_{d\text{-}diaph}$ = 3.0 (ASCE/SEI 7-22 Sec. 12.10.4.2.5)

$\delta_{e\text{-}dia}$ = 6.46 in. (an elastic response under strength-level forces)

$I_e$ = 1.0 (importance factor)

$$\delta_{DE\text{-}diaph} = \frac{C_{d-diaph}\delta_{e-dia}}{I_e} = \frac{3.0(6.46)}{1.0} = 19.4 \text{ in.}$$

It is important to recognize that $\delta_{DE\text{-}diaph}$ is based on some very simple and conservative assumptions likely causing it to be significantly overestimated (Lawson, 2019). The following is a list of some of those assumptions used here in determining $\delta_{DE\text{-}diaph}$ = 19.4 in.

- The three-term diaphragm deflection equation (SDPWS-2021 Equation 4.2-1) is a simplification of the more accurate four-term diaphragm deflection equation (SDPWS-2021 Equation C4.2.2-1), as it has combined the panel shear deformation with the nonlinear nail slip deformation contributions. This simplification often will significantly overestimate the deflection, and the use of the four-term equation would reduce this example's total diaphragm deflection calculation by approximately 30 percent.
- The flexural contribution from chord elongation ignores the significant stiffness of the perimeter reinforced concrete walls. Significant stiffness is indirectly obtained from the horizontal steel reinforcing within the concrete walls or the tension capacity of the concrete material itself. In this tilt-up concrete panel building, the steel angle chord acts as a tension/compression chord splice between the wall panels, and its elongation/shortening can be modeled as chord slip in the fourth term of the deflection equation. In this example, modeling the wall panels as chord elements but spliced by the steel angle with compression shortening and tension elongation, the calculation of the combined flexural and chord-slip contribution could potentially reduce in half depending on the steel angle's anchorage configuration to the wall panels. Ignoring the additional chord contributions to stiffness will overestimate the computed deflection.
- The contribution of shear deformations in Table 6-1 ignores extra stiffening caused by Nailing Zone 3 wrapping around the north and south sides of the building diaphragm, thus overestimating the deflection associated with this contribution.
- The shear deformation/nail slip term of SDPWS-2021 Equation 4.2-1 is based on the wider nail spacings at "other panel edges" without any consideration for the closer nail spacings at continuous panel edges that always occur in panelized wood panel roof systems. In this example, the additional edge nailing along the continuous panel edges results in the nail-slip contribution to diaphragm deflection being reduced by

approximately 20 percent. Ignoring this contribution to stiffness will overestimate the deflection.

- The deflection amplification factor, $C_{d\text{-}diaph}$, is 3.0 in this example and is dependent upon the assumptions discussed in Appendix Section C.3. These assumptions could be conservative or nonconservative.

After making adjustments for these conservative assumptions (however, still using $C_d$ = 3.0), it is estimated that the diaphragm deflection $\delta_{DE\text{-}diaph}$ in this example is more likely in the range of 9 inches to 13 inches. This compares more favorably with the design earthquake median diaphragm drift ratio (DDR) = 0.43 percent, reported for its matching archetype in Appendix C Table C-5 (The DDR is approximately equal to the building drift ratio, BDR, for these rigid wall archetypes). This 0.43 percent median DDR is equivalent to a diaphragm deflection of 10.3 inches. It should also be noted that various modeling assumptions were made in the FEMA P695 analyses, and these could have overestimated or underestimated system stiffness. Additionally, different assumptions or simplifications made by designers can also be a source of significant variation in resulting estimated diaphragm deflections.

For comparison, the diaphragm deflection for the traditional wood diaphragm design example illustrated in Chapter 3 can also be obtained. Using the same approach described in this section, the traditional wood diaphragm design has a conservative 29.4-inch deflection, $\delta_{DE\text{-}diaph}$ (using the simplistic three-term equation), but a more refined estimate after making similar adjustments is likely in the range of 15 inches to 20 inches. The larger computed deflections for the diaphragms designed with a traditional design are not a result of less stiffness but instead of higher design forces under the ELF procedure and a higher deflection amplification factor associated with the shear walls.

The computed elastic deflection ($\delta_{e\text{-}dia}$) of the diaphragm allows one to estimate the period of the diaphragm using Wilson's shear beam formula (Equation 4-1) as a guide. For the alternative RWFD design example, the result can be approximated as $T_{diaph} = (0.066\delta_e)^{0.5} = (0.066\times6.46"\times1/0.167)^{0.5}$ =1.6 seconds. Here $\delta_e$ is based on 1.0g of acceleration and the conservative three-term deflection equation, resulting in a period significantly longer than the 0.800 seconds one obtains using the alternative design procedure ($T_{diaph}$ = $0.002L$ = 0.002×400ft = 0.8 seconds for wood structural panel diaphragms). Computing the period using results from the four-term deflection equation with the discussed refinements provides an estimated period range from 1.1 seconds to 1.3 seconds. However, use of a longer period computed by other methods is not permitted for design.

### 6.1.2 Deflection of North/South Walls

It is anticipated that the diaphragm deflection will be the majority of the overall structural deformation; however, shear wall deflection should be added to the diaphragm deflection to obtain the total deformation used to evaluate its impact. The deflection of a cantilever shear wall has two components: a flexural component and a shear component from the following equation:

$$\delta_{wall} = \delta_{wall\ flexure} + \delta_{wall\ shear} \tag{6-4}$$

$$\delta_{wall} = \frac{Ph^3}{3EI} + \frac{1.2Ph}{GA} \tag{6-5}$$

The adjusted load onto the shear wall was computed in Section 5.1.11 as 440 kips, but a portion of this was from the diaphragm acting at the roof ($F_{v1}$ = 248.4 kips), and a portion was from the wall self-weight effectively acting at the mid-height ($F_{v2}$ = 191.4 kips). Thus, one approach to approximate the combined effect of these two forces is to place half the wall force at the roof height with the diaphragm force:

$$P = 248.4 + \frac{191.4}{2} = 344 \text{ kips}$$

$$h = 30 \text{ ft}$$

The material properties and section properties are computed for the eight 25-feet long concrete shear walls (9¼" thick, $f_c' = 4000$ psi):

$$E = 57\sqrt{f_c'} = 3.6 \times 10^3 \text{ ksi}$$

$$G = \frac{E}{2(1+v)} = \frac{3.6\times10^3}{2(1+0.2)} = 1.50 \times 10^3 \text{ ksi}$$

$$I_g = \frac{bh^3}{12} = \frac{9.25(25\times12)^3}{12} \times 8 \text{ walls} = 166.5 \times 10^6 \text{ in.}^4$$

$$A_g = bL = 9.25 \text{ in. } (25 \text{ ft} \times 12) \times 8 \text{ walls} = 22{,}200 \text{ in.}^2$$

The section properties $I_g$ and $A_g$ are for the gross section, but it is possible that the concrete members will crack, which will reduce the effective stiffnesses of the shear walls. ACI 318-19 Table 6.6.3.1.1(a) gives some guidance on approximating the reduced stiffness to determine lateral deflections in concrete members. More specifically, without a more accurate analysis, 35 percent of the gross moment of inertia is a conservative assumption and 100 percent of the gross cross-sectional area may be considered when there are significant portions of solid walls acting as shear wall elements.

$$\delta_{wall} = \frac{Ph^3}{3E(0.35I_g)} + \frac{1.2Ph}{GA_g}$$

$$= \frac{344(30\times12)^3}{3(3.6\times10^3)(0.35\times166.5\times10^6)} + \frac{1.2(344)(30\times12)}{1.5\times10^3\times22{,}200}$$

$$= 0.026 + 0.004 = 0.030 \text{ in.}$$

This contribution from the in-plane walls can also be affected by the stiffness of the foundation and connections to the foundation, but the magnitudes of these values is still expected to be relatively small.

To properly estimate the shear walls' maximum expected deflection, the earlier effects of dividing by response modification coefficient, *R,* must be partially reversed, and this is accomplished with the use of the deflection amplification factor, $C_d$. ASCE/SEI 7-22 Equation 12.8-1615 may be used to compute the maximum expected wall displacement, $\delta_{DE\text{-}wall}$:

$$\delta_{DE\text{-}wall} = \frac{C_d\delta_{e-wall}}{I_e}$$

$C_d$ = 4.0 (ASCE/SEI 7-22 Table 12.2-1)

$\delta_{e\text{-}wall}$ = 0.030 in. (an elastic response under strength-level forces)

$I_e$ = 1.0 (importance factor)

$$\delta_{DE\text{-}wall} = \frac{C_d\delta_{e-wall}}{I} = 0.12 \text{ in.}$$

The total system displacement is the sum of the two deflection components.

$$\delta_{DE} = \delta_{DE\text{-}diaph} + \delta_{DE\text{-}wall} = 19.4 + 0.12 = 19.5 \text{ in.}$$

This is the total estimated inelastic displacement during design seismic forces. As mentioned in Section 6.1.1, the diaphragm deflection component is likely very conservative. It is observed that the contribution from the shear walls is very small and could have been neglected in this situation. One of the prime characteristics of RWFD buildings is that the diaphragm dominates the response of the building, and this is evident here.

### *6.1.3 Limits on Diaphragm Deflection—Second-Order Effects and P-delta Instability*

One potential safety concern with large flexible diaphragms with large deflections is the rise in second-order effects, including *P*-delta instability. In addition, as the roof translates, the tops of columns and walls also translate, resulting in a leaning gravity system that generates additional lateral forces, further exacerbating the deflection, or the interstory drift.

One simple method to evaluate this concern is presented by Lawson and Koliou (2020) based on in-depth numerical analyses following the FEMA P695 procedure. This method is based on using the stability coefficient, $\theta$, of ASCE/SEI 7-22 Section 12.8.7. Although this stability coefficient, $\theta$, was not originally intended to be used to evaluate diaphragm deformations, with some simple adjustments it is a useful tool to investigate the diaphragm system stability under *P*-delta effects.

$$\theta = \frac{P_x / h_{sx}}{V_x / \Delta_{xe}} \qquad \text{ASCE/SEI 7-22 Eq. 12.8-18}$$

where:

$P_x$ = the vertical gravity load acting on the translating system, kips

$h_{sx}$ = the height of the translating system under consideration, inches

$V_x$ = the seismic shear force acting on the translating system under consideration, kips

$\Delta_{xe}$ = the weighted average elastic drift, inches

This equation evaluates the relative magnitude of the horizontal load added to the seismic-force-resisting system due to the corresponding drift (Lawson and Koliou, 2020). An increase of 10 percent or less ($\theta \leq 0.10$) is considered tolerable under ASCE/SEI 7-22 without a more detailed investigation.

The vertical gravity load acting on the translating system, $P_x$, has a component from the roof weight, $P_{x\ roof}$, and a component from the wall weight, $P_{x\ wall}$. As indicated by the applicable load combinations, the roof live load is excluded from the weight of the translating roof system. Because the wall's center of mass between the roof and slab-on-ground is only translating approximately half of that of the roof, the $P_{x\ wall}$ may be computed as the upper half of the wall plus any parapet. The load factors are 1.0 for this investigation.

$P_{x\ roof}$ = 12 psf (400 ft)(200 ft) = 960 kips

$$P_{x\ wall} = \frac{9.25 \text{ in}}{12}(150 \text{ pcf})\left(\frac{30 \text{ ft}}{2} + 3 \text{ ft}\right)400 \text{ ft}(2 \text{ sides}) = 1{,}665 \text{ kips}$$

$P_x = P_{x\ roof} + P_{x\ wall}$ = 960 + 1,665 = 2,625 kips

$h_{sx}$ = the height of the translating system under consideration

= 30 ft × 12 = 360 in.

$V_x$ = the seismic shear force acting on the translating system under consideration

= 1104 plf (400 ft) = 442 kips

$\Delta_{xe}$ = the weighted average elastic drift. A deflecting flexible diaphragm will approximate a parabolic shape, and thus the average translation of the roof and perpendicular walls due to the diaphragm will be two-thirds its maximum displacement. For this one-story building the system's drift is the combination of the diaphragm and shear wall drift components.

$$= \frac{2}{3}\delta_{e-dia} + \delta_{e-wall} = \frac{2}{3}(6.46) + 0.03 = 4.34 \text{ in.}$$

$$\theta = \frac{P_x / h_{sx}}{V_x / \Delta_{xe}} = \frac{2625/360}{442/4.34} = 0.071 \le 0.10 \text{ OK}$$

Because the stability coefficient is less than 10 percent, the *P*-delta effects on story shears, moments, and drifts need not be considered further.

It is worth mentioning here that according to ASCE/SEI 7-22 Section 12.8.6.5, diaphragm deflection is not included when evaluating the story drift limits of ASCE/SEI 7-22 Section 12.12.1. These limitations on building drift were developed primarily for the classic flexible frame system with a rigid diaphragm to prevent excessive distortion within the plane of the frame or shear wall. In masonry and concrete tilt-up buildings, the vertical elements deflect very little in-plane, with the bulk of translation occurring in the diaphragm. The story drift limits of the building code do not apply to the diaphragm deflection.

## 6.2 Steel Diaphragm Building Deflections Checks

### *6.2.1 Deflection of North/South Diaphragm*

Similar to the structural wood diaphragm example in Section 6.1, only the governing direction of the diaphragm, the north/south direction, will be checked. In-plane flexural deflections are generally considered negligible when compared to shear deflections in bare steel deck diaphragms. See DDM04 for further discussion. Thus, as introduced in Section 6.1.1, for diaphragms with multiple zones of width, $L_i$, and shear stiffness, $G'$, in kips/inch, and average shears, $v_{i\ ave}$, the total shear deformation at midspan, $\delta_n$, may be approximated as the summation of each zone contribution between the edge and the midspan of the diaphragm as:

$$\delta_n = \sum \frac{v_{i\ ave} L_i}{1000 G'} \tag{6-6}$$

where:

$\delta_n$ = maximum mid-span diaphragm deflection determined by elastic analysis, in.

$v_{i\ ave}$ = the average diaphragm shear within each shear stiffness zone

$L_i$ = the length of each shear stiffness zone measured perpendicular to loading

$G'$ = the shear stiffness of each shear stiffness zone

The diaphragm stiffness, $G'$, is determined per AISI S310-20 Section D5 (or by testing per AISI S907-17). $G'$ is determined from three sources of deformation under load: (1) the shear deformation of the deck profile; (2) the warping deformation of the deck profile; and (3) the relative slip contribution from the deck-to-framing structural connections and deck-to-deck sidelap connections. DDM04 provides all the necessary information for calculating the three deformation components, including stiffness for a number of proprietary fasteners, but manufacturer information may still be useful for specifics of the deck profile or use of connectors not listed in DDM04. In addition, the Steel Deck Institute and manufacturers (both deck and fastener companies) provide online tools for calculating $G'$ and deflection. Implementation of the deflection calculation for the example is aided by Table 6-2, where the average shear, length of the zones, and stiffness, $G'$, are provided for the bare steel deck roof example.

**Table 6-2 Bare Steel Deck Shear Deformation Computation Table**

| Zone | $v_{left}$ (plf) | $v_{right}$ (plf) | $v_{i\ ave}$ (plf) | $L_i$ (ft) | $G'$ (kip/in) | $\frac{v_{i\ ave}L_i}{1000G'}$ |
|---|---|---|---|---|---|---|
| 4 | 1468 | 1193 | 1331 | 37.5 | 234 | 0.21 in. |
| 3 | 1193 | 1009 | 1101 | 25 | 194 | 0.14 in. |
| 2 | 1009 | 734 | 872 | 37.5 | 131 | 0.25 in. |
| 1 | 734 | 0 | 367 | 100 | 101 | 0.36 in. |
| | | | | | ∑ = | 0.96 in. |

$$\delta_{dia} = \delta_n = \sum \frac{v_{i\ ave}L_i}{1000G'} = 0.96 \text{ in.}$$

To properly estimate the diaphragm's maximum expected inelastic deflection, we apply the deflection amplification factor, $C_{d\text{-}diaph}$. ASCE/SEI 7-22 Equation 12.8-16 may be used to compute the maximum design earthquake displacement of the diaphragm.

$$\delta_{DE\text{-}diaph} = \frac{C_{d-diaph}\delta_{e-dia}}{I_e}$$

$C_{d\text{-}diaph}$ = 3.0 (ASCE/SEI 7-22 Sec. 12.10.4.2.5)

$\delta_{e\text{-}dia}$ = 0.96 in. (an elastic response under strength-level forces)

$I_e$ = 1.0 (importance factor)

$$\delta_{DE\text{-}diaph} = \frac{C_{d-diaph}\delta_{e-dia}}{I_e} = \frac{3.0(0.96)}{1.0} = 2.88 \text{ in.}$$

As a side note, the computed elastic deflection ($\delta_{e\text{-}dia}$) of the diaphragm allows one to estimate the period of the diaphragm using Wilson's shear beam formula (Equation 4-1). The result can be approximated as $T_{diaph} = (0.066\delta_{e\text{-}dia})^{0.5} = (0.066\times0.96"\times1/0.222)^{0.5} = 0.53$ seconds, where $\delta_{e\text{-}dia}$ is based on 1.0g of acceleration, and results in a period reasonably close to what one obtains using the alternative design procedure's simplified formula (i.e., $T_{diaph} = 0.001L = 0.001\times400$ ft = 0.4 seconds) for bare steel structural panel diaphragms, as well as that obtained through more advanced modeling of the building with $T = 0.59$ seconds, as detailed in Appendix D.

### 6.2.2 Deflection of North/South Walls

The deflection of a cantilever shear wall has two components: a flexural component and a shear component:

$$\delta_{wall} = \delta_{wall\ flexure} + \delta_{wall\ shear}$$

$$\delta_{wall} = \frac{Ph^3}{3EI} + \frac{1.2Ph}{GA}$$

The adjusted load onto the shear wall was computed in Section 5.2.11 as 522 kips, but a portion of this was from the diaphragm acting at the roof ($F_{v1}$ = 330.3 kips), and a portion was from the wall self-weight effectively acting at the mid-height ($F_{v2}$ = 191.4 kips). Thus, one approach to approximate the combined effect of these two forces is to place half the wall force at the roof height with the diaphragm force.

$$P = 330.3 + \frac{191.4}{2} = 426 \text{ kips}$$

$h$ = 30 ft

The material properties and section properties are computed in Section 6.1.2 for the eight 25-ft long concrete shear walls (9¼-inch thick, $f_c'$ = 4000 psi).

To approximately consider the reduced in-plane stiffness of the concrete walls due to cracking, 35 percent of the gross moment of inertia and 100 percent of the gross cross-sectional area may be considered when significant portions of solid walls act as shear wall elements.

$$\delta_{wall} = \frac{Ph^3}{3EI(0.35I_g)} + \frac{1.2Ph}{GA_g}$$

$$= \frac{426(30\times12)^3}{3(3.6\times10^3)(0.35\times166.5\times10^6)} + \frac{1.2(426)(30\times12)}{1.5\times10^3\times22{,}200}$$

$$= 0.032 + 0.006 = 0.038 \text{ in.}$$

This contribution from the in-plane walls can also be affected by the stiffness of the foundation and connections to the foundation, but the magnitudes of these values are still expected to be relatively small.

The deflection amplification factor, $C_d$, may be used to compute the maximum expected wall deflection $\delta_{DE\text{-}wall}$:

$$\delta_{DE\text{-}wall} = \frac{C_d\delta_{e-wall}}{I_e}$$

where:

$C_d$ = 4.0 ASCE/SEI 7-22 Table 12.2-1

$\delta_{e\text{-}wall}$ = 0.038 in. (an elastic response under strength-level forces)

$I_e$ = 1.0 (importance factor)

$$\delta_{DE\text{-}wall} = \frac{C_d\delta_{e-wall}}{I} = 0.152 \text{ in.}$$

The total system displacement is the sum of the two deflection components.

$\delta_{DE} = \delta_{DE\text{-}diaph} + \delta_{DE\text{-}wall} = 2.88 + 0.152 = 3.03$ in.

This is the total estimated inelastic displacement during design seismic forces. It is observed that the contribution from the shear walls is very small and could have been neglected in this situation. One of the prime characteristics of RWFD buildings is that the diaphragm dominates the response of the building, which is evident here.

### 6.2.3 Limits on Diaphragm Deflection—Second-Order Effects and P-delta Instability

Similar to the approach provided in Section 6.1.3, the stability coefficient, $\theta$, of ASCE/SEI 7-22 Section 12.8.7 is used to investigate the diaphragm system stability under P-delta effects.

$$\theta = \frac{P_x/h_{sx}}{V_x/\Delta_{xe}}$$ ASCE/SEI 7-22 Eq. 12.8-18

where (per section 6.1.3):

$P_x$ = 2,625 kips

$h_{sx}$ = the height of the translating system under consideration

= 30 ft × 12 = 360 in.

$V_x$ = the seismic shear force acting on the translating system under consideration

= 1468 plf (400 ft) = 587.2 kips (Section 5.2.4)

$\Delta_{xe}$ = the weighted average elastic drift. A deflecting flexible diaphragm will approximate a parabolic shape, and thus the average translation of the roof and perpendicular walls due to the diaphragm will be two-thirds its maximum displacement.

$$= \frac{2}{3}\delta_{e-dia} + \delta_{e-wall} = \frac{2}{3}(0.96) + 0.038 = 0.68 \text{ in.}$$

$$\theta = \frac{P_x/h_{sx}}{V_x/\Delta_{xe}} = \frac{2625/360}{587.2/0.68} = 0.008 \le 0.10 \text{ OK}$$

Because the stability coefficient is less than 10 percent, the *P*-delta effects on story shears, moments, and drifts need not be considered further.

As discussed in Section 6.1.3, the story drift limits of the building code do not include the diaphragm deflection.

## 6.3 Limits on Diaphragm Deflection—Deformation Compatibility

To prevent damage to attached structural elements, including gravity load-carrying systems or any non-structural elements and their attachments, the engineer should be familiar with the expected building deflection and whether portions of the building are compatible with that deformation. Both ASCE/SEI 7-22 Section 12.12.4 and SDPWS-2021 Section 4.2.1 address the need to maintain structural integrity as a diaphragm deflects. SDPWS-2021 states the following regarding this:

> *"Permissible deflection shall be that deflection that will permit the diaphragm and any attached elements to maintain their structural integrity and continue to support their prescribed loads as determined by the applicable building code or standard."*

No prescriptive limits on deformation compatibility are given in SDPWS-2021, AISI S310-20, or ASCE/SEI 7-22 standards; instead, it is left to the structural engineer's judgment.

RWFD buildings typically occur as masonry or concrete shear wall buildings, and thus the diaphragm deflection results in the columns and

perpendicular walls rotating about their bases due to diaphragm translation at the top. This rotation is likely acceptable if the columns and walls were modeled with pinned bases during their individual design, even if some unintentional fixity exists. Research evaluating steel HSS-sections acting as interior columns undergoing interstory drift is available (Kong et al., 2019).

Perimeter walls often have significant out-of-plane fixity at the base because they are anchored to both the floor slab and foundation; thus, they should be evaluated as to their ability to yield and hinge at their base. The assumption of plastic hinges forming at the base of various elements prior to reaching the maximum design earthquake displacement, $\delta_{DE}$, is acceptable provided that these hinges do not result in an unstable structural mechanism or a loss of vertical support.

## 6.4 Limits on Diaphragm Deflection—Building Separations and Setbacks

Another diaphragm deflection limitation that must be investigated is building setbacks from property lines or adjacent buildings per ASCE/SEI 7-22 Section 12.12.2. For this investigation, the total $\delta_{DE}$ is computed as the sum of the shear walls' in-plane drift and the diaphragm's in-plane deflection. However, the in-plane drift of the stiff concrete or masonry shear walls is usually insignificant compared with the diaphragm and so is often ignored.

At property lines, the required building setback is $\delta_{DE}$. When evaluating two buildings on the same property, the required separation between those two buildings may be evaluated as the square-root-of-the-sum-of-the-squares (SRSS), $\delta_{SS}$, of the two independent $\delta_{DE}$*'s* per ASCE/SEI 7-22 Equation 12.12-2.

Where members span between structures, ASCE 7 Section 12.12.3 requires separations equal to the absolute sum of the maximum-considered-earthquake displacement, $\delta_{MCE}$, determined in accordance with ASCE/SEI 7-22 Section 12.8.6.

# Chapter 7

# Comparison of Designs Using Traditional Practice and the Alternative RWFD Procedure

This chapter presents a comparison of key design computations and results for example buildings using traditional practice (Chapter 3) and the alternative RWFD procedure (Chapter 5). A list of common design features is provided in Table 7-1. Section 7.1 presents a comparison of the diaphragm and shear wall designs for wood structural panel diaphragms, and Section 7.2 presents a comparison for bare steel deck diaphragms.

**Table 7-1 Common Features for Example Buildings**

| | |
|---|---|
| Diaphragm | Wood structural panel and bare steel deck diaphragms |
| Plan dimensions | 200 feet (north-south) × 400 feet (east-west) |
| Wall thickness | 9 1/4 inches |
| Wall height | 30 feet from slab-on-ground to diaphragm plus 3-foot-tall parapet |
| Seismic-Force-Resisting System | Intermediate precast concrete shear walls ($R$=4) |
| Roof design dead load | 12 psf |
| Spectral parameters | $S_{DS}$ = 1.0 and $S_{D1}$ = 0.6 |
| Seismic Design Category | D |

## 7.1 Wood Structural Panel Diaphragm Design

Comparison of design forces in Table 7-2 indicates that in general the alternative design procedure requires the diaphragm to be designed for lower forces. The exceptions are that the shear amplification for the north-south direction (transverse loading) results in essentially equivalent design force at the diaphragm boundary and end 10 percent regions and that the shear amplification in the east-west direction (longitudinal loading) results in higher diaphragm design forces along the boundary and end 10 percent regions. For the wood diaphragm, these observations are reflected in the nailing patterns that show that the alternative design procedure has less stringent nailing requirements in the interior of the diaphragm, the same

nailing requirement in the zone along the east and west edges, and more stringent nailing along the mid length of the north and south edges.

**Table 7-2 Comparison of Wood Diaphragm Designs Using Traditional Practice and the Alternative RWFD Procedure**

| Traditional Practice | Alternative RWFD Procedure |
|---|---|
| $R = 4$, $\Omega_o = 2.5$, and $C_d = 4$ | $R_{diaph} = 4.5$, $\Omega_{o\ diaph} = 2.0$, and $C_{d\ diaph} = 3.0$ |
| $T_a = C_T h_n^x = (0.02)30^{(0.75)} = 0.26$ seconds<br>ASCE/SEI 7-22 Eq. 12.8-7 | $T_{diaph} = 0.002(400\text{ ft}) = 0.800$ sec (north-south)<br>$T_{diaph} = 0.002(200\text{ ft}) = 0.400$ sec (east-west) |
| $C_S = \frac{S_{DS}}{R/I_e} = \frac{1.0}{4/1.0} = 0.25$ | North-south:<br>$C_S = \frac{S_{D1}}{T_{diaph}(R/I_e)} = \frac{0.6}{0.800(4.5/1.0)} = 0.167$<br>East-west:<br>$C_S = \frac{S_{DS}}{R_{diaph}/I_e} = \frac{1.0}{4.5/1.0} = 0.222$ |
| $F_p = 0.25w_p$ | North-south: $F_p = 0.167w_p$<br>East-west: $F_p = 0.222w_p$ |
| $w_{NS} = 1653$ plf<br>$w_{EW} = 2253$ plf | $w_{NS} = 1104$ plf<br>$w_{EW} = 2000$plf |
| Unit shear at diaphragm edge:<br>$v_{NS} = 1653$ plf<br>$v_{EW} = 563$ plf | Unit shear at diaphragm edge (amplified x 1.5):<br>$v_{NS} = 1104$ plf (1656 plf)<br>$v_{EW} = 500$ plf (750 plf) |
| Diaphragm nailing pattern from Figure 3-11:<br> 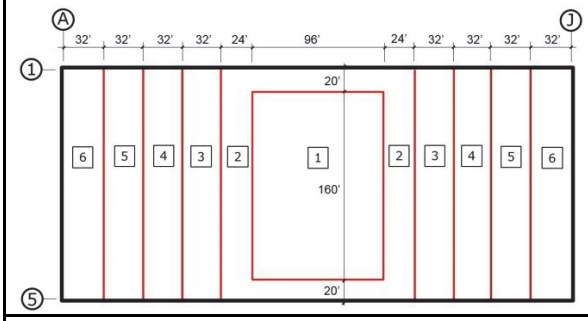 | Diaphragm nailing pattern from Figure 5-5:<br> 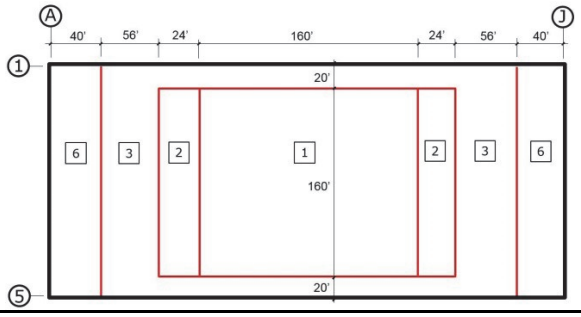 |
| North-south diaphragm chords:<br>$A_{s\ required} = 5.10$ in.$^2$<br>L5×5×5/8 steel angle, $A_s = 5.90$ in.$^2$<br>East-west diaphragm chords:<br>$A_{s\ required} = 0.87$ in.$^2$<br>L4×4×1/4 steel angle, $A_s = 1.93$ in.$^2$ | North-south diaphragm chords:<br>$A_{s\ required} = 3.41$ in.$^2$<br>L5×5×3/8 steel angle, $A_s = 3.65$ in.$^2$<br>East-west diaphragm chords:<br>$A_{s\ required} = 0.77$ in.$^2$<br>L4×4×1/4 steel angle, $A_s = 1.93$ in.$^2$ |
| Diaphragm deflection (north-south):<br>$\delta_{M\text{-}diaph} = 29.4$ in. (simplistic three-term equation) | Diaphragm deflection (north-south):<br>$\delta_{M\text{-}diaph} = 19.4$ in. (simplistic three-term equation) |

**Table 7-3 Comparison of Shear Wall Design Forces Using Traditional Practice and the Alternative RWFD Procedure**

| Traditional Practice | Alternative RWFD Procedure |
|---|---|
| $R = 4$, $\Omega_o = 2.5$, and $C_d = 4$ | $R_{wall} = 4$, $\Omega_{o\,wall} = 2.5$, and $C_{d\,wall} = 4$ |
| $T_a = C_T h_n^x = (0.02)30^{(0.75)} = 0.26$ seconds<br>ASCE/SEI 7-22 Eq. 12.8-7 | $T_{walls} = \frac{0.0019}{\sqrt{0.176}} 30 \text{ ft} = 0.136$ sec (north-south)<br>$T_{walls} = \frac{0.0019}{\sqrt{0.352}} 30 \text{ ft} = 0.096$ sec (east-west) |
| $C_S = \frac{S_{DS}}{R / I_e} = \frac{1.0}{4 / 1.0} = 0.25$ | North-south:<br>$C_S = \frac{S_{DS}}{R_{wall} / I_e} = \frac{1.0}{4 / 1.0} = 0.25$<br>East-west:<br>$C_S = \frac{S_{DS}}{R_{wall} / I_e} = \frac{1.0}{4 / 1.0} = 0.25$ |
| In-plane shear at base of shear walls:<br>$V_{NS} = 522$ kips<br>$V_{EW} = 608$ kips | In-plane shear at base of shear walls:<br>$V_{NS} = 440$ kips<br>$V_{EW} = 608$ kips |

## 7.2 Bare Steel Deck Diaphragm Design

Comparison of design forces in Table 7-4 indicates that in general the alternative design procedure requires the diaphragm to be designed for 11 percent lower forces. The exceptions are that the shear amplification for the north-south and east-west directions (transverse and longitudinal loading) results in higher design forces at the diaphragm boundary and end 10 percent regions. For the bare steel deck diaphragm design, these observations are reflected in an additional deck zone with a higher gage of steel deck at the ends of the diaphragms. The alternative design procedure has less sidelaps screws and deck thickness requirements in the interior of the diaphragm.

**Table 7-4 Comparison of Bare Steel Deck Diaphragm Designs Using Traditional Practice and the Alternative RWFD Procedure**

| Traditional Practice | Alternative RWFD Procedure |
|---|---|
| $R = 4$, $\Omega_o = 2.5$, and $C_d = 4$ | $R_{diaph} = 4.5$, $\Omega_{o\ diaph} = 2.0$, and $C_{d\ diaph} = 3.0$ |
| $T_a = C_T h_n^{(3/4)} = (0.02)30^{(0.75)} = 0.26$ seconds<br>ASCE/SEI 7-22 Eq. 12.8-7 | $T_{diaph} = 0.001(400\text{ ft}) = 0.400$ sec (north-south)<br>$T_{diaph} = 0.001(200\text{ ft}) = 0.200$ sec (east-west) |
| $C_S = \frac{S_{DS}}{R / I_e} = \frac{1.0}{4 / 1.0} = 0.25$ | North-South<br>$C_S = \frac{S_{DS}}{R_{diaph} / I_e} = \frac{1.0}{4.5 / 1.0} = 0.222$<br>East-West<br>$C_S = \frac{S_{DS}}{R_{diaph} / I_e} = \frac{1.0}{4.5 / 1.0} = 0.222$ |
| $F_p = 0.25 w_p$ | North-south: $F_p = 0.222 w_p$<br>East-west: $F_p = 0.222 w_p$ |
| $w_{NS} = 1653$ plf<br>$w_{EW} = 2253$ plf | $w_{NS} = 1468$ plf<br>$w_{EW} = 2000$plf |
| Unit shear at diaphragm edge:<br>$v_{NS} = 1653$ plf<br>$v_{EW} = 563$ plf | Unit shear at diaphragm edge (amplified x 1.5):<br>$v_{NS} = 1468$ plf (2202 plf)<br>$v_{EW} = 500$ plf (750 plf) |
| Diaphragm nailing pattern from Figure 3-8:<br> 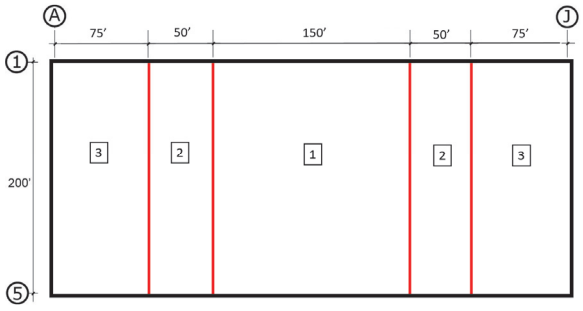 | Diaphragm nailing pattern from Figure 5-11:<br> 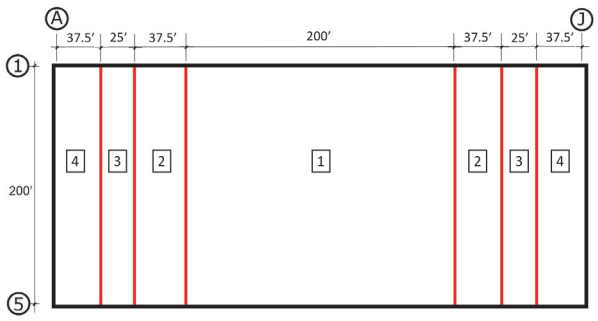 |
| North-south diaphragm chords:<br>$A_{S\ required} = 5.10$ in.$^2$<br>L5×5×5/8 steel angle, $A_s = 5.90$ in.$^2$<br>East-west diaphragm chords<br>$A_{S\ required} = 0.87$ in.$^2$<br>L4×4×1/4 steel angle, $As = 1.93$ in.$^2$ | North-south diaphragm chords:<br>$A_{S\ required} = 4.53$ in.$^2$<br>L5×5×1/2 steel angle, $A_s = 4.75$ in.$^2$<br>East-west diaphragm chords<br>$A_{S\ required} = 0.77$ in.$^2$<br>L4×4×1/4 steel angle, $As = 1.93$ in.$^2$ |
| Diaphragm deflection (north-south):<br>$\delta_{M\text{-}diaph} = 3.24$ in. | Diaphragm deflection (north-south):<br>$\delta_{M\text{-}diaph} = 2.88$ in. |

**Table 7-5 Comparison of Shear Wall Design Forces Using Traditional Practice and the Alternative RWFD Procedure**

| Traditional Practice | Alternative RWFD Procedure |
|---|---|
| $R = 4$, $\Omega_o = 2.5$, and $C_d = 4$ | $R_{wall} = 4$, $\Omega_{o\,wall} = 2.5$, and $C_{d\,wall} = 4$ |
| $T_a = C_T h_n^x = (0.02)30^{(0.75)} = 0.26$ seconds<br>ASCE/SEI 7-22 Eq. 12.8-7 | $T_{walls} = \frac{0.0019}{\sqrt{0.176}} 30 \text{ ft} = 0.136$ sec (north-south)<br>$T_{walls} = \frac{0.0019}{\sqrt{0.352}} 30 \text{ ft} = 0.096$ sec (east-west) |
| $C_S = \frac{S_{DS}}{R / I_e} = \frac{1.0}{4 / 1.0} = 0.25$ | North-south:<br>$C_S = \frac{S_{DS}}{R_{wall} / I_e} = \frac{1.0}{4 / 1.0} = 0.25$<br>East-west:<br>$C_S = \frac{S_{DS}}{R_{wall} / I_e} = \frac{1.0}{4 / 1.0} = 0.25$ |
| In-plane shear at base of shear walls:<br>$V_{NS} = 522$ kips<br>$V_{EW} = 608$ kips | In-plane shear at base of shear walls:<br>$V_{NS} = 522$ kips<br>$V_{EW} = 608$ kips |

# Chapter 8
# Future Studies for Design of RWFD Buildings

Recommendations for future study and research are provided in this chapter. These recommendations are intended to provide focus to future studies and research to benefit further development of design provisions for RWFD buildings. Recommendations presented are grouped as: (1) specific to the alternative RWFD design procedure; (2) extending the alternative RWFD design procedure to existing RWFD buildings; and (3) more general in nature such that they apply to all RWFD buildings regardless of the design procedure used. The chapter ends with a list of the five studies recommended to be prioritized for further study.

## 8.1 Studies Specific to the Alternative RWFD Procedure

The following recommended studies are applicable only to the RWFD procedure. They are listed in order of need, most urgent to least urgent.

### *8.1.1 Applicability to Buildings with Lightweight Enclosures, Steel Bracing Systems, and Other SFRSs*

The archetypes developed in conjunction with this project were selected to represent typical RWFD buildings in the United States. It is recognized that the alternative design procedure may apply to buildings with SFRSs not necessarily modeled as part of the work to validate the alternative RWFD procedure. Examples of other systems with stiff vertical elements for which the alternative RWFD procedure is allowed to be used in accordance with ASCE/SEI 7-22 Section 12.10.4.1 include ordinary and special steel concentrically braced frames, steel and concrete composite braced frames, and steel and concrete composite shear walls. In particular, braced frames are often used as interior lateral shear resisting elements, especially at interior thermal expansion joints.

If braced frame elements are used as the SFRS for the entire building, the exterior wall or cladding system, such as steel panels, often weighs much less than the concrete walls of the archetypes studied. A limited comparative study was conducted in conjunction with this report as described in Section 4.1, and the results suggest the building period may be independent of wall

mass. It would be beneficial to conduct further studies with these other SFRSs to better evaluate their performance under this alternative RWFD procedure even though ASCE/SEI 7-22 already allows their use. Many of the concepts of the alternative RWFD procedure are expected to be appropriate; however, the significant difference in mass due to the lightweight walls may lead to different behavior than that of the archetypes modeled in the studies that led to the alternative RWFD procedure.

Another concern is that braced frames or elements of other vertically oriented systems in some cases may not be significantly stronger and stiffer than the flexible diaphragm. This possibility was recognized in approving the alternative procedure in ASCE/SEI 7-22 but was thought to still result in safe designs. An additional study to better understand the effects of strength and stiffness differences between the diaphragm and vertical systems would result in better definition of the limits of applicability of the alternative RWFD procedure. The concern of the stiffness ratio between vertical lateral elements and the diaphragm has also been raised in relation to use of the two-stage analysis procedure. The recommended studies would also lead to a better understanding as to whether use of the two-stage analysis procedure requires further restriction than those imposed by ASCE/SEI 7-22 and whether there are cases for which the two-stage analysis may be overly conservative. An example of how the alternative RWFD procedure with the two-stage analysis might be overly conservative is if the vertical elements are ductile and yield. The diaphragm in this case may not be subjected to yielding and high ductility demands.

Although tension-only bracing is technically an ordinary concentrically braced frame, which would be allowed by ASCE/SEI 7-22, its strength and stiffness are likely close to or below those of the diaphragm. For that reason, the authors of this report recommend that tension-only bracing not be used with the alternative RWFD procedure.

The range of response modification coefficients ($R$) for braced frames and other systems is wide in comparison to the single value ($R = 4$) for an intermediate precast shear wall used for the archetypes in the studies for this report. This wide range in values of $R$ indicates that the range of ductility and overstrength is likely wide as well. The impact of the value of $R$, the proportion of $R$ related to overstrength, and the portion of $R$ related to ductility for various SFRSs could be studied to better understand how the diaphragm and overall building response is affected by the various systems.

### 8.1.2 Applicability to Buildings with Mezzanines and Multi-Story Buildings

Many RWFD buildings include mezzanines for a portion of the footprint. Often, these mezzanines are used for offices while the rest of the building has a separate use, such as storage. These mezzanines are often structurally attached to the building but are relatively small in plan. As a result, seismic performance of the building is likely to match that of the archetypes, but this has not been confirmed. Evaluating the effects of mezzanines of varying size and mass on the performance of RWFD buildings should be evaluated to determine whether any restrictions are required on their mass and configuration.

The principles discussed as part of the alternative design procedure could be transferred to design of certain multi-story buildings, but with caution. Often two-story tilt-up concrete or masonry buildings are built with large flexible diaphragms, and their behavior may be similar to that observed for the archetype buildings studied. Higher mode shapes and interaction between the two diaphragms remain a concern and should be studied further before extrapolating this alternative design procedure to multiple stories.

### 8.1.3 Deflection of Diaphragms

A simple means of computing or estimating the diaphragm deflection could likely be obtained from the analysis results performed to date. In comparison to the analyses of the wood diaphragm archetypes, deflections computed in accordance with SDPWS-2021 appear to substantially overestimate diaphragm displacement, as discussed in Section 6.1. Although overestimating deflection is conservative for computing second-order effects and building separations, the results could be unconservative if used to compute a period and that period were used to determine design forces. This was demonstrated in Section 6.1, where the estimated period of the diaphragm using Wilson's shear beam formula (Equation 4-1) exceeds $T_{diaph} = 0.002L$ for wood structural panel diaphragms.

In comparison to the analyses of bare steel deck diaphragm archetypes, deflections computed in accordance with AISI S310-20 or DDM04 may be modestly underestimated (Eatherton et al., 2020; Schafer, 2019). This may result in an under-estimation of second-order effects but be conservative from the standpoint of period estimation, which is the opposite of the situation for wood diaphragms.

The data from the archetype analyses could be studied to develop a means of estimating the diaphragm displacement at the design level and maximum

considered earthquakes. The results could be compared to analysis results of the three-dimensional modeling studies described in Section 8.1.6. Realistic estimates of displacements would eliminate unnecessarily conservative measures to maintain gravity system stability (see Section 8.3.3).

### 8.1.4 Comparison of Alternative Design Procedures

ASCE/SEI 7-22 includes a more general alternative design procedure for diaphragms in Section 12.10.3, in which one of the equations to determine a diaphragm's force depends on the inverse of the diaphragm design force reduction factor, $R_s$. The value of $R_s$ depends on the type and ductility of the diaphragm. A comparison of the resulting diaphragm designs using this alternative procedure to that of the alternative RWFD procedure for one-story structures with flexible diaphragms and rigid vertical elements would identify which one is likely to be used in practice. Such a study could be used to identify whether merging or syncing the procedures might be possible.

### 8.1.5 Compatibility of the Alternative RWFD Procedure with Design for Wind

The compatibility of the alternative procedure with wind design could be studied. Design for wind requires zones of higher uplift at corners and along the perimeter of building diaphragms. This results in more connectors in these zones, which is likely consistent with the zones of amplified shear strength of the alternative procedure. For buildings with interior lateral elements, the alternative design procedure will require zones of amplified strength not required for wind uplift design.

If a building is subjected to high wind forces relative to seismic forces, the diaphragm design strength may be controlled by wind. In these instances, the diaphragm wind design may require significantly more strength than that required for the alternative procedure.

The study could explore whether the increase in connectors required for wind uplift on the perimeter of a diaphragm would be adequate to obtain equivalent behavior to that of a diaphragm designed using the alternative RWFD procedure. Such a study could also explore the relative wind force to seismic force for which the alternative procedure design might be impacted.

### 8.1.6 Three-Dimensional Modeling Calibrated to the Response of Buildings and Tests

Several instrumented RWFD buildings have been exposed to strong ground shaking (Celebi et al., 1989; Bouwkamp et al., 1994), and several nonlinear

response analyses by others have been performed in an attempt to replicate the measured response (Wallace et al., 1999). Several of these analyses have been relatively successful, but more detailed models that include individual nonlinear connector response would be useful. Most, if not all, of the instrumented RWFD buildings have wood diaphragms. For RWFD buildings with bare steel deck diaphragms, there are no response data with strong motions. For bare steel deck diaphragms, a three-dimensional model could be compared to the approximately 70-foot-long diaphragms tested by Massarelli et al. (2012). Also, instrumentation of additional RWFD buildings, including ones with wood diaphragms and ones with bare steel deck diaphragms, is desirable.

### *8.1.7 Large-Scale Diaphragm Tests*

Large-scale cyclically loaded diaphragm tests or diaphragm tests for response to earthquake records could be performed to better understand the behavior of flexible diaphragms. Tests are desirable for both wood and bare steel deck diaphragms. The effect of connection ductility on global diaphragm ductility could be evaluated along with means of improving the spread of ductility. Tests could be used to determine the location of first yield and how to control this location with zones of amplified strength. Deformation compatibility issues could also be studied in conjunction with the diaphragm tests, though focused sub-assemblage tests are also likely needed to fully understand how to quantify or address concerns.

## 8.2 Studies Applicable to Extending the Alternative RWFD Procedure to Existing Buildings

Conceptually, it appears possible to use the alternative RWFD procedure to strengthen diaphragms of some existing RWFD buildings, although doing so comes with challenges. One of the first considerations is whether the approach will be to provide a ductile diaphragm or one that remains nearly elastic. If the approach is to provide strength for near elastic performance, ASCE/SEI 41-17 could be used. If the approach is to provide a ductile diaphragm, the concepts of the alternative RWFD might be implemented. For example, fasteners could potentially be added to the perimeter regions of the diaphragm to create strong end-of-span regions to encourage greater distribution of inelastic ductile behavior.

For wood diaphragms, consideration needs to be given to the type of sheathing and its connections to the existing framing and perimeter walls. Determinations need to be made regarding the existing sheathing and connectors, usually nails, and whether additional nails could be added to strengthen the diaphragm without splitting the existing wood. If structural

wood panels are required to be placed over the existing sheathing, it's important to consider how the new panels will interact with the existing sheathing (i.e., will the strength and stiffness be additive or less than the sum of the two?).

For bare steel deck diaphragms, the connector type and deck type will have a significant impact on retrofit approaches and possibilities. For example, if welds are used for framing connectors, the most logical approach may be to add more welds to achieve near elastic response. If the deck profile is an interlocking deck it may be difficult to add screwed sidelap connectors, but screws could be easily added for sidelaps of nested deck. Another consideration is if any existing connectors could be removed or broken to prevent adverse effects on the strengthened diaphragm. Many bare steel deck diaphragms in the western United States are constructed with proprietary sidelap connectors. These often are punched but result in a much stronger connection than button punching. Data on these connectors can be found in Torabian and Schafer (2021). Also, AISI S400-20 provides performance criteria for connectors that may be useful as a minimum representation of the strength and ductility of connectors that are added to strengthen a bare steel deck diaphragm.

Retrofitting existing diaphragms requires many considerations that are not required for new buildings. Although the concepts of the alternative RWFD procedure could be used to retrofit some existing RWFD buildings with weak diaphragms, ASCE/SEI 41-17 does not include a mechanism to do so without performing a nonlinear analysis. Retrofitting a diaphragm in accordance with the concepts of the alternative RWFD procedure would have to be in accordance with the 2021 *International Existing Building Code*, Section 104.11, Alternative Materials, Design and Methods of Construction, and Equipment (ICC, 2021). As the code official has the right of approval for such alternatives, it is unclear what supporting reports and tests would be required.

A study or studies focused on how to retrofit an existing RWFD building using the alternative RWFD procedure concepts would benefit the many industries that make use of this building type. Studies for wood diaphragms should focus on how realistic it is to create a zone of increased strength at the ends of the diaphragm spans. Studies could also explore the possibility of using alternative dowel-type connectors to supplement the strength of the existing nails. Studies of bare steel deck diaphragms should focus on the interactions of various connectors and whether nonductile connectors will have adverse effects on the performance of diaphragms. Studies should

consist of laboratory tests with combinations of connectors and detailed finite element analyses.

## 8.3 Studies Applicable to the Traditional and Alternative RWFD Procedures

The following recommended studies apply to both the traditional and alternative RWFD procedures. They are listed in order of need, most urgent to least urgent.

### *8.3.1 Irregular Plan Shapes, Abrupt Changes along Exterior Walls, and Nonparallel Walls*

RWFD buildings often have re-entrant corners and other abrupt changes in geometry. Examples include small wall pop-outs or setbacks of several feet to provide architectural relief for long walls and larger re-entrant corners to fit within a property line or to serve the operational needs of the occupants. Figure 8-1 shows an example of a large re-entrant corner, Figure 8-2 shows small wall pop-outs, and Figure 8-3 shows small wall setbacks. RWFD buildings also often include non-parallel (skewed) walls relative to the primary building axes, such as that shown in Figure 8-4 and Figure 8-5. Nonparallel walls are often used to match a nonparallel property line.

The effects of these discontinuities and nonparallel walls on performance due to a seismic event are not that well studied or understood, even for the traditional design procedure. Studying the effects of these discontinuities and nonparallel walls on nearby diaphragm connectors and the effect on diaphragm chords and collectors would be beneficial given the large number of RWFD buildings with these discontinuities. Such a study should explore the full range of small and large plan offsets and angles of wall skew. The study should also establish potential requirements regarding these discontinuities and nonparallel walls for both the traditional design procedure and for the alternative RWFD procedure.

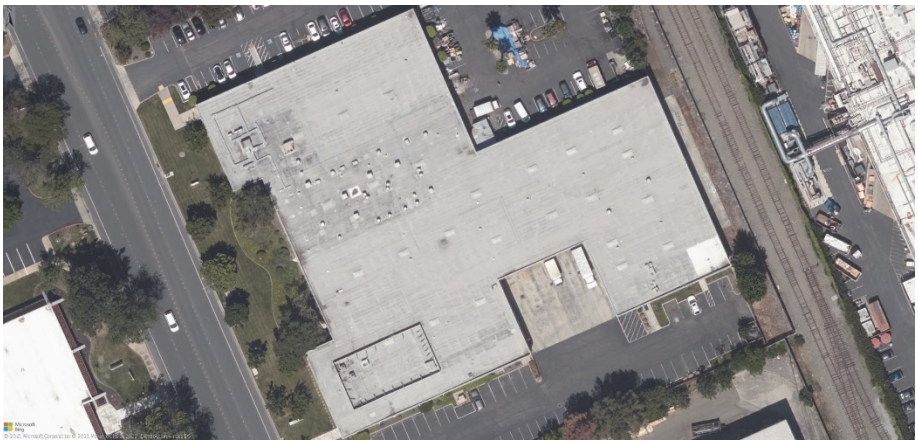

Figure 8-1 Example of a RWFD building with a large re-entrant corner (photo credit: ConnectExplorer).

Figure 8-2 Example of a RWFD building with a small wall pop-out (photo credit: VLMK Engineering + Design).

Figure 8-3 Example of a RWFD building with small wall setbacks (photo credit: ConnectExplorer).

Figure 8-4 Example of a RWFD building with nonparallel walls (photo credit: ConnectExplorer).

Figure 8-5 Example of a RWFD building with nonparallel walls (photo credit: ConnectExplorer).

### 8.3.2 C-Shaped Lateral-System Configurations

C-shaped lateral-system configurations occur when three of the four sides of a rectangular diaphragm are laterally supported but the fourth side is not. This configuration is commonly used for RWFD buildings with bare steel deck diaphragms in regions of low and moderate seismicity. Longer buildings with bare steel deck diaphragm often require one or more expansion joints. In a C-shaped lateral-system configuration, additional vertical elements are not provided within the interior of the building if there is a single expansion joint. The result is two building portions with C-shaped plan configurations for the exterior shear walls, as shown in Figure 8-6, resulting in diaphragms that are cantilevered or acting in rotation. This configuration is prohibited for wood structural panel diaphragms but not steel deck diaphragms. Although widely used, the expected seismic performance of this configuration has not been well studied. The alternative RWFD procedure is not permitted for this configuration because it requires lateral support on all four sides of a rectangular diaphragm. Additional studies are necessary to better understand how these buildings will respond to strong ground shaking and to determine whether the alternative RWFD procedure could be extended to these buildings.

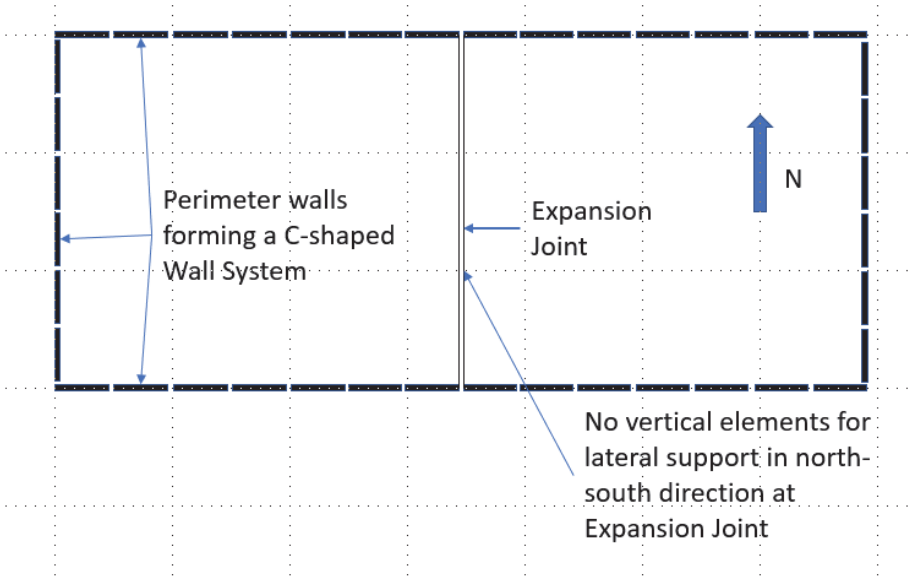


Figure 8-6 C-shaped lateral-system configuration.

If two or more expansion joints are provided, the interior building portions are typically constructed with steel braced frames at or near the parallel expansion joints. Diaphragm shears from the outer building portions may or may not be transferred across the expansion joint for lateral support from the braced frames of the interior portions. If such shear transfer is provided, the alternative RWFD procedure may also be applied to both interior and outer

building portions because each end of the rectangular diaphragm span is supported by vertical elements of an SFRS. If diaphragm shear is not transferred across the expansion joint, the outer building portions have a C-shaped plan configuration of walls, like buildings with a single expansion joint. If the expansion joints are large enough to accommodate seismic drifts and diaphragm deflections, the interior portions of the building could be designed using the alternative design procedure because they would be "stand-alone" building structures.

The diaphragms for portions of these buildings with C-shaped plan configurations for their lateral systems must be stiff and strong enough to transfer the loads to the vertical elements. Lateral load distribution to the vertical elements requires that diaphragms be treated as rigid or semi-rigid in accordance with ASCE/SEI 7-22 Section 12.3 because a flexible diaphragm requires a vertical element close to all four edges. C-shaped lateral systems are not consistent with the flexible diaphragm assumption, so lateral loads may not be distributed by tributary area. Neither the traditional RWFD design approach nor the alternative RWFD design procedure is applicable to buildings with C-shaped lateral-system configurations.

The archetypes studied for the alternative procedure did not include C-shaped plan configurations of the perimeter shear walls. The alternative RWFD procedure with modification has the potential to extend to these buildings. However, analyses of such buildings would have to be studied to develop appropriate design provisions.

The issues identified in this section are best studied with detailed, three-dimensional, nonlinear models subject to appropriately scaled earthquake time-histories.

### *8.3.3 Joist Seat Rollover for Shear Transfer*

In low and moderate seismic regions, joist rollover is often used to transfer diaphragm shear loads to the perimeter walls on which open-web steel joists are supported. The edge of the bare steel deck parallel with the walls is fastened to the horizontal leg of an upturned angle that is attached to the top of the joists at their bearings. The diaphragm shear is transferred from the deck to these upturned angles, from the angles to the joist top chords, and through the joist seat to either: (1) a pocketed embed plate in the wall panel (Figure 8-7) or (2) a seat angle (Figure 8-8). This shear must be transferred eccentrically through the joist seat depth, which causes a rollover action on the joist seat. Although joist manufacturers may have data on the strength and ductility of joist rollover, the strength and ductility of joist seat rollover

is generally not available to engineers designing RWFD buildings. Study of joist seat rollover through laboratory testing, reviewing of test results performed under the direction of joist manufacturers, or both is recommended.

Figure 8-7 Joist seat in bearing pocket of wall (photo credit: Joseph Steinbicker).

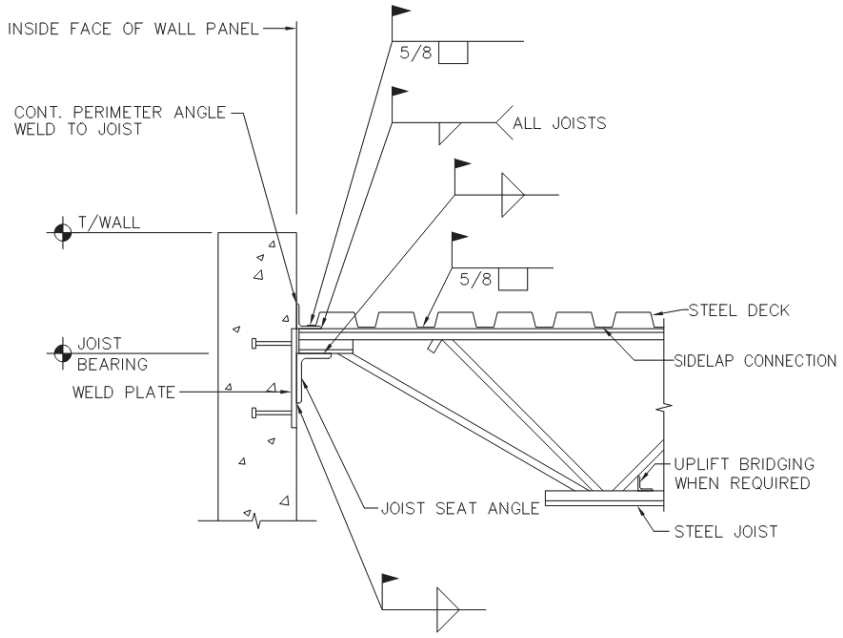


Figure 8-8 Example detail of joist seat supported by a seat angle (image credit: Joseph Steinbicker).

### 8.3.4 *Implications of Diaphragm Deflections on Structural and Nonstructural Elements*

Buildings with large flexible diaphragms can experience portions of the building displacing significant distances horizontally compared with buildings with rigid diaphragms. In buildings with rigid diaphragms, the diaphragm's horizontal displacement is likely only a little larger than the supporting frame or shear wall system; and the drift of these supporting SFRSs are limited by ASCE/SEI 7-22. Therefore, internal horizontal displacements of the rigid diaphragms are indirectly controlled.

However, the limitations on flexible diaphragm displacements in one-story buildings are less prescriptive than the drift limits for the SFRS, relying on the engineer's judgment of deformation compatibility discussed in Section 6.3. Furthermore, as demonstrated in Section 6.1.3 and Section 6.2.3, investigating second-order effects (*P*-delta) due to large diaphragm displacements involves modifying existing code provisions that were not originally intended for horizontal diaphragm usage.

Although the mainstay of RWFD buildings has traditionally been warehouse shells, it has become common for this system to be used in office buildings and commercial retail with numerous tenant improvements and partitions. The susceptibility of these latter two occupancies to damage due to large displacements is quite different, and limitations will likely be warranted.

A concern identified in ASCE/SEI 7-22 Commentary Section C12.10.4 is that the connectors of bare steel deck and structural wood panels to steel ledgers will be affected by prying as the wall rotates about its base. The authors of this document were shown the results of a proprietary test that indicates that the prying for bare steel deck connectors is partially, if not fully, alleviated by deformation of the flat base of the flute bending into a curved shape, as shown in Figure 8-9. As there is no force to restore the flute to flat, subsequent cycles to the same or smaller displacement would theoretically not result in prying. The limited testing is insufficient to dismiss the concern. Further testing of both wood structural panel and bare steel deck to ledger connections is necessary to confirm sufficient deformation capacity is obtained.

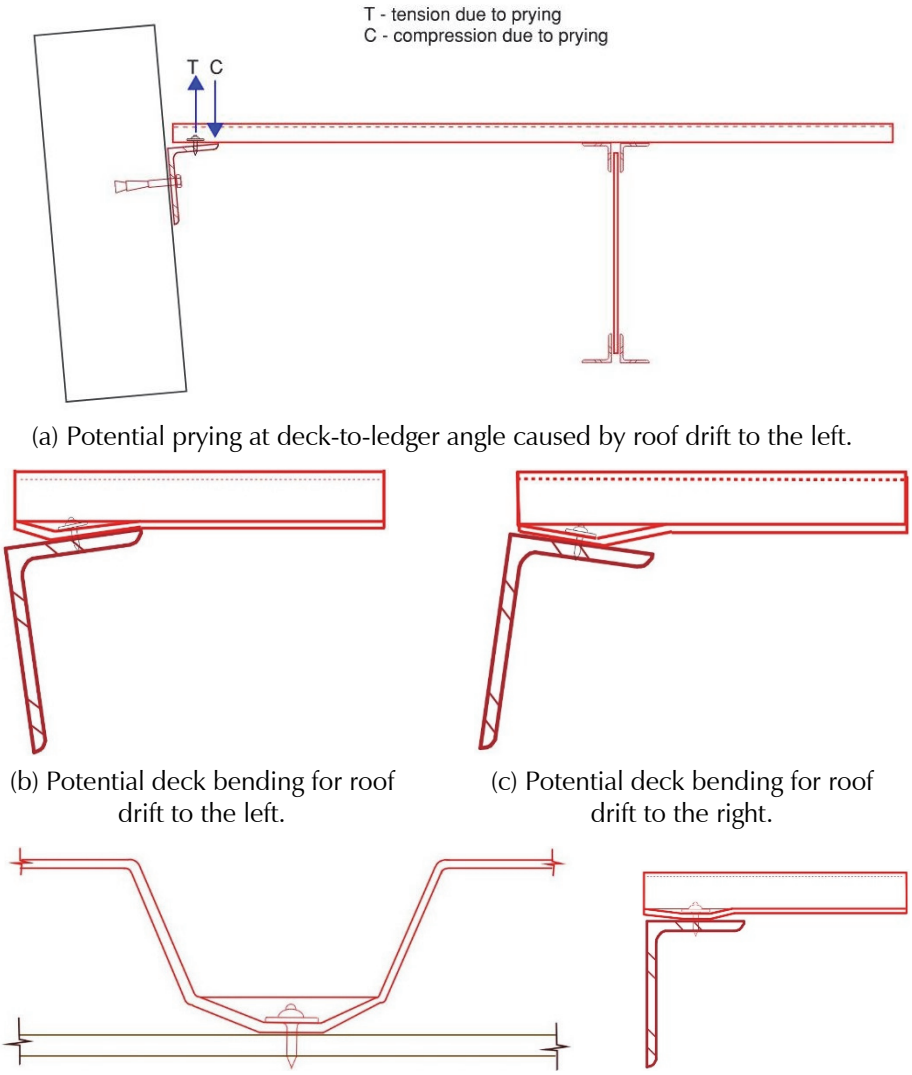


(a) Potential prying at deck-to-ledger angle caused by roof drift to the left.

(b) Potential deck bending for roof drift to the left.

(c) Potential deck bending for roof drift to the right.

(d) Potential deck bending that reduces prying due to roof drift.

Figure 8-9 Illustration of deck local bending that may reduce prying forces.

### *8.3.5 Out-of-Plane Top-of-Wall Anchorage Forces*

The results of an out-of-plane wall study (Lawson et al., 2018; Koliou et al., 2017) indicate that the wall anchorage provisions in ASCE/SEI 7-22, which are the same as those in ASCE/SEI 7-10 and ASCE/SEI 7-16 (ASCE, 2016), are likely adequate, except the analysis indicated that wall anchorage forces increased rather than decreased with shorter diaphragm spans. This suggests that the amplification factor for diaphragm flexibility, $k_a$, in Section 12.11.2.1 of ASCE/SEI 7-22 should be revisited and possibly replaced with a single coefficient equal to 2. The study also showed that there are corner effects that can occur and that wall forces varied substantially. This variation in the wall forces also showed up in the detailed three-dimensional analysis of the bare steel deck diaphragm building presented in Schafer (2019) and

discussed in Appendix D. Going forward, new studies need to determine whether current design practice leads to acceptable performance. Studies should focus on the following:

- Whether there is a need to increase anchorage design forces for shorter diaphragm spans to obtain desired performance.
- Whether the current out-of-plane design forces are large enough in situations where the diaphragm might remain elastic due to excess diaphragm strength provided to meet strength demands in the orthogonal direction. (This was studied to some extent as reported in Lawson et al., 2018).
- Whether further amplification of the forces on parapets and wall anchorages, particularly for taller parapets, that are common at the front of big-box retail stores is needed.
- Whether top of wall anchorages near building corners need to be designed for forces that are larger than currently required.
- Whether there is a need to combine the design for out-of-plane wall forces with in-plane diaphragm shears, which is not done in current practice.
- Whether shears in subdiaphragms should be combined with the main diaphragm shears, which is not done in current practice.
- The effect of non-parallel (skewed) walls on out-of-plane wall forces.

### *8.3.6 Combining Connector Forces from Shear Acting in Two Orthogonal Directions*

Diaphragm shears from two orthogonal directions both load a diaphragm connector. ASCE/SEI 7-22 does not require that connectors be designed for forces from orthogonal shears acting simultaneously. A study using three-dimensional nonlinear response models of diaphragms with individual diaphragm connectors could be used to determine whether the current practice of not combining shears from two orthogonal directions of loading is acceptable, or if these forces should be combined at the connector level. If combining forces from orthogonal directions of loading is required, then the models could be used to study how best to combine the forces on the connectors.

### *8.3.7 Forces on Continuity Ties*

In the direction that the deck spans, steel deck panels often serve as the wall anchorage continuity ties, as required by ASCE/SEI 7-22 Section 12.11, with interconnection ties required in Section 12.1.3. At end laps, continuity tie

forces are transferred through the framing connectors that attach the ends of deck panels to one another and to the support framing. These same connectors resist shear forces from the main diaphragm shear; however, current practice is to not combine these forces. A study to determine whether current practice is acceptable would be beneficial. If not acceptable, the study could provide clarification of how exactly to combine forces to the connectors from the diaphragm shear and continuity tie forces. The results could be used for both traditional practice and the alternative RWFD procedure.

For all wood diaphragms and occasionally for bare steel deck diaphragms, subdiaphragms are used to transfer the out-of-plane wall anchorage forces to limit the number of continuous ties. Subdiaphragms typically transfer the wall anchorage forces to continuous girder lines. For bare steel deck diaphragms, joist girders serve as the continuity ties, but this requires use of subdiaphragms to transfer the forces to joist girder lines.

### *8.3.8 Traditional Procedure versus Alternative RWFD Procedure for Design of Buildings with Bare Steel Deck Diaphragms*

Given that the FEMA P695 study results in Appendix B for traditional design with bare steel deck diaphragms failed to meet the targeted performance, it is evident that either a lower *R*-factor value is required than that currently allowed for use with the traditional design procedure or an alternative design procedure, such as the one presented in this report, is appropriate. With the introduction of special seismic detailing for bare steel deck diaphragms in AISI S400-20, these diaphragms are separated into two categories: those that meet the special detailing requirements and those that do not. The alternative RWFD procedure accommodates this difference with the use of a much lower value of $R_{diaph}$ for diaphragms not meeting the special detailing requirements than those that do. Thus, use of the traditional design procedure, which does not require use of a lower value *R*-factor, is more concerning for diaphragm designs not meeting the special detailing requirements. Although ASCE/SEI 7-22 allows use of the traditional method for bare steel deck diaphragms, including those not meeting the special detailing requirements, it appears necessary that the alternative RWFD procedure or another approach with a low value *R*-factor for diaphragm design be mandated for bare steel deck diaphragms not meeting the special detailing requirements. Such a mandate has not yet been adopted by consensus committees, such as the NEHRP Provisions Update Committee or the ASCE/SEI 7 Seismic Subcommittee. A study on how to transition from traditional design of RWFD buildings to mandated designs procedures that meet the targeted performance, such as the alternative RWFD procedure

does, is needed. The study could also explore how to expand the applicability of the alternative RWFD procedure to better represent the breadth of design configurations for the built environment.

## 8.4 Study Priorities

It is recommended that the following five studies, in the order presented, should be the highest priority among those described in prior sections:

1. Applicability to Buildings with Lightweight Enclosures, Steel Bracing Systems, and Other SFRSs (Section 8.1.1)
2. Irregular Plan Shapes, Abrupt Changes along Exterior Walls, and Nonparallel Walls (Section 8.3.1)
3. Applicability to Buildings with Mezzanines and Multi-Story Buildings (Section 8.1.2)
4. C-Shaped Lateral-System Configurations (Section 8.3.2)
5. Joist Seat Rollover for Shear Transfer (Section 8.3.3)

Applicability to buildings with lightweight enclosures and steel bracing systems is the highest priority because there is uncertainty about the need for restrictions regarding the strength and stiffness of steel braced frames. The irregular plan shapes, abrupt changes and nonparallel walls is second because these conditions are common in RWFD building construction. Applicability to buildings with mezzanines and multi-story buildings is third because there are many of these buildings and there is a need to define when mezzanines essentially act as a second level. C-shaped lateral system configuration is fourth because many buildings are constructed with this configuration in low and moderate seismic zones. Similarly, joist seat rollover is fifth because its use is so prevalent.

Although not making the list of highest priorities, comparison of alternative design procedures (Section 8.1.3) and compatibility of the alternative RWFD procedure with wind design (Section 8.1.4) would likely be the least costly to address.

# Chapter 9
# Conclusions

This report has presented an alternative procedure to design single-story RWFD buildings with wood structural panel or bare steel deck diaphragms within the existing framework of ASCE/SEI 7-22. A version of the alternate design procedure presented herein was adopted by the 2020 *NEHRP Recommended Seismic Provisions for New Buildings and Other Structures* prior to being considered for inclusion in ASCE/SEI 7-22. The alternative design procedure presented is relatively simple to implement and is based on yielding and energy dissipation in the diaphragm rather than yielding, rocking, or sliding of the walls. FEMA P695 collapse assessment studies have demonstrated improved seismic performance of buildings designed using the alternative procedure, beyond the seismic performance anticipated using traditional design practice for these buildings.

The flow, sale, and manufacturing of goods in the United States is heavily dependent upon RWFD buildings. Big box retail stores, logistical storage, and manufacturing facilities could be at risk because the building code provisions traditionally used for seismic design do not appropriately address how earthquakes affect these buildings. With this disconnect between the intent of traditional design practice and the behavior of these buildings, difficulty exists in evaluating this building stock for seismic vulnerabilities. The alternative procedure presented in this report is intended to fill this gap.

The alternative RWFD design procedure has been included in ASCE/SEI 7-22, which is anticipated to be adopted by the 2024 *International Building Code*. Within ASCE/SEI 7-22, the alternative RWFD procedure is not mandatory because the traditional design procedure is maintained. However, as practicing engineers become more familiar with the alternative procedure and as confidence in its reliability increases, it could become the most common design approach for RWFD buildings. Addressing the issues identified in Chapter 8 could help increase its use.

For an existing building, using this procedure may not result in a building that complies with the ASCE/SEI 41 elastic procedure. However, a diaphragm strengthened to meet the intent of the alternative design procedure would likely meet the nonlinear procedures. The alternative procedure offers the possibility of limiting strengthening of a roof to only a strip of roof

structure along the perimeter of the diaphragm rather than the entire diaphragm. However, further study is required to establish requirements for strengthening diaphragms in existing buildings.

Recommendations for future studies and research are provided in Chapter 8. The intention of including these recommendations is to provide focus for future studies and research so that they directly benefit development of design provisions for RWFD buildings.

# Appendix A

# Evaluating RWFD Buildings Using FEMA P695 Methodology

This appendix provides an overview of the FEMA P695 studies that provide the basis for the alternative RWFD procedure. The FEMA P695 studies described here were primarily conducted as part of the development of the 2015 edition of FEMA P-1026, but some new material has been added.

The FEMA P695 methodology is used to quantify building system performance and provide guidance in the selection of appropriate seismic design coefficients when ASCE/SEI 7 linear design methods are applied. The primary design performance objective of FEMA P695 is to obtain an acceptably low probability of collapse of the SFRS under maximum considered earthquake (MCE) ground motions. The evaluation must use a representative nonlinear numerical building model that includes both detailed design information of the system, as well as comprehensive test data on the post-yield performance of system components and subassemblies.

When using FEMA P695, a structural system and design methodology are evaluated with collapse fragility curves. Incremental Dynamic Analyses (IDA) are conducted on a representative sample of numerical models that account for the range of the design space using a pre-determined ensemble of earthquake ground motions. Collapse fragility curves are then developed from the IDAs. The number of archetypes selected was based on appropriately representing typical RWFD buildings, including the range of variation reasonably expected and likely to affect performance. The archetypes were assigned to performance groups for the evaluation process.

The RWFD building archetypes were designed for locations with high and moderate seismic hazard. For the evaluations, high-seismic hazard was defined as having design acceleration parameters $S_{DS}$ equal to 1.0 and $S_{D1}$ equal to 0.60. These acceleration parameters were used for the SDC $D_{max}$ evaluation in accordance with FEMA P695. Moderate-seismic hazard was defined as having design spectral response acceleration parameters $S_{DS}$ equal to 0.499 and $S_{D1}$ equal to 0.199, which are the boundary values for SDC C and SDC D. This is referred to as SDC $C_{max}$ for the evaluations.

The FEMA P695 Far-Field Ground Motion Ensemble was used. This ensemble contains twenty-two historical ground motions listed in Table A-1, with two horizontal components each recorded at the same station. This results in forty-four ground motion records for use in analyzing each archetype. This ground motion ensemble is considered representative of the seismicity in the western United States.

**Table A-1 FEMA P695 Earthquake Ground Motion Ensemble**

| EQ Index | Earthquake Event | | | | Recording Station | PGA(g)* |
|---|---|---|---|---|---|---|
| | Name | | Year | $M_w$ | | |
| | EQ ID | Earthquake | | | | |
| 1 | 12011 | Northridge | 1994 | 6.7 | Beverly Hills – Mulhol | 0.52 |
| 2 | 12012 | Northridge | 1994 | 6.7 | Canyon Country–WLC | 0.48 |
| 3 | 12041 | Duzce, Turkey | 1999 | 7.1 | Bolu | 0.82 |
| 4 | 12052 | Hector Mine | 1999 | 7.1 | Hector | 0.34 |
| 5 | 12061 | Imperial Valley | 1979 | 6.5 | Delta | 0.35 |
| 6 | 12062 | Imperial Valley | 1979 | 6.5 | El Centro Array#11 | 0.38 |
| 7 | 12071 | Kobe, Japan | 1995 | 6.9 | Nishi – Akashi | 0.51 |
| 8 | 12072 | Kobe, Japan | 1995 | 6.9 | Shin – Osaka | 0.24 |
| 9 | 12081 | Kocaeli, Turkey | 1999 | 7.5 | Duzce | 0.36 |
| 10 | 12082 | Kocaeli, Turkey | 1999 | 7.5 | Arcelik | 0.22 |
| 11 | 12091 | Landers | 1992 | 7.3 | Yermo Fire Station | 0.24 |
| 12 | 12092 | Landers | 1992 | 7.3 | Coolwater | 0.42 |
| 13 | 12101 | Loma Prieta | 1989 | 6.9 | Capitola | 0.53 |
| 14 | 12102 | Loma Prieta | 1989 | 6.9 | Gilroy Array#3 | 0.56 |
| 15 | 12111 | Manjil, Iran | 1990 | 7.4 | Abbar | 0.51 |
| 16 | 12121 | Superstition Hills | 1987 | 6.5 | El Centro Imp. Co. | 0.36 |
| 17 | 12122 | Superstition Hills | 1987 | 6.5 | Poe Road (temp) | 0.45 |
| 18 | 12132 | Cape Mendocino | 1992 | 7.0 | Rio Dell Overpass | 0.55 |
| 19 | 12141 | Chi-Chi, Taiwan | 1999 | 7.6 | CHY 101 | 0.44 |
| 20 | 12142 | Chi-Chi, Taiwan | 1999 | 7.6 | TCU045 | 0.51 |
| 21 | 12151 | San Fernando | 1971 | 6.6 | LA – Hollywood Stor. | 0.21 |
| 22 | 12171 | Friuli, Italy | 1976 | 6.5 | Tolmezzo | 0.35 |

The collapse margin ratio (*CMR*) is determined from the IDA and fragility curves. *CMR* is defined as the median spectral collapse intensity at the fundamental elastic period of the building archetype under analysis, $S_{CT}[T]$, obtained from nonlinear dynamic analyses, divided by the ground motion spectral demand, $S_{MT}[T]$, at the maximum considered earthquake (MCE)

intensity level at the same fundamental elastic period. The collapse margin ratio is multiplied by a spectral shape factor (SSF) to obtain an adjusted collapse margin ratio (*ACMR*). The spectral shape factor is a function of the fundamental period, the period-based ductility, $\mu_T$, and the applicable seismic design category of the archetype under analysis. The *ACMR* for both individual archetypes and the archetype performance groups are compared to acceptable *ACMR*s that account for uncertainties judged to be within the evaluation process. The acceptable *ACMR* for a performance group targets less than 10 percent probability of collapse in an MCE event, and the acceptable *ACMR* for individual archetypes targets less than 20 percent probability of collapse in an MCE event.

For this study, the acceptable *ACMR*s were computed using the uncertainty (beta) factors listed in Table A-2. The value for the design requirement uncertainty was based on an assumed improved design procedure, so a larger value might be more appropriate for evaluating the traditional design procedure. The combined uncertainty, $\beta_{Total}$, was computed as the square-root-sum-of-the-squares of the individual uncertainties. For $\beta_{Total}$ equal to 0.66, the acceptable *ACMR* is 1.73 and 2.30 for 20 percent and 10 percent probability of collapse at MCE ground motion, respectively. Thus, the acceptable *ACMR* applicable for the performance of individual archetypes was 1.73, and the acceptable *ACMR* of performance groups was 2.30.

**Table A-2 Beta Factors for Determining Acceptable Collapse Margin Ratios**

| Description | Beta Factor | Value of $\beta$ |
|---|---|---|
| Record-to-record uncertainty | $\beta_{TR}$ | 0.40 |
| Design requirements uncertainty | $B_{DR}$ | 0.20 |
| Test data uncertainty | $\beta_{TD}$ | 0.35 |
| Modeling uncertainty | $B_{MDL}$ | 0.35 |
| Combined uncertainty | $\beta_{Total}$ | 0.66 |

## A.1 Modeling Framework

Large wood structural panel and steel deck diaphragms can have thousands of connectors. Yielding of these connectors is the primary means of obtaining ductility and dissipating energy. Although modeling the nonlinear behavior of all or many of these connectors in a detailed three-dimensional analysis would be the ideal means of evaluating RWFD systems, taking this approach is unrealistic at this time given the thousands of hours of computer run time it would require. For example, such a model took more than three hours to run one-half of a comparatively short record. Because the computer

run time necessary to perform nonlinear response history analyses of detailed three-dimensional models is too long, a modeling framework was developed that allows for a relatively simplified model to be used.

The modeling framework developed to analyze RWFD buildings included three steps, as illustrated in Figure A-1. These three steps were as follows:

1. Create a database of connectors that have been cyclically tested and develop analytical models to capture their responses (Koliou and Filiatrault, 2017). Based on the test results, determine the hysteretic parameters of Wayne-Stewart (Stewart, 1987) or SAWS (Folz and Filiatrault, 2001) nonlinear cyclic springs for each connector. A representation of the parameters for the Wayne-Stewart and SAWS springs are shown in Figure A-2. Examples for nailed and welded framing connectors are illustrated in Figure A-3 and Figure A-4.
2. Create an analytical model in MATLAB (MATLAB, 2013) of one-half of each archetype's diaphragm (due to symmetry) that accounts for the stiffness of the panels, diaphragm chords, and each diaphragm connector. Divide the diaphragm model into horizontal segments and load the diaphragm by a cyclic point load at its mid-span. Combine the response of the elements and connectors within each diaphragm segment to form a single nonlinear hysteretic spring that represents the cyclic response of the segment. This step is illustrated in Figure A-5. Variable connector spacing is accounted for in this model.
3. Create a two-dimensional building model in RUAUMOKO2D (Carr, 2007) that consists of one-half of the archetype (due to symmetry) and includes a spring and mass for each horizontal diaphragm segment, beam elements with nonlinear hinges to represent the out-of-plane wall response, and springs and masses to represent the in-plane wall at the end of the diaphragm. A representation of the simplified model is shown in Figure A-6. *P*-delta effects are incorporated into the model by applying the roof weight on leaning columns between the ground and the roof diaphragm. Localized effects that account for shear concentration in subdiaphragms, at corners, at openings, or at regions receiving wall anchorage forces are not accounted for in this analysis. This model also cannot account for loading from the two orthogonal directions acting simultaneously.

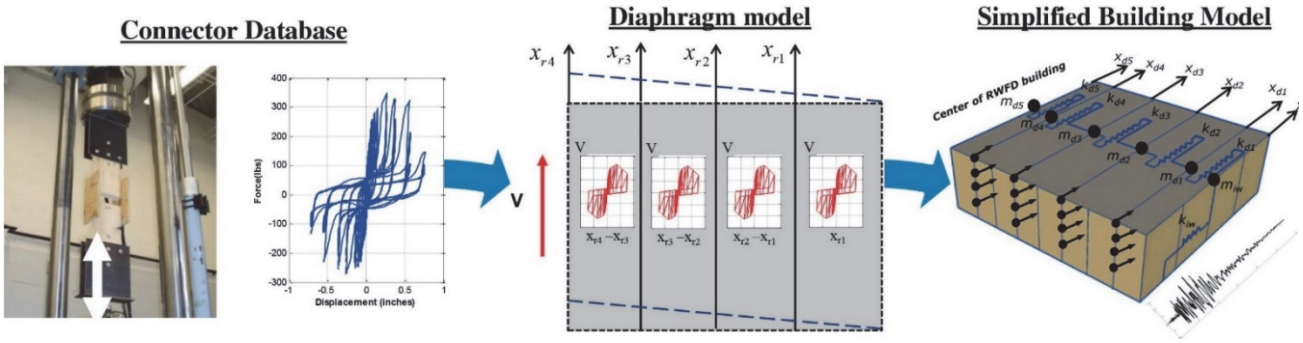


Figure A-1 Three-step modeling framework.

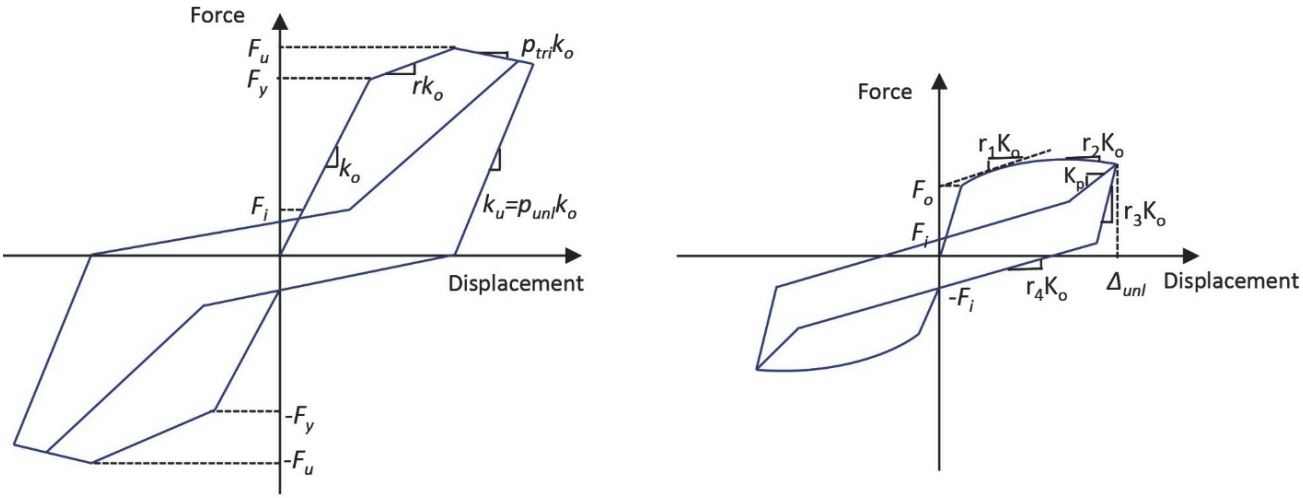


Figure A-2 Illustration of hysteretic models: (a) Wayne-Stewart; and (b) SAWS.

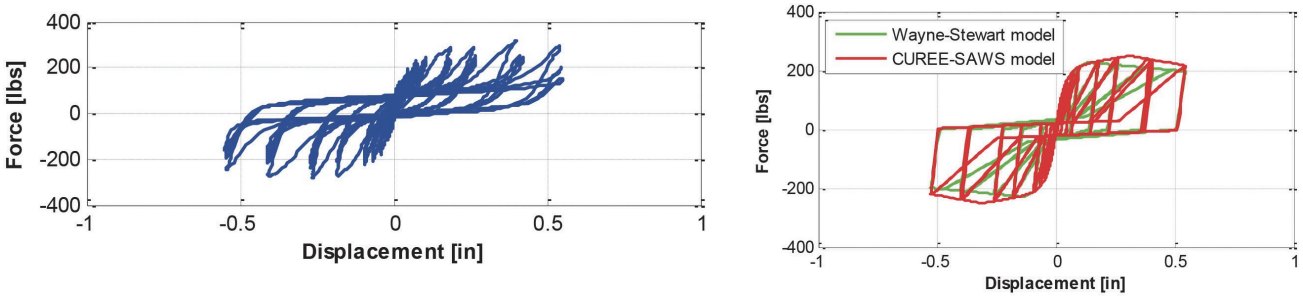


Figure A-3 Comparison of hysteretic response for 10d common nail and wood deck: (a) example of experimental data (Coyne, 2007) and (b) best fit numerical model based on data from several tests (Koliou, 2014).

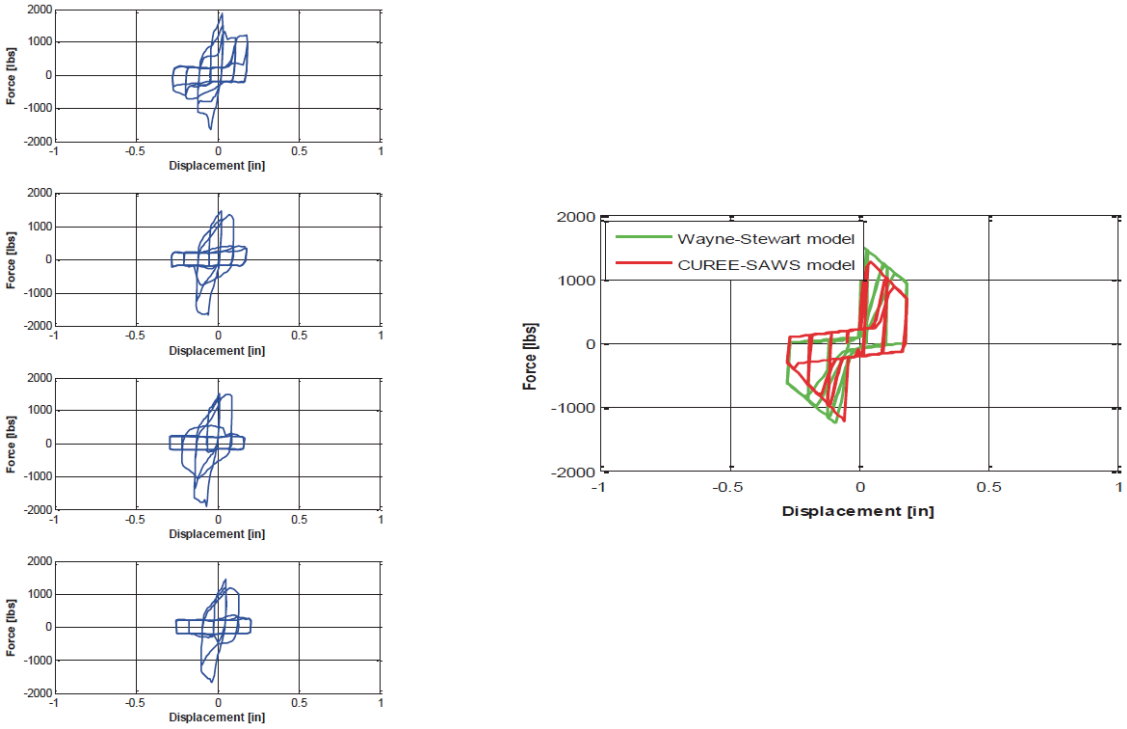


(a) (b)

Figure A-4 Comparison of hysteretic response for 2-ply, 22-gage framing welds to 0.25 in. plate: (a) experimental (Guenfoud et al., 2010) and (b) fitted optimal hysteretic models.

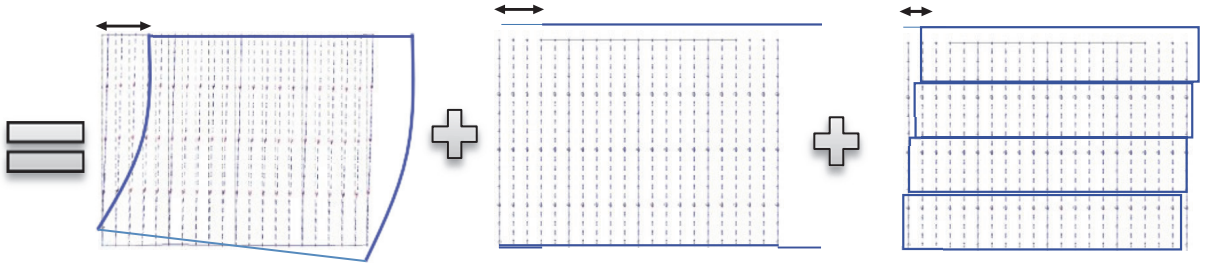

Figure A-5 In-plane displacement components of the analytical inelastic roof diaphragm model.

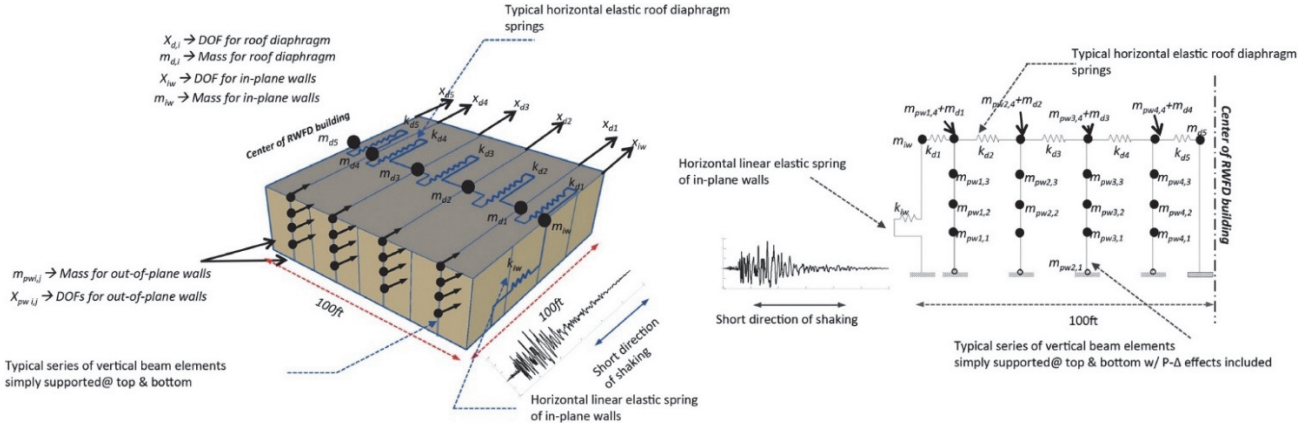


(a) (b)

Figure A-6 Illustration of a simplified RWFD building model developed in the RUAUMOKO2D platform.

Cyclic test data for the 10d common nails are from Coyne (2007), Fonseca et al. (2002), and Christovasilis et al. (2009). Cyclic data for button punch, screw, and top seam weld sidelap connectors between deck sheets are from Rogers and Tremblay (2003a). Cyclic data for welds, powder actuated fasteners, and screws that connect steel deck to steel plates are from Guenfoud et al. (2010) and from Rogers and Tremblay (2003b). A list of the database of cyclic test data for nails and steel deck connectors is included in Table A-3, Table A-4, and Table A-5.

## A.2 Modeling Framework Validation

The two-dimensional model of the diaphragm, Step 2, was validated by comparing predicted results to cyclic diaphragm test results of Tremblay et al. (2004). The predicted and tested shear for monotonic loading are normalized to the applicable maximum shear and compared in Figure A-7. The results of shear versus deformation for one main cycle predicted by the diaphragm submodel versus the test results are compared in Figure A-8. Two validation methods were used for the simplified model, Step 3. First, the initial elastic periods were obtained from the simplified model using eigenvalue analysis and compared to first and second mode periods predicted by the detailed Finite Element Model developed by Olund (2009). The periods from the simplified model were approximately 3 percent longer than Olund's model, indicating good correlation.

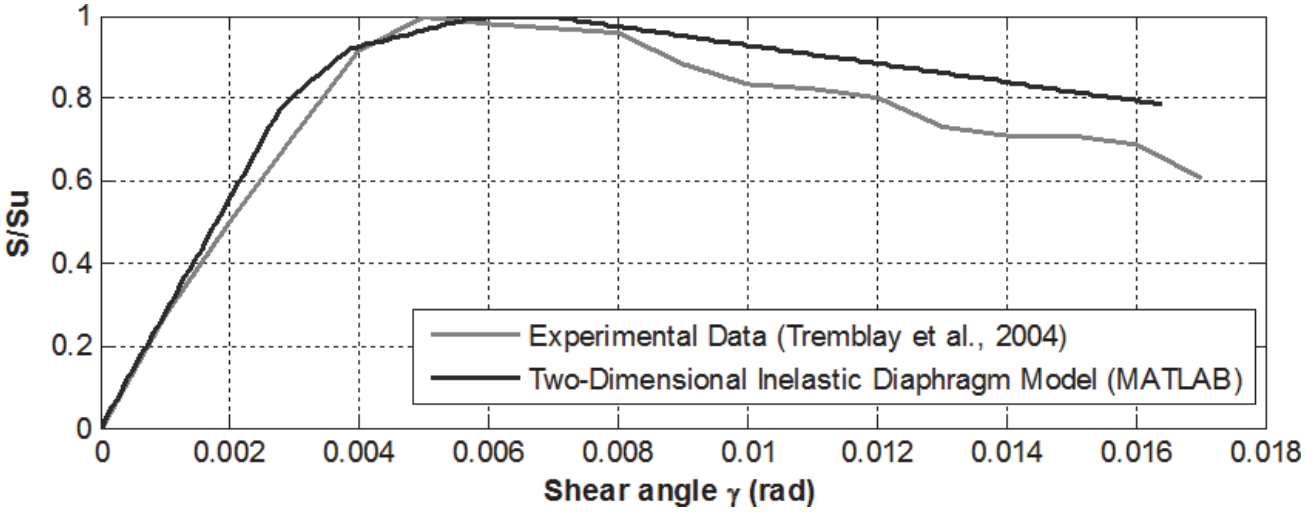


Figure A-7 Validation/comparison of inelastic roof diaphragm for monotonic loading.

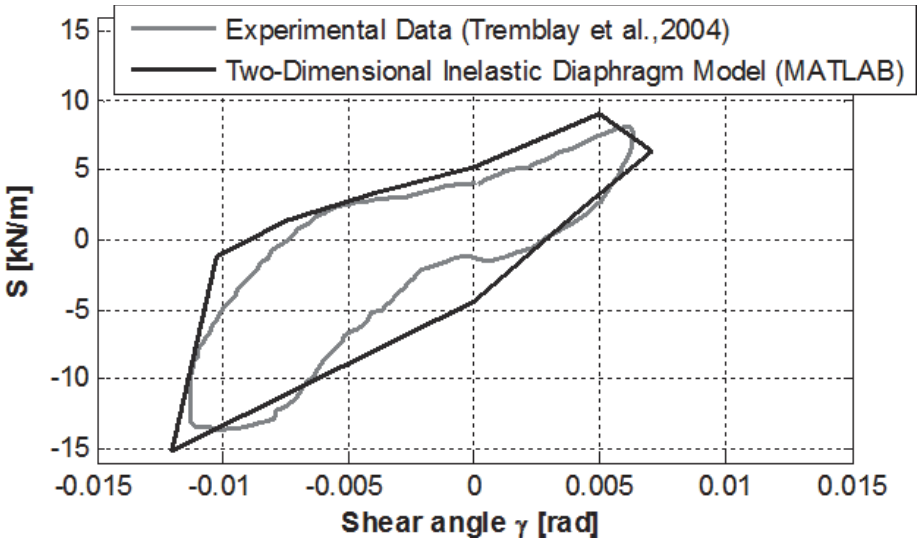


Figure A-8 Validation/comparison of inelastic roof diaphragm for cyclic loading (one main cycle).

As a second validation for Step 3, the RWFD simplified model was used to compare the probability of the roof drift exceeding 3 percent, with similar data available from Olund. Olund set the limit state for a RWFD as a roof drift equal to 3 percent. For the purpose of comparing results of Olund's detailed model to those of the simplified building model, the limit state was set equal to 3 percent diaphragm drift, but for analysis results for the FEMA P695 evaluations, the limit state was equated to a load-displacement (*P*-delta) sidesway instability.

The simplified building model overestimates the probability of exceedance by a factor of up to 3 at low $S_a$ values. However, in the range of most interest ($S_a$ between 2 and 3), the simplified building model is within approximately 9 percent of the Olund probability of exceedance.

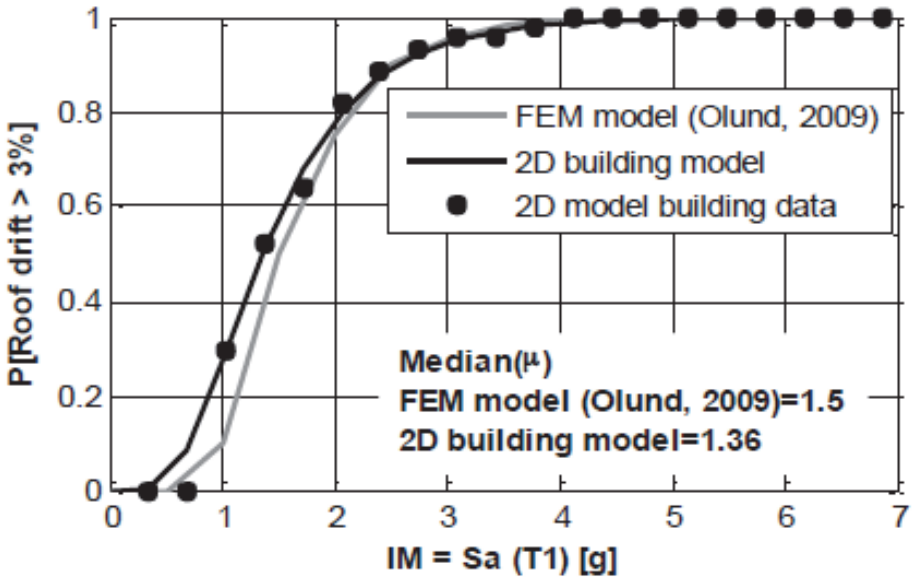


Figure A-9 Incremental dynamic analysis results/comparison.

A limitation of the modeling framework was that it could not account for simultaneous loading of framing connectors at ends of steel deck sheets from the in-plane diaphragm shears and the continuity tie or out-of-plane wall anchorage forces. Therefore, the archetypes designed and analyzed were based on the requirements to resist shear only. However, the magnitudes of these two sources of loading are not compatible with one another. Specifically, out-of-plane wall forces were not reduced to account for ductility, and the connections supporting the wall were expected to behave elastically, while the forces acting on these same connectors from diaphragm shear resistance were based on an assumption that the connections will yield. There seems to be a philosophical conflict in the intended behavior of the fastener when exposed to both diaphragm shear forces and wall anchorage forces, which occur simultaneously in some regions of the diaphragm. Further analyses beyond those for the FEMA P695 evaluations are recommended to study this issue. Studying this issue will require nonlinear response history analyses of detailed, three-dimensional models with nonlinear connections.

## A.3 List of Connectors in Database

Cyclic test data are essential for analyzing flexible roof diaphragms. At the time the FEMA P695 analyses were performed, the data for common nail connectors were relatively complete. Additional connection tests have since been performed for bare steel deck diaphragms as presented in Appendix D. The connections included in the database assembled by Koliou (2014) and Koliou and Filiatrault (2017), and the sources of the test data are included in

Table A-3, Table A-4, and Table A-5. The fitted parameters for the Wayne-Stewart hysteretic model and the SAWS hysteretic model are included in Koliou (2014) and Koliou and Filiatrault (2017).

**Table A-3 Cyclic Test Data for Nails**

| Connection Type | Specimen Characteristics | Number of Specimens Tested | Source |
|---|---|---|---|
| 6d common nails (d, diameter=0.113 in.; l, length=2.0 in.) | 7/16 OSB std. | 10 | Coyne (2007) |
| 8d common nails (d=0.113 in., l=2.5 in.) | 2x4 Hem Fir. & 7/16 OSB std. | 19 | Christovasilis et al. (2009) |
| | 2x6 Hem Fir. & 7/16 OSB std. | 17 | |
| 8d common nails (d=0.131 in., l=2.5 in.) | 7/16 OSB std. | 10 | Coyne (2007) |
| 10d common nails (d=0.148 in., l=3.0 in.) | 7/16 OSB std. | 10 | |
| | 5/8 OSB std. | 10 | |
| | 3/4 OSB std. | 10 | |
| 10d box nails (d=0.131 in., l=3.0 in.) | DF-L & 19/32 T&G | 20 | Fonseca et al. (2002) |
| | DF-L & 19/32 OSB std. | 20 | |
| #10 Rolled – Hardened screws (d=0.113 in., l=2.0 in.) | DF-L & 7/16 OSB std. | 20 | |

**Table A-4 Cyclic Test Data for Steel Deck Sidelap Connectors**

| Connection Type | Specimen Characteristics | Number of Specimens Tested | Corresponding Publication |
|---|---|---|---|
| Button punch (0.39 in. diameter) | 22 ga deck | 2 | Rogers and Tremblay (2003a) |
| | 20 ga deck | 2 | |
| Screws (10-14×7/8 in.) | 22 ga deck | 2 | |
| | 20 ga deck | 2 | |
| Welds (1.38 in. length) | 22 ga deck | 2 | |

**Table A-5 Cyclic Test Data for Steel Deck Framing Connectors**

| Connection Type | Specimen Characteristics | Number of Specimens Tested | Corresponding Publication |
|---|---|---|---|
| Powder-Actuated Fasteners (Hilti EDNK22-THO12 and Buildex BX12) | 22 ga deck to 0.12 in. plate | 4 | Rogers and Tremblay (2003b) |
| | 20 ga deck to 0.12 in. plate | 4 | |
| Powder-Actuated Fasteners (Hilti ENPH2-21-L15 and Buildex BX14) | 22 ga deck to 0.79 in. plate | 4 | |
| | 20 ga deck to 0.79 in. plate | 4 | |
| Buildex Screws (12-14x in.) | 22 ga deck to 0.12 in. plate | 2 | |
| | 20 ga deck to 0.12 in. plate | 2 | |
| Hilti Screws (12-24x7/8 in.) | 22 ga deck to 0.12 in. plate | 2 | |
| | 20 ga deck to 0.12 in. plate | 2 | |
| Welds (0.63 in. arc spot) & Washer | 22 ga deck to 0.12 in. plate | 1 | |
| Welds (0.63 in. arc spot) | 22 ga deck to 0.12 in. plate | 2 | |
| | 22 ga deck to 0.79 in. plate | 1 | |
| | 20 ga deck to 0.12 in. plate | 2 | |
| Welds (0.63 in. – 0.75 in. arc spot) | 2 ply – 16 ga deck to 0.25 in. plate | 4 | Guenfoud, Tremblay & Rogers (2010) |
| | 2 ply – 18 ga deck to 0.25 in. plate | 4 | |
| | 2 ply – 20 ga deck to 0.25 in. plate | 4 | |
| | 2 ply – 22 ga deck to 0.25 in. plate | 4 | |
| | 4 ply – 16 ga deck to 0.25 in. plate | 4 | |
| | 4 ply – 18 ga deck to 0.25 in. plate | 3 | |
| | 4 ply – 20 ga deck to 0.25 in. plate | 4 | |
| | 4 ply – 22 ga deck to 0.25 in. plate | 4 | |

## A.4 Common Formulas and Abbreviations Used in FEMA P695 Studies

Table A-6 contains common formulas and abbreviations used in Appendix A through Appendix D to describe the FEMA P695 studies.

**Table A-6 Common Formulas and Abbreviations Used in FEMA P695 Studies**

| Abbreviation | Description |
|---|---|
| *ACMR* | Adjusted Collapse Margin Ratio, where: $ACMR = SSF_i \times CMR_i$ |
| *BDR* | Building Drift Ratio, where: *BDR*(%) = *DDR*(%) + *WDR*(%) |
| *CMR* | Collapse Margin Ratio, where: $CMR_i = \frac{S_{CT}}{S_{MT}}$ |
| DE | Design Earthquake |
| *DDR* | Diaphragm Drift Ratio (%), where: $DDR(\%) = \frac{X_{mid,roof}}{L_f / 2} \times 100$<br>$X_{mid,roof}$ is the diaphragm deflection at mid length<br>$L_f$ is the diaphragm span in feet |
| MCE | Maximum Considered Earthquake |
| *SSF* | Spectral Shape Function |
| $S_{CT}$ [*T*] | Median collapse intensity obtained from nonlinear dynamic analysis at the fundamental elastic period |
| $S_{MT}$ [*T*] | Ground motion spectral demand at maximum considered earthquake (MCE) intensity level at the fundamental elastic period |
| WDR(%) | In-plane Wall Drift Ratio, where: $WDR(\%) = \frac{X_{in\text{-}plane\ walls}}{h_{wall}} \times 100$<br>$X_{in\text{-}plane\ walls}$ is the deflection at the roof level of the in-plane walls<br>$h_{wall}$ is the height of roof above the foundation |
| $\mu_T$ | Period based ductility, where: $\mu_T = \frac{\delta_u}{\delta_{y,eff}}$<br>$\delta_u$ is the ultimate building drift ratio (BDR)<br>$\delta_{y,eff}$ is the effective yield building drift ratio (BDR) |

# Appendix B

# Evaluation of Traditional Design Procedure Using FEMA P695

The traditional design procedure was used to develop a set of archetype RWFD buildings, and FEMA P695 analyses were applied to these designs to provide a baseline of performance and to demonstrate that changes to the design procedure are necessary. This chapter provides a summary of the archetypes used to evaluate the traditional design procedure and provides a summary of the FEMA P695 evaluation results. Both wood and steel deck diaphragms are addressed.

## B.1 Description of Archetypes

Evaluations were performed on archetypes as described for high- and moderate-seismic hazard as defined in Appendix A. For these evaluations, archetypes were designed with either wood structural panel or steel deck diaphragms. The archetype naming convention is shown in Figure B-1. Detailed descriptions of the archetypes and diaphragm construction are provided in Table B-1 through Table B-3 and Figure B-2 through Figure B-5.

The archetypes are grouped by diaphragm type, either wood or steel deck, and whether the diaphragm is relatively large or small. The archetypes have plan aspect ratios of 1:1, 2:1, and 1:2. Large diaphragms are 400 feet long and either 400 feet or 200 feet wide. The small diaphragms with aspect ratios of 2:1 or 1:2 are 200 feet long by 100 feet wide, whereas those with 1:1 aspect ratios are 100 feet by 100 feet. The wood diaphragms are wood structural panels constructed of oriented-strand board (OSB) nailed to wood nailers that are attached to open-web steel joists. This design is commonly called a hybrid panelized roof structure. The steel deck diaphragms are attached to the joists with arc spot welds, PAFs, or self-drilling screws. Adjacent steel deck sheets are attached along their sides (sidelaps) with top seam welds, button punches, or self-drilling screws. Many steel deck diaphragms include proprietary sidelap connections in the western United States, which includes regions of high seismicity. Archetypes are not included with the proprietary sidelap connections because cyclic test data for

the response of these connectors are not available. The steel deck diaphragms were designed using 22-gage and 20-gage deck because connection data were available for these sizes. Thicker gage deck results in less ductile connections, so the steel deck diaphragm results presented herein are limited to only diaphragms with 22-gage or 20-gage deck.

The archetype walls are constructed of reinforced concrete panels measuring 25 feet wide, 33 feet tall (from the top of the slab-on-grade), and 9 1/4 inch thick for high-seismic hazard and 7 1/4 inch thick for moderate-seismic hazard. The roof level is 30 feet above the top of the slab-on-grade, with the walls cantilevering as a parapet 3 feet higher than the roof level.

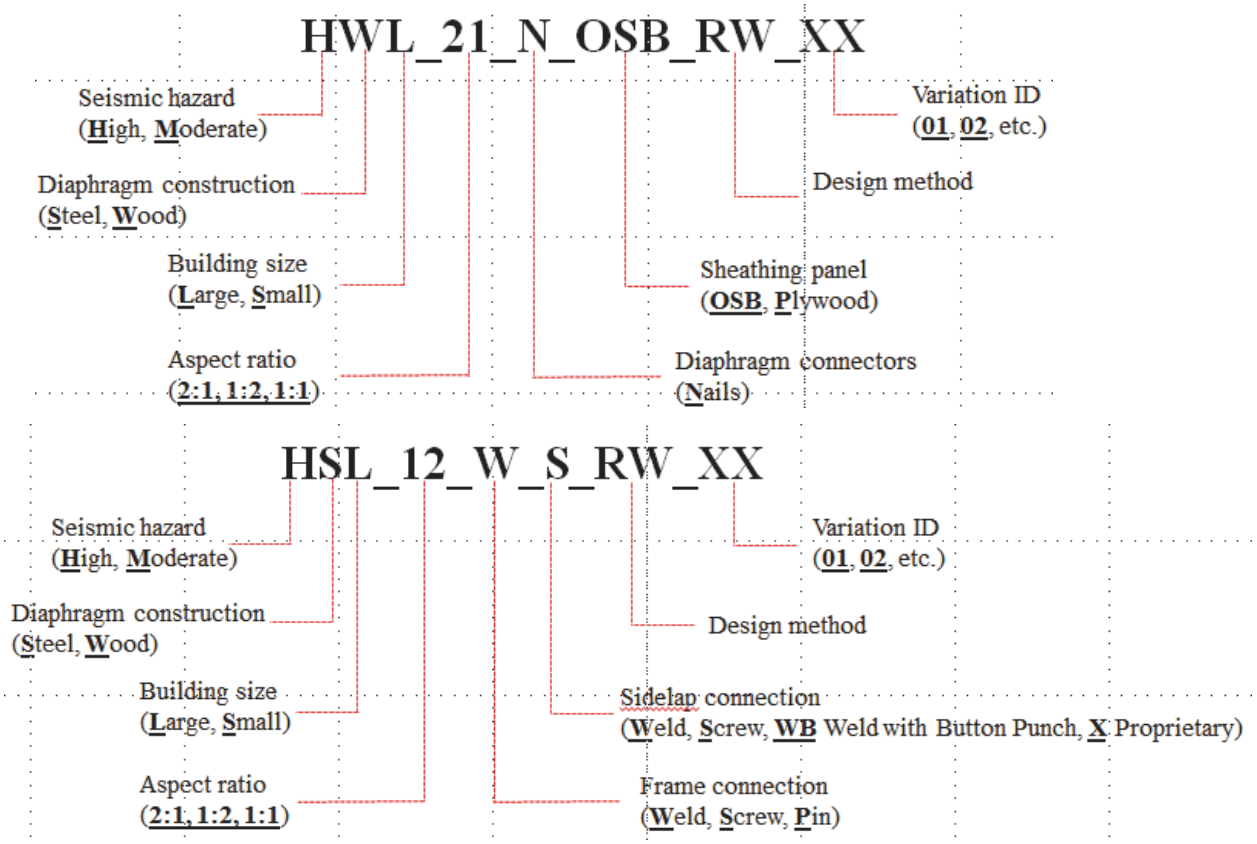


Figure B-1 Archetype naming convention.

The archetypes, which were designed in conformance to ASCE/SEI 7-10, have intermediate precast shear walls with a response modification coefficient ($R$) of 4. The design period for each direction of each archetype was computed using the approximate period equation, ASCE/SEI 7 Equation 12.8-7, for $T_a$, which is consistent with traditional practice. For the 30-foot roof height of the archetypes, the approximate period is 0.26 seconds. This value is less than the transition period, $T_s$, equal to 0.60 seconds for high-seismic-hazard (SDC $D_{max}$) archetypes and 0.40 seconds for moderate-

seismic-hazard (SDC $C_{max}$) archetypes. Therefore, the archetypes for the traditional design procedure were designed using a base shear coefficient of 0.25 for the high-seismic hazard (SDC $D_{max}$) and using a base shear coefficient of 0.125 for the moderate-seismic hazard (SDC $C_{max}$).

The diaphragms for the archetypes are zoned with different fastener spacings similar to zoning commonly used in practice. Details about the diaphragm fastener zoning are provided in Figure B-2 through Figure B-5.

**Table B-1 Descriptions of Archetypes with Wood Diaphragms—Traditional Design**

| Archetype ID | Diaphragm Construction | Building Size | Diaphragm Aspect Ratio | Building Dimensions (ft) | Connector Type | Seismic Design Category |
|---|---|---|---|---|---|---|
| HWL_21_N_OSB_RW4_04 | Wood | Large | 2:1 | 400×200 | Common nails | $D_{max}$ |
| HWL_12_N_OSB_RW4_02 | Wood | Large | 1:2 | 200×400 | Common nails | $D_{max}$ |
| HWL_11_N_OSB_RW4_01 | Wood | Large | 1:1 | 400×400 | Common nails | $D_{max}$ |
| HWS_21_N_OSB_RW4_01 | Wood | Small | 2:1 | 200×100 | Common nails | $D_{max}$ |
| HWS_12_N_OSB_RW4_01 | Wood | Small | 1:2 | 100×200 | Common nails | $D_{max}$ |
| HWS_11_N_OSB_RW4_01 | Wood | Small | 1:1 | 100×100 | Common nails | $D_{max}$ |
| HWS_11_N_OSB_RW4_02 | Wood | Small | 1:1 | 100×100 | Common nails | $D_{max}$ |
| MWL_11_N_OSB_RW4_01 | Wood | Large | 1:1 | 400×400 | Common nails | $C_{max}$ |
| MWL_21_N_OSB_RW4_01 | Wood | Large | 2:1 | 400×200 | Common nails | $C_{max}$ |
| MWL_12_N_OSB_RW4_01 | Wood | Large | 1:2 | 200×400 | Common nails | $C_{max}$ |
| MWS_11_N_OSB_RW4_01 | Wood | Small | 1:1 | 100×100 | Common nails | $C_{max}$ |
| MWS_21_N_OSB_RW4_01 | Wood | Small | 2:1 | 200×100 | Common nails | $C_{max}$ |
| MWS_12_N_OSB_RW4_01 | Wood | Small | 1:2 | 100×200 | Common nails | $C_{max}$ |

## Archetype: HWL_11_N_OSB_RW4_01

Top of Wall = 33-ft
Top of Roof = 30-ft

9¼" concrete wall panels (f'c=4ksi) with #5@10"o.c. (fy=60ksi)

15/32" Structural I rated OSB, fully blocked

Nail Spacings (inches) — Continuous Edges of Panels / Other Edges of Panels / Intermediate (Field)

1. 10d at 6,6,12
2. 10d at 4,6,12
3. 10d at 2½,4,12
4. 10d at 2,3,12 w/ 3x framing

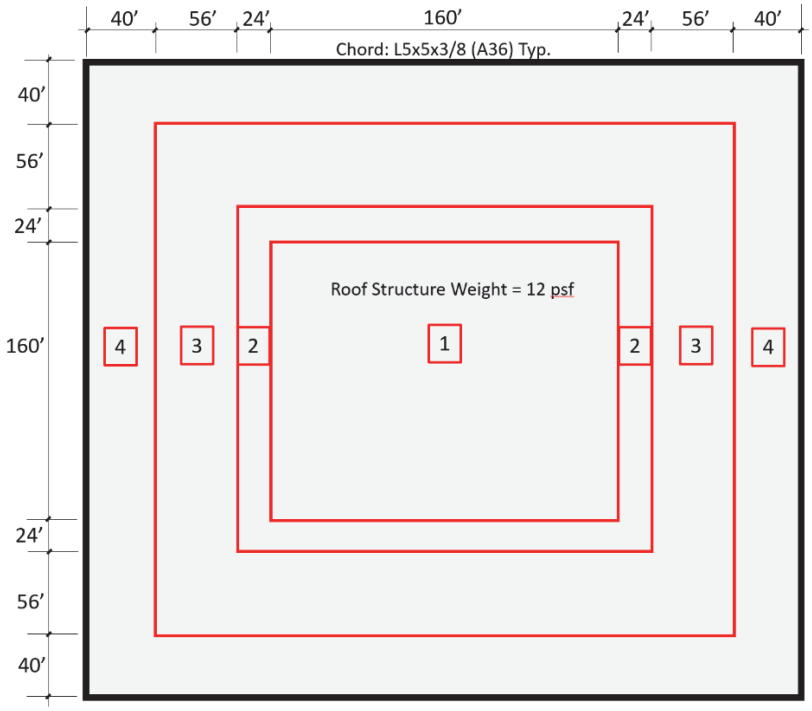


## Archetype: HWL_21_N_OSB_RW4_01 HWL_12_N_OSB_RW4_01

Top of Wall = 33-ft
Top of Roof = 30-ft

9¼" concrete wall panels (f'c=4ksi) with #5@10"o.c. (fy=60ksi)

15/32" Structural I rated OSB, fully blocked

Nail Spacings (inches) — Continuous Edges of Panels / Other Edges of Panels / Intermediate (Field)

1. 10d at 6,6,12
2. 10d at 4,6,12
3. 10d at 2½,4,12
4. 10d at 2,3,12 w/ 3x framing
5. 2 lines of 10d at 2½,4,12 w/ 4x framing
6. 2 lines of 10d at 2½,3,12 w/ 4x framing

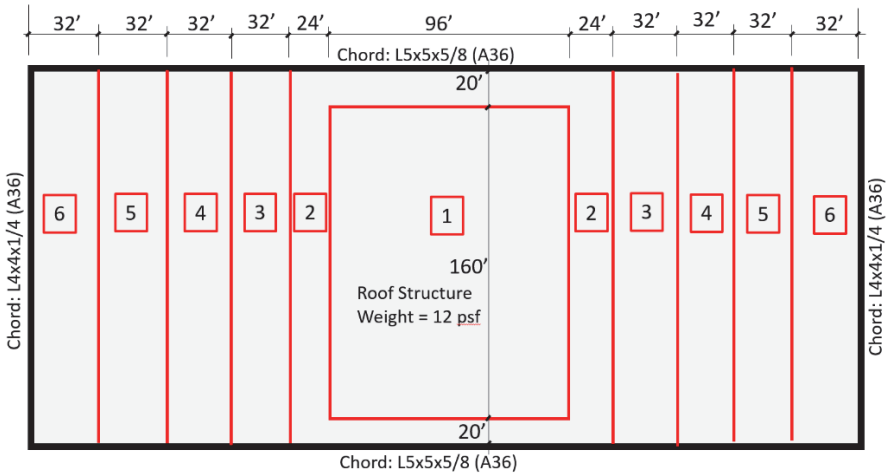


Figure B-2 Design details for the "large" archetypes with wood diaphragms designed for high-seismic hazard (traditional procedure).

## Archetype:
## HWS_21_N_OSB_RW4_01
## HWS_12_N_OSB_RW4_01

Top of Wall = 33-ft
Top of Roof = 30-ft

9¼" concrete wall panels (f'c=4ksi)
with #5@10"o.c. (fy=60ksi)

15/32" Structural I rated OSB,
fully blocked

Nail Spacings (inches) — Continuous Edges of Panels / Other Edges of Panels / Intermediate (Field)

| | |
|---|---|
| 1 | 10d at 6,6,12 |
| 2 | 10d at 4,6,12 |
| 3 | 10d at 2½,4,12 |
| 4 | 10d at 2,3,12 w/ 3x framing |
| 5 | 2 lines of 10d at 2½,4,12 w/ 4x framing |

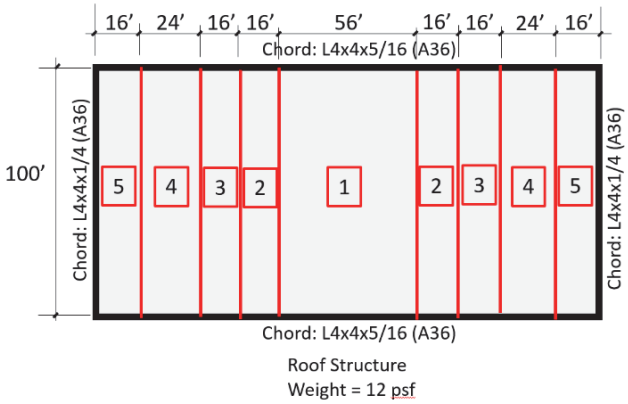


## Archetype:
## HWS_11_N_OSB_RW4_01
## HWS_11_N_OSB_RW4_02

Top of Wall = 33-ft
Top of Roof = 30-ft

9¼" concrete wall panels (f'c=4ksi)
with #5@10"o.c. (fy=60ksi)

15/32" Structural I rated OSB,
fully blocked

Nail Spacings (inches) — Continuous Edges of Panels / Other Edges of Panels / Intermediate (Field)

| | |
|---|---|
| 1 | 10d at 6,6,12 |
| 6 | 2 lines of 10d at 2½,3,12 w/ 4x framing |

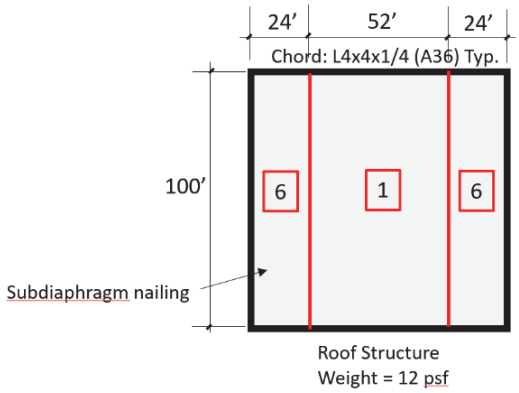


Figure B-3 Design details for the "small" archetypes with wood diaphragms designed for high-seismic hazard (traditional procedure).

## Archetype: MWL_11_N_OSB_RW4_01

Top of Wall = 33-ft
Top of Roof = 30-ft

7¼" concrete wall panels (f'c=4ksi) with #5@14"o.c. (fy=60ksi)

15/32" Structural I rated OSB, fully blocked

Nail Spacings (inches) — Continuous Edges of Panels / Other Edges of Panels / Intermediate (Field)

| | |
|---|---|
| 1 | 10d at 6,6,12 |
| 2 | 10d at 4,6,12 |

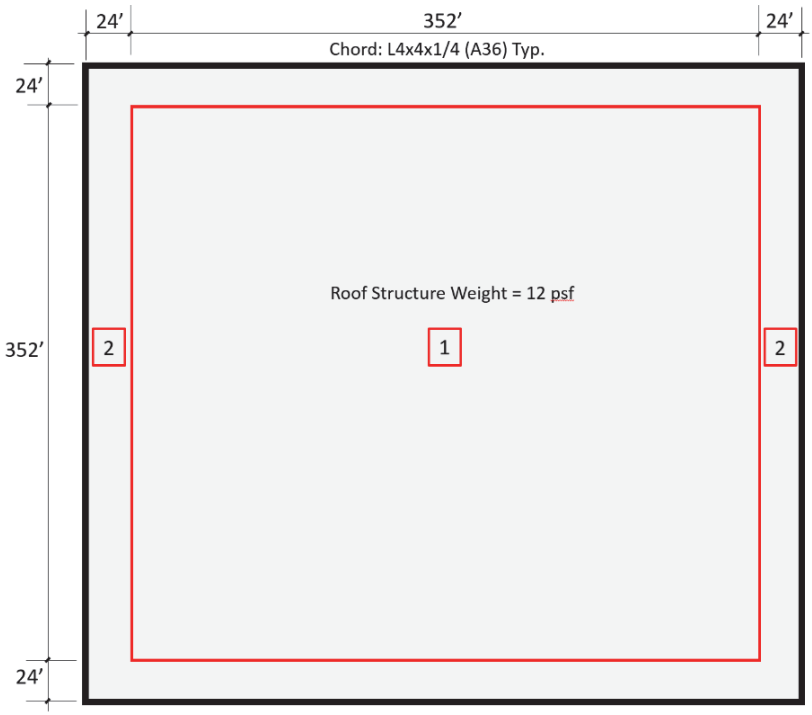


## Archetype: MWL_21_N_OSB_RW4_01 MWL_12_N_OSB_RW4_01

Top of Wall = 33-ft
Top of Roof = 30-ft

7¼" concrete wall panels (f'c=4ksi) with #5@14"o.c. (fy=60ksi)

15/32" Structural I rated OSB, fully blocked

Nail Spacings (inches) — Continuous Edges of Panels / Other Edges of Panels / Intermediate (Field)

| | |
|---|---|
| 1 | 10d at 6,6,12 |
| 2 | 10d at 4,6,12 |
| 3 | 10d at 2½,4,12 |

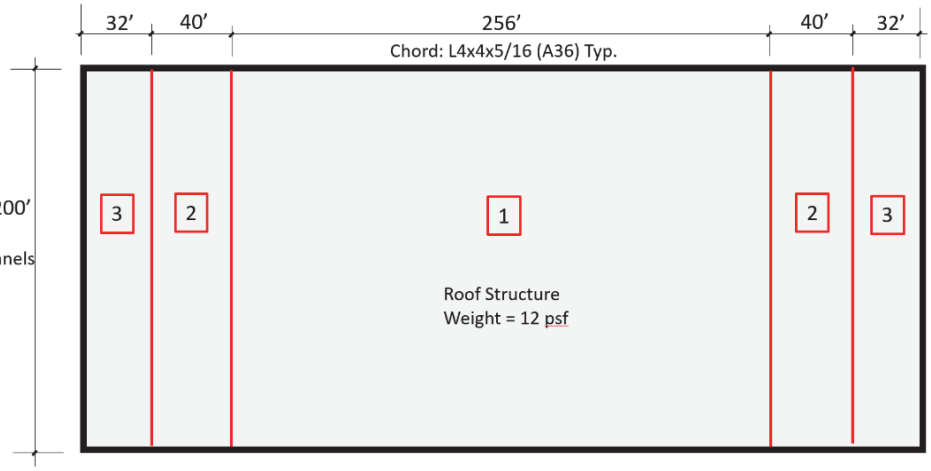


Figure B-4 Design details for "large" archetypes with wood diaphragms designed for moderate-seismic hazard (traditional procedure).

## Archetype:
## MWS_11_N_OSB_RW4_01

Top of Wall = 33-ft
Top of Roof = 30-ft

7¼" concrete wall panels (f'c=4ksi)
with #5@14"o.c. (fy=60ksi)

15/32" Structural I rated OSB,
fully blocked

Nail Spacings (inches)
Continuous Edges of Panels
Other Edges of Panels
Intermediate (Field)

| | |
|---|---|
| 1 | 10d at 6,6,12 |
| 2 | 10d at 4,6,12 |

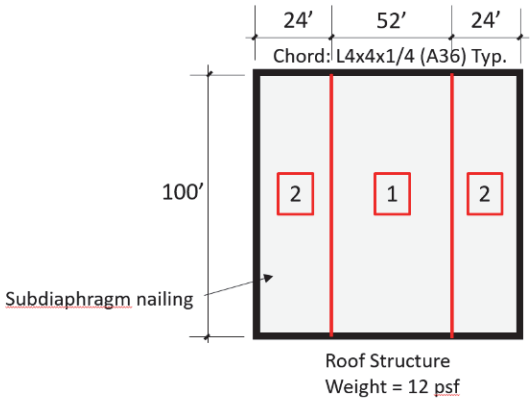


## Archetype:
## MWS_21_N_OSB_RW4_01
## MWS_12_N_OSB_RW4_01

Top of Wall = 33-ft
Top of Roof = 30-ft

7¼" concrete wall panels (f'c=4ksi)
with #5@14"o.c. (fy=60ksi)

15/32" Structural I rated OSB,
fully blocked

Nail Spacings (inches)
Continuous Edges of Panels
Other Edges of Panels
Intermediate (Field)

| | |
|---|---|
| 1 | 10d at 6,6,12 |
| 2 | 10d at 4,6,12 |

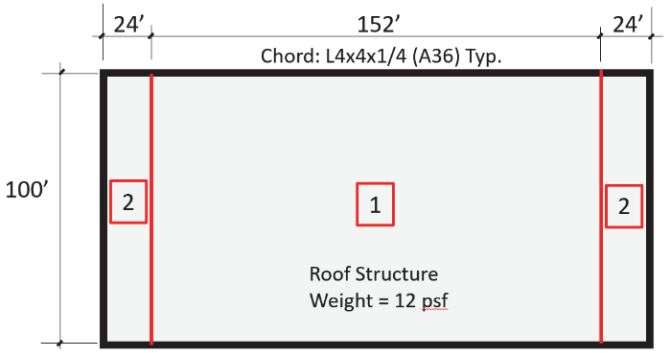


Figure B-5 Design details for "small" archetypes with wood diaphragms designed for moderate-seismic hazard (traditional procedure).

**Table B-2 Descriptions of Archetypes with Steel Diaphragms (High-Seismic Hazard)—Traditional Design**

| Archetype Designation | Diaphragm Dimensions (ft) | Zone | Zone Width (ft) | Connector Pattern / Deck Gage | Framing Connectors | Sidelap Connectors | Sidelap Spacing |
|---|---|---|---|---|---|---|---|
| **High Seismicity – Large Buildings** | | | | | | | |
| HSL_11_P_S_RW4 | 400×400 | 3 | 56 | 36/11 – 22 ga | PAF | #10 screw | 6 in. |
| | | 2 | 24 | 36/9 – 22 ga | PAF | #10 screw | 9 in. |
| | | 1 | 120 | 36/9 – 22 ga | PAF | #10 screw | 18 in. |
| HSL_11_W_WB_RW4 | 400×400 | 3 | 56 | 36/7 – 22 ga | 1/2 in. dia. welds | TSW | 12 in. |
| | | 2 | 24 | 36/7 – 22 ga | 1/2 in. dia. welds | BP | 12 in. |
| | | 1 | 120 | 36/7 – 22 ga | 1/2 in. dia. welds | BP | 24 in. |
| HSL_21_W_WB_RW4_01 | 400×200 | 3 | 0 | 36/7 – 22 ga | 1/2 in. dia. effective area welds (5/8 and 3/4 in. dia. at the surface) | TSW | 6 in. |
| | | 2 | 54 | 36/7 – 22 ga | 1/2 in. dia. effective area welds (5/8 and 3/4 in. dia. at the surface) | TSW | 12 in. |
| | | 1 | 96 | 36/7 – 22 ga | 1/2 in. dia. effective area welds (5/8 and 3/4 in. dia. at the surface) | BP | 12 in. |
| HSL_21_P_S_RW4_01 | 400×200 | 3 | 50 | 36/9 – 20 ga | PAF | #10 screws | 3 in. |
| | | 2 | 60 | 36/9 – 22 ga | PAF | #10 screws | 6 in. |
| | | 1 | 90 | 36/5 – 22 ga | PAF | #10 screws | 6 in. |
| HSL_11_S_S_RW4 | 400×400 | 3 | 66 | 36/11 – 22 ga | #12 or #14 HWH self-drilling screws by Hilti | #10 screws | 3 in. |
| | | 2 | 24 | 36/9 – 22 ga | #12 or #14 HWH self-drilling screws by Hilti | #10 screws | 6 in. |
| | | 1 | 120 | 36/9 – 22 ga | #12 or #14 HWH self-drilling screws by Hilti | #10 screws | 9 in. |
| HSL_12_W_WB_RW4 | Refer to HSL_21_W_WB for design | | | | | | |
| HSL_12_P_S_RW4 | Refer to HSL_21_P_S for design | | | | | | |

**Table B-2 Descriptions of Archetypes with Steel Diaphragms (High-Seismic Hazard)—Traditional Design (continued)**

| ArchetypeDesignation | Diaphragm Dimensions (ft) | Zone | Zone Width (ft) | Connector Pattern / Deck Gage | Framing Connectors | Sidelap Connectors | Sidelap Spacing |
|---|---|---|---|---|---|---|---|
| **High Seismicity – Small Buildings** | | | | | | | |
| HSS_11_W_B_RW4 | 100×100 | 3 | 50 | 36/5 – 22 ga | 1/2 in. dia effective welds (5/8 in. and 3/4 in. at the surface) | BP | 12 in. |
| | | 2 | 50 | 36/5 – 22 ga | 1/2 in. dia. effective welds (5/8 in. and 3/4 in. at the surface) | BP | 12 in. |
| | | 1 | 50 | 36/5 – 22 ga | 1/2 in. dia. effective welds (5/8 in. and 3/4 in. at the surface) | BP | 12 in. |
| HSS_21_W_WB_RW4 | 200×100 | 3 | 0 | 36/7 – 22 ga | 1/2 in. dia. effective welds (5/8 in. and 3/4 in. dia. puddle welds at the surface) | TSW | 9 in. |
| | | 2 | 40 | 36/7 – 22 ga | 1/2 in. dia. effective welds (5/8 in. and 3/4 in. dia. puddle welds at the surface) | TSW | 9 in. |
| | | 1 | 60 | 36/7 – 22 ga | 1/2 in. dia. effective welds (5/8 in. and 3/4 in. dia. puddle welds at the surface) | BP | 12 in. |
| HSS_12_W_WB_RW4 | Refer to HSS_21_W_WB_RW4 | | | | | | |
| HSS_11_P_S_RW4 | 100×100 | 3 | 0 | 36/9 – 22 ga | PAF | #10 screws | 18 in. |
| | | 2 | 0 | 36/9 – 22 ga | PAF | #10 screws | 18 in. |
| | | 1 | 50 | 36/9 – 22 ga | PAF | #10 screws | 18 in. |
| HSS_11_S_S_RW4 | 100×100 | 3 | 0 | 36/9 – 22 ga | #12 | #10 screws | 9 in. |
| | | 2 | 0 | 36/9 – 22 ga | #12 | #10 screws | 9 in. |
| | | 1 | 50 | 36/9 – 22 ga | #12 | #10 screws | 9 in. |
| HSS_21_P_S_RW4 | 200×100 | 3 | 0 | 36/9 – 22 ga | PAF | #10 screws | 3 in. |
| | | 2 | 40 | 36/9 – 22 ga | PAF | #10 screws | 3 in. |
| | | 1 | 60 | 36/9 – 22 ga | PAF | #10 screws | 9 in. |
| HSS_12_P_S_RW4 | Refer to HSS_21_P_S_RW4 | | | | | | |
| HSS_21_S_S_RW4 | 200×100 | 3 | 0 | 36/11 – 20 ga | #12 | #10 screws | 3 in. |
| | | 2 | 40 | 36/11 – 20 ga | #12 | #10 screws | 3 in. |
| | | 1 | 60 | 36/9 – 22 ga | #12 | #10 screws | 6 in. |
| HSS_12_S_S_RW4 | Refer to HSS_21_S_S_RW4 | | | | | | |

**Table B-3 Descriptions of Archetypes with Steel Diaphragms (Moderate-Seismic Hazard)—Traditional Design**

| Archetype Designation | Diaphragm Dimensions (ft) | Zone | Zone Width (ft) | Connector Pattern / Deck Gage | Framing Connectors | Sidelap Connectors | Sidelap Spacing |
|---|---|---|---|---|---|---|---|
| **Moderate Seismicity – Large Buildings** | | | | | | | |
| MSL_21_P_S_RW4 | 400×200 | 3 | 32 | 36/9 – 22 ga | PAF | #10 screws | 15 in. |
| | | 2 | 36 | 36/9 – 22 ga | PAF | #10 screws | 27 in. |
| | | 1 | 132 | 36/5 – 22 ga | PAF | #10 screws | 15 in. |
| MSL_12_P_S_RW4 | Refer to MSL_21_P_S_RW4 | | | | | | |
| MSL_21_S_S_RW4 | 400×200 | 3 | 32 | 36/9 – 22 ga | #12 Hilti HWH screws | #10 screws | 6 in. |
| | | 2 | 36 | 36/9 – 22 ga | #12 Hilti HWH screws | #10 screws | 12 in. |
| | | 1 | 132 | 36/5 – 22 ga | #12 Hilti HWH screws | #10 screws | 9 in. |
| MSL_12_S_S_RW4 | Refer to MSL_21_S_S_RW4 | | | | | | |
| MSL_21_W_S_RW4 | 400×200 | 3 | 32 | 36/7 – 22 ga | 3/4 in. welds | #10 screws | 6 in. |
| | | 2 | 36 | 36/7 – 22 ga | 3/4 in. welds | #10 screws | 12 in. |
| | | 1 | 132 | 36/5 – 22 ga | 5/8 in. welds | #10 screws | 9 in. |
| MSL_12_W_S_RW4 | Refer to MSL_21_W_S_RW4 | | | | | | |
| MSL_11_P_S_RW4 | 400×400 | 3 | 32 | 36/5 – 22 ga | PAF | #10 screws | 12 in. |
| | | 2 | 36 | 36/5 – 22 ga | PAF | #10 screws | 21 in. |
| | | 1 | 132 | 36/5 – 22 ga | PAF | #10 screws | 36 in. |
| MSL_11_S_S_RW4 | 400×400 | 3 | 32 | 36/5 – 22 ga | #12 Hilti HWH screws | #10 screws | 9 in. |
| | | 2 | 36 | 36/5 – 22 ga | #12 Hilti HWH screws | #10 screws | 12 in. |
| | | 1 | 132 | 36/5 – 22 ga | #12 Hilti HWH screws | #10 screws | 21 in. |
| MSL_11_W_S_RW4 | 400×400 | 3 | 32 | 36/5 – 22 ga | 5/8 in. dia. welds | #10 screws | 9 in. |
| | | 2 | 36 | 36/5 – 22 ga | 5/8 in. dia. welds | #10 screws | 18 in. |
| | | 1 | 132 | 36/5 – 22 ga | 5/8 in. dia. welds | #10 screws | 21 in. |
| MSL_21_W_W_RW4_01 | 400×200 | 3 | 40 | 36/7 – 22 ga | 3/4 in. dia. welds | TSW | 18 in. |
| S | | 2 | 40 | 36/5 – 22 ga | 3/4 in. dia. welds | TSW | 24 in. |
| | | 1 | 120 | 36/5 – 22 ga | 3/4 in. dia. welds | TSW | 36 in. |
| MSL_12_W_W_RW4_01 | Refer to MSL_21_W_W_RW4_01 | | | | | | |
| MSL_11_W_W_RW4_01 | 400×400 | 3 | 40 | 36/5 – 22 ga | 3/4 in. dia. welds | TSW | 36 in. |
| | | 2 | 40 | 36/4 – 22 ga | 3/4 in. dia. welds | TSW | 36 in. |
| | | 1 | 120 | 36/4 – 22 ga | 3/4 in. dia. welds | TSW | 72 in. |

**Table B-3 Descriptions of Archetypes with Steel Diaphragms (Moderate-Seismic Hazard)—Traditional Design (continued)**

| Archetype Designation | Diaphragm Dimensions (ft) | Zone | Zone Width (ft) | Connector Pattern / Deck Gage | Framing Connectors | Sidelap Connectors | Sidelap Spacing |
|---|---|---|---|---|---|---|---|
| **Moderate Seismicity – Small Buildings** | | | | | | | |
| MSS_11_S_S_RW4 | 100×100 | 3 | 0 | 36/5 – 22 ga | #12 HWH Hilti screw | #10 screws | 36 in. |
| | | 2 | 0 | 36/5 – 22 ga | #12 HWH Hilti screw | #10 screws | 36 in. |
| | | 1 | 50 | 36/5 – 22 ga | #12 HWH Hilti screw | #10 screws | 36 in. |
| MSS_11_P_S_RW4 | 100×100 | 3 | 0 | 36/5 – 22 ga | PAF | #10 screws | 36 in. |
| | | 2 | 0 | 36/5 – 22 ga | PAF | #10 screws | 36 in. |
| | | 1 | 50 | 36/5 – 22 ga | PAF | #10 screws | 36 in. |
| MSS_11_W_S_RW4 | 100×100 | 3 | 0 | 36/5 – 22 ga | 5/8 in. puddle welds | #10 screws | 36 in. |
| | | 2 | 0 | 36/5 – 22 ga | 5/8 in. puddle welds | #10 screws | 36 in. |
| | | 1 | 50 | 36/5 – 22 ga | 5/8 in. puddle welds | #10 screws | 36 in. |
| MSS_21_S_S_RW4 | 200×100 | 3 | 22 | 36/7 – 22 ga | #12 HWH Hilti screw | #10 screws | 9 in. |
| | | 2 | 0 | 36/5 – 22 ga | #12 HWH Hilti screw | #10 screws | 12 in. |
| | | 1 | 78 | 36/5 – 22 ga | #12 HWH Hilti screw | #10 screws | 12 in. |
| MSS_12_S_S_RW4 | Refer to MSS_21_S_S_RW4 | | | | | | |
| MSS_21_P_S_RW4 | 200×100 | 3 | 22 | 36/7 – 22 ga | PAF | #10 screws | 12 in. |
| | | 2 | 0 | 36/5 – 22 ga | PAF | #10 screws | 21 in. |
| | | 1 | 78 | 36/5 – 22 ga | PAF | #10 screws | 21 in. |
| MSS_12_P_S_RW4 | Refer to MSS_21_P_S_RW4 | | | | | | |
| MSS_21_W_S_RW4 | 200×100 | 3 | 22 | 36/7 – 22 ga | 5/8 in. puddle welds | #10 screws | 9 in. |
| | | 2 | 0 | 36/5 – 22 ga | 5/8 in. puddle welds | #10 screws | 12 in. |
| | | 1 | 78 | 36/5 – 22 ga | 5/8 in. puddle welds | #10 screws | 12 in. |
| MSS_12_W_S_RW4 | Refer to MSS_21_W_S_RW4 | | | | | | |
| MSL_21_P_S_RW4 | 400×200 | 3 | 32 | 36/9 – 22 ga | PAF | #10 screws | 15 in. |
| | | 2 | 36 | 36/9 – 22 ga | PAF | #10 screws | 27 in. |
| | | 1 | 132 | 36/5 – 22 ga | PAF | #10 screws | 15 in. |
| MSL_12_P_S_RW4 | Refer to MSL_21_P_S_RW4 | | | | | | |
| MSL_21_S_S_RW4 | 400×200 | 3 | 32 | 36/9 – 22 ga | #12 Hilti HWH screws | #10 screws | 6 in. |
| | | 2 | 36 | 36/9 – 22 ga | #12 Hilti HWH screws | #10 screws | 12 in. |
| | | 1 | 132 | 36/5 – 22 ga | #12 Hilti HWH screws | #10 screws | 9 in. |
| MSL_12_S_S_RW4 | Refer to MSL_21_S_S_RW4 | | | | | | |
| MSL_21_W_S_RW4 | 400×200 | 3 | 32 | 36/7 – 22 ga | 3/4 in. welds | #10 screws | 6 in. |
| | | 2 | 36 | 36/7 – 22 ga | 3/4 in. welds | #10 screws | 12 in. |
| | | 1 | 132 | 36/5 – 22 ga | 5/8 in. welds | #10 screws | 9 in. |
| MSL_12_W_S_RW4 | Refer to MSL_21_W_S_RW4 | | | | | | |

## B.2 Summary of FEMA P695 Analysis Results for Traditional Design

Incremental Dynamic Analyses (IDA) (Vamvatsikos and Cornell, 2002) using the FEMA P695 Far-Field Ground Motion Ensemble were performed using the simplified building models described in Appendix A to compute the median collapse intensity. For the analysis results, the median collapse intensity is defined as the median spectral intensity at the fundamental period that causes side-sway *P*-delta instability.

Summaries of the collapse margin ratio results for the performance groups of wood and steel archetypes are provided in Table B-4 and Table B-5. *ACMR*s and acceptable *ACMR*s for the individual archetypes and the archetype groups are also included in this section. The acceptable *ACMR* applicable for the performance of individual archetypes is 1.73, and the acceptable *ACMR* of performance groups is 2.30.

Diaphragms designed using the traditional design procedure of ASCE/SEI 7-10 did not pass the FEMA P695 collapse criteria for the small archetype performance groups with wood diaphragms. Each small wood diaphragm archetype had an individual *ACMR* that exceeded the acceptable value of 1.73, indicating each archetype passed the criterion. However, the small archetype performance groups for both high-seismic and moderate-seismic hazard had *ACMR* values of 2.11 and 1.98, respectively, which is less than the acceptable *ACMR* of 2.30. Thus, these performance groups did not pass the criterion. The small archetypes had short periods and remained in the short-period range as yielding occurred. In this region, period shifts can result in resonance with large spikes in the short-period range that can lead to much larger spectral accelerations and displacements than predicted using the design-spectrum plateau. This issue of short-period structures having higher seismic demands leading to the lowest level of collapse performance has been well documented, starting with Newmark and Hall (1973). Section 9.5.1 of FEMA P695 describes this issue with short-period structures in greater detail. But studies documented in FEMA P-2139-1, *Short-Period Building Collapse Performance and Recommendations for Improving Seismic Design* (FEMA, 2020b), have shown that the concern raised by Newmark and Hall is offset by other factors captured in detailed models. These results suggest that more detailed modeling of smaller buildings designed in accordance with FEMA P-1026 could potentially also show more favorable performance.

The larger archetype wood diaphragm performance groups had *ACMR*s of 2.68 and 2.80 for the high-seismic and moderate-seismic hazard performance

groups, which exceed the acceptable *ACMR* of 2.30. Each large wood diaphragm archetype had an individual *ACMR* that exceeded the acceptable value of 1.73. The large wood archetypes performed better because the elastic periods were often off the design response spectrum's plateau, but the diaphragms were designed as though the elastic period was on the plateau of the spectrum. Also, as the diaphragm yields, its period lengthens, which in general leads to lower forces.

Both the large and small steel deck diaphragm performance groups did not pass the criteria. For individual archetypes with high-seismic hazard, five of seven large archetypes and one of nine small archetypes had *ACMR*s less than the acceptable *ACMR* of 1.73. For individual archetypes with moderate-seismic hazard, three of twelve large archetypes and three of nine small archetypes had *ACMR*s less than acceptable. The *ACMR*s for the large archetype groups of 1.71 and 1.87 for high-seismic hazard and 1.95 and 1.88 for moderate-seismic hazard performed slightly worse than the small archetype groups. The small archetype groups had values of 2.23 and 1.92 for high-seismic hazard and a value of 1.86 for moderate-seismic hazard. The reason for the difference relative to what was observed for the wood diaphragms is that the larger steel diaphragms are relatively stiffer than the larger wood diaphragms and have periods that are on or close to the design spectrum plateau. Differences in *ACMR*s of the archetypes with various combinations of welds, PAFs, screws and button punches are not significant enough to distinguish definitive differences in performance of the connectors. However, connection tests clearly demonstrate that PAF and screw fasteners provide significantly more ductility than welded and button punch connections. Tests results of proprietary punch systems were not reviewed as they are not in the public domain.

**Table B-4 Summary of Collapse Margin Ratio Results for Wood Diaphragm Archetype Performance Groups for Traditional Design**

| Performance Group | Seismicity | Size | Computed *ACMR* | Acceptable *ACMR* | Pass/Fail |
|---|---|---|---|---|---|
| PG-1E | High | Large | 2.68 | 2.30 | Pass |
| PG-2E | High | Small | 2.11 | | Fail |
| PG-3E | Moderate | Large | 2.80 | | Pass |
| PG-4E | Moderate | Small | 1.98 | | Fail |

**Table B-5 Summary of Collapse Margin Ratio Results for Steel Deck Diaphragm Archetype Performance Groups for Traditional Design**

| Performance Group | Seismicity | Size | Framing Connectors | Sidelaps | Computed *ACMR* | Acceptable *ACMR* | Pass/Fail |
|---|---|---|---|---|---|---|---|
| PG-5E | High | Large | Welds | Welds / button punches | 1.71 | 2.30 | Fail |
| PG-6E | High | Large | PAFs / screws | Screws | 1.87 | | Fail |
| PG-7E | High | Small | Welds | Button punches | 2.23 | | Fail |
| PG-8E | High | Small | PAFs / screws | Screws | 1.92 | | Fail |
| PG-9E | Moderate | Large | Welds / PAFs/ screws | Screws | 1.95 | | Fail |
| PG-10E | Moderate | Large | Welds / PAFs/ screws | Welds | 1.88 | | Fail |
| PG-11E | Moderate | Small | Welds /PAFs / screws | Screws | 1.86 | | Fail |

The results indicate that, based on the FEMA P695 methodology, the traditional design procedure may not be adequate for either wood structural panel or steel deck diaphragms. Therefore, a modified or new design procedure was desired. The results also indicate that if a single response modification coefficient were to be used for the diaphragm parallel to design of SFRS vertical elements, its value would need to be less than 4. For the wood diaphragms, considering that the lowest ratio of *ACMR* to acceptable *ACMR* (1.98/2.3) is 0.86 leads to the expectation that traditional design using a response modification coefficient, *R*, of about 3 to 3.5 (i.e., 0.86×4) is appropriate. For steel deck diaphragms, consider that the lowest ratio of *ACMR* to acceptable *ACMR* (1.71/2.3) is 0.74, which leads to the expectation that traditional design using an *R* of about 2.5 to 3 may be appropriate for 20-gage and 22-gage steel deck diaphragms. Although these results did not clearly demonstrate the need to differentiate between connector type, the connection test results clearly showed that PAFs and screws were more ductile than welded and button punch connections.

The analysis results also showed that the diaphragm's inelastic behavior was concentrated at the ends of the diaphragm. The global ductility of the

diaphragm is lower than the ductility of the connectors because connector yielding is not spreading well into the diaphragm. Response of these buildings would improve if a means of spreading connection yielding deeper into the diaphragm were developed. For the steel deck diaphragms, the response would also be improved if the post-yield stiffness of the connector were positive to a larger displacement value. Tests indicate positive post-yield stiffness only to 1 mm or 2 mm. The exact displacement needed for improved behavior is not known at this time, but a value such as 10 mm is expected to be more than adequate.

## B.3 Detailed FEMA P695 Evaluation Results for the Traditional Design Procedure

Summaries of collapse results for individual wood and bare steel deck diaphragm archetypes are provided in Table B-6 through Table B-8 for the wood diaphragm archetypes and Table B-9 for the bare steel deck diaphragm archetypes. Values for the median collapse intensity, $S_{CT}[T]$, ground motion spectral demand, $S_{MT}[T]$, building drift ratios (*BDR*) for the design level earthquake and maximum considered earthquake, the spectral shape factor (*SSF*), fundamental elastic period, and period-based ductility, $\mu_T$, are provided.

The *BDR*, which equals the sum of the wall drift ratio (*WDR*) and the diaphragm drift ratio (*DDR*), is essentially the same as the *DDR* for the archetypes in this study because the *WDR*s in this study are very small.

**Table B-6 Summary of Collapse Results for RWFD Archetypes with Wood Diaphragms—Traditional Design**

| Archetype ID | Design Configuration | | | | Pushover and IDA Results | | | Relevant Analysis Parameters | | |
|---|---|---|---|---|---|---|---|---|---|---|
| | Building Size | Diaphragm Aspect ratio | Diaphragm Construction | SDC | $S_{MT}[T]$ (g) | $S_{CT}[T]$ (g) | *CMR* | Period (sec) | Median *BDR* @ DE (%) | Median *BDR* @ MCE (%) |
| **Performance Group No. PG-1E (Wood, Large Building, Existing Design)** | | | | | | | | | | |
| HWL_21_N_OSB_RW4_07 | Large | 2:1 | Wood Panelized | $D_{max}$ | 1.06 | 2.00 | 1.89 | 0.85 | 0.29 | 0.55 |
| HWL_12_N_OSB_RW4_02 | Large | 1:2 | Wood Panelized | $D_{max}$ | 1.50 | 3.36 | 2.24 | 0.49 | 0.42 | 0.64 |
| HWL_11_N_OSB_RW4_01 | Large | 1:1 | Wood Panelized | $D_{max}$ | 1.05 | 1.68 | 1.60 | 0.87 | 0.32 | 0.53 |
| **Performance Group No. PG-2E (Wood, Small Building, Existing Design)** | | | | | | | | | | |
| HWS_21_N_OSB_RW4_01 | Small | 2:1 | Wood Panelized | $D_{max}$ | 1.41 | 1.98 | 1.40 | 0.54 | 0.56 | 1.16 |
| HWS_12_N_OSB_RW4_01 | Small | 1:2 | Wood Panelized | $D_{max}$ | 1.50 | 2.64 | 1.76 | 0.38 | 0.72 | 1.72 |
| HWS_11_N_OSB_RW4_01 | Small | 1:1 | Wood Panelized | $D_{max}$ | 1.50 | 2.21 | 1.47 | 0.36 | 0.65 | 1.68 |
| HWS_11_N_OSB_RW4_02 | Small | 1:1 | Wood Panelized | $D_{max}$ | 1.50 | 2.32 | 1.55 | 0.37 | 0.68 | 1.63 |
| **Performance Group No. PG-3E (Wood, Large Building, Existing Design)** | | | | | | | | | | |
| MWL_21_N_OSB_RW4_01 | Large | 2:1 | Wood Panelized | $C_{max}$ | 0.50 | 1.28 | 2.56 | 0.90 | 0.31 | 0.52 |
| MWL_12_N_OSB_RW4_01 | Large | 1:2 | Wood Panelized | $C_{max}$ | 0.75 | 1.75 | 2.33 | 0.55 | 0.39 | 0.63 |
| MWL_11_N_OSB_RW4_01 | Large | 1:1 | Wood Panelized | $C_{max}$ | 0.51 | 1.09 | 2.14 | 0.92 | 0.35 | 0.55 |
| **Performance Group No. PG-4E (Wood, Small Building, Existing Design)** | | | | | | | | | | |
| MWS_21_N_OSB_RW4_01 | Small | 2:1 | Wood Panelized | $C_{max}$ | 0.75 | 1.15 | 1.50 | 0.58 | 0.51 | 0.89 |
| MWS_12_N_OSB_RW4_01 | Small | 1:2 | Wood Panelized | $C_{max}$ | 0.75 | 1.35 | 1.72 | 0.43 | 0.55 | 0.98 |
| MWS_11_N_OSB_RW4_01 | Small | 1:1 | Wood Panelized | $C_{max}$ | 0.75 | 1.47 | 1.96 | 0.45 | 0.59 | 1.15 |

**Table B-7 Computed and Acceptable Adjusted Collapse Margin Ratios for RWFD Archetypes with Wood Diaphragms—Traditional Design**

| Archetype ID | Design Configuration | | | | Collapse Margin Parameters | | | | Acceptance Check | |
|---|---|---|---|---|---|---|---|---|---|---|
| | Building Size | Diaphragm Aspect Ratio | Diaphragm Construction | SDC | *CMR* | $\mu_T$ | *SSF* | *ACMR* | Accept. *ACMR* | Pass/Fail |
| **Performance Group No. PG-1E (Wood, Large Building, Existing Design)** | | | | | | | | | | |
| HWL_21_N_OSB_RW4_07 | Large | 2:1 | Wood | $D_{max}$ | 1.89 | 8.07 | 1.43 | 2.70 | 1.73 | Pass |
| HWL_12_N_OSB_RW4_02 | Large | 1:2 | Wood | $D_{max}$ | 2.24 | 8.95 | 1.36 | 3.05 | 1.73 | Pass |
| HWL_11_N_OSB_RW4_01 | Large | 1:1 | Wood | $D_{max}$ | 1.60 | 8.42 | 1.43 | 2.29 | 1.73 | Pass |
| Mean of Performance Group: | | | | | 1.91 | 8.48 | 1.41 | 2.68 | 2.30 | Pass |
| **Performance Group No. PG-2E (Wood, Small Building, Existing Design)** | | | | | | | | | | |
| HWS_21_N_OSB_RW4_01 | Small | 2:1 | Wood | $D_{max}$ | 1.40 | 7.20 | 1.31 | 1.84 | 1.73 | Pass |
| HWS_12_N_OSB_RW4_01 | Small | 1:2 | Wood | $D_{max}$ | 1.76 | 8.95 | 1.36 | 2.39 | 1.73 | Pass |
| HWS_11_N_OSB_RW4_01 | Small | 1:1 | Wood | $D_{max}$ | 1.55 | 8.32 | 1.36 | 2.10 | 1.73 | Pass |
| HWS_11_N_OSB_RW4_02 | Small | 1:1 | Wood | $D_{max}$ | 1.55 | 8.51 | 1.36 | 2.11 | 1.73 | Pass |
| Mean of Performance Group: | | | | | 1.57 | 8.25 | 1.35 | 2.11 | 2.30 | Fail |
| **Performance Group No. PG-3E (Wood, Large Building, Existing Design)** | | | | | | | | | | |
| MWL_21_N_OSB_RW4_01 | Large | 2:1 | Wood | $C_{max}$ | 2.56 | 8.15 | 1.14 | 2.92 | 1.73 | Pass |
| MWL_12_N_OSB_RW4_01 | Large | 1:2 | Wood | $C_{max}$ | 2.33 | 8.79 | 1.14 | 2.66 | 1.73 | Pass |
| MWL_11_N_OSB_RW4_01 | Large | 1:1 | Wood | $C_{max}$ | 2.14 | 8.54 | 1.14 | 2.44 | 1.73 | Pass |
| Mean of Performance Group: | | | | | 2.34 | 8.49 | 1.14 | 2.67 | 2.30 | Pass |
| **Performance Group No. PG-4E (Wood, Small Building, Existing Design)** | | | | | | | | | | |
| MWS_21_N_OSB_RW4_01 | Small | 2:1 | Wood | $C_{max}$ | 1.50 | 8.05 | 1.16 | 1.74 | 1.73 | Pass |
| MWS_12_N_OSB_RW4_01 | Small | 1:2 | Wood | $C_{max}$ | 1.72 | 8.49 | 1.14 | 1.96 | 1.73 | Pass |
| MWS_11_N_OSB_RW4_01 | Small | 1:1 | Wood | $C_{max}$ | 1.96 | 8.09 | 1.14 | 2.23 | 1.73 | Pass |
| Mean of Performance Group: | | | | | 1.73 | 8.21 | 1.15 | 1.98 | 2.30 | Fail |

**Table B-8 Summary of Collapse Results for RWFD Archetypes with Steel Diaphragms—Traditional Design**

| Archetype ID | Design configuration | | | | Pushover and IDA Results | | | Relevant Analysis Parameters | | |
|---|---|---|---|---|---|---|---|---|---|---|
| | Building Size | Diaphragm Aspect Ratio | Diaphragm Construction | SDC | $S_{MT}[T]$ (g) | $S_{CT}[T]$ (g) | *CMR* | Period (sec) | Median *BDR* @ DE (%) | Median *BDR* @ MCE (%) |
| **Performance Group No. PG-5E (Steel, Large Building, Welds and Button Punches as Sidelap Connectors, Existing Design)** | | | | | | | | | | |
| HSL_21_W_WB_RW4_01 | Large | 2:1 | Steel (WR Deck) | $D_{max}$ | 1.50 | 1.56 | 0.99 | 0.52 | 0.19 | 0.45 |
| HSL_12_W_WB_RW4_01 | Large | 1:2 | Steel (WR Deck) | $D_{max}$ | 1.50 | 2.85 | 1.90 | 0.39 | 0.28 | 0.71 |
| HSL_11_W_WB_RW4_01 | Large | 1:1 | Steel (WR Deck) | $D_{max}$ | 1.50 | 1.43 | 0.95 | 0.49 | 0.13 | 0.42 |
| **Performance Group No. PG-6E (Steel, Large Building, Screws as Sidelap Connectors, Existing Design)** | | | | | | | | | | |
| HSL_21_P_S_RW4_01 | Large | 2:1 | Steel (WR Deck) | $D_{max}$ | 1.50 | 1.85 | 1.23 | 0.54 | 0.15 | 0.33 |
| HSL_12_P_S_RW4_01 | Large | 1:2 | Steel (WR Deck) | $D_{max}$ | 1.50 | 3.10 | 2.07 | 0.41 | 0.25 | 0.56 |
| HSL_11_P_S_RW4_01 | Large | 1:1 | Steel (WR Deck) | $D_{max}$ | 1.50 | 1.69 | 1.13 | 0.56 | 0.18 | 0.34 |
| HSL_11_S_S_RW4_01 | Large | 1:1 | Steel (WR Deck) | $D_{max}$ | 1.50 | 1.73 | 1.15 | 0.51 | 0.16 | 0.29 |
| **Performance Group No. PG-7E (Steel, Small Building, Button Punches as Sidelap Connectors, Existing Design)** | | | | | | | | | | |
| HSS_11_W_B_RW4_01 | Small | 1:1 | Steel (WR Deck) | $D_{max}$ | 1.50 | 2.59 | 1.73 | 0.21 | 0.17 | 0.39 |
| HSS_21_W_B_RW4_01 | Small | 2:1 | Steel (WR Deck) | $D_{max}$ | 1.50 | 2.13 | 1.42 | 0.35 | 0.21 | 0.44 |
| HSS_12_W_B_RW4_01 | Small | 1:2 | Steel (WR Deck) | $D_{max}$ | 1.50 | 2.85 | 1.90 | 0.26 | 0.15 | 0.35 |
| **Performance Group No. PG-8E (Steel, Small Building, Screws as Sidelap Connectors, Existing Design)** | | | | | | | | | | |
| HSS_11_P_S_RW4_01 | Small | 1:1 | Steel (WR Deck) | $D_{max}$ | 1.50 | 2.33 | 1.55 | 0.23 | 0.16 | 0.41 |
| HSS_11_S_S_RW4_01 | Small | 1:1 | Steel (WR Deck) | $D_{max}$ | 1.50 | 2.15 | 1.43 | 0.25 | 0.14 | 0.36 |
| HSS_21_P_S_RW4_01 | Small | 2:1 | Steel (WR Deck) | $D_{max}$ | 1.50 | 1.99 | 1.33 | 0.37 | 0.19 | 0.35 |
| HSS_12_P_S_RW4_01 | Small | 1:2 | Steel (WR Deck) | $D_{max}$ | 1.50 | 2.56 | 1.71 | 0.24 | 0.17 | 0.31 |
| HSS_21_S_S_RW4_01 | Small | 2:1 | Steel (WR Deck) | $D_{max}$ | 1.50 | 1.87 | 1.25 | 0.42 | 0.15 | 0.42 |
| HSS_12_S_S_RW4_01 | Small | 1:2 | Steel (WR Deck) | $D_{max}$ | 1.50 | 2.13 | 1.42 | 0.22 | 0.14 | 0.39 |

**Table B-8** **Summary of Collapse Results for RWFD Archetypes with Steel Diaphragms—Traditional Design (continued)**

| Archetype ID | Design Configuration | | | | Pushover and IDA Results | | | Relevant Analysis Parameters | | |
|---|---|---|---|---|---|---|---|---|---|---|
| | Building Size | Diaphragm Aspect Ratio | Diaphragm Construction | SDC | $S_{MT}[T]$ (g) | $S_{CT}[T]$ (g) | *CMR* | Period (sec) | Median *BDR* @ DE (%) | Median *BDR* @ MCE (%) |
| **Performance Group No. PG-9E (Steel, Large Building, Screws as Sidelap Connectors, Existing Design)** | | | | | | | | | | |
| MSL_21_P_S_RW4_01 | Large | 2:1 | Steel (WR Deck) | $D_{max}$ | 0.68 | 0.93 | 1.35 | 0.66 | 0.29 | 0.41 |
| MSL_12_P_S_RW4_01 | Large | 1:2 | Steel (WR Deck) | $D_{max}$ | 0.75 | 1.50 | 2.01 | 0.53 | 0.19 | 0.33 |
| MSL_21_S_S_RW4_01 | Large | 2:1 | Steel (WR Deck) | $D_{max}$ | 0.63 | 0.96 | 1.52 | 0.71 | 0.22 | 0.35 |
| MSL_12_S_S_RW4_01 | Large | 1:2 | Steel (WR Deck) | $D_{max}$ | 0.75 | 1.41 | 1.88 | 0.55 | 0.21 | 0.32 |
| MSL_21_W_S_RW4_01 | Large | 2:1 | Steel (WR Deck) | $D_{max}$ | 0.62 | 1.15 | 1.41 | 0.73 | 0.20 | 0.31 |
| MSL_12_W_S_RW4_01 | Large | 1:2 | Steel (WR Deck) | $D_{max}$ | 0.75 | 1.47 | 1.96 | 0.52 | 0.23 | 0.34 |
| MSL_11_P_S_RW4_01 | Large | 1:1 | Steel (WR Deck) | $D_{max}$ | 0.70 | 1.27 | 1.81 | 0.65 | 0.24 | 0.39 |
| MSL_11_S_S_RW4_01 | Large | 1:1 | Steel (WR Deck) | $D_{max}$ | 0.70 | 1.10 | 1.58 | 0.65 | 0.21 | 0.45 |
| MSL_11_W_S_RW4_01 | Large | 1:1 | Steel (WR Deck) | $D_{max}$ | 0.67 | 1.11 | 1.66 | 0.68 | 0.25 | 0.47 |
| **Performance Group No. PG-10E (Steel, Large Building, Welds as Sidelap Connectors, Existing Design)** | | | | | | | | | | |
| MSL_21_W_W_RW4_01 | Large | 2:1 | Steel (WR Deck) | $C_{max}$ | 0.73 | 1.02 | 1.39 | 0.62 | 0.19 | 0.35 |
| MSL_12_W_W_RW4_01 | Large | 1:2 | Steel (WR Deck) | $C_{max}$ | 0.75 | 1.50 | 1.99 | 0.51 | 0.24 | 0.41 |
| MSL_11_W_W_RW4_01 | Large | 1:1 | Steel (WR Deck) | $C_{max}$ | 0.74 | 1.13 | 1.52 | 0.61 | 0.18 | 0.36 |

**Table B-8 Summary of Collapse Results for RWFD Archetypes with Steel Diaphragms—Traditional Design (continued)**

| Archetype ID | Design Configuration | | | | Pushover and IDA Results | | | Relevant Analysis Parameters | | |
|---|---|---|---|---|---|---|---|---|---|---|
| | Building Size | Diaphragm Aspect Ratio | Diaphragm Construction | SDC | $S_{MT}[T]$ (g) | $S_{CT}[T]$ (g) | *CMR* | Period (sec) | Median *BDR* @ DE (%) | Median *BDR* @ MCE (%) |
| Performance Group No. PG-11E (Steel, Small Building, Screws as Sidelap Connectors, Existing Design) | | | | | | | | | | |
| MSS_11_S_S_RW4_01 | Small | 1:1 | Steel (WR Deck) | $C_{max}$ | 0.75 | 1.26 | 1.67 | 0.32 | 0.15 | 0.36 |
| MSS_11_P_S_RW4_01 | Small | 1:1 | Steel (WR Deck) | $C_{max}$ | 0.75 | 1.34 | 1.78 | 0.30 | 0.17 | 0.41 |
| MSS_11_W_S_RW4_01 | Small | 1:1 | Steel (WR Deck) | $C_{max}$ | 0.75 | 0.98 | 1.30 | 0.28 | 0.14 | 0.37 |
| MSS_21_S_S_RW4_01 | Small | 2:1 | Steel (WR Deck) | $C_{max}$ | 0.75 | 1.05 | 1.39 | 0.54 | 0.19 | 0.48 |
| MSS_12_S_S_RW4_01 | Small | 1:2 | Steel (WR Deck) | $C_{max}$ | 0.75 | 1.39 | 1.85 | 0.31 | 0.15 | 0.29 |
| MSS_21_P_S_RW4_01 | Small | 2:1 | Steel (WR Deck) | $C_{max}$ | 0.75 | 1.17 | 1.55 | 0.59 | 0.20 | 0.44 |
| MSS_12_P_S_RW4_01 | Small | 1:2 | Steel (WR Deck) | $C_{max}$ | 0.75 | 1.48 | 1.97 | 0.28 | 0.16 | 0.32 |
| MSS_21_W_S_RW4_01 | Small | 2:1 | Steel (WR Deck) | $C_{max}$ | 0.75 | 1.08 | 1.43 | 0.55 | 0.18 | 0.36 |
| MSS_12_W_S_RW4_01 | Small | 1:2 | Steel (WR Deck) | $C_{max}$ | 0.75 | 1.28 | 1.71 | 0.33 | 0.17 | 0.31 |

**Table B-9** **Computed and Acceptable Adjusted Collapse Margin Ratios for RWFD Archetypes with Steel Diaphragms—Traditional Design**

| Archetype ID | Design configuration | | | | Collapse Margin Parameters | | | | Acceptance Check | |
|---|---|---|---|---|---|---|---|---|---|---|
| | Building Size | Diaphragm Aspect Ratio | Diaphragm Construction | SDC | *CMR* | $\mu_T$ | *SSF* | *ACMR* | Accept. *ACMR* | Pass/Fail |
| **Performance Group No. PG-5E (Steel, Large Building, Welds and Button Punches as Sidelap Connectors, Existing Design)** | | | | | | | | | | |
| HSL_21_W_WB_RW4_01 | Large | 2:1 | Steel | $D_{max}$ | 0.99 | 8.09 | 1.34 | 1.33 | 1.73 | Fail |
| HSL_12_W_WB_RW4_01 | Large | 1:2 | Steel | $D_{max}$ | 1.90 | 8.26 | 1.33 | 2.53 | 1.73 | Pass |
| HSL_11_W_WB_RW4_01 | Large | 1:1 | Steel | $D_{max}$ | 0.95 | 8.16 | 1.33 | 1.27 | 1.73 | Fail |
| **Mean of Performance Group:** | | | | | **1.28** | **8.17** | **1.33** | **1.71** | **2.30** | **Fail** |
| **Performance Group No. PG-6E (Steel, Large Building, Screws as Sidelap Connectors, Existing Design)** | | | | | | | | | | |
| HSL_21_P_S_RW4_01 | Large | 2:1 | Steel | $D_{max}$ | 1.23 | 8.24 | 1.35 | 1.67 | 1.73 | Fail |
| HSL_12_P_S_RW4_01 | Large | 1:2 | Steel | $D_{max}$ | 2.07 | 8.14 | 1.33 | 2.75 | 1.73 | Pass |
| HSL_11_P_S_RW4_01 | Large | 1:1 | Steel | $D_{max}$ | 1.13 | 8.26 | 1.36 | 1.53 | 1.73 | Fail |
| HSL_11_S_S_RW4_01 | Large | 1:1 | Steel | $D_{max}$ | 1.15 | 8.01 | 1.33 | 1.53 | 2.73 | Fail |
| **Mean of Performance Group:** | | | | | **1.40** | **8.16** | **1.34** | **1.87** | **2.30** | **Fail** |
| **Performance Group No. PG-7E (Steel, Small Building, Button Punches as Sidelap Connectors, Existing Design)** | | | | | | | | | | |
| HSS_11_W_B_RW4_01 | Small | 1:1 | Steel | $D_{max}$ | 1.73 | 7.94 | 1.32 | 2.28 | 1.73 | Pass |
| HSS_21_W_B_RW4_01 | Small | 2:1 | Steel | $D_{max}$ | 1.42 | 8.05 | 1.33 | 1.89 | 1.73 | Pass |
| HSS_12_W_B_RW4_01 | Small | 1:2 | Steel | $D_{max}$ | 1.90 | 7.91 | 1.32 | 2.51 | 1.73 | Pass |
| **Mean of Performance Group:** | | | | | **1.68** | **7.97** | **1.32** | **2.23** | **2.30** | **Fail** |
| **Performance Group No. PG-8E (Steel, Small Building, Screws as Sidelap Connectors, Existing Design)** | | | | | | | | | | |
| HSS_11_P_S_RW4_01 | Small | 1:1 | Steel | $D_{max}$ | 1.55 | 8.02 | 1.33 | 2.07 | 1.73 | Pass |
| HSS_11_S_S_RW4_01 | Small | 1:1 | Steel | $D_{max}$ | 1.43 | 8.15 | 1.33 | 1.91 | 1.73 | Pass |
| HSS_21_P_S_RW4_01 | Small | 2:1 | Steel | $D_{max}$ | 1.33 | 8.33 | 1.33 | 1.76 | 1.73 | Pass |
| HSS_12_P_S_RW4_01 | Small | 1:2 | Steel | $D_{max}$ | 1.71 | 8.25 | 1.33 | 2.27 | 1.73 | Pass |
| HSS_21_S_S_RW4_01 | Small | 2:1 | Steel | $D_{max}$ | 1.25 | 7.85 | 1.32 | 1.65 | 1.73 | Fail |
| HSS_12_S_S_RW4_01 | Small | 1:2 | Steel | $D_{max}$ | 1.42 | 8.06 | 1.33 | 1.89 | 1.73 | Pass |
| **Mean of Performance Group:** | | | | | **1.45** | **8.11** | **1.33** | **1.92** | **2.30** | **Fail** |

**Table B-9** **Computed and Acceptable Adjusted Collapse Margin Ratios for RWFD Archetypes with Steel Diaphragms—Traditional Design (continued)**

| Archetype ID | Design Configuration | | | | Collapse Margin Parameters | | | | Acceptance Check | |
|---|---|---|---|---|---|---|---|---|---|---|
| | Building Size | Diaphragm Aspect Ratio | Diaphragm Construction | SDC | CMR | $\mu_T$ | *SSF* | *ACMR* | Accept. *ACMR* | Pass/Fail |
| **Performance Group No. PG-9E (Steel, Large Building, Screws as Sidelap Connectors, Existing Design)** | | | | | | | | | | |
| vMSL_21_P_S_RW4_01 | Large | 2:1 | Steel | $C_{max}$ | 1.35 | 8.32 | 1.15 | 1.55 | 1.73 | Fail |
| MSL_12_P_S_RW4_01 | Large | 1:2 | Steel | $C_{max}$ | 2.01 | 7.85 | 1.13 | 2.27 | 1.73 | Pass |
| MSL_21_S_S_RW4_01 | Large | 2:1 | Steel | $C_{max}$ | 1.52 | 8.02 | 1.18 | 1.80 | 1.73 | Pass |
| MSL_12_S_S_RW4_01 | Large | 1:2 | Steel | $C_{max}$ | 1.88 | 8.38 | 1.15 | 2.16 | 1.73 | Pass |
| MSL_21_W_S_RW4_01 | Large | 2:1 | Steel | $C_{max}$ | 1.41 | 8.20 | 1.18 | 1.66 | 1.73 | Fail |
| MSL_12_W_S_RW4_01 | Large | 1:2 | Steel | $C_{max}$ | 1.96 | 8.02 | 1.15 | 2.25 | 1.73 | Pass |
| MSL_11_P_S_RW4_01 | Large | 1:1 | Steel | $C_{max}$ | 1.81 | 7.99 | 1.15 | 2.08 | 1.73 | Pass |
| MSL_11_S_S_RW4_01 | Large | 1:1 | Steel | $C_{max}$ | 1.58 | 8.15 | 1.15 | 1.81 | 1.73 | Pass |
| MSL_11_W_S_RW4_01 | Large | 1:1 | Steel | $C_{max}$ | 1.66 | 8.22 | 1.17 | 1.94 | 1.73 | Pass |
| **Mean of Performance Group:** | | | | | **1.69** | **8.13** | **1.16** | **1.95** | **2.30** | **Fail** |
| **Performance Group No. PG-10E (Steel, Large Buildings, Welds as Sidelap connectors, Existing Design)** | | | | | | | | | | |
| MSL_21_W_W_RW4_01 | Large | 2:1 | Steel | $C_{max}$ | 1.39 | 7.76 | 1.15 | 1.59 | 1.73 | Fail |
| MSL_12_W_W_RW4_01 | Large | 1:2 | Steel | $C_{max}$ | 1.99 | 8.15 | 1.14 | 2.27 | 1.73 | Pass |
| MSL_11_W_W_RW4_01 | Large | 1:1 | Steel | $C_{max}$ | 1.52 | 8.09 | 1.16 | 1.76 | 1.73 | Pass |
| **Mean of Performance Group:** | | | | | **1.63** | **8.00** | **1.15** | **1.88** | **2.30** | **Fail** |
| **Performance Group No. PG-11E (Steel, Small Building, Screws as Sidelap Connectors, Existing Design)** | | | | | | | | | | |
| MSS_11_S_S_RW4_01 | Small | 1:1 | Steel | $C_{max}$ | 1.67 | 8.15 | 1.14 | 1.91 | 1.73 | Pass |
| MSS_11_P_S_RW4_01 | Small | 1:1 | Steel | $C_{max}$ | 1.78 | 8.26 | 1.14 | 2.03 | 1.73 | Pass |
| MSS_11_W_S_RW4_01 | Small | 1:1 | Steel | $C_{max}$ | 1.30 | 7.78 | 1.13 | 1.47 | 1.73 | Fail |
| MSS_21_S_S_RW4_01 | Small | 2:1 | Steel | $C_{max}$ | 1.39 | 8.05 | 1.15 | 1.60 | 1.73 | Fail |
| MSS_12_S_S_RW4_01 | Small | 1:2 | Steel | $C_{max}$ | 1.85 | 8.56 | 1.14 | 2.11 | 1.73 | Pass |
| MSS_21_P_S_RW4_01 | Small | 2:1 | Steel | $C_{max}$ | 1.55 | 8.12 | 1.16 | 1.80 | 1.73 | Pass |
| MSS_12_P_S_RW4_01 | Small | 1:2 | Steel | $C_{max}$ | 1.97 | 7.88 | 1.14 | 2.25 | 1.73 | Pass |
| MSS_21_W_S_RW4_01 | Small | 2:1 | Steel | $C_{max}$ | 1.43 | 7.97 | 1.15 | 1.65 | 1.73 | Fail |
| MSS_12_W_S_RW4_01 | Small | 1:2 | Steel | $C_{max}$ | 1.71 | 8.02 | 1.14 | 1.95 | 1.73 | Pass |
| **Mean of Performance Group:** | | | | | **1.63** | **8.09** | **1.14** | **1.86** | **2.30** | **Fail** |

## B.4 Fundamental Period of the Archetypes

The results of the simplified building model analyses show that the fundamental period of each archetype is dominated by the diaphragm response. A summary of the elastic periods is included in Table B-10. The elastic fundamental periods for the archetypes were obtained from the analyses and are included in Table B-6 and Table B-8.

**Table B-10 Summary of Elastic Periods for Archetypes Designed Using the Traditional Procedure**

| Span Length | Period for High-Seismic Archetypes | Period for Moderate-Seismic Archetypes |
|---|---|---|
| **Wood Diaphragms** | | |
| 400 ft | 0.85 to 0.87 sec | 0.90 to 0.92 sec |
| 200 ft | 0.49 to 0.54 sec | 0.55 to 0.58 sec |
| 100 ft | 0.36 to 0.38 sec | 0.43 to 0.45 sec |
| **Steel Diaphragms** | | |
| 400 ft | 0.49 to 0.56 sec | 0.61 to 0.73 sec |
| 200 ft | 0.35 to 0.42 sec | 0.51 to 0.59 sec |
| 100 ft | 0.21 to 0.26 sec | 0.28 to 0.33 sec |

Using the initial elastic periods from the analyses of the high-seismic wood diaphragm archetypes and the high-seismic steel deck diaphragm archetypes, empirical formulas were developed for the fundamental periods of wood and steel deck diaphragms, respectively. The following formula is proposed for computing the fundamental period, $T_{wood}$, of the wood diaphragm buildings with concrete or masonry shear walls:

$$T_{wood} = \frac{0.0019}{\sqrt{C_w}} h_n + 0.002 L_f \qquad \text{(B-1)}$$

Where $L_f$ is the diaphragm span in feet between vertical elements of the seismic-force-resisting system, $C_w$ is a coefficient defined by Equation 12.8-10 in ASCE/SEI 7-10:

$$C_w = \frac{100}{A_B} \sum_{i=1}^{x} \frac{A_i}{1 + 0.83 \left( \frac{h_i}{D_i} \right)^2} \qquad \text{(B-2)}$$

$A_B$ is the area of the base of the building in square feet, $A_i$ is the web area of the in-plane shear wall $i$ in square feet, $D_i$ is the length of the in-plane shear wall $i$ in square feet, $h_i$ is the height of the in-plane shear wall $i$ in square feet, and $h_n$ is the height of the roof framing in feet.

The following formula is proposed for computing the fundamental period, $T_{steel}$, of the steel deck diaphragm buildings:

$$T_{steel} = \frac{0.0019}{\sqrt{C_w}} h_n + 0.001 L_f \qquad \text{(B-3)}$$

Periods derived from the proposed equations, along with the periods determined from the simplified building model analyses, are plotted in Figure B-6 for the wood diaphragm archetypes and in Figure B-7 for the steel

diaphragm archetypes. For comparison, periods derived from ASCE/SEI 7-10 equations and, for the wood archetypes, periods derived from equations proposed by Freeman et al. (1995) are also plotted.

Although the periods are derived from analyses of single-span diaphragms, the deformations were shear dominated. Therefore, the proposed period equations are valid for multi-span diaphragms. The archetypes used to develop these formulas included heavy walls. In general, archetypes with more or less mass will have a corresponding diaphragm design with more or less stiffness, thus offsetting the mass variation. Therefore, the proposed period equations are thought to be generally independent of mass (i.e., the same formula for period applies). An additional study was conducted of two archetypes, one with lightweight walls loading the diaphragm (HWL_N_OSB_P1026_04) and another with heavyweight walls loading the diaphragm (HWL_N_OSB_P1026_01), with both designed using the alternative RWFD procedure. As reported in Appendix C, this study found both had similar elastic periods in the transverse direction, thus supporting this conclusion. In the longitudinal direction, where nailing patterns are controlled by the orthogonal direction of loading, such an offset to the mass variation might not occur to this degree.

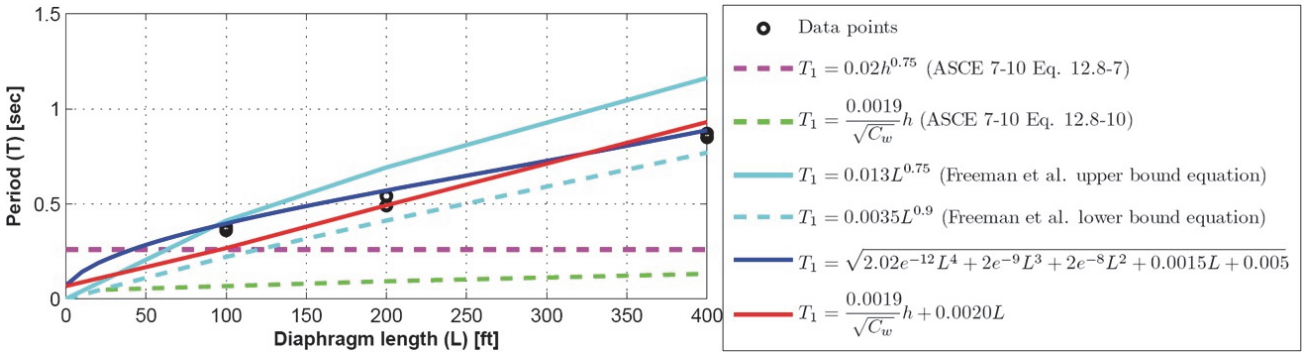


Figure B-6 Comparison of fundamental periods from analyses of wood panel archetypes to those predicted by the proposed formula (Equation B-1), ASCE/SEI 7-10 equations, a best fit curve, and those proposed by Freeman et al. (1995).

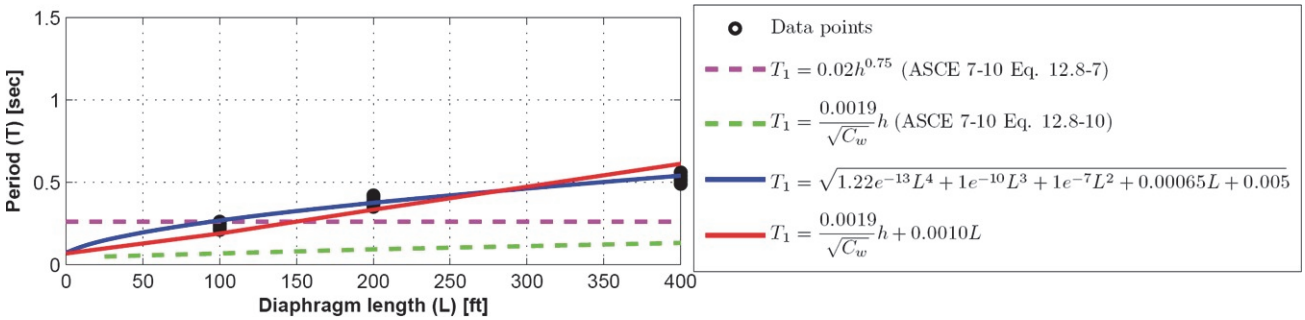


Figure B-7 Comparison of fundamental periods from analyses of steel deck archetypes to those predicted by the proposed formula (Equation B-3), ASCE/SEI 7-10 equations, and a best fit curve.

# Appendix C

# Evaluation of Alternative RWFD Design Procedure for Wood Diaphragms

This appendix describes the archetypes with wood diaphragms used to evaluate the alternative RWFD procedure and provides a summary of the FEMA P695 evaluation results.

## C.1 Description of Archetypes

Evaluations were performed on archetypes designed for high- and moderate-seismic hazard as defined in Appendix A. For these evaluations, archetypes were designed with wood structural panel diaphragms. Details of these archetypes are in Table C-1, and summary figures with detailed descriptions of diaphragm zones for the archetypes are in Figure C-1 through Figure C-7.

The archetypes are grouped by whether the diaphragm is relatively large or small. The archetypes have plan aspect ratios of 1:1, 2:1, and 1:2. Large diaphragms are 400 feet long and either 400 feet or 200 feet wide. The small diaphragms with aspect ratios of 2:1 and 1:2 are 200 feet long by 100 feet wide, whereas those with 1:1 aspect ratios are 100 feet by 100 feet. The wood diaphragms are OSB wood structural panels nailed to wood nailers that are attached to open-web steel joists.

The archetype walls are constructed of reinforced concrete panels measuring 25 feet in length. All high- and moderate-seismic hazard archetype groups include walls 33 feet tall (measured from the top of slab-on-grade) that are 9 1/4 inch thick for high-seismic hazard and 7 1/4 inch thick for moderate-seismic hazard. The roof level of these archetypes is set at 30 feet above the top of slab-on-grade with parapet walls cantilevering 3 feet higher than the roof level.

Additional high-seismic hazard archetypes were developed to investigate the effects of building height on performance. For the large diaphragm archetypes, 20-foot-roof-level and 40-foot-roof-level building designs were developed with 6-inch-thick and 11 1/4-inch-thick reinforced concrete wall panels, respectfully.

An additional study was conducted on a large 2:1 diaphragm archetype designed with lightweight longitudinal walls (10 psf) to investigate the performance of RWFD buildings without heavy wall weight interacting with the diaphragm. For these archetypes, only the wall weight and corresponding diaphragm nailing were changed, while the in-plane stiffness of the walls remained the same. Among the types of structures this archetype might represent are structurally separated interior portions of large RWFD buildings, as these separate sections are often braced with steel braced frames in one orthogonal direction and concrete or masonry walls in the other direction. These archetypes also provide a bounding condition for commercial buildings that might have a limited amount of concrete or masonry wall on one or more sides in combination with light cladding systems.

In the early development of the alternative RWFD design procedure, archetype designs were developed based on a building period of $T_a = T_{diaph} + T_{walls}$, which is similar to the approach in ASCE/SEI 41-13 Equation 7-19; however, this longer design period was abandoned for direct use of the diaphragm period, $T_{diaph}$, in the alternative RWFD design procedure for simplicity and conservativism. In these earlier studies, the interior diaphragm portions between the amplified shear boundary zones were left as a single nailing pattern because it was believed that this was a worst-case configuration by discouraging distribution of inelastic behavior. These earlier studies are presented in Koliou et al. (2016c) and showed similar increases in performance over traditional design.

**Table C-1 Descriptions of Archetypes with Wood Diaphragms (High- and Moderate-Seismic Hazard)—Alternative RWFD Design**

| Archetype ID | Diaphragm Dimensions | Roof Height | Wall Material | Wall Weight |
|---|---|---|---|---|
| **High-Seismicity Wood, Large Buildings** | | | | |
| HWL_21_N_OSB_P1026_01<br>HWL_12_N_OSB_P1026_01 | 400×200 ft | 30 ft | 9¼ in. Concrete | 116 psf |
| HWL_21_N_OSB_P1026_02<br>HWL_12_N_OSB_P1026_02 | 400×200 ft | 20 ft | 6 in. Concrete | 75 psf |
| HWL_21_N_OSB_P1026_03<br>HWL_12_N_OSB_P1026_03 | 400×200 ft | 40 ft | 11¼ in. Concrete | 141 psf |
| HWL_21_N_OSB_P1026_04 | 400×200 ft | 30 ft | Lightweight | 10 psf |
| HWL_11_N_OSB_P1026_01 | 400×400 ft | 30 ft | 9¼ in. Concrete | 116 psf |
| HWL_11_N_OSB_P1026_02 | 400×400 ft | 20 ft | 6 in. Concrete | 75 psf |
| HWL_11_N_OSB_P1026_03 | 400×400 ft | 40 ft | 11¼ in. Concrete | 141 psf |
| **High-Seismicity Wood, Small Buildings** | | | | |
| HWS_21_N_OSB_ P1026_01<br>HWS_12_N_OSB_ P1026_01 | 200×100 ft | 30 ft | 9¼ in. Concrete | 116 psf |
| HWS_11_N_OSB_P1026_01<br>HWS_11_N_OSB_P1026_02 | 100×100 ft | 30 ft | 9¼ in. Concrete | 116 psf |
| **Moderate-Seismicity Wood, Large Buildings** | | | | |
| MWL_21_N_OSB_P1026_01<br>MWL_12_N_OSB_P1026_01 | 400×200 ft | 30 ft | 9¼ in. Concrete | 116 psf |
| MWL_11_N_OSB_P1026_01 | 400×400 ft | 30 ft | 9¼ in. Concrete | 116 psf |
| **Moderate-Seismicity Wood, Small Buildings** | | | | |
| MWS_21_N_OSB_P1026_01<br>MWS_12_N_OSB_P1026_01 | 200×100 ft | 30 ft | 9¼ in. Concrete | 116 psf |
| MWS_11_N_OSB_P1026_01<br>MWS_11_N_OSB_P1026_02 | 100×100 ft | 30 ft | 9¼ in Concrete | 116 psf |

## Archetype: HWL_11_N_OSB_P1026_01

Top of Wall = 33-ft
Top of Roof = 30-ft

9¼" concrete wall panels (f'c=4ksi)
with #5@10"o.c. (fy=60ksi)

15/32" Structural I rated OSB,
fully blocked

Nail Spacings (inches) — Continuous Edges of Panels / Other Edges of Panels / Intermediate (Field)

| | |
|---|---|
| 1 | 10d at 6,6,12 |
| 2 | 10d at 4,6,12 |
| 4 | 10d at 2,3,12 w/ 3x framing |

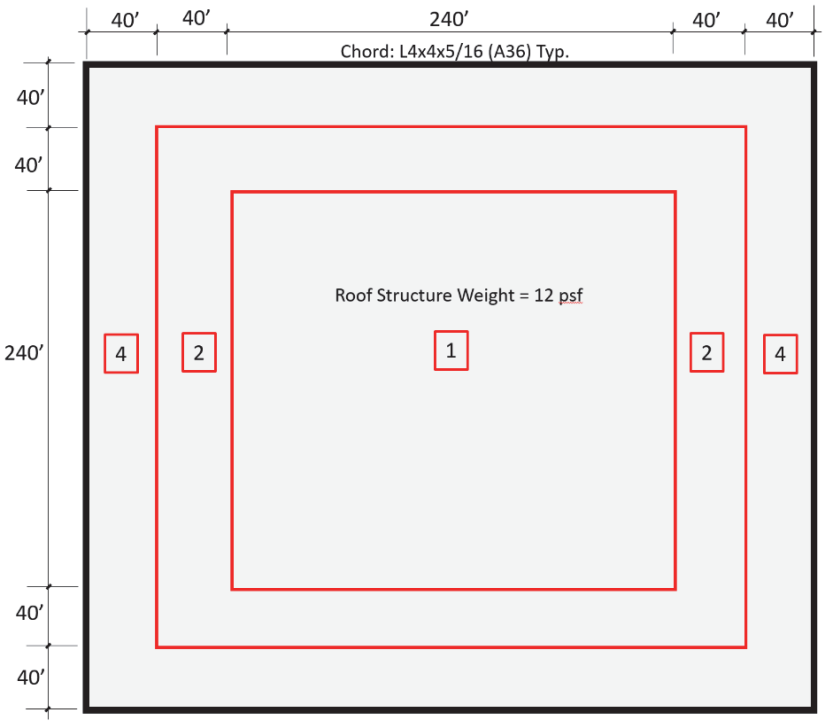


## Archetype: HWL_11_N_OSB_P1026_02

Top of Wall = 23-ft
Top of Roof = 20-ft

6" concrete wall panels (f'c=4ksi)
with #5@17"o.c. (fy=60ksi)

15/32" Structural I rated OSB,
fully blocked

Nail Spacings (inches) — Continuous Edges of Panels / Other Edges of Panels / Intermediate (Field)

| | |
|---|---|
| 1 | 10d at 6,6,12 |
| 3 | 10d at 2½,4,12 |

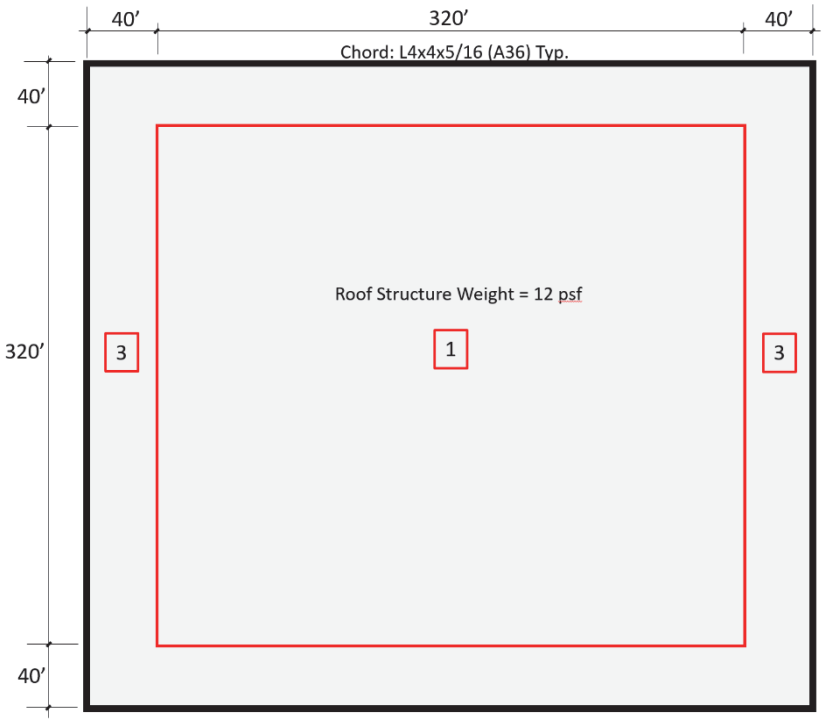


Figure C-1 Design details for archetypes with wood diaphragms designed for high-seismic hazard, part 1 (alternative RWFD procedure).

## Archetype:
## HWL_11_N_OSB_P1026_03

Top of Wall = 43-ft
Top of Roof = 40-ft

11.25" concrete wall panels (f'c=4ksi) with #5@10"o.c. each face (fy=60ksi, d=8.22")

15/32" Structural I rated OSB, fully blocked

Nail Spacings (inches)
Continuous Edges of Panels
Other Edges of Panels
Intermediate (Field)

| | |
|---|---|
| 1 | 10d at 6,6,12 |
| 2 | 10d at 4,6,12 |
| 3 | 10d at 2½,4,12 |
| 5 | 2 lines of 10d at 2½,4,12 w/ 4x framing |

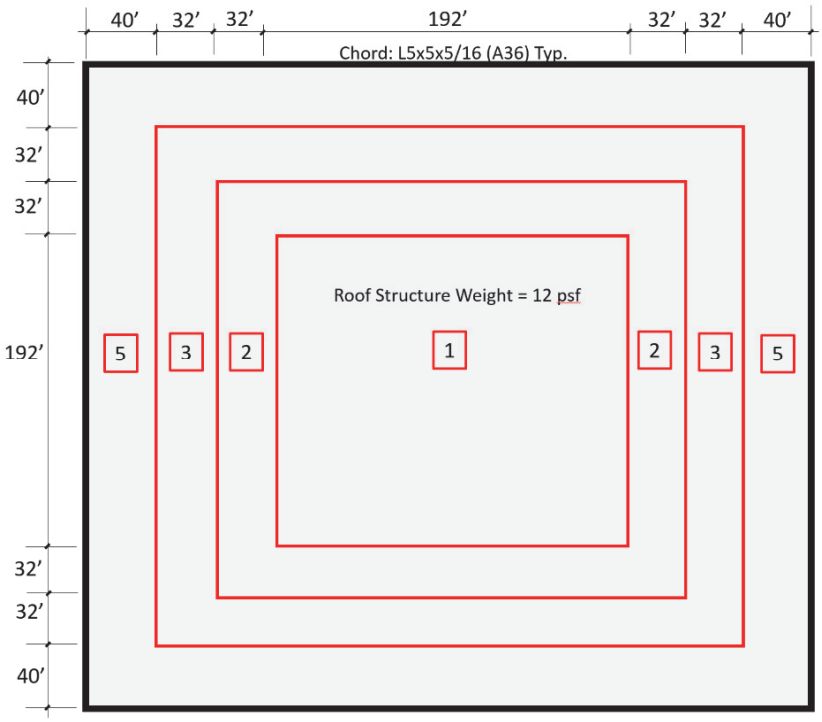


## Archetype:
## HWL_21_N_OSB_P1026_01
## HWL_12_N_OSB_P1026_01

Top of Wall = 33-ft
Top of Roof = 30-ft

9¼" concrete wall panels (f'c=4ksi) with #5@10"o.c. (fy=60ksi)

15/32" Structural I rated OSB, fully blocked

Nail Spacings (inches)
Continuous Edges of Panels
Other Edges of Panels
Intermediate (Field)

| | |
|---|---|
| 1 | 10d at 6,6,12 |
| 2 | 10d at 4,6,12 |
| 3 | 10d at 2½,4,12 |
| 6 | 2 lines of 10d at 2½,3,12 w/ 4x framing |

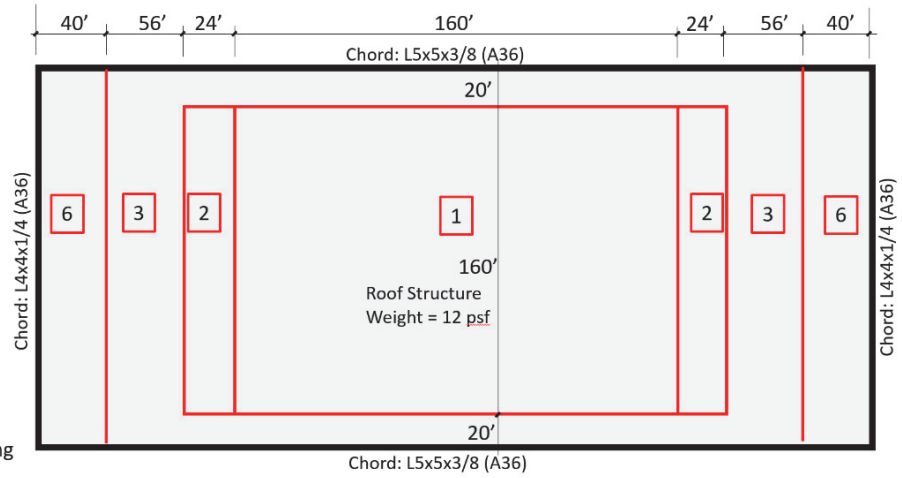


Figure C-2 Design details for archetypes with wood diaphragms designed for high-seismic hazard, part 2 (alternative RWFD procedure).

## Archetype:
## HWL_21_N_OSB_P1026_02
## HWL_12_N_OSB_P1026_02

Top of Wall = 23-ft
Top of Roof = 20-ft

6" concrete wall panels (f'c=4ksi) with #5@17"o.c. (fy=60ksi)

15/32" Structural I rated OSB, fully blocked

Nail Spacings (inches)
Continuous Edges of Panels
Other Edges of Panels
Intermediate (Field)

1 10d at 6,6,12
2 10d at 4,6,12
4 10d at 2,3,12 w/ 3x framing

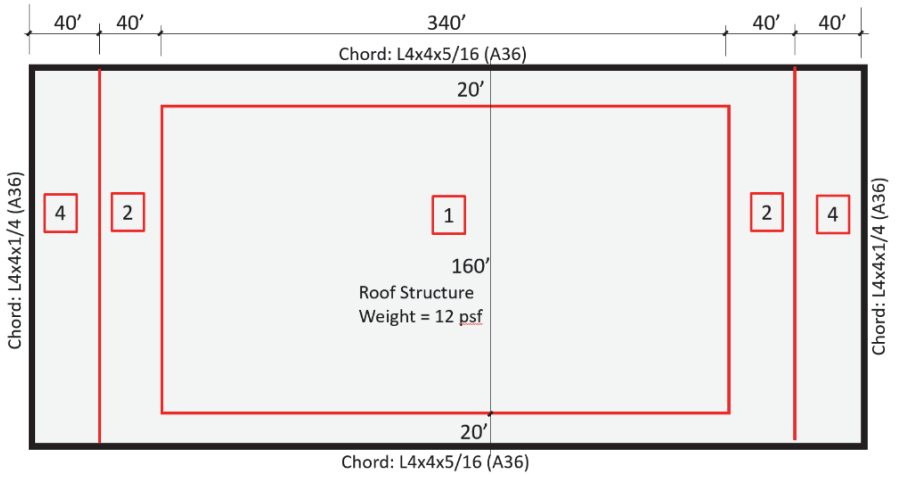


## Archetype:
## HWL_21_N_OSB_P1026_03
## HWL_12_N_OSB_P1026_03

Top of Wall = 43-ft
Top of Roof = 40-ft

11.25" concrete wall panels (f'c=4ksi) with #5@10"o.c. each face (fy=60ksi, d=8.22")

15/32" Structural I rated OSB, typical except Zone 7, fully blocked

Nail Spacings (inches)
Continuous Edges of Panels
Other Edges of Panels
Intermediate (Field)

1 10d at 6,6,12
2 10d at 4,6,12
3 10d at 2½,4,12
4 10d at 2,3,12 w/ 3x framing
5 2 lines of 10d at 2½,4,12 w/ 4x framing
7 2 lines of 10d at 2½,3,12 w/ 4x framing

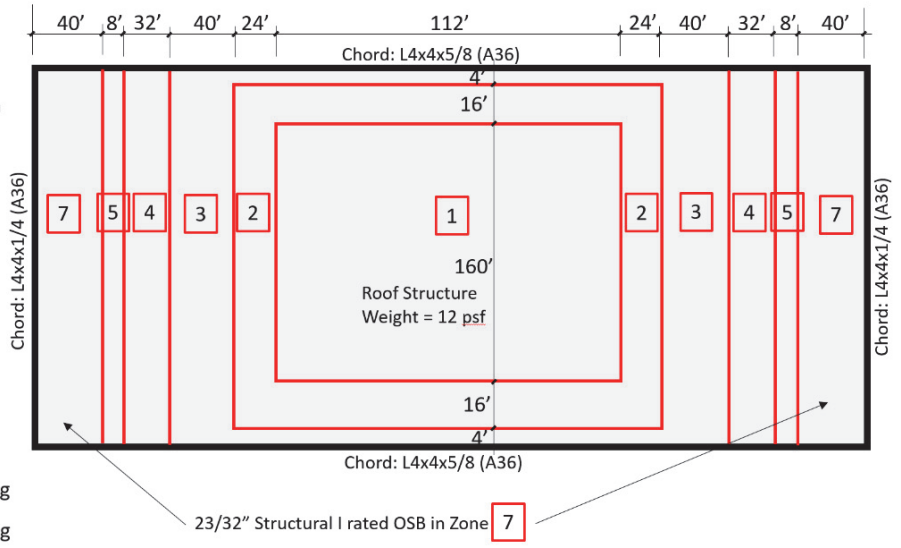


Figure C-3 Design details for archetypes with wood diaphragms designed for high-seismic hazard, part 3 (alternative RWFD procedure).

## Archetype:
## HWS_21_N_OSB_P1026_01
## HWS_12_N_OSB_P1026_01

Top of Wall = 33-ft
Top of Roof = 30-ft

9¼" concrete wall panels (f'c=4ksi)
with #5@10"o.c. (fy=60ksi)

15/32" Structural I rated OSB,
fully blocked

Nail Spacings (inches)
Continuous Edges of Panels
Other Edges of Panels
Intermediate (Field)

| | |
|---|---|
| 1 | 10d at 6,6,12 |
| 2 | 10d at 4,6,12 |
| 3 | 10d at 2½,4,12 |
| 4 | 10d at 2,3,12 w/ 3x framing |
| 6 | 2 lines of 10d at 2½,3,12 w/ 4x framing |

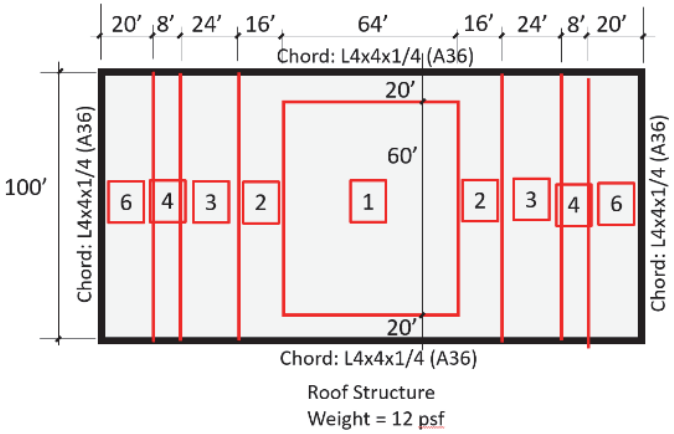


## Archetype:
## HWL_21_N_OSB_P1026_04

Top of Wall = 33-ft
Top of Roof = 30-ft

Lightweight Cladding on longitudinal
wall elevations (10 psf)

15/32" Structural I rated OSB,
fully blocked

Nail Spacings (inches)
Continuous Edges of Panels
Other Edges of Panels
Intermediate (Field)

| | |
|---|---|
| 1 | 10d at 6,6,12 |
| 2 | 10d at 4,6,12 |
| 3 | 10d at 2½,4,12 |

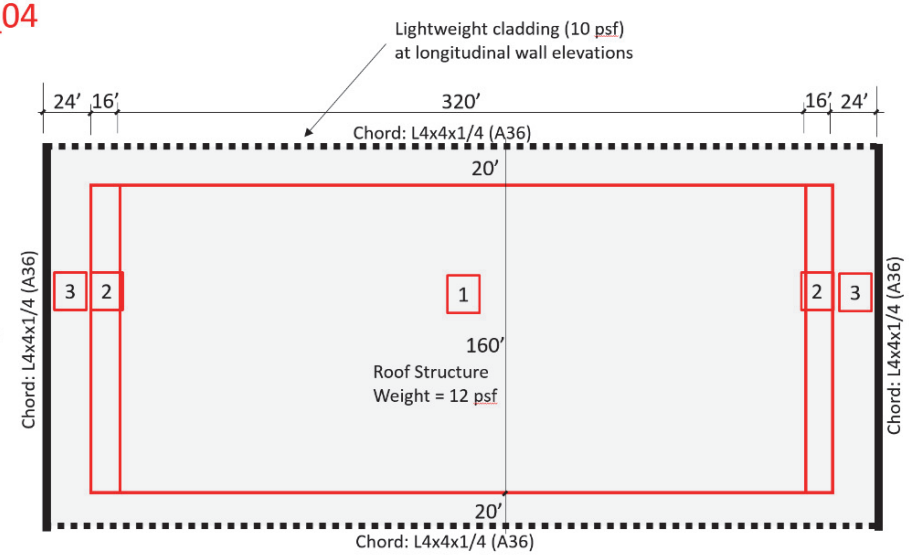


Figure C-4 Design details for archetypes with wood diaphragms designed for high-seismic hazard, part 4 (alternative RWFD procedure).

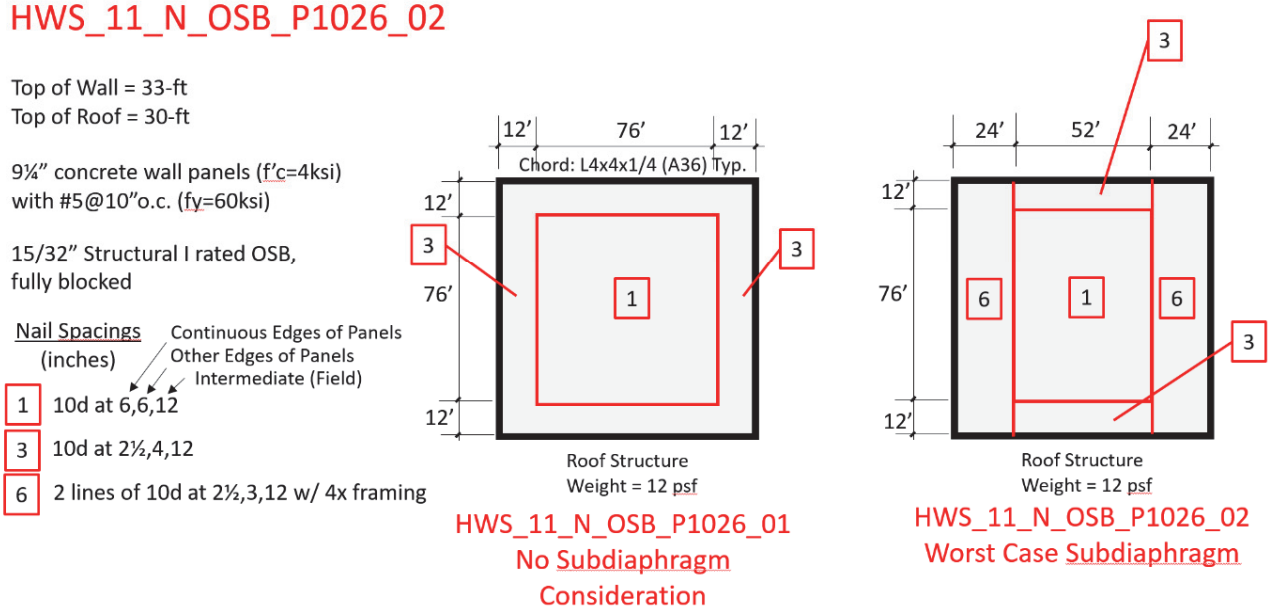


Figure C-5 Design details for archetypes with wood diaphragms designed for high-seismic hazard, part 5 (alternative RWFD procedure).

## Archetype:
## MWL_11_N_OSB_P1026_01

Top of Wall = 33-ft
Top of Roof = 30-ft

7¼" concrete wall panels (f'c=4ksi)
with #5@14"o.c. (fy=60ksi)

15/32" Structural I rated OSB,
fully blocked

Nail Spacings (inches)
Continuous Edges of Panels
Other Edges of Panels
Intermediate (Field)

1 10d at 6,6,12

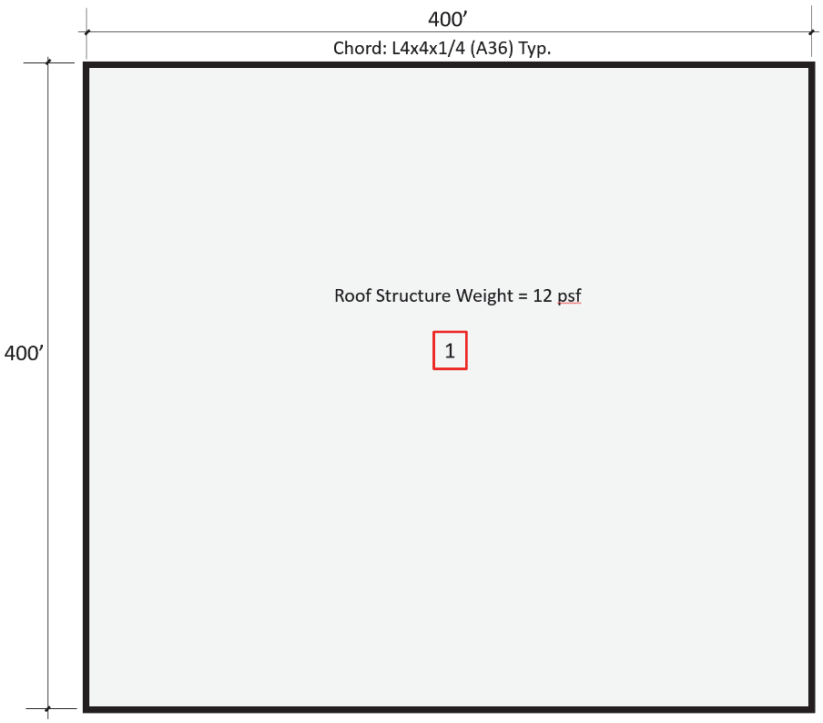


## Archetype:
## MWL_21_N_OSB_P1026_01
## MWL_12_N_OSB_P1026_01

Top of Wall = 33-ft
Top of Roof = 30-ft

7¼" concrete wall panels (f'c=4ksi)
with #5@14"o.c. (fy=60ksi)

15/32" Structural I rated OSB,
fully blocked

Nail Spacings (inches)
Continuous Edges of Panels
Other Edges of Panels
Intermediate (Field)

1 10d at 6,6,12
2 10d at 4,6,12

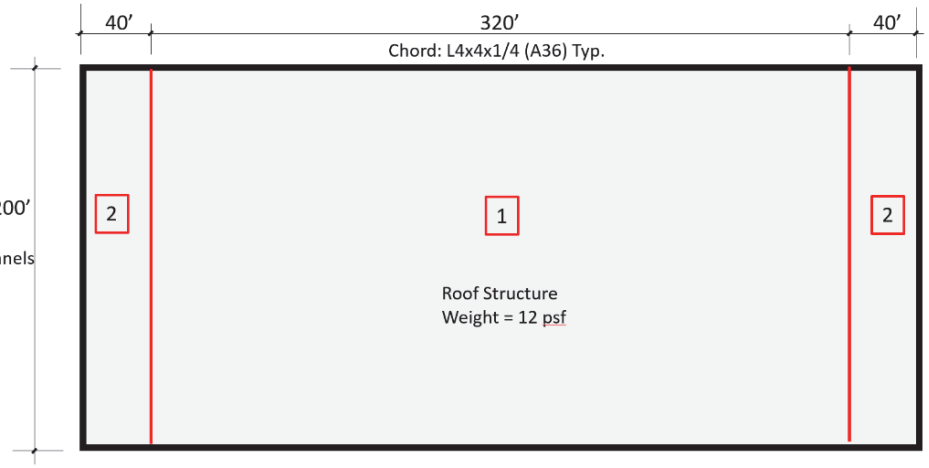


Figure C-6 Design details for archetypes with wood diaphragms designed for moderate-seismic hazard, part 1 (alternative RWFD procedure).

## Archetype:
## MWS_21_N_OSB_P1026_01
## MWS_12_N_OSB_P1026_01

Top of Wall = 33-ft
Top of Roof = 30-ft

7¼" concrete wall panels (f'c=4ksi)
with #5@14"o.c. (fy=60ksi)

15/32" Structural I rated OSB,
fully blocked

Nail Spacings (inches)
Continuous Edges of Panels
Other Edges of Panels
Intermediate (Field)

1 10d at 6,6,12

3 10d at 2½,4,12

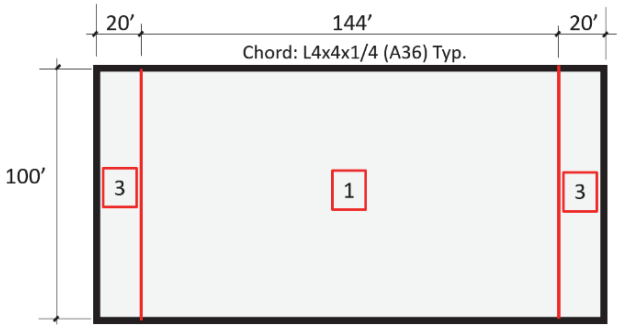


## Archetype:
## MWS_11_N_OSB_P1026_01
## MWS_11_N_OSB_P1026_02

Top of Wall = 33-ft
Top of Roof = 30-ft

7¼" concrete wall panels (f'c=4ksi)
with #5@14"o.c. (fy=60ksi)

15/32" Structural I rated OSB,
fully blocked

Nail Spacings (inches)
Continuous Edges of Panels
Other Edges of Panels
Intermediate (Field)

1 10d at 6,6,12

3 10d at 2½,4,12

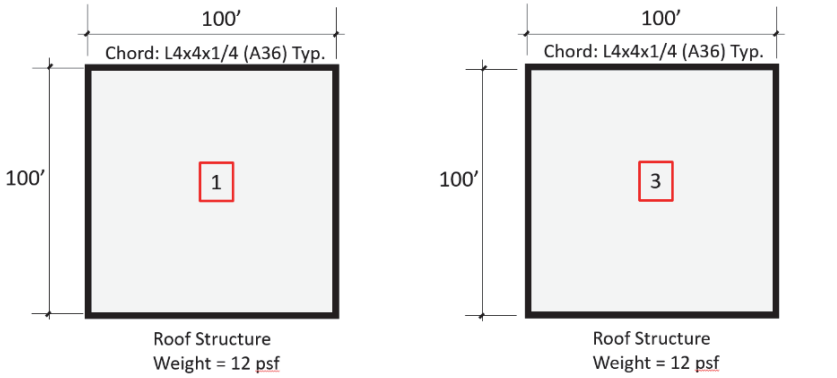


MWS_11_N_OSB_P1026_01
No Subdiaphragm
Consideration

MWS_11_N_OSB_P1026_02
Worst Case Subdiaphragm with
Simplified Nailing

Figure C-7 Design details for archetypes with wood diaphragms designed for moderate-seismic hazard, part 2 (alternative RWFD procedure).

## C.2 Summary of FEMA P695 Analysis Results for the Alternative RWFD Design Procedure

Incremental Dynamic Analyses (IDA) using the FEMA P695 Far-Field Ground Motion Ensemble were performed using the simplified models described in Appendix A to compute median collapse intensities (see Table A-6 for notations and abbreviations). Summaries of collapse results for individual wood diaphragm archetypes are included in Section C.4. Computed and acceptable *ACMR* values for the individual archetypes and the archetype groups are also included in Section C.4. The acceptable *ACMR* values are computed using the beta factors listed in Table A-2. The combined uncertainty, $\beta_{Total}$, is computed as the square-root-sum-of-the-squares of the individual uncertainties. For $\beta_{Total}$ equal to 0.66, the acceptable *ACMR* is 1.73 and 2.30 for 20 percent and 10 percent probability of collapse at MCE ground motion, respectively. Therefore, the acceptable *ACMR* applicable for the performance of individual archetypes is 1.73, and the acceptable *ACMR* of performance groups is 2.30. These targets were achieved by each wood diaphragm archetype and each performance group designed using the alternative RWFD design procedure. Summaries of the adjusted collapse margin ratio results for the performance groups of wood archetypes are provided in Table C-2.

**Table C-2 Summary of Collapse Margin Ratio Results for Wood Diaphragm Archetype Performance Groups for Alternative RWFD Design**

| Performance Group | Seismicity | Size | Computed *ACMR* | Acceptable *ACMR* | Pass/Fail |
|---|---|---|---|---|---|
| PG-1N | High | Large | 3.42 | 2.30 | Pass |
| PG-2N | High | Small | 2.54 | | Pass |
| PG-3N | Moderate | Large | 3.92 | | Pass |
| PG-4N | Moderate | Small | 3.14 | | Pass |

The elastic periods for the archetypes designed in accordance with the alternative RWFD design procedure are listed in Table C-3. In the majority of cases, the computed periods are no more than 6 percent longer than the computed periods in Table B-10 for the corresponding archetypes designed using the traditional procedure. In some cases, periods were approximately 16 percent longer than those designed to the traditional procedure.

The archetypes with large diaphragms performed better, with higher *ACMR*s, than the archetypes with small diaphragms, and the archetypes designed for moderate seismicity performed better than the ones designed for high seismicity. The small archetypes designed for high seismicity had the lowest *ACMR*. The range of fundamental elastic periods for the high-seismicity archetypes shown in Table C-3 is less than the transition period of 0.6

seconds for most of the small, 100-foot and 200-foot diaphragms. The *ACMR* for small archetypes designed for moderate seismicity have longer periods than those designed for high seismicity, and the transition period is lower at 0.4 seconds. The elastic period values in Table C-3 are all well above the transition period for the wood archetypes that are 400-feet long, pointing to a reason for high *ACMR*s (i.e., better performance) for the large wood diaphragm performance groups, PG-1N and PG-3N.

**Table C-3 Summary of Elastic Periods for Archetypes Designed Using the Alternative RWFD Design Procedure**

| Wood Diaphragm Span Length | Period for High-Seismic Archetypes | Period for Moderate-Seismic Archetypes |
|---|---|---|
| 400 ft | 0.89 to 0.94 sec | 0.91 to 0.93 sec |
| 200 ft | 0.49 to 0.63 sec | 0.54 to 0.60 sec |
| 100 ft | 0.38 to 0.44 sec | 0.43 to 0.46 sec |

The ranges of building drift ratios (*BDR*) for the 30-foot-high-roof-level archetypes within the performance groups are provided in Table C-4. The *BDR* is the sum of the wall drift ratio (*WDR*) and the diaphragm drift ratio (*DDR*) and often serves as a damage index. The *WDR* is computed as the in-plane wall deformation divided by the height of the roof, and the *DDR* is computed as the diaphragm displacement divided by one-half of the diaphragm span. The *WDR*s for the rigid wall archetypes were negligible, resulting in the *BDR* approximately equal to the *DDR* for each archetype.

A study of building height was conducted on the large diaphragm archetypes under high seismicity. Table C-5 provides a comparison of the *BDR*s within PG-1N for large diaphragm archetypes of different heights to the roof level. The taller buildings have larger *BDR*s, which would normally indicate higher potential damage. However, this can be misleading where the drift is dominated by the diaphragm because the *BDR*s fail to capture the fact that shorter buildings may have significantly greater P-delta stability concerns compared with taller buildings when given similar diaphragm deflections. To illustrate this point, Table C-6 provides a comparison of the *ACMR*s within PG-1N for large diaphragm archetypes of different heights to the roof level, and the shorter buildings have less margin from collapse. As mentioned in Appendix B, for evaluating performance acceptability, archetype limit states are equated to a load-displacement *P*-delta sidesway instability, not an arbitrary *BDR* limit.

**Table C-4 Range of Building Drift Ratios (*BDR*s) for the 30-foot-High-Roof-Level Archetypes within Wood Diaphragm Performance Groups**

| Performance Group | Seismicity | Size | Median *BDR* @ DE (%) | Median *BDR* @ MCE (%) |
|---|---|---|---|---|
| PG-1N | High | Large | 0.30 to 0.51 | 0.53 to 0.83 |
| PG-2N | High | Small | 0.78 to 0.82 | 1.11 to 1.35 |
| PG-3N | Moderate | Large | 0.31 to 0.42 | 0.54 to 0.63 |
| PG-4N | Moderate | Small | 0.51 to 0.68 | 0.92 to 1.25 |

**Table C-5 Range of Building Drift Ratios (*BDR*s) for High-Seismicity Archetypes of Different Roof Heights within Wood Diaphragm Performance Group PG-1N**

| Performance Group | Size | Roof Height | Median *BDR* @ DE (%) | Median *BDR* @ MCE (%) |
|---|---|---|---|---|
| PG-1N | 400×200 ft | 20 ft | 0.39 | 0.53 |
| | | 30 ft | 0.43 | 0.58 |
| | | 40 ft | 0.46 | 0.60 |
| PG-1N | 200×400 ft | 20 ft | 0.47 | 0.81 |
| | | 30 ft | 0.51 | 0.83 |
| | | 40 ft | 0.53 | 0.84 |
| PG-1N | 400×400 ft | 20 ft | 0.28 | 0.50 |
| | | 30 ft | 0.30 | 0.53 |
| | | 40 ft | 0.35 | 0.58 |

**Table C-6 Adjusted Collapse Margin Ratios (*ACMR*s) for High-Seismicity Archetypes of Different Roof Heights within Wood Diaphragm Performance Group PG-1N**

| Performance Group | Size | Roof Height | *ACMR* | Acceptable *ACMR* |
|---|---|---|---|---|
| PG-1N | 400×200 ft | 20 ft | 3.45 | 1.73 |
| | | 30 ft | 3.87 | 1.73 |
| | | 40 ft | 3.91 | 1.73 |
| PG-1N | 200×400 ft | 20 ft | 3.09 | 1.73 |
| | | 30 ft | 3.28 | 1.73 |
| | | 40 ft | 3.39 | 1.73 |
| PG-1N | 400×400 ft | 20 ft | 2.80 | 1.73 |
| | | 30 ft | 3.38 | 1.73 |
| | | 40 ft | 3.50 | 1.73 |

## C.3 Overstrength and Deflection Amplification Factors for the Diaphragm

Section 7.6 of FEMA P695 describes derivation of the system overstrength factor, $\Omega_0$, from the archetype overstrength factor, $\Omega$, calculated for each performance group. It indicates that $\Omega_0$ should not be taken as less than the

largest value of $\Omega$, should not be taken as less than 3, and should be judgmentally rounded to half-unit intervals. For the FEMA P-1026 wood diaphragm archetypes, the assigned $\Omega_{0\text{-}diaph}$ of 2 was selected based on the $\Omega$ values assigned to the two high-seismic performance groups (2.14 and 1.72). Although notably larger $\Omega$ values (4.01 and 2.50) were calculated for moderate-seismic performance groups, higher overstrength factors are understood to be common for moderate-seismic groups across all systems, and it is not standard practice to assign $\Omega_0$ based on these higher values. Based on the judgement of those involved in the development of the ASCE/SEI 7-22 provisions, $\Omega_{0\text{-}diaph}$ was rounded to 2.

Values for the overstrength factor, $\Omega$, computed from the results of a nonlinear pushover analysis are included in Table C-9. The overstrength factors, $\Omega$, of all performance groups proposed for the system range from 1.72 to 4.01.

The deflection amplification factor, $C_d$, included in the ASCE/SEI 7 provisions was derived from the FEMA P-1026 nonlinear response history analysis (NLRHA) studies in conformance with FEMA P695 procedures (developed for vertical elements of the seismic-force-resisting system) with some modifications. According to FEMA P695, vertical systems with typical damping are assigned a deflection amplification factor, $C_d$, equal to the response modification factor, $R$. For the case where bare steel deck diaphragms with special seismic detailing and wood diaphragms are designed according to ASCE/SEI 7-22 Section 12.10.4, a deflection amplification factor, $C_{d\text{-}diaph}$, of 3.0 (less than $R_{diaph}$ of 4.5) is deemed appropriate for several reasons: (1) the boundary zones are designed for 1.5 times the design shear value, equating to $R_{diaph}$ of 3.0 at the boundaries; (2) the inelastic deformations in diaphragms concentrate at the diaphragm perimeter and at transitions in strength and stiffness (e.g., transitions in nailing patterns), leaving large portions of the diaphragm elastic; and (3) numerical studies underlying FEMA P-1026 found that the ratio of median design-basis-earthquake drift to yield drift (approximation of predicted drift) was between 1.4 and 2.9, with an average value of 2.1, suggesting that $C_{d\text{-}diaph}$ of 3.0 is conservative.

Numerical studies used as the basis for this report provide data on analytical predictions of average peak diaphragm displacements. Diaphragm drift ratios published in Koliou et al. (2016a) and summarized in Appendix B are average peak ratios for archetypes representing traditional design practice, using the FEMA P695 ground motion suite scaled to $S_{DS}$ = 1.0. The reported diaphragm drift ratios correspond to an average peak diaphragm deflection of 7 inches for the Chapter 3 example of the 400 foot-by-200 foot diaphragm

designed using traditional provisions. For the alternative RWFD design procedure, the diaphragm drift ratios are reported in Table C-7 and correspond to an average peak roof deflection of 10 inches for the Chapter 5 and Chapter 6 examples of the 400 foot-by-200 foot diaphragm. Higher drift ratios associated with the alternative RWFD design procedure do not correlate with higher probability of collapse, because the alternative RWFD design procedure more effectively distributes the inelastic ductile behavior over a wider portion of the diaphragm.

In Chapter 6, use of the diaphragm's deflection amplification factor with the best-estimate calculated elastic deflection closely approaches the analytically predicted deflection of 10 inches computed using nonlinear response history analysis.

## C.4 FEMA P695 Evaluation Results for the Alternative RWFD Design Procedure

Results for the FEMA P695 collapse analyses for the alternative RWFD design procedure are presented in Table C-7, Table C-8, and Table C-9.

**Table C-7 Summary of Collapse Results for RWFD Archetypes with Wood Diaphragms—Alternative RWFD Design**

| Archetype ID | Design Configuration | | | | Pushover and IDA Results | | | Relevant Analysis Parameters | | |
|---|---|---|---|---|---|---|---|---|---|---|
| | Building Size | Diaphragm Aspect Ratio | Roof Height | SDC | $S_{MT}[T]$ (g) | $S_{CT}[T]$ (g) | *CMR* | Period (sec) | Median *BDR* @ DE (%) | Median *BDR* @ MCE (%) |
| **Performance Group No. PG-1N (High-Seismic Hazard, Wood, Large Building, New Design)** | | | | | | | | | | |
| HWL_21_N_OSB_P1026_01 | Large | 2:1 | 30 ft | $D_{max}$ | 0.95 | 2.54 | 2.67 | 0.94 | 0.43 | 0.58 |
| HWL_21_N_OSB_P1026_02 | Large | 2:1 | 20 ft | $D_{max}$ | 1.00 | 2.40 | 2.40 | 0.90 | 0.39 | 0.53 |
| HWL_21_N_OSB_P1026_03 | Large | 2:1 | 40 ft | $D_{max}$ | 0.96 | 2.59 | 2.70 | 0.93 | 0.46 | 0.60 |
| HWL_21_N_OSB_P1026_04 | Large | 2:1 | 30 ft | $D_{max}$ | 0.96 | 2.34 | 2.44 | 0.93 | 0.44 | 0.54 |
| HWL_12_N_OSB_P1026_01 | Large | 1:2 | 30 ft | $D_{max}$ | 1.50 | 3.70 | 2.47 | 0.51 | 0.51 | 0.83 |
| HWL_12_N_OSB_P1026_02 | Large | 1:2 | 20 ft | $D_{max}$ | 1.50 | 3.48 | 2.32 | 0.49 | 0.47 | 0.81 |
| HWL_12_N_OSB_P1026_03 | Large | 1:2 | 40 ft | $D_{max}$ | 1.50 | 3.82 | 2.55 | 0.50 | 0.53 | 0.84 |
| HWL_11_N_OSB_P1026_01 | Large | 1:1 | 30 ft | $D_{max}$ | 0.98 | 2.30 | 2.35 | 0.91 | 0.30 | 0.53 |
| HWL_11_N_OSB_P1026_02 | Large | 1:1 | 20 ft | $D_{max}$ | 1.01 | 1.96 | 1.94 | 0.89 | 0.28 | 0.50 |
| HWL_11_N_OSB_P1026_03 | Large | 1:1 | 40 ft | $D_{max}$ | 0.96 | 2.32 | 2.41 | 0.93 | 0.35 | 0.58 |
| **Performance Group No. PG-2N (High-Seismic Hazard, Wood, Small Building, New Design)** | | | | | | | | | | |
| HWS_21_N_OSB_P1026_01 | Small | 2:1 | 30 ft | $D_{max}$ | 1.42 | 2.56 | 1.80 | 0.63 | 0.80 | 1.11 |
| HWS_12_N_OSB_P1026_01 | Small | 1:2 | 30 ft | $D_{max}$ | 1.50 | 3.02 | 2.02 | 0.44 | 0.82 | 1.20 |
| HWS_11_N_OSB_P1026_01 | Small | 1:1 | 30 ft | $D_{max}$ | 1.50 | 2.88 | 1.92 | 0.39 | 0.78 | 1.32 |
| HWS_11_N_OSB_P1026_02 | Small | 1:1 | 30 ft | $C_{max}$ | 1.50 | 2.80 | 1.86 | 0.38 | 0.80 | 1.35 |
| **Performance Group No. PG-3N (Moderate-Seismic Hazard, Wood, Large Building, New Design)** | | | | | | | | | | |
| MWL_21_N_OSB_P1026_01 | Large | 2:1 | 30 ft | $C_{max}$ | 0.49 | 1.69 | 3.46 | 0.91 | 0.31 | 0.54 |
| MWL_12_N_OSB_P1026_01 | Large | 1:2 | 30 ft | $C_{max}$ | 1.00 | 2.79 | 2.79 | 0.54 | 0.42 | 0.63 |
| MWL_11_N_OSB_P1026_01 | Large | 1:1 | 30 ft | $C_{max}$ | 0.48 | 1.69 | 3.52 | 0.93 | 0.39 | 0.57 |

**Table C-7 Summary of Collapse Results for RWFD Archetypes with Wood Diaphragms—Alternative RWFD Design (continued)**

| Archetype ID | Design Configuration | | | | Pushover and IDA Results | | | Relevant Analysis Parameters | | |
|---|---|---|---|---|---|---|---|---|---|---|
| | Building Size | Diaphragm Aspect Ratio | Roof Height | SDC | $S_{MT}[T]$ (g) | $S_{CT}[T]$ (g) | *CMR* | Period (sec) | Median *BDR* @ DE (%) | Median *BDR* @ MCE (%) |
| **Performance Group No. PG-4N (Moderate-Seismic Hazard, Wood, Small Building, New Design)** | | | | | | | | | | |
| MWS_21_N_OSB_P1026_01 | Small | 2:1 | 30 ft | $C_{max}$ | 0.73 | 1.58 | 2.17 | 0.60 | 0.51 | 0.92 |
| MWS_12_N_OSB_P1026_01 | Small | 1:2 | 30 ft | $C_{max}$ | 0.74 | 2.08 | 2.82 | 0.43 | 0.66 | 0.97 |
| MWS_11_N_OSB_P1026_01 | Small | 1:1 | 30 ft | $C_{max}$ | 0.75 | 2.35 | 3.13 | 0.46 | 0.61 | 1.21 |
| MWS_11_N_OSB_P1026_02 | Small | 1:1 | 30 ft | $C_{max}$ | 0.75 | 2.11 | 2.82 | 0.45 | 0.68 | 1.25 |

**Table C-8 Computed and Acceptable Collapse Margin Ratios for RWFD Archetypes with Wood Diaphragms—Alternative RWFD Design**

| Archetype ID | Design Configuration | | | | Collapse Margin Parameters | | | | Acceptance Check | |
|---|---|---|---|---|---|---|---|---|---|---|
| | Building Size | Diaphragm Aspect Ratio | Roof Height | SDC | *CMR* | $\mu_T$ | SSF | *ACMR* | Accept. *ACMR* | Pass/Fail |
| **Performance Group No. PG-1N (High-Seismic Hazard, Wood, Large Building, New Design)** | | | | | | | | | | |
| HWL_21_N_OSB_P1026_01 | Large | 2:1 | 30 ft | $D_{max}$ | 2.67 | 8.40 | 1.45 | 3.87 | 1.73 | Pass |
| HWL_21_N_OSB_P1026_02 | Large | 2:1 | 20 ft | $D_{max}$ | 2.40 | 8.35 | 1.44 | 3.45 | 1.73 | Pass |
| HWL_21_N_OSB_P1026_03 | Large | 2:1 | 40 ft | $D_{max}$ | 2.70 | 8.41 | 1.45 | 3.91 | 1.73 | Pass |
| HWL_21_N_OSB_P1026_04 | Large | 2:1 | 30 ft | $D_{max}$ | 2.44 | 8.43 | 1.45 | 3.54 | 1.73 | Pass |
| HWL_12_N_OSB_P1026_01 | Large | 1:2 | 30 ft | $D_{max}$ | 2.47 | 8.65 | 1.33 | 3.28 | 1.73 | Pass |
| HWL_12_N_OSB_P1026_02 | Large | 1:2 | 20 ft | $D_{max}$ | 2.32 | 8.73 | 1.33 | 3.09 | 1.73 | Pass |
| HWL_12_N_OSB_P1026_03 | Large | 1:2 | 30 ft | $D_{max}$ | 2.55 | 8.77 | 1.33 | 3.39 | 1.73 | Pass |
| HWL_11_N_OSB_P1026_01 | Large | 1:1 | 30 ft | $D_{max}$ | 2.35 | 8.44 | 1.44 | 3.38 | 1.73 | Pass |
| HWL_11_N_OSB_P1026_02 | Large | 1:1 | 30 ft | $D_{max}$ | 1.94 | 8.35 | 1.44 | 2.80 | 1.73 | Pass |
| HWL_11_N_OSB_P1026_03 | Large | 1:1 | 30 ft | $D_{max}$ | 2.41 | 8.37 | 1.45 | 3.50 | 1.73 | Pass |
| **Mean of Performance Group:** | | | | | **2.42** | **8.49** | **1.41** | **3.42** | **2.30** | **Pass** |

**Table C-8 Computed and Acceptable Collapse Margin Ratios for RWFD Archetypes with Wood Diaphragms—Alternative RWFD Design (continued)**

| Archetype ID | Design Configuration | | | | Collapse Margin Parameters | | | | Acceptance Check | |
|---|---|---|---|---|---|---|---|---|---|---|
| | Building Size | Diaphragm Aspect Ratio | Roof Height | SDC | *CMR* | $\mu_T$ | SSF | *ACMR* | Accept. *ACMR* | Pass/Fail |
| **Performance Group No. PG-2N (High-Seismic Hazard, Wood, Small Building, New Design)** | | | | | | | | | | |
| HWS_21_N_OSB_ P1026_01 | Small | 2:1 | 30 ft | $D_{max}$ | 1.80 | 8.10 | 1.36 | 2.45 | 1.73 | Pass |
| HWS_12_N_OSB_ P1026_01 | Small | 1:2 | 30 ft | $D_{max}$ | 2.02 | 8.13 | 1.33 | 2.68 | 1.73 | Pass |
| HWS_11_N_OSB_ P1026_01 | Small | 1:1 | 30 ft | $D_{max}$ | 1.92 | 8.41 | 1.33 | 2.55 | 1.73 | Pass |
| HWS_11_N_OSB_P1026_02 | Small | 1:1 | 30 ft | $D_{max}$ | 1.86 | 8.43 | 1.33 | 2.48 | 1.73 | Pass |
| **Mean of Performance Group:** | | | | | **1.90** | **8.27** | **1.34** | **2.54** | **2.30** | **Pass** |
| **Performance Group No. PG-3N (Moderate-Seismic Hazard, Wood, Large Building, New Design)** | | | | | | | | | | |
| MWL_21_N_OSB_P1026_01 | Large | 2:1 | 30 ft | $C_{max}$ | 3.46 | 8.18 | 1.22 | 4.22 | 1.73 | Pass |
| MWL_12_N_OSB_P1026_01 | Large | 1:2 | 30 ft | $C_{max}$ | 2.79 | 8.28 | 1.15 | 3.21 | 1.73 | Pass |
| MWL_11_N_OSB_P1026_01 | Large | 1:1 | 30 ft | $C_{max}$ | 3.52 | 8.64 | 1.23 | 4.33 | 1.73 | Pass |
| **Mean of Performance Group:** | | | | | **3.26** | **8.37** | **1.20** | **3.92** | **2.30** | **Pass** |
| **Performance Group No. PG-4N (Moderate-Seismic Hazard, Wood, Small Building, New Design)** | | | | | | | | | | |
| MWS_21_N_OSB_P1026_01 | Small | 2:1 | 30 ft | $C_{max}$ | 2.17 | 8.19 | 1.19 | 2.58 | 1.73 | Pass |
| MWS_12_N_OSB_P1026_01 | Small | 1:2 | 30 ft | $C_{max}$ | 2.82 | 8.42 | 1.14 | 3.21 | 1.73 | Pass |
| MWS_11_N_OSB_P1026_01 | Small | 1:1 | 30 ft | $C_{max}$ | 3.13 | 8.39 | 1.14 | 3.57 | 1.73 | Pass |
| MWS_11_N_OSB_P1026_02 | Small | 1:1 | 30 ft | $C_{max}$ | 2.82 | 8.32 | 1.14 | 3.21 | 1.73 | Pass |
| **Mean of Performance Group:** | | | | | **2.73** | **8.33** | **1.15** | **3.14** | **2.30** | **Pass** |

**Table C-9 Overstrength Parameters for RWFD Archetypes with Wood Diaphragms—Alternative RWFD Design**

| Archetype ID | Design configuration | | | | $\Omega$ |
|---|---|---|---|---|---|
| | Building Size | Diaphragm Aspect Ratio | Roof Height | SDC | |
| **Performance Group No. PG-1N (High-Seismic Hazard, Wood, Large Building, Alternative RWFD Design)** | | | | | |
| HWL_21_N_OSB_P1026_01 | Large | 2:1 | 30 ft | $D_{max}$ | 2.44 |
| HWL_21_N_OSB_P1026_02 | Large | 2:1 | 20 ft | $D_{max}$ | 2.47 |
| HWL_21_N_OSB_P1026_03 | Large | 2:1 | 40 ft | $D_{max}$ | 2.48 |
| HWL_21_N_OSB_P1026_04 | Large | 2:1 | 30 ft | $D_{max}$ | 2.46 |
| HWL_12_N_OSB_P1026_01 | Large | 1:2 | 30 ft | $D_{max}$ | 1.60 |
| HWL_12_N_OSB_P1026_02 | Large | 1:2 | 20 ft | $D_{max}$ | 1.65 |
| HWL_12_N_OSB_P1026_03 | Large | 1:2 | 40 ft | $D_{max}$ | 1.64 |
| HWL_11_N_OSB_P1026_01 | Large | 1:1 | 30 ft | $D_{max}$ | 2.30 |
| HWL_11_N_OSB_P1026_02 | Large | 1:1 | 20 ft | $D_{max}$ | 2.15 |
| HWL_11_N_OSB_P1026_03 | Large | 1:1 | 40 ft | $D_{max}$ | 2.24 |
| **Mean of Performance Group** | | | | | **2.14** |
| **Performance Group No. PG-2N (High-Seismic Hazard, Wood, Small Building, Alternative RWFD Design)** | | | | | |
| HWS_21_N_OSB_P1026_01 | Small | 2:1 | 30 ft | $D_{max}$ | 1.67 |
| HWS_12_N_OSB_P1026_01 | Small | 1:2 | 30 ft | $D_{max}$ | 1.75 |
| HWS_11_N_OSB_P1026_01 | Small | 1:1 | 30 ft | $D_{max}$ | 1.73 |
| HWS_11_N_OSB_P1026_02 | Small | 1:1 | 30 ft | $D_{max}$ | 1.72 |
| **Mean of Performance Group** | | | | | **1.72** |
| **Performance Group No. PG-3N (Moderate-Seismic Hazard, Wood, Large Building, Alternative RWFD Design)** | | | | | |
| MWL_21_N_OSB_P1026_01 | Large | 2:1 | 30 ft | $C_{max}$ | 4.71 |
| MWL_12_N_OSB_P1026_01 | Large | 1:2 | 30 ft | $C_{max}$ | 2.83 |
| MWL_11_N_OSB_P1026_01 | Large | 1:1 | 30 ft | $C_{max}$ | 4.50 |
| **Mean of Performance Group** | | | | | **4.01** |
| **Performance Group No. PG-4N (Moderate-Seismic Hazard, Wood, Small Building, Alternative RWFD Design)** | | | | | |
| MWS_21_N_OSB_P1026_01 | Small | 2:1 | 30 ft | $C_{max}$ | 2.77 |
| MWS_12_N_OSB_P1026_01 | Small | 1:2 | 30 ft | $C_{max}$ | 2.53 |
| MWS_11_N_OSB_P1026_01 | Small | 1:1 | 30 ft | $C_{max}$ | 2.34 |
| MWS_11_N_OSB_P1026_02 | Small | 1:1 | 30 ft | $C_{max}$ | 2.36 |
| **Mean of Performance Group** | | | | | **2.50** |

## C.5 Analysis of Archetypes Using Uniform Nailing

Table C-10 includes a comparison of archetypes designed using the alternative RWFD design procedure versus those using one pattern of uniform nailing. For the archetypes with uniform nailing, the nailing in the edge zone, where the shear is amplified by 1.5, was extended across the diaphragm. This is essentially designing for $R_{diaph}$ equal to 3 without reducing the nailing across the diaphragm. This nailing is likely to cause a concentration of yielding along the diaphragm edge with little opportunity for yielding to spread into the diaphragm. For the archetypes studied, the less desirable nailing lowered the *ACMR* but in no case did it reduce it below the acceptable level of 1.73 for an individual archetype. This result indicates that adequate overstrength and ductility exists for this less-than-desirable nailing. It also means that the location of the transition of amplified shear to unamplified shear can be extended toward the center of the diaphragm, if necessary, with only modest reductions in the seismic performance.

**Table C-10 Comparison of Archetypes**

| Performance Group ID | Design Configuration | | | | Collapse Margin | | Pass/Fail |
|---|---|---|---|---|---|---|---|
| | Archetype ID | Building Size | Diaphragm Construction | SDC | *ACMR* | Acceptable *ACMR* | |
| PG-1 | HWL_12_N_OSB_P1026_01 | Large | Wood Panelized | $D_{max}$ | 3.28 | 1.73 | Pass |
| | HWL_12_N_OSB_RD3_01 | Large | Wood Panelized | $D_{max}$ | 2.93 | | Pass |
| | Performance Group (*ACMR*=3.42) | Projected *ACMR* of PG=*ACMR*×(2.93/3.28) | | | 3.06 | 2.30 | Pass |
| PG-2 | HWS_21_N_OSB_ P1026_01 | Small | Wood Panelized | $D_{max}$ | 2.45 | 1.73 | Pass |
| | HWS_21_N_OSB_RD3_01 | Small | Wood Panelized | $D_{max}$ | 2.25 | | Pass |
| | Performance Group (*ACMR*=2.54) | Projected *ACMR* of PG=*ACMR*×(2.25/2.45) | | | 2.33 | 2.30 | Pass |
| PG-3 | MWL_12_N_OSB_P1026_01 | Large | Wood Panelized | $C_{max}$ | 3.21 | 1.73 | Pass |
| | MWL_12_N_OSB_RD3_01 | Large | Wood Panelized | $C_{max}$ | 2.76 | | Pass |
| | Performance Group (*ACMR*=3.92) | Projected *ACMR* of PG=*ACMR*×(2.76/3.21) | | | 3.37 | 2.30 | Pass |
| PG-4 | MWS_21_N_OSN_ P1026_01 | Small | Wood Panelized | $C_{max}$ | 2.58 | 1.73 | Pass |
| | MWS_21_N_OSN_RD3_01 | Small | Wood Panelized | $C_{max}$ | 2.05 | | Pass |
| | Performance Group (*ACMR*=3.14) | Projected *ACMR* of PG=*ACMR*×(2.05/2.58) | | | 2.50 | 2.30 | Pass |

# Appendix D

# Extension of FEMA P-1026 to Bare Steel Deck Roof Diaphragms

The first edition of FEMA P-1026 (2015) introduced and explained an alternative procedure for seismic design of RWFD buildings. At that time, the method was not fully developed for bare steel deck roof diaphragms and was limited to wood structural panel roof diaphragms. This appendix summarizes the additional work completed to extend the procedure to bare steel deck roof diaphragms.

## D.1 Background

The stiffness, strength, and ductility of bare steel deck diaphragms are derived from the deck profile, deck thickness, deck material, deck-to-deck (sidelap) connections, and deck-to-framing (structural) connections. Stiffness and strength may be determined by calculation or test as stipulated in AISI S310-20. Ductility of bare steel deck diaphragms under cyclic loads may be assessed by cantilever diaphragm testing per AISI S907-17 (AISI, 2018). Prior to ASCE/SEI 7-22, the ductility of steel deck diaphragms was not explicitly considered, so designs were governed only by the stiffness and strength of the diaphragm.

A large database of cantilever diaphragm tests was compiled by O'Brien et al. (2017) and detailed and assessed by Eatherton et al. (2020). These test results show that ductile response is commonly observed in bare steel deck diaphragms, but care must be taken with the details. The observed ductility and post-peak residual-force capacity at large deformations is determined by both the deck and its connectors, and relative contributions between the two depend on the specific details. Connectors, both sidelap and structural, and their selected attachment patterns have an important influence on the response and are thus separately considered. Unlike wood sheathed diaphragms, they are not the only, nor always even the primary, source of nonlinear response for the system.

## D.2 Connector Strength and Ductility

Previous work to develop FEMA P-1026 (2015) compiled and characterized available cyclic data on sidelap and structural connections for steel deck (Koliou, 2014; Koliou et al., 2016a; Koliou and Filiatrault, 2017). At that time, the data were relatively limited and primarily derived from the testing of Rogers and Tremblay (2003a, b) and Guenfoud et al. (2010). Available testing covered common cases but did not include proprietary sidelap connections or current generations of PAFs, both of which are in common use today. Additionally, the test setup of Rogers and Tremblay (Figure D-1a) employed relatively short lengths of the deck (280 mm), and in some cases, substantial and undesirable deformations were observed outside of the connection region. In addition, many of the welded specimens exhibited a high degree of residual-force capacity after failure due to the test setup. As shown in Figure D-1, the test setup was relatively short and allowed a portion of the deck to torque and resist deformation through bearing and bending even after weld detachment.

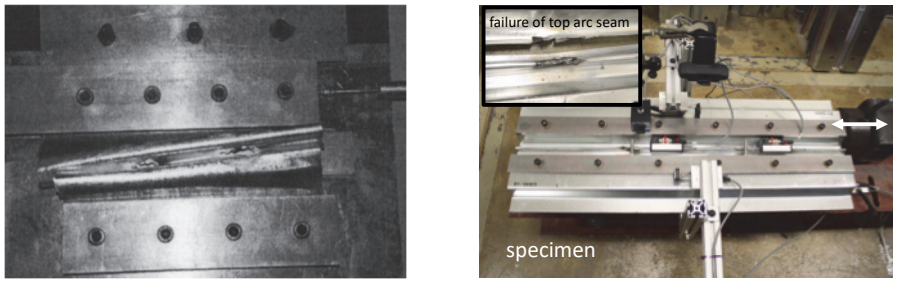


(a) Rogers and Tremblay (2003b) (b) Torabian and Schafer (2021)

Figure D-1 Comparison of testing for top-arc seam weld as employed for connector data: (a) as used in Koliou (2014) based on Rogers and Tremblay (2003b), and (b) as used herein based on Torabian and Schafer (2021).

Given the limitations of the available data, a comprehensive set of cyclic sidelap and structural deck connection testing was performed using the test setup of Figure D-1(b), as reported in Torabian and Schafer (2021) and consistent with AISI S905 (2017). Structural connectors play a critical role in the overall diaphragm performance of the deck system, as they provide the load path between the deck under shear and the substructure and perimeter framing. A deck with damaged sidelap connectors has greatly reduced shear strength, but a deck with a substantial loss of structural connectors has no load path for redistribution. The two primary structural connections in use are welds and mechanical fasteners, such as PAFs. Cyclic test results for these two common structural connectors are compared in Figure D-2. Individual welded deck connections provide high stiffness and strength but little-to-no ductility or post-peak residual-force capacity. PAF deck

connections provide more limited stiffness and strength but excellent ductility and post-peak residual-force capacity.

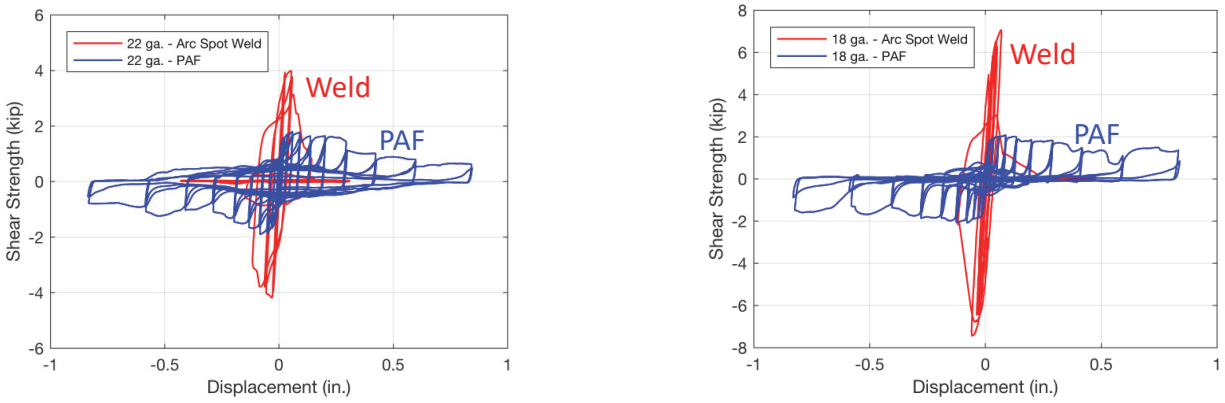


(a) 22 gage, 1.5-in. WR deck (b) 18 gage, 1.5-in. WR deck

Figure D-2 Performance of PAF vs. arc-spot-weld structural connectors (image credit: Schafer, 2019 based on data in Torabian and Schafer, 2021).

For each cyclic test in Torabian and Schafer (2021), the force-deformation response backbone was characterized and reported. Key parameters in this characterization include the initial stiffness ($k_i$), the peak strength ($P_{peak}$), the displacement after the peak where the strength drops to 80 percent of peak ($\delta_{pp80}$), the maximum displacement on the connector ($\delta_4$), and the residual force ($P_4$) available at this maximum displacement. Each of these quantities play a critical role in the dynamic response of the connection. For sidelap and structural connectors in 22-gage, 1.5-inch wide rib (WR) deck, the results are excerpted from Torabian and Schafer (2021) in Table D-1. Mechanically fastened connectors (screwed sidelap with PAF structural connections) have larger drift capacity, ductility, and residual force capacity.

**Table D-1 Average Connector Response for 22-gage, 1.5-inch WR Deck from Cyclic Testing (Torabian and Schafer, 2021)**

| Type | Connector | $k_i$ kip/in | $P_{peak}$ lb | $\delta_{pp80}$ in | $\delta_{pp80}/\delta_y$ ($\mu$)[1] | $\delta_4/\delta_y$ | $P_4/P_{peak}$ (c)[2] |
|---|---|---|---|---|---|---|---|
| Sidelap | Screw Sidelap | 58.2 | 787 | 0.303 | 23 | 41 | 0.25 |
| | Top Arc Seam Weld | 40.5 | 2428 | 0.126 | 2 | 5 | 0.03 |
| | PunchLok II crimp | 33.1 | 2046 | 0.264 | 4 | 11 | 0.18 |
| | Button Punch | 10.3 | 157 | 0.154 | 10 | 20 | 0.44 |
| Structural | Arc Spot Weld | 168.5 | 4002 | 0.063 | 3 | 5 | 0.02 |
| | Arc Seam Weld | 167.9 | 4676 | 0.075 | 3 | 6 | 0.18 |
| | PAF to 4.76 mm plate | 132.5 | 1798 | 0.232 | 17 | 42 | 0.40 |
| | PAF to 9.53 mm plate | 143.9 | 1798 | 0.228 | 18 | 39 | 0.43 |

(1) $\mu = \delta_{pp80}/\delta_y$ and $\delta_y = P_{peak}/k_i$

(2) Residual force at $\delta_4$ normalized by peak force $P_{peak}$

## D.3 Diaphragm Strength and Ductility

The strength and stiffness of bare steel deck diaphragms are commonly assessed by full-scale cantilever diaphragm tests using AISI S907-17 and its earlier incarnations. A comprehensive database of such testing was assembled by O'Brien et al. (2017) and summarized and assessed in Eatherton et al. (2020). The tests typically consist of three to five intermediate joists, decks attached to the joists and to the perimeter, and a perimeter structural frame that deforms in pure shear consistent with Figure D-3(a). This test database was assessed to develop a basic understanding of the ductility of steel-deck diaphragms and the sensitivity of that ductility to detailing and other considerations.

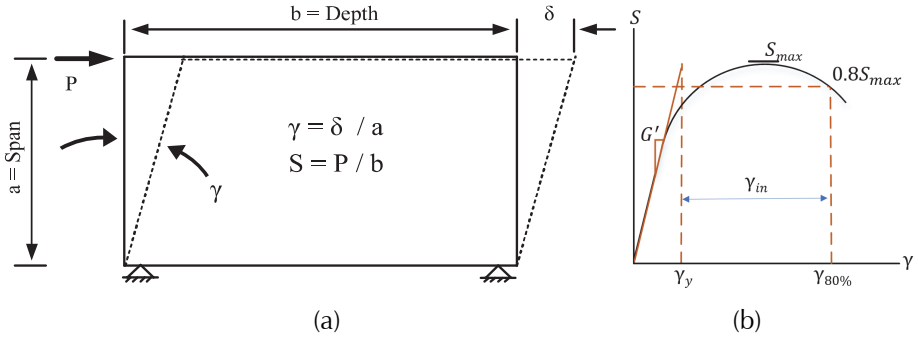


Figure D-3 Definition of: (a) shear angle ($\gamma$) and normalized load ($S$) in typical cantilever test, and (b) stiffness ($G'$), strength ($S_{max}$), and subassembly ductility ($\mu_{sub}$) evaluated from test results (figure credits: (a) O'Brien et al., 2017; (b) Schafer, 2019).

Although a significant number of monotonic cantilever diaphragm tests have been conducted, the number of cyclic (or dynamic) tests is relatively small. Nonetheless, it is possible to assess the basic ductility observed in these tests as summarized in Table D-2. The cyclic performance of mechanically fastened cantilever bare steel deck diaphragms is superior to welds. However, the ductility of mechanically fastened deck systems is not as great as the connection-level testing suggests, nor is the detriment in ductility for welded systems as substantial as the connection-level testing suggests. Nonetheless, the cyclic degradation for welded systems is substantial, and the performance of mechanically fastened systems is generally superior.

**Table D-2 Subsystem Ductility ($\mu$) from Cantilever Diaphragm Tests (Schafer, 2019)[1]**

| Connector | | Monotonic | | | Cyclic | | | |
|---|---|---|---|---|---|---|---|---|
| Structural | Sidelap | $n$ | $\mu_m$ | $\sigma_m$ | $n$ | $\mu_c$ | $\sigma_c$ | $\mu_c/\mu_m$ |
| PAF[2] | Screw | 19 | 3.6 | 1.8 | 19 | 2.9 | 1.0 | 80% |
| Weld[3] | (all connectors) | 28 | 3.2 | 1.1 | 8 | 1.7 | 0.5 | |
| | Button Punch | 8 | 2.6 | 0.4 | 6 | 1.5 | 0.4 | 60% |
| | Screw | 8 | 3.4 | 1.3 | 1 | 2.0 | - | 59% |
| | Top Arc Seam | 7 | 3.9 | 1.0 | 1 | 2.6 | - | 68% |
| | Arc Seam Weld | 5 | 3.2 | 1.3 | - | - | - | |

(1) n: number of samples; σ: standard deviation.

(2) Martin (2002) tests 29 and 35 included in O'Brien et al. (2017) statistics but removed here because testing was not conducted deep enough into post-peak to reliably establish 80 percent post-peak strength.

(3) Tremblay et al. (2004) developed a system using spot welds with washers for structural connections. This system has moderate ductility and little cyclic degradation. Related data are not included in this table under "weld" since the details are non-standard.

Eatherton et al. (2020) and Schafer (2019) provide additional analysis utilizing the database of O'Brien et al. (2017). Notable findings from these analyses include: (a) deck orientation has little-to-no observed impact on shear performance; (b) endlap details only have a minor effect on the ductility of bare steel deck diaphragms (slightly beneficial from a ductility and deformation standpoint for welded endlaps and slightly detrimental for fastened endlaps); (c) modest overstrength (1.2 × nominal strength) is observed in mechanically fastened bare steel deck diaphragms; and (d) welded diaphragms have little-to-no post-peak residual-force capacity, whereas systems with PAF mechanical fasteners have as much as 40 percent residual-force capacity even at shear angles as high as 5 percent.

Complete details of the considered specimens may be found in O'Brien et al. (2017). For convenience, the envelope of the tested specimens with mechanically fastened (PAF/Screw) connections are summarized here:

**Deck**

- 36-inch-wide B deck (B deck is a WR deck)
- $T$ = 0.0276 inch to 0.05748 inch (24 to 16 gage)
- $F_y$ = 36 to 56 ksi, $\varepsilon_u$ > 20 percent (one specimen – $F_u$ = 96ksi, $\varepsilon_u$ = 10 percent specimen)
- Cellular deck removed from dataset

**Structural Connectors**

- Hilti X-HSN 24, X-ENP-19L15, X-EDNK22-THQ12; Buildex BX12
- 3-inch, 6-inch, 9-inch, 12-inch spacing

**Sidelap connectors**

- #12
- 6-inch, 12-inch spacing

This envelope of tested specimens provided the initial categorization for specimens pre-qualified to provide ductile seismic performance as adopted in AISI S400-20 and discussed in Section D.5. The categorization was augmented by fastener testing as discussed in Section D.2 and committee input during the balloting process for changes to AISI S400-20.

## D.4 Archetype Building Assessment with 3D Models (Traditional Practice)

As detailed in Appendix C, a suite of RWFD building archetypes was developed for FEMA P-1026 (2015). These archetypes were evaluated using a 2D nonlinear model capturing essential nonlinearities as detailed in Koliou et al. (2016a) and Appendix C. The studied steel-deck archetypes, designed by traditional practice consistent with Chapter 3, failed a FEMA P695 assessment (Koliou et al., 2016a). The large building archetype, same dimensions as that examined in Chapter 3 and Chapter 5, was the worst performing of the studied steel deck roof archetypes and was thus selected for more detailed investigation.

The nature of the nonlinear shear response in wood sheathed and steel deck diaphragms is different. For steel-deck diaphragms, both the connector and the profile itself contribute substantially to the response, whereas for wood diaphragms the primary nonlinearity is from the connectors (i.e., the nail connections). In addition, steel-deck connectors include both deck-to-deck (sidelap) connections and deck-to-framing (structural) connectors. The impact of damage to sidelap connections is much more favorable to the overall shear-deformation response than damage to the structural connections.

As a result of these issues, a 3D modeling approach was developed to examine the seismic performance of steel deck roof diaphragms in RWFD buildings more closely. The large building archetype (200 feet × 400 feet in plan) was revisited and new roof designs, consistent with Chapter 3, completed for a mechanically fastened steel deck roof that employs PAF

structural connectors and screwed sidelaps, and for a welded steel deck roof that employs arc spot welds for the structural connectors and either top-arc seam welds or button punching for the sidelap connectors completed (details are provided in Schafer, 2019).

The 3D modeling strategy is depicted in Figure D-4. The connector tests described in Section D.2 were utilized to develop hysteretic models for all sidelap and structural connections. Based on the archetype design, cyclic cantilever diaphragm tests were simulated for each roof zone. The cantilever diaphragm simulation included material and geometric nonlinearity (yielding and buckling) and employed shell elements for the deck and experimentally determined nonlinear hysteretic models for the connectors. The resulting nonlinear shear response for the simulated test was characterized and then used in the roof of the 3D model of the full building via nonlinear truss elements—in an area equal to the joist spacing by the deck width. Thus, the shear behavior of the roof followed exactly that determined in the roof zone simulations. All walls, columns, joists, and joist girders were explicitly modeled in the building, as detailed in Schafer (2019).

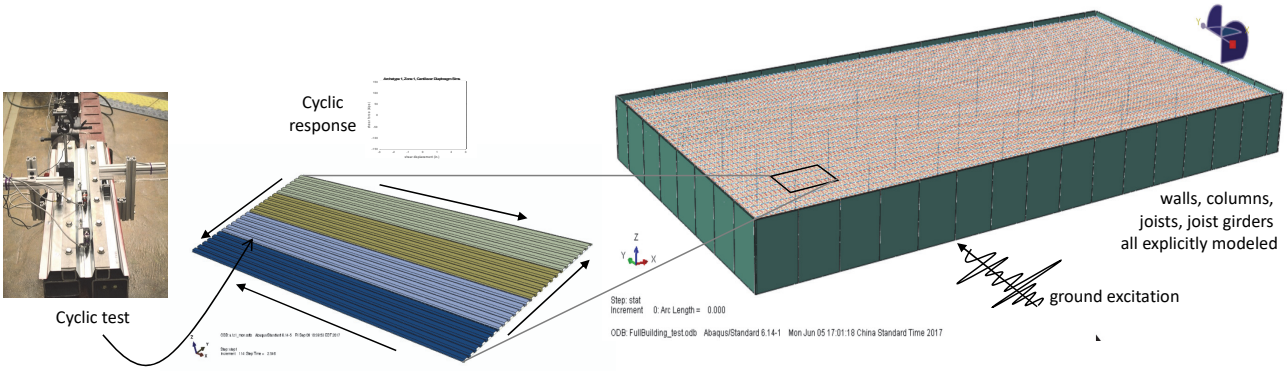


(a) connector tests (b) 3D roof submodel (c) 3D building model

Figure D-4 3D building model employed in simulations (figure credit: Schafer, 2019).

Example results from the cantilever diaphragm simulations for the roof zone closest to the edge of the building are provided in Figure D-5. Both roof systems (mechanically fastened and welded) have the same demands, and both have adequate capacity. However, the mechanically fastened system has modestly higher overstrength (capacity/demand is 1.3) due to the need to increase thickness to 18-gage deck to meet the demands, whereas the welded system was able to provide sufficient capacity with 20-gage deck (capacity/demand is 1.1). More importantly, the mechanically fastened system has substantial post-peak residual-force capacity, whereas the welded system has the minimal post-peak capacity, as shown in Figure D-5.

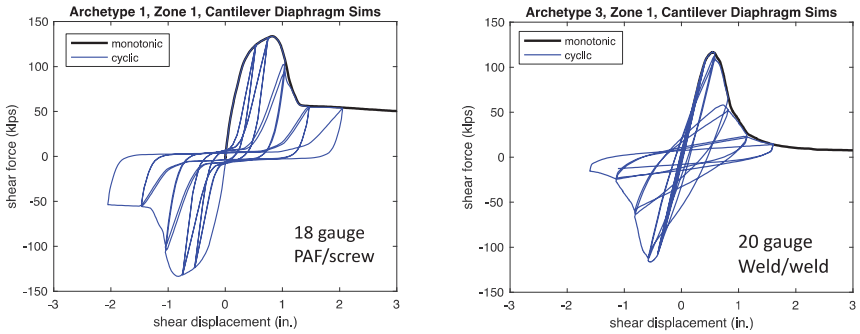


(a) mechanically fastened (b) welded

Figure D-5 Response in cantilever diaphragm simulation comparing the roof zone closest to the edge of the building for roof that is: (a) mechanically fastened, and (b) welded (figure credit: Schafer, 2019).

The FEMA P695 methodology was employed to assess the performance of the building models. Due to high computational overhead, instead of performing the incremental dynamic analysis (IDA) with the FEMA P695 Far-Field Ground Motion Ensemble, the FEMA P695 Appendix F criterion for collapse evaluation of individual buildings was utilized. In a typical P695 evaluation, the computed adjusted collapse margin ratio ($SSF \times CMR$) is compared with an acceptable collapse margin ratio at a given failure probability, such as 10 percent ($ACMR_{10\%}$), resulting in the probability of failure passing FEMA P695 written mathematically as:

$$SSF \times CMR > ACMR_{10\%} \tag{D-1}$$

Where the $CMR$ is traditionally established from IDA based on the median collapse ratio scaled to the MCE level:

$$SSF \times (S_{CT} / S_{MT}) > ACMR_{10\%} \tag{D-2}$$

If this is solved for $S_{CT}$ directly, then one can establish the scale factor at which 50 percent of the buildings must survive the earthquake suite to ensure an acceptable overall failure probability (e.g., $ACMR_{10\%}$) at MCE level:

$$S_{CT} > (ACMR_{10\%} / SSF)\, S_{MT} \tag{D-3}$$

First, in this procedure, the scale factor $S_{CT}$ consistent with $ACMR_{10\%}$ is established, then the forty-four nonlinear time history analyses are run at this level. If half of the buildings pass at this level, the building passes. Next, to establish the acceptable collapse margin ratio (target), the uncertainty in the earthquake records, design methods, test data used to support the analysis, and the model itself must be assessed. This process is summarized for the two studied systems in Table D-3. All assessments are in the weak (north-south) direction of the building. See Schafer (2019) for additional discussion of the response in the strong (east-west) direction.

**Table D-3 Summary of Vibration, Pushover, and Determination of Earthquake Scaling Factor for 3D Building Model with Bare steel deck Diaphragms**

| | Large (200′ × 400′) Building Archetype | | |
|---|---|---|---|
| | P695 Parameter | Mechanically Fastened Roof | Welded Roof |
| Model results (vibration & pushover) | $T^{1}$ | 0.59 | 0.70 |
| | $\Omega$ | 1.30 | 1.22 |
| | $\mu_T$ | 1.28 | 1.06 |
| | $SSF$ | 1.07 | 1.04 |
| P695 Uncertainty Parameters | $\beta_{RTR}$ | 0.23 | 0.21 |
| | $\beta_{DR}$ | 0.20 | 0.20 |
| | $\beta_{TD}$ | 0.20 | 0.20 |
| | $\beta_{MDL}$ | 0.20 | 0.20 |
| | $\beta_{TOT}$ | 0.41 | 0.40 |
| | $ACMR_{10\%}$ | 1.70 | 1.69 |
| | $S_{MT}$ | 1.50 | 1.50 |
| Evaluation | $S_{CT} > (ACMR_{10\%}/SSF)S_{MT}$ | 2.38 | 2.41 |

(1) may be compared with $T \sim 0.001L = 0.4$ seconds.

The typical collapse criteria employed in FEMA P695 analyses is story drift; however, this is a poor metric for failure in the roof. Therefore, the maximum shear angle in the roof was monitored. At the scale factor established in Table D-3, the Cumulative Distribution Function (CDF) (across the forty-four earthquakes) of the maximum recorded shear angle in the roof is provided for the two fastening systems in Figure D-6. The welded system experienced shear angles 1.6 to 2.0 times greater than the mechanically fastened steel deck roof. Further, the median (across the earthquakes) of the maximum shear angle on the welded roof system was 7.4 percent, which is far in excess of shear angles for which welded steel deck systems can provide successful response. However, the mechanically fastened system had a median shear angle of 4.5 percent, which is large but obtainable for mechanically fastened systems.

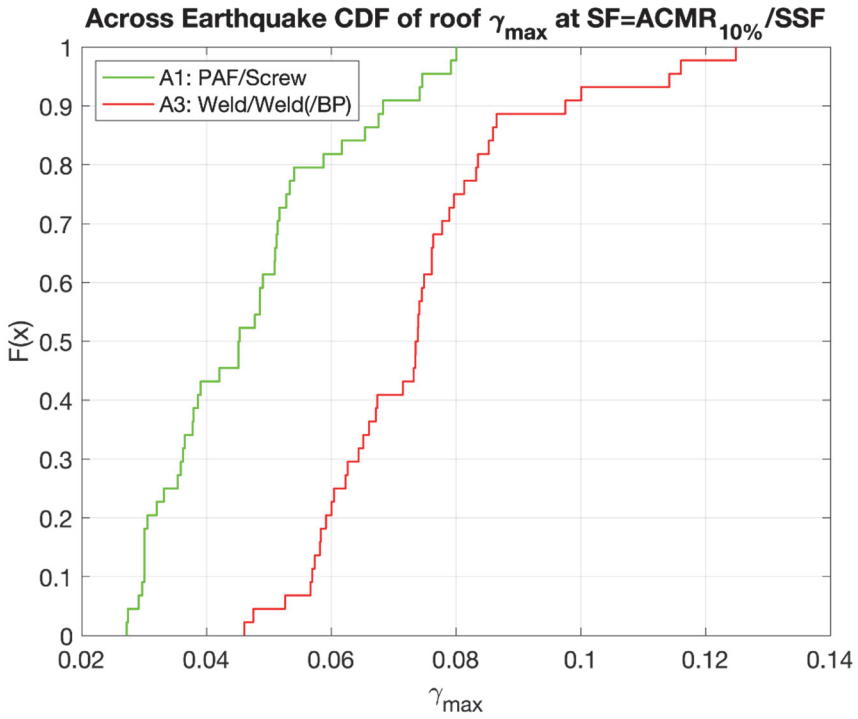


Figure D-6 CDF of peak diaphragm shear strain for large building archetype, mechanically fastened (designated as A1) and welded (designated as A3) across forty-four FEMA P695 earthquakes.

A more nuanced examination of the roof shear angle demand is provided in Figure D-7. In this figure, the diaphragm shear strain across the mid-width of the 400-foot-long roof, at the moment of maximum recorded shear strain demand, for each of the forty-four studied earthquakes is provided for the two studied large building roof archetypes. The locations where the diaphragm shear strain increases are at the roof-zone boundaries. The mechanically fastened system provides reduced shear strain demands and a more consistent response than the welded roof archetype.

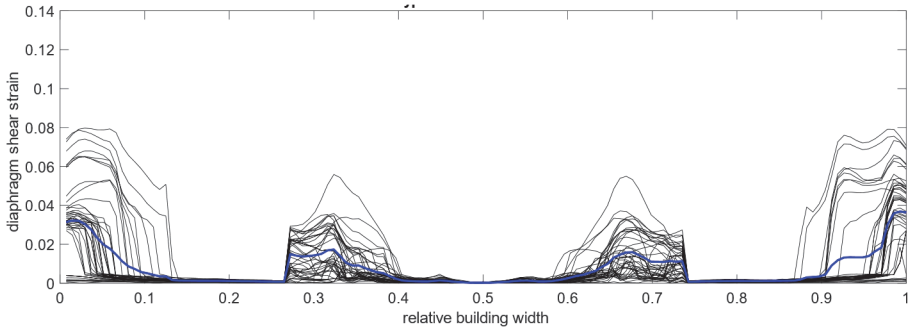


(a) mechanically fastened steel-deck roof

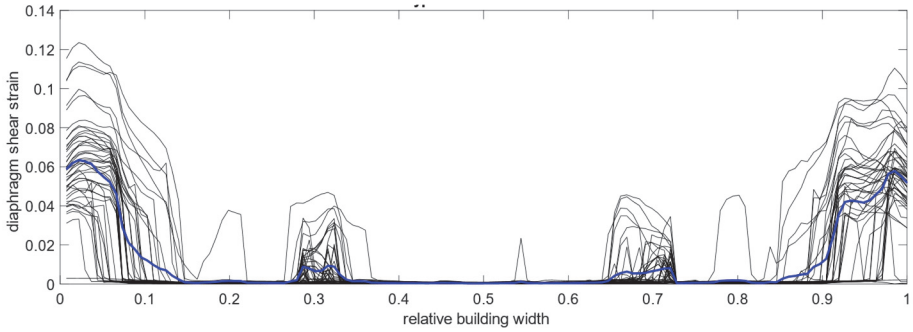


(b) welded steel-deck roof

Figure D-7 Trace of peak mid-width diaphragm shear strain across 400-foot roof width for forty-four earthquake records with average in blue for: (a) mechanically fastened roof, and (b) welded roof.

Selecting 5 percent as the maximum shear angle for the median demand, per Figure D-6, one concludes that traditionally designed, mechanically fastened roof systems are acceptable per FEMA P695; however, welded systems are likely not acceptable. This provides some nuance to the conclusions of Koliou et al. (2016a) regarding the performance of traditionally designed steel-deck diaphragms.

## D.5 Special-Seismic-Detailing Requirements

Based in part on the findings summarized in this appendix, AISI S400-20 adopted provisions for special seismic detailing of bare steel deck diaphragms. These provisions are triggered by ASCE/SEI 7-22 when utilizing the alternative RWFD procedure and $R_{diaph} = 4.5$. The seismic detailing provisions of AISI S400-20 Section F3.5 provide both prescriptive and performance-based requirements.

The prescriptive requirements, found in AISI S400-20 Section F3.5.1, define the deck panel type, thickness, material, type of connector, and attachment and spacing parameters for meeting special seismic detailing. The criteria are based on the tested cantilever diaphragms as summarized in Section D.3 and the fastener testing summarized in Section D.2. Specifically, AISI S400-20 Section F3.5.1 requires:

- The steel deck panel type shall be 36 inch-wide (914 mm), 1.5 inch-deep (38.1 mm) wide rib, 6 inch-pitch (152.4 mm) deck.
- The steel-deck base steel thickness shall be greater than or equal to 0.0295 inches (0.749 mm) and less than or equal to 0.0598 inches (1.52 mm).
- The steel deck material shall conform to AISI S100 Section A3.1.1.
- The steel deck structural connection between the steel deck and the supporting steel member, with a minimum thickness of 1/8 inch (3.18 mm), shall be limited to mechanical connectors qualified in accordance with Section F3.5.1.1. This section provides performance criteria, and testing reported in Torabian and Schafer (2021) indicates PAFs that can meet these requirements.
- The steel deck structural connection perpendicular to the steel deck ribs shall be no less than a 36/4 pattern (12 inches, or 305 mm, on center) and no more than a 36/9 pattern (6 inches, or 152 mm, on center) with double fasteners in the last panel rib.
- The steel deck structural connection parallel to the steel deck ribs shall be spaced no less than 3 inches (76.2 mm) and no more than 24 inches (610 mm) and shall not be greater than the sidelap connection spacing.
- The sidelap connection between steel deck shall be limited to #10, #12, or #14 screws sized such that shear in the screws is not the controlling limit state or connectors qualified in accordance with Section F3.5.1.2.
- The sidelap connection shall be spaced no less than 6 inches (152 mm) and no more than 24 inches (610 mm).

The alternative, performance-based requirements, defined in AISI S400-20 Section F3.5.2, allow either cyclic cantilever diaphragm tests or simulations of cyclic cantilever diaphragm tests to establish the required ductility, deformation capacity, and residual-force capacity in the diaphragm. Performance targets are based on the response of mechanically fastened systems shown to provide adequate seismic behavior.

## D.6 Resolution of FEMA P-1026 (2015) Concerns

FEMA P-1026 (2015) did not extend the use of the alternative RWFD design philosophy to steel deck diaphragms despite modeling results that indicated its successful performance (Koliou, 2014). This decision was due to issues that are listed in Table D-4. Resolution of these issues, along with the additional research explained in this appendix, led to the adoption of

provisions for bare steel deck diaphragms in FEMA P-1026 (2021) and ASCE/SEI 7-22.

**Table D-4 Resolution of FEMA P-1026 (2015) Comments on Application to Bare Steel Deck Roof Diaphragms in RWFD Buildings**

| FEMA P-1026 (2015) reservation | Resolution |
|---|---|
| (1) Tests results of a large-scale diaphragm showed significantly less distribution of yielding than the analyses show when loaded parallel to deck edges (Massarelli et al., 2012). | Broader evaluation of testing and 3D building modeling mitigated this concern. However, it was found that mechanically fastened deck systems were more successful at distributing inelasticity in the roof, and this became part of the basis for requiring special seismic detailing for bare steel deck diaphragms. |
| (2) Steel-deck diaphragms have not been envisioned to be yielding elements, and as such design strengths are based on monotonic tests. | Bare steel deck diaphragms do have sufficient inelasticity derived from the deck profile, deck-to-deck, and deck-to-framing connections. Cyclic fastener testing, cantilever diaphragm testing, and building models demonstrated successful performance so long as details for special seismic performance were maintained. |
| (3) Data for reverse cyclically loaded connections are sparse and missing for many commonly used deck gages. | New testing was conducted as summarized in Schafer (2019) and Torabian and Schafer (2021). |
| (4) The post-yield stiffness of connectors is positive for only a small deformation, 1 mm to 2 mm. | This observation is important, but only true for welded connectors. This is part of the reason mechanically fastened and welded systems have been separated in the implementation. |
| (5) Few reverse cyclically loaded diaphragm tests have been performed, but FEMA P695 requires comprehensive test data. | A broader set of existing cyclically loaded diaphragm tests were collated in O'Brien et al. (2017) and Eatherton et al. (2020) and provided the basis for evaluation. |
| (6) Many diaphragms in high-seismic regions are designed using proprietary sidelaps for which no test data were available to include in the study. | Torabian and Schafer (2021) includes testing on proprietary sidelaps, and the special seismic detailing requirements in AISI S400-20 have a performance-based path that such sidelaps can utilize to qualify for special seismic detailing as appropriate. |
| (7) End lap connectors that are expected to resist diaphragm shears in a ductile manner, while at the same time resisting out-of-plane wall anchorage forces in an elastic manner, must be further studied and understood. This issue will likely require design limitations that have yet to be identified | Cantilever tests on endlaps do not indicate a unique concern, though it is recognized that particularly for welded endlaps the multi-ply configuration requires significant care. The issue of wall anchorage forces may deserve further study; however, the systems that distribute inelasticity in the diaphragm have the most uniform prediction for anchorage forces. Thus, the special seismic detailing is expected to mitigate this issue. |

## D.7 Re-Assessment of Koliou (2014) 2D RWFD Model for Bare steel deck Diaphragms

In Koliou (2014), the FEMA P-1026 (2015) method (separate $T$, two-stage analysis, $R_{diaph} = 4.5$, amplified shear by 1.5 in the $0.1L$ end zones) was also applied to steel deck diaphragms. Time history analyses indicated that the revised procedure would be successful in better distributing inelasticity in the diaphragm and the method passed the FEMA P695 criteria. The reservations detailed in Section D.6 precluded the steel deck results from being utilized in 2015; however, with the more recent work described in this appendix, the bulk of Koliou's analysis results may now be utilized.

An important proviso in utilizing this past work for steel decks is that the results for welded steel deck need to be removed. As detailed in Schafer (2019) and discussed in Section D.2, in several cases, the hysteretic characterizations in the past work are overly optimistic due to details of the testing. This is especially true for welded sidelap connections using top arc seam welds and welded endlap structural connections based on Rogers and Tremblay (2003b) and Guenfoud et al. (2009) as utilized in Koliou (2014). In these cases, the connector models included large artificial residual-force capacities (and potential for load redistribution) that were not realized in other testing and are not expected to be present for a weld in the post-peak damage state.

Including only mechanically fastened systems, Koliou (2014) summary results are provided for the SDC $D_{max}$ building archetypes in Figure D-8 and may be compared with those for wood sheathed roofs in Table C-8. Both individually and as performance groups, all of the buildings pass FEMA P695, thus providing final justification for the extension of FEMA P-1026 (2015) to bare steel deck diaphragm systems that meet special seismic detailing requirements.

| Archetype ID | Design configuration | | | | Collapse margin parameters | | | | Acceptance check | |
|---|---|---|---|---|---|---|---|---|---|---|
| | Building size | Diaphragm aspect ratio | Diaphragm construction | Seismic SDC | CMR | $\mu_T$ | SSF | ACMR | Accept. ACMR | Pass/Fail |
| **Performance Group No. PG-6N (Steel, Large Building, Screws as sidelap Connectors, New Design)** | | | | | | | | | | |
| HSL_21_P_S_RD4.5-1.5_01 | Large | 2:1 | Steel | $D_{max}$ | 1.47 | 8.38 | 1.37 | 2.02 | 1.73 | Pass |
| HSL_12_P_S_RD4.5-1.5_01 | Large | 1:2 | Steel | $D_{max}$ | 2.56 | 8.15 | 1.36 | 3.48 | 1.73 | Pass |
| HSL_11_P_S_RD4.5-1.5_01 | Large | 1:1 | Steel | $D_{max}$ | 2.12 | 8.51 | 1.37 | 2.90 | 1.73 | Pass |
| HSL_11_S_S_RD4.5-1.5_01 | Large | 1:1 | Steel | $D_{max}$ | 1.96 | 8.11 | 1.36 | 2.67 | 1.73 | Pass |
| **Mean of Performance Group:** | | | | | **2.03** | **8.29** | **1.37** | **2.77** | **2.30** | **Pass** |
| **Performance Group No. PG-8N (Steel, Small Building, Screws as sidelap Connectors, New Design)** | | | | | | | | | | |
| HSS_11_P_S_RD4.5-1.5_01 | Small | 1:1 | Steel | $D_{max}$ | 1.98 | 8.17 | 1.33 | 2.63 | 1.73 | Pass |
| HSS_11_S_S_RD4.5-1.5_01 | Small | 1:1 | Steel | $D_{max}$ | 1.72 | 7.99 | 1.33 | 2.29 | 1.73 | Pass |
| HSS_21_P_S_RD4.5-1.5_01 | Small | 2:1 | Steel | $D_{max}$ | 1.59 | 8.09 | 1.33 | 2.11 | 1.73 | Pass |
| HSS_12_P_S_RD4.5-1.5_01 | Small | 1:2 | Steel | $D_{max}$ | 2.01 | 8.14 | 1.33 | 2.67 | 1.73 | Pass |
| HSS_21_S_S_RD4.5-1.5_01 | Small | 2:1 | Steel | $D_{max}$ | 1.63 | 7.96 | 1.33 | 2.17 | 1.73 | Pass |
| HSS_12_S_S_RD4.5-1.5_01 | Small | 1:2 | Steel | $D_{max}$ | 1.92 | 7.98 | 1.33 | 2.55 | 1.73 | Pass |
| **Mean of Performance Group:** | | | | | **1.81** | **8.06** | **1.33** | **2.40** | **2.30** | **Pass** |

Figure D-8 Performance of FEMA P-1026 (2015) mechanically fastened steel roof archetypes by design performance group for SDC $D_{max}$ cases (figure credit: Koliou, 2014).

For steel deck roofs that do not meet the special-seismic-detailing requirements, it should still be permitted to use the overall FEMA P-1026 design philosophy: separate *T* for roof, separate forces from the design spectra for roof, and carry roof forces down to walls (two-stage analysis). But the large inelastic $R_{diaph}$ force reductions should not be allowed, and instead, the roof should be designed at elastic or near elastic levels.

## D.8 Summary of Updated Design Procedure for Bare Steel Deck Roof Diaphragms and Related Future Work

With the addition of the special seismic detailing, AISI S400-20 provides a clear path to achieve inelastic response from steel deck diaphragms. The RWFD design method of FEMA P-1026 implemented in ASCE/SEI 7-22 Section 12.10.4 utilizes this feature through $R_{diaph,}$ as does the alternative diaphragm design method in ASCE/SEI 7-22 Section 12.10.3 through $R_s$. Beyond the special-seismic-detailing requirements, the design method implemented for bare steel deck diaphragms parallels that of wood diaphragms.

The estimated period for steel deck roof diaphragms (Equation 4-3) may deserve additional study. The limited 3D building models completed here exhibited longer periods than Equation 4-3 (see Table D-3). Accurate period estimation can be important for the economy of the method, as long-period diaphragms see reduced demand forces.

The prescriptive special seismic detailing of AISI S400-20 provides the easiest path for designers. Expanding the solutions available should be a priority, particularly with respect to different deck profiles, material yield stress, and sidelap connection solutions. Given the variety of diaphragm ductility that is possible with steel deck systems, it could be desirable to create ordinary, intermediate, and special-seismic-detailing requirements and commensurate $R_{diaph}$ factors to go with these systems. In particular, welded systems, which are currently forced to be designed as near elastic, do exhibit limited ductility, and appropriate $R_{diaph}$ factors could be developed. Additional commentary on future work, related more broadly to the alternative design procedure and not bare steel deck specifically, is provided in Chapter 8.

# Acronyms

| | |
|---|---|
| ACI | American Concrete Institute |
| ACMR | adjusted collapse margin ratio |
| ASCE | American Society of Civil Engineers |
| ASD | allowable stress design |
| AWC | American Wood Council |
| BDR | building drift ratio |
| CMR | collapse margin ratio |
| CUREE | Consortium of Universities for Research in Earthquake Engineering |
| DDR | diaphragm drift ratio |
| DE | design earthquake |
| DF/L | Douglas-Fir/Larch |
| DM | damage measure |
| EERI | Earthquake Engineering Research Institute |
| ELF | equivalent lateral force |
| FEMA | Federal Emergency Management Agency |
| g | gravity |
| IBC | International Building Code |
| ICBO | International Conference of Building Officials |
| ICC | International Code Council |
| IDA | incremental dynamic analysis |
| IM | intensity measure |
| MCE | maximum considered earthquake |

| | |
|---|---|
| NEHRP | National Earthquake Hazards Reduction Program |
| NIST | National Institute of Standards and Technology |
| NLRHA | Nonlinear response history analysis |
| NOAA | National Oceanic and Atmospheric Administration |
| NRC | National Research Council of National Academy of Sciences |
| o.c. | on center |
| OSB | oriented-strand board |
| PCF | pounds per cubic foot |
| PEER | Pacific Earthquake Engineering Research Center |
| PG | performance group |
| PGA | peak ground acceleration |
| plf | pounds per linear foot |
| PSI | pounds per square inch |
| P-delta | axial load-deflection |
| RWFD | rigid wall-flexible diaphragm |
| SAWS | Seismic Analysis of Woodframe Structures |
| SDC | seismic design category |
| SDI | Steel Deck Institute |
| SDPWS | Special Design Provisions for Wind and Seismic |
| SEAOC | Structural Engineers Association of California |
| SEAONC | Structural Engineers Association of Northern California |
| sec | seconds |
| SFRS | seismic-force-resisting system |
| SRSS | square root sum of the squares |
| SSF | spectral shape factor |
| UBC | Uniform Building Code |

WDR wall drift ratio

WR Deck wide rib deck

# References


ACI, 2015, *Design Guide for Tilt-Up Concrete Panels,* ACI 551.2R-15, American Concrete Institute, Farmington Hills, Michigan.

ACI, 2019, *Building Code Requirements for Structural Concrete and Commentary,* ACI 318-19, American Concrete Institute, Farmington Hills, Michigan.

AISI, 2017, *Test Standard for Determining the Strength and Deformation Characteristics of Cold-Formed Steel Connections*, AISI S905-17, American Iron and Steel Institute, Washington, D.C.

AISI, 2018, *Test Standard for Determining the Strength and Stiffness of Cold-Formed Steel Diaphragms by the Cantilver Test Method*, AISI S907-17, American Iron and Steel Institute, Washington, D.C.

AISI, 2020a, *North American Standard for the Design of Profiled Steel Diaphragm Panels*, AISI S310-20, American Iron and Steel Institute, Washington, D.C.

AISI, 2020b, *North American Standard for Seismic Design of Cold-Formed Steel Structural Systems*, AISI S400-20, American Iron and Steel Institute, Washington, D.C.

ASCE, 2010, *Minimum Design Loads for Buildings and Other Structures*, ASCE/SEI 7-10, American Society of Civil Engineers, Reston, Virginia.

ASCE, 2016, *Minimum Design Loads and Associated Criteria for Buildings and Other Structures*, ASCE/SEI 7-16, American Society of Civil Engineers, Reston, Virginia.

ASCE, 2017, *Seismic Evaluation and Retrofit of Existing Buildings*, ASCE/SEI 41-17, American Society of Civil Engineers, Reston, Virginia.

ASCE, 2022, *Minimum Design Loads and Associated Criteria for Buildings and Other Structures*, ASCE/SEI 7-22, American Society of Civil Engineers, Reston, Virginia. At the time of preparing the final manuscript for this report, the public comment period for ASCE/SEI

7-22 was completed and the document was under final editorial review.

AWC, 2021, *Special Design Provisions for Wind and Seismic,* ANSI/AWS SDPWS-2021, American Wood Council, Leesburg, Virginia.

Bouwkamp, J.G., Hamburger, R.O., Gillengerten, J.D., 1994, *Degradation of Plywood Roof Diaphragms Under Multiple Earthquake Loading*, Data Utilization Report CSMIP/94-02, California Strong Motion Instrumentation Program, California Department of Conservation, Division of Mines and Geology, Sacramento, California.

Brandow, G.E., 2010, *SEI Case Study: Large Retail Building, Yucca Valley, California*, Structural Engineering Institute of the American Society of Civil Engineers, Reston, Virginia.

Carr, J., 2007, RUAUMOKO, University of Canterbury, Christchurch, New Zealand.

Celebi, M., Bongiovanni, G., Safak, E., Brady, A.G., 1989, "Seismic response of a large-span roof diaphragm," *Earthquake Spectra*, Vol. 5, No. 2.

Christovasilis, I. P., Filiatrault, A., and Wanitkorkul, A., 2009, *Seismic Testing of a Full-Scale Two-Story Light-Frame Wood Building: NEESWood Benchmark Test*, Technical Report MCEER-09-0005, Multidisciplinary Center for Earthquake Engineering Research, University at Buffalo, Buffalo, New York.

Coyne, T., 2007, *NEESWood: Framing to Sheathing Connection Tests*, unpublished REU report under faculty advisor Dr. Andre Filiatrault, The State University of New York at Buffalo, Buffalo, New York.

Eatherton, M.R., O'Brien, P.E., Easterling, W.S., 2020, "Examination of ductility and seismic diaphragm design force-reduction factors for steel deck and composite diaphragms," *Journal of Structural Engineering*, Vol. 146, No. 11.

EERI, 1985, "The Morgan Hill Earthquake of April 24, 1984," *Earthquake Spectra*, Vol. 1, No. 3.

FEMA, 2009, *Quantification of Building Seismic Performance Factors*, FEMA P695, prepared by the Applied Technology Council for the Federal Emergency Management Agency, Washington, D.C.

FEMA, 2015, *Seismic Design of Rigid Wall-Flexible Diaphragm Buildings: An Alternate Procedure*, FEMA P-1026, prepared by the Building

Seismic Safety Council of the National Institute of Building Sciences for the Federal Emergency Management Agency, Washington, D.C.

FEMA, 2020a, *NEHRP Recommended Seismic Provisions for New Buildings and Other Structures*, FEMA P-2082, Federal Emergency Management Agency, Washington, D.C.

FEMA, 2020b, *Short-Period Building Collapse Performance and Recommendations for Improving Seismic Design, Volume 1 – Overarching Findings, Conclusions, and Recommendations*, FEMA P-2139-1, prepared by the Applied Technology Council for the Federal Emergency Management Agency, Washington, D.C.

Folz, B., and Filiatrault, A., 2001, "Cyclic analysis of wood shear walls," *Journal of Structural Engineering,* Vol. 127, No. 4, pp. 433-441.

Fonseca, F. S., Rose, S. K., and Campbell, S. H., 2002, *Nail, Wood Screw, and Staple Fastener Connections*, CUREE Publication No. W-16, Consortium of Universities for Research in Earthquake Engineering, Richmond, California.

Freeman, S.A., Gilmartin, U.A., and Searer, G.R., 1995, "Tilt-up construction: proposed seismic design procedures developed from strong motion research," *Proceedings of the NEHRP Conference and Workshop on Research on the Northridge, California Earthquake of January 17, 1994,* Consortium of Universities for Research in Earthquake Engineering, Richmond, California.

Freeman, S., Searer, G., and Gilmartin, U., 2002, "Proposed seismic design provisions for rigid shear wall / flexible diaphragm structures," *Proceedings of the Seventh U.S. National Conference on Earthquake Engineering* (7NCEE), Earthquake Engineering Research Institute, Oakland, California.

Guenfoud, N., Tremblay, R., and Rogers, C.A., 2010, "Shear capacity and tension capacity of arc-spot welds for multi-overlap deck panels," *Journal of Constructional Steel Research*, Vol. 66, No. 8-9, pp. 1018-1029.

Hamburger, R.O., McCormick, D.L., and Hom, S., 1988, "The Whittier Narrow earthquake of October 1, 1987—performance of tilt-up buildings," *Earthquake Spectra*, Vol. 4, No. 2, pp. 219-254.

ICBO, 1988, *Uniform Building Code*, International Conference of Building Officials, Whittier, California.

ICBO, 1997, *Uniform Building Code*, International Conference of Building Officials, Whittier, California.

ICC, 2018, *International Building Code*, International Code Council, Inc., Country Club Hills, Illinois.

ICC, 2021, *International Existing Building Code*, International Code Council, Inc., Country Club Hills, Illinois.

Koliou, M., 2014, *Seismic Analysis and Design of Rigid Wall-Flexible Roof Diaphragm Structures*, Ph.D. Dissertation, The State University of New York at Buffalo, Buffalo, New York.

Koliou, M. and Filiatrault, A., 2017, "Development of wood and steel diaphragm hysteretic connector database for performance-based earthquake engineering," *Bulletin of Earthquake Engineering*, Vol. 15, pp. 4319-4347.

Koliou, M., Filiatrault, A., Kelly, D.J., and Lawson, J., 2016a, "Distributed yielding concept for improved seismic collapse performance of rigid wall-flexible diaphragm buildings," *Journal of Structural Engineering*, Vol. 142, No. 2.

Koliou, M., Filiatrault, A., Kelly, D.J., and Lawson, J., 2016b, "Buildings with rigid walls and flexible roof diaphragms I: Evaluation of current U. S. seismic provisions," *Journal of Structural Engineering*, Vol. 142, No. 3.

Koliou, M., Filiatrault, A., Kelly, D.J., and Lawson, J., 2016c, "Buildings with rigid walls and flexible roof diaphragms II: Evaluation of a new seismic design approach based on distributed diaphragm yielding," *Journal of Structural Engineering*, Vol. 142, No. 3.

Koliou, M., van de Lindt, J.W., and Filiatrault, A., 2016d, "Evaluation of an alternative seismic design approach for rigid wall flexible wood roof diaphragm buildings through probabilistic loss estimation and disaggregation," *Engineering Structures*, Vol. 127, pp. 31-39.

Koliou, M., Lawson, J., Filiatrault, A., and Kelly, D.J., 2017, "Evaluation of out-of-plane wall anchorage force provisions in buildings with rigid walls and flexible roof diaphragms," *Earthquake Spectra*, Vol. 33, No. 1, pp. 1-23.

Kong, H., Eatherton, M., and Schafer, B., 2019, "Design of fixed-base hollow structural section columns subject to large seismic drift," *Proceedings of the Annual Stability Conference*, Structural Stability Research Council, St. Louis, Missouri.

Lawson, J., 2013, *Seismic Design of Timber Panelized Roof Structures*, WoodWorks, Wood Products Council, Washington, D.C.

Lawson, J., 2019, "Improving the accuracy of wood diaphragm deflection computations and its impact on ASCE 41 pseudo-lateral force estimates," *SEAOC 2019 Convention Proceedings*, Structural Engineers Association of California, Squaw Valley, California.

Lawson J., Koliou, M., Filiatrault, A., and Kelly, D.J., 2018, "The Evaluation of current wall-to-roof anchorage force provisions for single-story concrete and masonry buildings with lightweight flexible diaphragms," *SEAOC 2018 Convention Proceedings*, Structural Engineers Association of California, Palm Desert, California.

Lawson, J., and Koliou, M., 2020, "Evaluating second-order effects in rigid wall-flexible roof diaphragm buildings," *Earthquake Spectra*, Vol. 36, No. 4.

Massarelli, R., Franquet, J.-E., Shrestha, K., Tremblay, R., and Rogers, C., 2012, "Seismic testing and retrofit of steel deck roof diaphragms for building structures," *Thin-Walled Structures*, Vol. 61, pp. 239-247.

MATLAB, 2013, version 8.10.1.604, The MathWorks Inc, Natick, Massachusetts.

Mays, T. and Steinbicker, J., 2013, *Engineering Tilt-Up*, Tilt-Up Concrete Association, Mount Vernon, Iowa.

Newmark, N.M., and Hall, W.J., 1973, "Seismic design criteria for nuclear reactor facilities," *Building Practices for Disaster Mitigation,* Report No. 46, National Bureau of Standards, U.S. Department of Commerce, Washington, D.C.

NIST, 2004, *Voluntary Product Standard PS 2-04*, *Performance Standard for Wood-Based Structural-Use Panels*, National Institute of Standards and Technology, Gaithersburg, Maryland.

NRC, 1973, *The Great Alaska Earthquake of 1964*, National Research Council: Committee on the Alaska Earthquake, National Academy of Sciences, Washington, D.C.

O'Brien, P., Eatherton, M.R., Easterling, W.S., Schafer, B.W., Hajjar, J.F., 2017, *Steel Deck Diaphragm Test Database v1.0*, CFSRC R-2017-03, Cold-Formed Steel Research Consortium Report Series, Johns Hopkins University Library, John Hopkins University, Baltimore, Maryland. (jhir.library.jhu.edu/handle/1774.2/40634)

Olund, O., 2009, *Analytical Study to Investigate the Seismic Performance of Single Story Tilt-Up Structures*, Master's Thesis, University of British Columbia, Vancouver, Canada.

PEER, 2004, *Evaluation and Application of Concrete Tilt-up Assessment Methodologies*, PEER Lifelines Task 509, Degenkolb Engineers, San Francisco, California.

Phipps, M., and Jirsa, J., 1990, "Performance of industrial facilities and implications for design of new structures and upgrading of existing hazardous buildings," *Proceedings: Putting the Pieces Together – The Loma Prieta Earthquake One Year Later,* Bay Area Regional Earthquake Preparedness Project (BAREPP), San Francisco, California.

Rogers, C. A., and Tremblay, R., 2003a, "Inelastic seismic response of side lap fasteners for steel roof deck diaphragms," *Journal of Structural Engineering,* Vol. 129, No. 12, pp. 1637-1646.

Rogers, C.A., and Tremblay, R., 2003b, "Inelastic seismic response of frame fasteners for steel roof deck diaphragms," *Journal of Structural Engineering,* Vol. 129, No. 12.

Schafer, B.W., 2019, *Research on the Seismic Performance of Rigid Wall Flexible Diaphragm Buildings with Bare Steel Deck Diaphragms*, CFSRC R-2019-02, Cold-Formed Steel Research Consortium Report Series, Johns Hopkins University Library, John Hopkins University, Baltimore, Maryland. (https://jscholarship.library.jhu.edu/handle/1774.2/60360)

SDI, 2015, *Diaphragm Design Manual*, *4th Edition*, DDM04, Steel Deck Institute, Glenshaw, Pennsylvania.

SEAOC, 1999, *Recommended Lateral Force Requirements and Commentary, 7th Edition,* Structural Engineers Association of California, Sacramento, California.

SEAONC, 2001, *Guidelines for Seismic Evaluation and Rehabilitation of Tilt-Up Buildings and Other Rigid Wall/Flexible Diaphragm Structures,* Structural Engineers Association of Northern California, San Francisco, California.

Shipp, J., 2010, "Case studies – documentation to support a separate structural engineering practice act," *Structures Congress 2010*, American Society of Civil Engineers, Reston, Virginia.

SSC, 1995, *Northridge Earthquake: Turning Loss to Gain*, SSC Report No. 95-01, Seismic Safety Commission, State of California, Sacramento, California.

Stewart, W.G., 1987, *The Seismic Design of Plywood Sheathed Shear Walls*, Ph.D. Dissertation, University of Canterbury, Christchurch, New Zealand.

TMS, 2016, *Building Code Requirements for Masonry Structures*, The Masonry Society, Longmont, Colorado.

Torabian, S., and Schafer, B.W., 2021, "Cyclic experiments on sidelap and structural connectors in steel deck diaphragms," *Journal of Structural Engineering*, Vol. 147, No. 4.

Tremblay, R., Martin, E., Yang, W., and Rogers, C.A., 2004, "Analysis, testing and design of steel roof deck diaphragms for ductile earthquake resistance," *Journal of Earthquake Engineering*, Vol. 8, No. 5, pp. 775- 816.

USGS, 1971, *The San Fernando, California, Earthquake of February 9, 1971*, Geological Survey Professional Paper 733, U.S. Geological Survey and the National Oceanic and Atmospheric Administration, Washington, D.C.

Vamvatsikos, D., and Cornell, A.C., 2002, "Incremental dynamic analysis," *Earthquake Engineering and Structural Dynamics,* Vol. 31, No. 3, pp. 491-514.

Wallace, J.W., Stewart, J.P., and Whittaker, A.S., 1999, *Building Vulnerability Studies: Modeling and Evaluation of Tilt-up and Steel Reinforced Concrete Buildings*, PEER Report 1999/13, Pacific Earthquake Engineering Research Center, University of California at Berkeley, Berkeley, California.

Wilson, A., Quenneville, P., and Ingham, J., 2013, "Natural period and seismic idealization of flexible timber diaphragms," *Earthquake Spectra*, Vol. 29, No. 3.

# Project Participants

## SECOND EDITION PROJECT TEAM

### Federal Emergency Management Agency

Mai (Mike) Tong (Project Officer)
Federal Emergency Management Agency
400 C Street, SW
Washington, D.C. 20472

William T. Holmes (Technical Advisor)
Federal Emergency Management Agency
2600 La Cuesta Avenue,
Oakland, California 94611

### Applied Technology Council

Jon A. Heintz (Project Executive)
Applied Technology Council
201 Redwood Shores Parkway, Suite 240
Redwood City, California 94065

Justin Moresco (Project Manager)
Applied Technology Council
201 Redwood Shores Parkway, Suite 240
Redwood City, California 94065

### Project Technical Committee

Dominic J. Kelly (Project Technical Director)
Simpson Gumpertz & Heger
41 Seyon Street
Building 1, Suite 500
Waltham, Massachusetts 02453

Benjamin Schafer
Johns Hopkins University
105 Latrobe Hall
3400 North Charlies Street
Baltimore, Maryland 21218

Kelly Cobeen
Wiss, Janney, Elstner Associates, Inc.
2000 Powell Street, Suite 1650
Emeryville, California 94608

Robert Tremblay
Polytechnique Montreal
2500, chemin de Polytechnique
Montreal, Quebec H3T 1J4

John Lawson
California Polytechnic State University
1 Grand Avenue
Building 21, Office 110A
San Luis Obispo, California 93407

### Project Review Panel

Ryan Kersting (ATC Board Contact)
Buehler
600 Q Street, Suite 200
Sacramento, California 95811

Phil Line
American Wood Council
222 Catoctin Circle SE, Suite 201
Leesburg, Virginia 20175

Bonnie Manley
American Iron and Steel Institute
41 Tucker Road
Norfolk, Massachusetts 02081

David McCormick
Simpson Gumpertz & Heger
1999 Harrison Street, Suite 2400
Oakland, California 94612

Trent Nagele
VLMK Engineering + Design
3933 S Kelly Avenue
Portland, Oregon 97239

Joe Steinbicker
Steinbicker & Co, LLC
1206 Chantry Place
Lake Mary, Florida 32746

### Project Working Group

Maria Koliou
Texas A&M University
201 Dwight Look Engineering Building
College Station, Texas 77843

Shahab Torabian
Simpson Gumpertz & Heger
1625 Eye Street NW, Suite 900
Washington, D.C. 20006

## FIRST EDITION PROJECT TEAM

### Principal Authors

John Lawson
California Polytechnic State University
1 Grand Avenue
Building 21, Office 110A
San Luis Obispo, California 93407

Dominic J. Kelly
Simpson Gumpertz & Heger
41 Seyon Street
Building 1, Suite 500
Waltham, Masssachusetts 02453

### Contributing Authors

Andre Filiatrault
University at Buffalo
212 Ketter Hall
Buffalo, New York 14260

Maria Koliou
University at Buffalo
212 Ketter Hall
Buffalo, New York 14260

### Reviewers

Kelly Cobeen
Wiss, Janney, Elstner Associates, Inc.
2000 Powell Street, Suite 1650
Emeryville, California 94608

David McCormick
Simpson Gumpertz & Heger
1999 Harrison Street, Suite 2400
Oakland, California 94612

### Project Management Committee

William T. Holmes (Chair)
Federal Emergency Management Agency
2600 La Cuesta Avenue,
Oakland, California 94611

James R. Harris
J R Harris & Co
1775 Sherman Suite #2000
Denver, Colorado 80203

John D. Hooper
Magnusson Klemencic Associates
1301 5th Ave #3200
Seattle, Washington 98101

Barry H. Welliver
BHW Engineers, LLC
5 Bon Air Rd # 222
Larkspur, California 94939

Dominic J. Kelly
Simpson Gumpertz & Heger
41 Seyon Street
Building 1, Suite 500
Waltham, Massachussets 02453

### Project Review Panel

Ryan Kersting
Buehler
600 Q Street, Suite 200
Sacramento, California 95811

Joe Steinbicker
Steinbicker & Co, LLC
1206 Chantry Place
Lake Mary, Florida 32746

James Kramer
MHP Structural Engineers
3900 Cover St
Long Beach, California 90808

Doug Thompson
STB Structural Engineers, Inc.
21084 Bake Pkwy # 100
Lake Forest, California 92630

Trent Nagele
VLMK Engineering + Design
3933 S Kelly Avenue
Portland, Oregon 97239

### Project Review Panel Workshop Participants

Thomas Gangel
Wallace Engineering
123 North Martin Luther King Jr. Boulevard
Tulsa, Oklahoma 74103

Bonnie Manley
American Iron and Steel Institute
41 Tucker Road
Norfolk, Massachusetts 02081

Nathan Hauer
Structural Engineering Group, Target Stores

Lawrence Novak
Portland Cement Association
5420 Old Orchard Road
Skokie, Illinois 60077

Philip Line
American Wood Council
222 Catoctin Circle SE, Suite 201
Leesburg, Virginia 20175

### Project Oversight

Mai Tong
Federal Emergency Management Agency
400 C Street, SW
Washington, D.C. 20472

Robert D. Hanson
Federal Emergency Management Agency
5885 Dunabbey Loop
Dublin, Ohio 43017

Philip Schneider
National Institute of Building Sciences
1090 Vermont Avenue NW, Suite 700
Washington, D.C.  20005


FEMA

FEMA P-1026